Damir Radan

Integrated Control of Marine Electrical Power Systems

THESIS FOR THE DEGREE OF PHILOSOPHIAE DOCTOR

Department of Marine Technology
Norwegian University of Science and Technology
2008

NTNU

NTNU
Norwegian University of Science and Technology

Thesis for the degree of philosophiae doctor

Faculty of Engineering Science & Technology
Department of Marine Technology

ISBN 978-82-471-6633-8 (printed ver.)
ISBN 978-82-471-6647-5 (electronic ver.)
ISSN 1503-8181

Theses at NTNU, 2008:37

Printed at Tapir Uttrykk

Abstract

This doctoral thesis presents new ideas and research results on control of marine electric power system.

The main motivation for this work is the development of a control system, power management system (PMS) capable to improve the system robustness to blackout, handle major power system faults, minimize the operational cost and keep the power system machinery components under minimal stress in all operational conditions.

Today, the electric marine power system tends to have more system functionality implemented in integrated automation systems. The present state of the art type of tools and methods for analyzing marine power systems do only to a limited extent utilize the increased knowledge available within each of the mechanical and electrical engineering disciplines.

As the propulsion system is typically consisted of the largest consumers on the vessel, important interactions exists between the PMS and vessel propulsion system. These are interacted through the dynamic positioning (DP) controller, thrust allocation algorithm, local thruster controllers, generators' local frequency and voltage controllers. The PMS interacts with the propulsion system through the following main functions: available power static load control, load rate limiting control and blackout prevention control (i.e. fast load reduction). These functions serve to prevent the blackout and to ensure that the vessel will always have enough power.

The PMS interacts with other control systems in order to prevent a blackout and to minimize operational costs. The possibilities to maximize the performance of the vessel, increase the robustness to faults and decrease a component wear-out rate are mainly addressed locally for the individual control systems. The solutions are mainly implicative (for e.g. local thruster control, or DP thrust allocation), and attention has not been given on the interaction between these systems, the power system and PMS. Some of the questions that may arise regarding the system interactions, are as follows: how the PMS functionality may affect a local thruster control, how the local thruster control may affect the power system performance, how some consumers may affect the power system performance in normal operations and thus affect other consumers, how the power system operation may affect the susceptibility to faults and blackout, how various operating and weather conditions may affect the power system performance and thus propulsion performance though the PMS power limiting control, how propulsion performance may affect the overall vessel performance, which kind of faults can be avoided if the control system is re-structured, how to minimize the operational costs and to deal with the conflicting goals. This PhD thesis aims to provide answers to such questions.

The main contributions of this PhD thesis are:

- A new *observer-based fast load reduction system* for the blackout prevention control has been proposed. When compared to the existing fast load reduction systems, the proposed controller gives much faster blackout detection rate, high reliability in the detection and faster and more precise load reduction (within 150 miliseconds).
- New *advanced energy management control* strategies for reductions in the operational costs and improved fuel economy of the vessel.
- *Load limiting controllers* for the reduction of thruster wear-out rate. These controllers are based on the probability of torque loss, real-time torque loss and the thruster shaft

accelerations. The controllers provide means of redistributing thrust from load fluctuating thrusters to less load fluctuating ones, and may operate independently of the thrust allocation system. Another solution is also proposed where the load limiting controller based on thrust losses is an integrated part of DP thrust allocation algorithm.

- A new concept of totally integrated thrust allocation system, local thruster control and power system. These systems are integrated through PMS functionality which is contained within each thruster PLC, thereby distributed among individual controllers, and independent of the communications and dedicated controllers.
- *Observer-based inertial controller* and *direct torque-loss controller* (soft anti-spin controller) with particular attention to the control of machine wear-out rate. These controller contribute to general shaft speed control of electrical thrusters, generators and main propulsion prime movers.

The proposed controllers, estimators and concepts are demonstrated through time-domain simulations performed in MATLAB/SIMULINK. The selected data are typical for the required applications and may differ slightly for the presented cases.

Acknowledgments

This thesis is the main result of my doctoral studies, undertaken in the period September 2004 through December 2007 at the *Norwegian University of Technology and Science* (NTNU). My funding has been provided by a scholarship from the *Research Council of Norway* (NFR), and in part also by the project on *Energy Efficient All-Electric Ship* (EEAES), sponsored by the NFR.

The work of this thesis has been supervised by Dr.Ing. Alf-Kåre Ådnanes and Professor Asgeir J. Sørensen, both from the Department of Marine Technology and Professor Tor Arne Johansen from the Department of Engineering Cybernetics. I would like to thank my supervisor, Professor Asgeir J. Sørensen at the *Department of Marine Technology* for taking me in as a PhD student and for guiding me through the PhD. I would like to thank him for his guidance and enthusiastic encouragement, for backing me up and providing advices both within research and life in general when needed. I would like to thank to my supervisor, Alf-Kåre Ådnanes for introducing me to the design of marine electrical power systems and sharing from his immense knowledge of marine power plants. I also want to thank him for finding time for meetings even in the times when he was in short visit in Trondheim. Special thanks also to my supervisor, Professor Tor Arne Johansen from the *Department of Engineering Cybernetics* for the guidance on the PhD work and collaboration on papers. I would like to thank him for fruitful discussions throughout this project.

I have received valuable help from Professor Roy Nilsen and PhD student William Gullvik, from the *Department of Electrical Power Engineering*, NTNU for the discussions related to modeling of marine power systems and marine electric thruster drives.

I also need to thank to Mr. Jan-Peter Westergard from the *Wärtsila* for his help in defining the engine responses with regards to blackout prevention and for valuable discussions.

I would also like to thank my fellow PhD students for a good working environment, and especially Øyvind Smogeli, for collaboration on joint publication. Thanks also to Jostein Bakkeheim, Eivind Ruth and Luca Pivano for discussions on control of propulsion systems.

Thanks to the MSc students to whom I was advisor: Terje Arntsen for the work on optimization of power management load dependent start tables, and to Haakon Ellingsen for the work on speed control of marine engines.

I would also like to thank my colleges and in particular the administration Marianne Kjølås for the organization and help.

I would like to express my gratitude to all my family for their support and patience, and especially to my parents Boris and Ana for their continued support in my choices. Finally, to my wife Lejla and children Dominik and Lana for their love, patience and encouragement when it was most required.

Trondheim, December 3rd, 2007 Damir Radan

Contents

Nomenclature

Abbreviations

CO_2	Carbon dioxide
CPP	Controllable pitch propeller
CPU	Control processing unit
DP	Dynamic positioning
EB-FLR	Event-Based fast load reduction
EMS	Energy management system
FLR	Fast load reduction
FPBS	Frequency Sensitive Phased Back System
FPP	Fixed pitch propeller
GES	Globally exponentially stable
HVAC	Heating ventilation air-conditioning
IACS	International association of classification societies
I/O	Input/Output
ITO	Inertial torque observer
LCU	Local control unit
LNG	Liquefied natural gas
Low pass	Butterworth second order low pass filter based PI controller
LSC	Local speed controller
NOx	Nitrogen oxides
Obs-FLR	Observer-based frequency sensitive fast load reduction system
OSV	Offshore supply vessel
Qmg-Luen	Mechanical torque Luenberger observer
Qmg- Sliding	Mechanical torque Sliding mode observer
PCS	Process Control Stations
PI	Proportional integral (controller)
PO	Proportional observer
PID	Proportional integral derivational (controller)
PIO	Proportional integral observer
PIOM	Modified proportional-integral observer
PLC	Programmable logic controller
PRC	Power redistribution control
PS	Processing station
PSV	Platform supply vessel
PWM-VSI	Pulse width modulated voltage source inverter
DC	Direct current

PMS	Power management system
RMS	Root mean square
RPU	Remote Processor Units
SBFC	Specific break fuel consumption
SOx	Sulphur oxides
SS	Sea state
TRAN	Transit
VMS	Vessel management system

Lowercase

$a_{j,gi}$	BSFC approximation constant for each generating set i
$a_{max,g}$	maximum permitted engine load constant
$b_{e,gi}$	specific brake fuel consumption for each unit
c_0	sensitivity constant for the high load cost
d_x, d_y	faults or disturbances appearing in state and output equations respectively
d_ω	speed measurement noise
e_0	constant for emission cost
g	acceleration of gravity
h_0	nominal propeller shaft immersion measured in still water
k	number of generating sets online
k_{1g}, k_{2g}	sliding observer gains
$k_{FLR,p}$	controller gain for FLR
k_{thp1}	controller gain for quasi-static load limiting controller
k_{Pp}, k_{Ip}, k_{Dp}	proportional, integral and derivative control gains
k_{gp}	controller total gain for PRC
k_c	proportional gain for PRC
$k_{iner,p}$	inertial controller gain
$k_{\beta,,p}$	direct torque loss controller gain
l_{1g}, l_{2g}	observer gains for generator FLR control
l_{1p}, l_{2p}	observer gains for thruster load torque observer
m	designating number of the vessel operating mode
m_0	maintenance cost when the unit is unloaded
m_1	linear constant between m_0 and m_2
m_2	is the specified maintenance cost in an ideal case
n_{crit}	critical speed of the propeller when the ventilation occurs
q_h	threshold for the relative torque values i.e. torque loss factor
r_p	harmonic vertical relative displacement of the point $P(x_b, y_b, z_b)$
$r_{pa1/3}$	significant response amplitude of the propeller
s	Laplace operator (time derivative)

t	time or the number of new time step recorded (for discrete time)
t_{com}	time to execute the load reduction
$t_{FR,,i}$	response time of the fast load reduction (FLR) system
t_{mp}	time response of the frequency converter
$t_{\theta,com}$	time response due to communications and computations
th	number of thrusters connected on-line to the network
t_p	thust configuration vector
u	input vector
v_0	constant for the load variation cost
$w_g(k)$	weighting terms for the generators
w_p	maximum loading individually set for each thruster (consumer)
$w_{r,gi}$	installed power ratio for generators
w_{th}	weight factor for propulsion participation in the available power control
x	state vector
$\tilde{x}$	state estimation error vector
$\hat{x}$	state estimation vector
y	output vector
z_p	absolute vertical displacement of the point P

Uppercase

A	state matrix
B	input matrix
B_{gi}	status of the breaker and the generator load sharing
C_{HL}^t	generator high load cost
C_{LL}^t	generator low load cost
C_v^t	generator load variation cost
$C_{\text{stand-by}}^t$	generator stand-by cost
C_{sw}^t	generator switching cost
C_e^t	generator exhaust emission cost
D_g	generator damping coefficient
E	output noise vector
F	vector of thrust forces
FC_g	total instantaneous fuel consumption for the engine (generating-set)
FC_{gi}^{tran}	instantaneous transient fuel consumption for the engine
G	set of generators available to start
H_i	inertial time constant for each generating-set in seconds,
H_w	significant wave height

J_{comb}	combined cost function
J_{FC}	cost function for the instantaneous fuel consumption
J_{FCyear}	cost function per year of vessel operations
J_p	thruster moment of inertia
K	set of generators selected to start
K_Q, K_T	propeller torque and thrust constants respectively
L_P, L_I	proportional and integral observer gain vector
$L^*_{s,thp}$	optimized limit per thruster determined by DP controller
N_{comp}	number of separated compartments (sub-systems)
N_f	number of faulty generators
N_g	total number of installed units per system
N_p	total number of zero-crossings per hour
$N_{p,loss}$	expected number of times per hour that the thrust loss will occur
OP	time spent in the selected operational mode of the vessel
P_{ap}	thruster load power
P_{0p}	thruster nominal power reference (set-point)
P_{cp}	commanded power on thruster
P_{gf}	load for the generators at the moment of trip (pre-fault load)
P_{gi}	generator load
P_{rg}	installed generating power capacity
$P_{r,gi}$	generator power rating
P_{rsg}	required power generating capacity
$P_{\text{start},gi}(k)$	unit power when the next unit starts
P_g	total consumed load,
$P_{r,av}(k)$	available power is based on the maximum power capacity
P_{th}	total propulsion load
P_{av}	available power
$P_{c\text{-}ns}$	sheddable consumers other consumers then propulsion
$P_{av,start}$	available power based on the start dependent load tables
$P_{s,thp}$	power limit (static) per thruster
$P_{d,thp}$	dynamic part of the load limiting control
Q_{dg}	system damping torque
Q_{eg}	system electrical torque
Q_{mg}	system mechanical torque
Q_{mp}	motor torque of thruster
Q_{ap}	load torque of thruster
Q_{fp}	friction torque of thruster
Q_c^f	low pass filtered commanded torque
Q_{0p}	nominal propeller torque
$Q_{iner,p}$	inertial torque on propeller
$R_{mg\text{-}un}$	power slew rate magnitudes for generator unload

$R_{mg\text{-}up}$	power slew rate magnitudes for generator loading
R_{ω}	weight matrix in thrust allocation algorithm
$S_{gi}(k)$	load sharing constant
SR_g	engine load torque rates
SR_p	propeller (thruster) load torque rates
$S_{\zeta}(\omega)$	wave energy spectrum
T_{mp}	time constant for the thrust motor
T_{mg}	time constant for the generator
$T_{f,th}$	filter time constant
$T_{start\text{-}up,gi}$	time to start the unit
T_{Qf}	low pass filter time constant for the thrust loss factor filtering
$T(\alpha)$	thrust configuration matrix
T_{0p}	thrust force per thruster
$\hat{T}_{a,p}$	load torque real-time estimate
V_s	speed of the vessel
W	cost matrix

Greek

α_p	thruster azimuth angle
$\beta_{loss,p}$	torque loss factor of the propeller
$\overline{\beta}_{loss,p}$	average propeller torque loss factor
$\delta_g(t)$	frequency deviation between the mean and the nominal speed
ε	constant used to avoid singular solution
γ	weighting terms for the combined cost function J_{comb}
ΔQ_p	torque deviation on thruster
$\Delta P_{\mathrm{gi}}^{\max}$	engine maximum load step capability
$\Delta P_{\mathrm{FLR},g}^{\max}$	maximum power available for the FLR
$\Delta P_{FLR,gi}$	load to be reduced by the FLR
$\Delta\gamma_{start,g}$	relaying control limit
$\Delta\gamma_{ss}$	load shedding limit
$\Delta\omega_{FLR,gi}$	permitted frequency drop during load reduction
$\Delta\omega_{\mathrm{gi}}$	class rule permitted frequency deviation from nominal ω_{0gi}
$\Delta\omega_{gi}^{\mathrm{osc}}$	oscillating frequency deviation from the nominal
$\Delta\omega_p$	speed deviation on thruster
η_{pd}	efficiency of thruster (propulsion drive)
ν	load dependent stop constant
μ	vessel-wave heading angle

Π_p , ψ_p	weights in thrust allocation algorithm
ρ	penalty constant
τ_{gI}	time constant for the network frequency low pass filter
τ	total required thrust
ζ_a	wave amplitude
ω	wave frequency
ω_e	vessel-wave encounter frequency
ω_{0gi}	nominal engine speed (frequency)
ω_g	mean rotor angular speed for all generators in the system
$\omega_{FLR,p}^{\max}$	maximum limit frequency for FLR activation
$\bar{\hat{\omega}}_g$	filtered network frequency

Chapter 1

Introduction

1.1 Background

Electrical installations are present in any ship, from powering of communication and navigation equipment, alarm and monitoring system, running of motors for pumps, fans or winches, to high power installation for electric propulsion. The concept of electric propulsion is originated more than 100 years ago. However, with the possibility to control electrical motors with variable speed in a large power range with compact, reliable and cost competitive solutions, the use of electrical propulsion has emerged in new application areas during the 80's and 90's (Ådnanes, 2004).

Typically, ships with electric propulsion tend to have more system functionality implemented in integrated automation systems, partially because such functionalities are regarded to be necessary for safe and optimal operation, but also because the electric propulsion plant enables the use of such functions. In the commercial market the offshore vessels in addition to cruise ships and ice breakers have been technology drivers concerning automation, power and propulsion systems. They are characterized by the required ability to conduct complex marine operations, operational availability, safety focus, cost effectiveness and flexibility in operational profile concerning transit, station keeping, maneuverability and to some extent also a significant vessel or process load system. These rather complex power plants opened up for an increasing use of fully *all-electric ships* and the introduction of fully integrated computer-controlled systems in order to operate safely and cost efficiently. Such concepts are today applied in an increasing number of ship applications (Hansen, 2000; Sørensen and Ådnanes, 2005).

Power Management System (PMS) is a crucial part of the automation and power systems on marine vessels, and in particular for ships with electric propulsion and station keeping thrusters. The PMS controls the power system in order to maximize the blackout prevention capabilities and minimize the fuel consumption. It also serves to decrease the maintenance costs through protecting the equipment against faults and malfunctions; see e.g. Häkkinen (2003). Through interaction between the PMS and other control systems, the performance of the vessel can be maximized. The purpose of the PMS is to assure adequate and reliable electrical power supply to the various consumers. This is achieved by the following main tasks (May and Foss, 2000):

1. *Generator allocation control* (generator auto-start and auto-stop): The PMS will control the number of generators online according to the available load on the network and operational conditions;
2. *Propulsion load limiting control*: Under normal operating conditions (i.e. generator loading less than 100 %) the PMS will prohibit an excessive load increase by controlling the maximum individual consumption of e.g. thrusters, drilling units, and compressors. The power limit signals also features a *load increase rate* function (slew rate limits);
3. *Fast load reduction*: The power consumption of variable frequency drives (thrusters, drilling) is controlled in order to avoid overloading the generators. Should an overload

occur e.g. caused by a shut down of a generator set, the PMS will force load reduction of some or all of the variable frequency drives until the situation is recovered;

4. *Regenerated power control*: regenerated power from e.g. the drilling drawworks is limited to avoid a reverse power situation for the generators. The draw works on drilling vessels is able to generate power which in some installations may be regenerated to the network. To prevent tripping of generators on reverse power, the amount of re-generated power will be limited by the drilling control system in accordance with signals from the PMS;
5. *Blackout restart*: The PMS will perform blackout restart of the power system in the event of a total or partial blackout;
6. Further, the PMS includes the *Redundancy and Criticality Assessment* system, an operator support system that monitors the "health" of the electric power system. All generators, switchboards and thruster drives, including all auxiliary systems, are monitored and compared with specific requirements for the defined operational modes of the vessel. Any important alarm or non-conformance with respect to equipment condition or set-up is reported to the engineers as well as to the DP-operators.

This thesis deals mainly with first three PMS functionalities, namely: *generator allocation control*, *propulsion load limiting control* and *fast load reduction*.

Electric propulsion is an emerging area where various competence areas meet. Successful solutions for vessels with electric propulsion are found in environments where naval architects, hydrodynamic and propulsion engineers, and electrical engineering expertise cooperate under constructional, operational, and economical considerations (Ådnanes, 2004). However, the present state of the art type of tools and methods for analyzing marine power systems do only to a limited extent utilize the increased knowledge available within each of the mechanical and electrical engineering disciplines. The today's solutions are kind of ad-hoc approaches in overall optimization, and analytical approach to large extent has been missing in the design.

The complex interaction between vessel sub-systems is demonstrated in Fig. 1.1. In Fig. 1.1 the overall propulsion control structure is presented for typical dynamically positioned (DP) vessel, equipped with electric propulsion. The control structure consists of:

- DP controller;
- Thrust allocation;
- Local thruster controller;
- Power plant with generator's frequency and voltage controllers;
- PMS distributed controllers with relevant functionalities for the propulsion including:
  - Generator allocation control;
  - Available power based propulsion static load control;
  - Propulsion load rate limiting control;
  - Blackout prevention control (fast load reduction).

The high level controller, which can be a dynamic positioning (DP) controller, position mooring (PM) controller, or joystick controller, computes the forces in surge and sway and moment in yaw needed to counteract the environmental loads and track the desired path. The thrust allocation controller calculates the thrust set points for each propulsion unit according to a given optimization criterion, e.g. minimization of power consumption, see Fossen (2002) and references therein. The low-level thruster controllers control the thrusters to produce the thrust forces given by the set points from the thrust allocation system. The PMS is limiting

and redistributing the power on consumers in order to avoid the blackout, see e.g. Kallah (1997), Lauvdal and Ådnanes (2000), May and Foss (2000), Savoy (2002), May (2003). As the PMS is affecting the overall propulsion, its action has to be coordinated between a number of controllers in the control loop, as shown in Fig.1.1. Moreover, the controllers have to be set with regards to the level of system protection and selectivity. This has to be done in opposite direction as well, i.e. the protection must be set to comply with the operation of power system in various operating conditions. Spurious trips of the equipment have to be avoided during normal operation transients but the protection system must be sensitive to the real faults. These possibly conflicting goals have to be accomplished by careful coordination between various controllers and protection systems. The protection system, other then the fast load reduction (FLR) system, has not been dealt in this thesis. However, the PMS performance has been analyzed in order to improve the robustness to faults and the speed of the fault/ blackout detection.

The interaction of all controllers must be coordinated in order to obtain an optimal operation of the vessel. A special responsibility lies with the system integration responsible, and experience has shown that it might be a challenging work to coordinate the overall system robustness and optimization.

One of the important controllers for the blackout prevention is FLR system. Various types of FLR algorithms have been applied on board the marine vessels, see e.g. May and Foss (2000), Kundur (1994), Lauvdal and Ådnanes (2000), Savoy (2002), May (2003). The frequency based FLR algorithm will be triggered regardless to the real cause of the frequency drop. This FLR algorithm may execute during normal operations involving transients, such as e.g. propeller load fluctuations. Another type of FLR algorithm is based on the signal received from the switchboard, i.e. circuit breaker. This one is considered to be prone to the transmission noise in the cables, dependent on the communication and computational delays and faults within the PMS control system. A new hybrid type of the FLR algorithm, integrated in the system but with distributed functionality, has been proposed in the thesis.

In dynamic positioning (DP) of the vessel, the propeller loadings will change depending on the various factors, among the most important are: the controller modes, weather conditions, vessel performance and the tuning of the DP controller, see e.g. Fossen (2002), Johansen (2004), Johansen *et al.* (2004a), Johansen *et al.* (2004b), Fossen and Johansen (2006), Nguyen *et al.* (2007a), Nguyen *et al.* (2007b), Ruth *et al.* (2007) and the references therein. Fast load fluctuations, continuously present during a storm, are mainly responsible for the network frequency fluctuations. These are also generated by the propeller thrust losses, see e.g. Sørensen *et al.* (1997), Smogeli *et al.* (2004a), Smogeli *et al.* (2004b), Smogeli (2006), Ruth (2005), Ruth and Smogeli (2006), Bakkeheim *et al.* (2006), Bakkeheim *et al.* (2007a), Bakkeheim *et al.* (2007b), Radan *et al.* (2006b), Radan *et al.* (2007a), Pivano *et al.* (2007a), Pivano *et al.* (2007b) and references therein.

The interconnecting point for all installed power equipment is the power distribution system. By starting and inrush transients, load variations, and network disturbances from harmonic effects the load and generators are interacting and influencing each other. Optimum operation and control of the power system is essential for safe operation with a minimum of fuel consumption. The optimization-based power and energy management strategies are mainly introduced to improve the fuel economy on on-land vehicles equipped with energy storage device (battery), see e.g. Aoyagi *et al.* (2001), Lin *et al.* (2003), Emadi (2003), Barsali *et al.* (2004), Sciarretta *et al.* (2004), Koot *et al.* (2005), He and Jang (2006),

Guzzella and Sciarretta (2007), Sciarretta and Guzzella (2007) and references therein. These methods had limited application on board marine vessel despite the need for improved frequency control of generators. These issues are considered in this thesis and as an outcome a new idea for the complete functional integration of consumers and generators has been proposed.

Due to relatively low number of units installed and low variety of prime mover types and fuels used, the energy management control found today in the marine vessel is fairly simple, see Hansen (2000), Arntsen (2005), Davey (2005), and Levander (2006). The generators are committed according to pre-set load dependent start and stop tables, as explained in e.g. Hansen (2000), Radan *et al.* (2005), Radan *et al.* (2006a). The extensive knowledge contained in the literature for the on-land power generation and distribution has limited use in the marine application. These methods may provide potentially significant operational cost savings together with the improvements in planning and intelligent handling of the power plant; see e.g. Wood and Wollenberg (1996), Tupper (1996), Michalewicz *et al.* (1996), Olsbu *et al.* (1988), Karnavas and Papadopoulos (1999), Watson (2002), Klimstra, (2004b), Klimstra, (2004c), Matt *et al.*, (2005), Perez-Guerrero and Cedenio-Maldonado (2005), Bansal (2006), Lee and Chen (2007). Therefore, the important aim of this thesis is to make a contribution towards decreasing operational costs of the marine vessel and to increase the level of automatic control in the marine power plant.

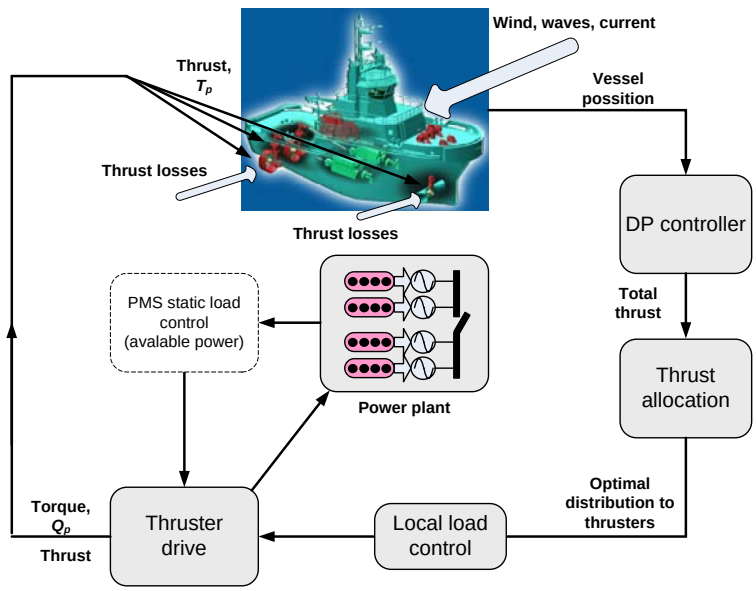

Fig. 1.1. Propulsion control structure

1.2 Problem statement

The types of the future required methods for analysis of marine power system are not only to optimize the steady state performance, but also to include analysis of dynamic behavior in operational cases for the total system, including low level control and energy management system.

Therefore, the main aim is to develop high-level power/energy management system (PMS/EMS) which monitors and has the overall control functionality of the power system and which will be the integrating element in a totally integrated power, automation, and positioning system.
The functionally integrated control system should provide means of:

- Optimal allocation and distribution of energy onboard with minimum operational costs, including fuel consumption;
- Reduce thrusters damages and wear-out rate of thruster components;
- Reduce the network load fluctuations, thereby reduce the mechanical vibrations and wear of generating-set parts;
- Reduce the network frequency and voltage fluctuations, thereby reduce the stress to electrical equipment and machines supplied from the network;
- Maximize blackout prevention through reducing the frequency fluctuations and improving the blackout detection speed and reliability;
- Improve the controller and system robustness to faults and disturbances.

These objectives should be accomplished in all circumstances, i.e. when the vessel is subject to varying operational conditions, safety requirements and operational availability. The high-level control system has to be robust to faults and errors in readings. It should also be well integrated with the low level controllers. The integrated system should provide an optimal interaction between the control and the protection of the distribution system.

1.3 Main contributions

The main contributions found in this thesis are summarized here. Parts of this thesis have earlier been published. References to these publications are given below:

– The blackout prevention control has been analyzed in Chapter 3. Among the numbers of methods used for *fast load reduction* a new observer-based method has been proposed. The result has been presented in Radan *et al.* (2007b). It has been demonstrated that the proposed method can improve the reliability and speed of detection of circuit breaker trip and provide more robust and faster load reduction.

– By using advanced energy management control strategies the fuel consumption on the vessel can be reduced from 6 to 8 % for offshore supply vessels. Similar methodology can be applied to other vessels as well. The energy management system has been presented in Chapter 4. Part of these results have been presented in Radan *et al.* (2005) and Radan *et al.* (2006a). However, the *short-time unit commitment* control strategies have not been previously published.

– In Chapter 5 a high-level propulsion *quasi-static load limiting controller* has been proposed. The load limiting controller is based on the probability of torque loss published in Radan *et al.* (2006b). Other controllers are also proposed: the real-time torque loss and on the thruster shaft acceleration. The controllers provide means of redistributing thrust from load fluctuating thrusters to less load fluctuating ones, and may operate independently of the thrust allocation system.

– The work in this thesis has shown how the marine power system can have complete integrated functionality between the thrust allocation system, local thruster control and power system. The power can be re-distributed between the generators and consumers in order to obtain the minimum load fluctuations on generating-sets and thrusters while the average thrust remains unchanged. This has been confirmed through the simulations and presented in Chapter 6 and Radan *et al.* (2008), Radan *et al.* (2007b). Moreover, it has been demonstrated that the fuel economy can also be improved up to 13%.

– Chapter 7 explores the benefits of integrated network control concept for increased robustness to faults and blackout. Attention has been given to integration aspects of PMS with thrust allocation. The concept of *frequency-based load limiting control*, based on PRC is also proposed.

– In Chapter 8, another contribution to general speed control of electrical thrusters, generators and main propulsion prime movers is proposed. Two controllers are proposed: *observer-based inertial controller* and *direct torque-loss controller* (soft anti-spin controller). Part of this work has been published in Radan *et al.* (2007a). Both of the controllers can lower the speed and torque fluctuations on thrusters and improve the robustness to noise present in the speed measurements. In Chapter 8, various types of observers are compared in order to improve the noise filtering in the speed measurement signal for frequency drives and engines.

1.4 Organization of the thesis

Chapter 2 introduces the design of power management system and explains the most important issues regarding the vessel vulnerability to faults. The emphasis is given on the controller interaction for optimal performance.

Chapter 3 presents the blackout prevention control. Different blackout prevention control strategies are analyzed, and a new control strategy is proposed. The proposed controller is compared with the existing ones.

Chapter 4 gives the comparison between the on-land and the offshore unit commitment optimization and economic load dispatch. The operating costs and number of constraints of the offshore vessel are defined. The convex and non-convex methods for the solution are analyzed. The long-term and short-term unit commitment strategies are proposed.

Chapter 5 is about the propulsion load limiting control. It describes the load fluctuations influence to the network and classifies the loads depending on the importance to inject the load fluctuations to the network. Several slowly varying off-line and real-time controllers are proposed.

Chapter 6 proposes a new strategy to completely attenuate the frequency and voltage fluctuations on the network and significantly improve the network stability. The proposed control is termed the *Power Redistribution Control* (PRC) as it will redistribute power around nominal (set-points) on individual thrusters, depending on the network frequency fluctuations.

Chapter 7 proposes a new concept of integrated power network control. The robustness to faults and blackout is analyzed with regards to the existing and proposed control systems. The new aspects of integration of PRC with thrust allocation and quasi-static load limiting controllers have been proposed. Moreover, frequency-based load limiting control is also proposed.

Chapter 8 is about the speed control of thrusters and generators. Effect of noise on shaft speed control has been analyzed, and several state observers for improved noise filtering have been proposed. These observers have been compared for optimal noise versus control response. The inertial controller and direct torque loss controller (soft anti-spin) controllers have been proposed.

Chapter 9 summarizes the main conclusions of this thesis and proposes further work.

Appendix A describes the modeling of marine power system.

Appendix B gives the control plant models for the generator and thruster.

Chapter 2

Functionality of power management system

2.1 PMS functionality

The Power Management System (PMS) is a crucial part of the automation and power systems on marine vessels, and in particular for ships with electric propulsion and station keeping thrusters. The PMS controls the power system in order to maximize the blackout prevention capabilities and minimize the fuel consumption. It also serves to decrease the maintenance costs through protecting the equipment against faults and malfunctions. Through interaction between the PMS and other control systems, the performance of the vessel can be maximized. In order to give an overview of the functionality of existing PMS, as well as to propose new challenges and ideas, the main topics of the design and operation of the marine power plant have been described.

2.2 Overall fault vulnerability and redundancy

2.2.1 Power system fault vulnerability

The minimum power generating capacity and the number of the generating sets are dependant upon the required thruster power to maintain position and heading of the vessel under the most severe environmental conditions, services load and the auxiliary systems, see e.g. Kallah, (1997), and May and Foss (2000).

Depending on class notation, some vessel must be resistant to single faults. In such vessels, the actual total installed capacity is governed by the available power after a single fault according to the following equation (May and Foss, 2000):

$$P_{rg} = P_{rsg} \cdot \frac{N_{comp}}{N_{comp} - 1} \tag{2.1}$$

where P_{rg} is the installed generating power capacity, P_{rsg} is the required power generating capacity, and N_{comp} is the number of separated sub-systems. The generating sets, thrusters and their auxiliaries are housed in separate compartments. Eq. (2.1) is based on equal capacity in each of the sub-systems, which is commonly applied in ship designs.

According to (2.1), the amount of installed power decreases with the number of split sub-systems or number of the engine compartments. The highest P_{rg} is obtained with two subsystems, N_{comp}=2, where $P_{rg} = 2\ P_{rsg}$. As the N_{comp} increases, P_{rg} becomes closer to the P_{rsg}, $P_{rg} \approx P_{rsg}$.

The design optimum lies in the point where the reduction in the installed power capacity P_{rg} fully compensates for the increase in the cost of additional compartments, each with auxiliaries and services. The following conflicting objectives and constraints are part of the optimization trade-offs:

- *Constraint*: vulnerability to single faults with the possibility to extend to multiple faults;
- *Constraint*: mission accomplishment (operational and weather conditions);
- *Objective*: minimize the installed power;
- *Objective*: minimize the complexity of the power system and costs of additional auxiliaries;
- *Objective*: minimize the operating costs, among the highest is the fuel consumption.

The mission accomplishment is specified as the most severe environmental conditions for the vessel to perform operations, e.g. 10 years winter storm conditions (May and Foss, 2000).

In order to obtain more flexibility in satisfying these objectives, the component-based optimization can be used, as shown in Fig. 2.1 (Ådnanes, 2004). Several levels of power system redundancy for one or two engine rooms have been defined:

- *Power generation level*: defines the number of generating sets;
- *Power distribution level*: defines the number of switchboards, bus-ties, etc.;
- *Electric part of propulsion system*: number of frequency converters, electric motors, etc.;
- *Mechanical part of propulsion system*: number of shafts, gears, propellers, etc.

For each of these levels, the objectives and constraints, defined above, can be included in the optimization. The design constraints are influencing the power availability in the vessel operations. The design constraints also influence the reliability of machinery systems; see e.g. Häkkinen (2003), and Conachey (2005).

Thus, the PMS operation will depend to a large extent on a number of fixed parameters, such as: the power system configuration, DP class, the installed power, number of generating sets, and similar; see e.g. Hansen (2000), Arntsen (2005), Davey (2005), Radan *et al.* (2005), Levander (2006), and Radan *et al.* (2006a).

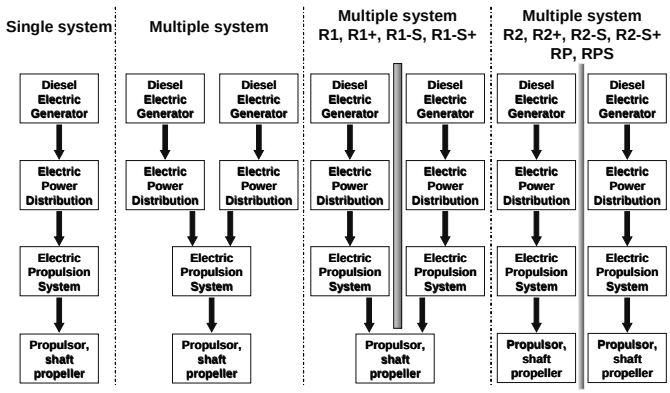

Fig. 2.1. Various levels of power system redundancy
for one or two engine rooms, Ådnanes, (2004)

2.2.2 PMS fault vulnerability

In conventional machinery space with lower automation level, the control system is centralized in one control processing unit (CPU), and a number of local control units (LCU) which are distributed in the machinery space. The main operator station is located at the same place as the CPU – machinery control room or bridge.

On highly automated systems found today, more common concept is to distribute PMS functions in several units (Lauvdal and Ådnanes, 2000). Fig. 2.2 shows a concept of system integration with network between operating stations, programmable logic controllers (PLCs) and thruster drives. Process Control Stations (PCS, PCU) or Remote Processor Units (RPU) are PLCs. All PMS substations or PCS that take part in the PMS are performing calculations based on the information received from its own bus segment. They also share information from the other PMS substations (Savoy, 2002). In cases when the vessel must continue to operate with opened bus-tie (power system is divided on two or more subsystems which are isolated), each power system will have its own PMS substation, and each PMS substation can act as autonomous unit. The system is not dependant on central computer, and a high redundancy of the control system is achieved.

For smaller vessels, another concept is typically used. There each controller takes care of the whole plant, with a duty/stand-by functionality.

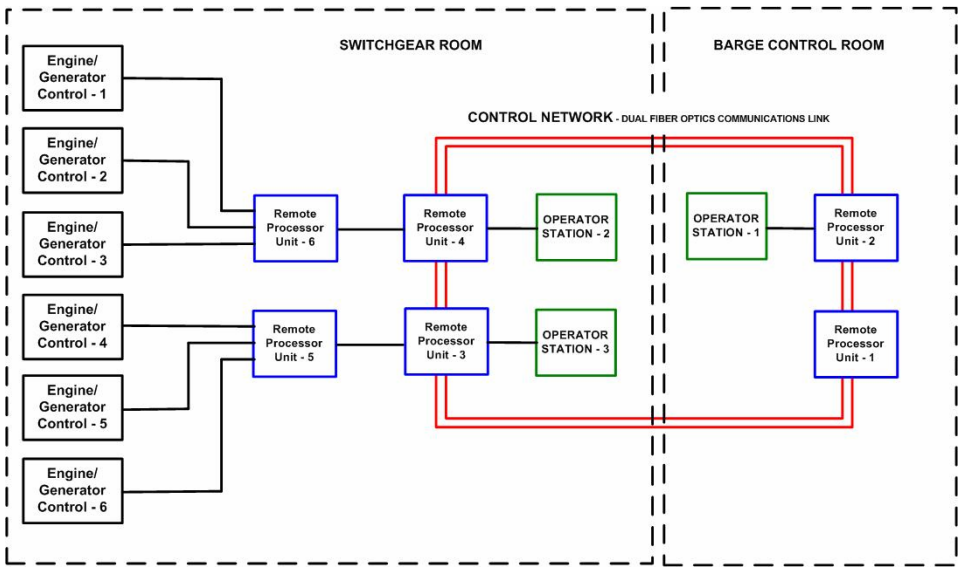

Figure 2.2. Functional integration and information distribution in PMS, Savoy (2002)

2.3 Generator allocation control

2.3.1 Single point failure and maximum transient load

The PMS monitors the total power demand and compares it to the available supply. The PMS can automatically start and stop generator sets to coincide with the load changes in accordance with the pre-calculated load dependent start/stop tables (May, 2002; Radan *et al.*, 2005; Radan *et al.*, 2006a). In case of sudden failure of the generating set, the power system loading will be transferred to the remaining generators online. Then, the remaining generators on-line must take the rest of the system load. The transient frequency deviation is limited to ±10% according to the class society rules (IACS, 2004). Activating the under frequency limit will initiate opening of the circuit breaker(s) for the remaining generator(s) online. This will have a blackout as a consequence. In order to prevent the blackout, the FLR system must reduce the load before the frequency reaches the under-frequency limit. The transient load step in the system when N_f units are tripped (fail) with k units online is defined:

$$\Delta P_{\text{tran}}(k, N_f) = \sum_{f=1}^{N_f} P_{gf}(k, N_f), \tag{2.2}$$

where P_{gf} is the load for the generators that are tripped. The main requirement from the class societies is the resistance to single failure. In that respect, the limits are usually calculated for the situation in which the unit with the highest loading fails:

$$P_{gf}(k) = \max_i P_{gi}(k), \text{ for } j \in [1, k], \tag{2.3}$$

where P_{gi} is the current load of the generator. Each generator contributes an amount of power proportional to its inertia, i.e. its inertial time constant H_i and power rating $P_{r,gi}$. Assuming that the generators remain in the synchronism, the following equation to calculate the load step per generator can be used (Machowski et al., 1997):

$$\Delta P_{\text{tran},gi}(k, N_f) = \frac{H_i P_{r,gi}(k)}{\sum_{i=1}^{k-N_f} H_i P_{r,gi}} \Delta P_{\text{tran}}(k, N_f), \tag{2.4}$$

where H_i is the inertial time constant for each generating-set in seconds, and $P_{r,gi}$ is the generator power rating. When the fault occurs, the N_f faulty generators will be disconnected and $k–N_f$ generating-sets will remain on-line.

The transient load per generator is determined as the sum of the generator load and transient load step:

$$P_{\text{tran},gi}(k, N_f) = P_{gi} + \Delta P_{\text{tran},gi}(k, N_f). \tag{2.5}$$

2.3.2 Load depended start of generating sets

For the power system equipped with FLR system, as well as for those without FLR, the blackout can be prevented as long as the maximum transient load step is lower or equal to the permitted, according to:

$$\Delta P_{\text{tran},gi}(k, N_f) \le \min\left[\Delta P^{\max}_{\text{tran},gi}\left(a_{\max,g}, t_{FLR,i}\right), \Delta P^{\max}_{\text{FLR},gi}\right], \tag{2.6}$$

$$\Delta P^{\max}_{\text{tran},gi}\left(a_{\max,g}, t_{FLR,i}\right) = \begin{cases} \min\left(a_{\max,g} P_{r,gi} - P_{gi}, \Delta P^{\max}_{\text{gi}}\right), & \text{without FLR system} \\ \Delta P^{\max}_{\text{tran},gi}\left(t_{FLR,i}\right), & \text{with FLR system} \end{cases}$$

$$\Delta P^{\max}_{\text{FLR},gi} = \frac{H_i P_{r,gi}(k)}{\sum_{i=1}^{k-N_f} H_i P_{r,gi}} \Delta P^{\max}_{\text{FLR},g},$$

where:

- $\Delta P^{\max}_{\text{FLR},g}$ is the maximum power available for the FLR, dependant on the load of the consumers available for the FLR. Through out the thesis, it will be assumed $\Delta P^{\max}_{\text{FLR},g} \ge \Delta P^{\max}_{\text{tran},gi}\left(a_{\max,g}, t_{FLR,i}\right)$, so $\Delta P^{\max}_{\text{FLR},g}$ will be omitted in eq. (2.6);
- $a_{\max,g}$ is the maximum permitted engine load constant;
- $\Delta P^{\max}_{\text{gi}}$ is the engine maximum load step capability, defined in the text below;
- $t_{FR,,i}$ is the FLR system response time needed to reduce the load on the consumers. The permitted transient load step, for the systems equipped with the FLR system, is dependant on the time needed for the control system to reduce the load on consumers $t_{FR,,i}$. This will be defined later in this Chapter.

Without the FLR system the maximum transient load could not be higher than the maximum permitted engine load $a_{\max,g}P_{rg,i}$. The constant $a_{max,g}$ differs among the different engine manufacturers and depends on details in the engine design. It is typically:

$$1.1 \le a_{\max,g} \le 1.15\,. \tag{2.7}$$

Typically, diesel engines are not capable to accept at once the load step higher than $0.25P_{rgi}$ to $0.33P_{rgi}$, see e.g. MAN Diesel SE (2006). Due to engine limitations in the load step acceptance, the following limit must be included:

$$\Delta P_{\text{gi}}(k, N_f) \le \Delta P^{\max}_{\text{gi}}\,. \tag{2.8}$$

Therefore, special problem represents operating with only 2 generating sets on-line, since for two equal rated units: ΔP_{gi} (k=2, N_f=1) = $0.55P_{rgi}$.

The maximum continuous safe loading limit (blackout limit) for the generator is determined when (2.6) is substituted in (2.5) according to:

$$P_{\text{cont},gi}^{\max}(k, N_f) = P_{\text{tran},gi}(k, N_f) - \Delta P_{\text{tran},gi}^{\max}\left(a_{\max,g}, t_{FLR,i}\right). \quad (2.9)$$

With respect to k number of generating sets online, the next unit must start before the load reaches the maximum continuous safe limit. Thus, the safe generator operational region $P_{gi}(k)$ for starting units is limited to:

$$P_{gi}(k) \le P_{\text{start},gi}(k) \le \min\left(P_{\text{cont},gi}^{\max}(k, N_f), P_{rgi}\right), \quad (2.10)$$

where $P_{\text{start},gi}(k)$is the power when the next unit k+1 starts for the situation with k units online i.e. $P_{\text{start},gi}(k) = P_{gi}(k) = P_{gi}(k+1)$. The *min* function determines the minimum value among maximum continuous safe limit and rated power. Although the maximum permitted engine load determines maximum engine load capability, continuous operation is not allowed in the region: $a_{\max,g} P_{rg,i} > P_{rg,i}$.

The maximum permitted continuous load is usually pre-calculated in the so-called *load dependent start tables*, as shown in the example given in Table 2.1 (MAN Diesel SE, 2006). The table shows the situation when one of the equally rated units fails. It is assumed that the load sharing between generating sets is equal, i.e. all units are equally loaded.

Table 2.1. Load dependent start table for equally rated generators

Number of generators connected	Generator load–pre fault $P_{gi}(k)/P_{rgi}$	Generator load–post fault $P_{gi}(k, N_f)/P_{rgi}$	Maximum load step, $\Delta P_{gi}(k, N_f)/P_{rgi}$
2	0.55	0.55 2/1= 1.10	0.55
2	0.60	0.60 2/2 = 0.90	0.20
4	0.74	0.74 4/2 = 0.98	0.24
5	0.80	0.80 5/4 ≈ 1.00	0.2
6	0.82	0.82 6/5 ≈ 1.00	0.17
7	0.86	0.86 7/6 ≈ 1.00	0.14

Load sharing

The load per unit depends on the load sharing constant, determined by the PMS:

$$P_{gi}(k) = S_{gi}(k) P_g, \quad (2.11)$$

where $S_{gi}(k)$ is the load sharing constant which depends on the number of on-line units k. The following equation must hold in order to avoid the load limiting or the reverse power condition on any generator:

$$P_g = \sum_{i=1}^{k} S_{gi}(k) P_g = \sum_{i=1}^{k} P_{gi}(k), \quad (2.12)$$

which means that the total contribution from all generators that share the total consumed load P_g must be equal to that load. Then, the main load sharing constraint must be fulfilled:

$$\sum_{i=1}^{k} S_{gi}(k) = 1. \quad (2.13)$$

According to the class society rules, equal load sharing between generating sets must be obtained:

$$\frac{P_{gi}(k)}{P_{rgi}(k)} = \frac{P_{g,i+1}(k)}{P_{rg,i+1}(k)}, \text{ for all } i \in [1, N_g], \tag{2.14}$$

where N_g is the total number of installed units per system, which means that the following equation must hold in normal steady conditions, according to class society rules:

$$\frac{S_{gi}(k)}{P_{rgi}(k)} = \frac{S_{g,i+1}(k)}{P_{rg,i+1}(k)}, \text{ for all } i \in [1, N_g]. \tag{2.15}$$

Equally rated units

According to (2.15), if $P_{r,gi}(k) = P_{r,gi+1}(k)$, then $S_{gi}(k) = S_{gi+1}(k)$. Then (2.12) becomes:

$$P_g = \sum_{i=1}^{k} S_{gi}(k) P_g = k\ P_{gi}(k)\ . \tag{2.16}$$

The load sharing for equally rated units is then:

$$S_{gi}(k) = \frac{1}{k}\ . \tag{2.17}$$

Usually, all generating sets installed in the vessel are supplied from the same manufacturer. Therefore, equally rated generators will have the same inertia time constant $H_i = H_{i+1}$.

The load step per generator for equally rated units is calculated from (2.4). If all units have equal ratings, inertias, and share load equally, the (2.4) simplifies to:

$$\Delta P_{tran,gi}(k, N_f) = \frac{P_{r,gi}(k)}{kP_{r,gi}(k, N_f) - N_f P_{r,gi}(k, N_f)} N_f P_{gf}(k, N_f)\ . \tag{2.18}$$

Finally, the simplified equation for the load step with equally rated units when one unit fails is obtained:

$$\Delta P_{tran,,gi}(k, N_f = 1) = \frac{1}{k-1} P_{gi}(k)\ . \tag{2.19}$$

One can notice that the safe operational region will increase with the number of generators online k due to decrease in the transient load step per generator $\Delta P_{tran,gi}(k, N_f)$.

2.3.3 Load depended start/stop of generating sets

The load dependent start table has to be optimized in order to obtain the lowest possible fuel consumption, considering the blackout as an important constraint, see e.g. Radan *et al.* (2005). In the load increasing operations, when the load per generator becomes higher than allowed in eq. (2.10), the next generator in the start sequence must be started, synchronized and connected to the network.

When the load per generator becomes lower than recommended by the engine manufacturers, the number of units on-line can be disconnected and stopped. This is usually done in order to save fuel and decrease the wear and resulting maintenance costs due to low load running of the engines.

Thus, the load operational region $P_{gi}(k)$ for start/stop of the units is defined according to:

$$a_{\min,g} P_{r,gi} \le P_{\text{stop},gi}(k) \le P_{gi}(k) \le P_{\text{start},gi}(k) \le \min\left(P^{\max}_{\text{cont},gi}(k, N_f), P_{r,gi}\right), \qquad (2.20)$$

where $P_{\text{stop},gi}(k)$ is the power when the next unit in the sequence k–1 stops for the situation with k units online i.e. $P_{\text{stop},gi}(k) = P_{gi}(k) = P_{gi}(k–1)$. The $a_{\min,g}$ is a constant that determines the recommended minimum load on the engine, as described above. For diesel engines a continuous operation below 0.15 $P_{rg,i}$ is not recommended (MAN B&W, 2004). Thus, the minimum engine load can be defined as:

$$0.15 \le a_{\min,g} \le 0.30\,. \qquad (2.21)$$

If the engines are to be loaded down to this low load constraint, the total power system load would be too low before one unit is stopped making all engines to run on relatively low load. Therefore, the existing criterion is that the load dependent stop tables must not coincide with the load dependent start tables:

$$P_{\text{start},g}(k) \le P_{\text{stop},g}(k+1) \le P_{\text{start},g}(k+1)\,. \qquad (2.22)$$

2.3.4 Available power

In order to prevent a blackout, the system must always have a sufficient power reserve or available power to its full online capacity. The minimum available power based on the maximum power ratings is determined according to:

$$P_{r,av}(k) = P_{r,g}(k) - P_g(k) = \sum_{i=1}^{k} P_{r,gi} - P_g\,, \qquad (2.23)$$

where $P_{r,g}$ is the generating capacity or sum of the power ratings $P_{r,gi}$ for all the generators on-line, P_g is the total consumed load, shared among generating sets, each loaded P_{gi}. In the real applications, the power generating capacity is calculated from the status of the generator breakers (ON/OFF) and the power ratings of the generating sets according to:

$$P_{r,g}(k) = \sum_{i=1}^{N_g} P_{r,gi}\ B_{gi}\ , \tag{2.24}$$

$$B_{gi} = \begin{cases} 1 & \textit{if} \quad \text{breaker is ON AND } S_{gi}(k)/P_{rgi}(k) \approx S_{g,i+1}(k)/P_{rg,i+1}(k) \\ 0 & \textit{else} \end{cases},$$

$$k = \sum_{i=1}^{N_g} B_{gi}\ ,$$

where B_{gi} is the checking status of the breaker and the generator load sharing. If the generator is ON but does not share load equally according to (2.15), its power capacity will not be included in the total power capacity calculation. This requirement is to assure that recently started generator can not participate in the available power calculation.

The minimum available power, based on the generator failure cases is determined according to:

$$P^{\min}_{\text{cont},av}(k, N_f) = \sum_{i=1}^{k} \min\left(P^{\max}_{\text{cont},gi}(k, N_f), P_{rgi}\right) - \sum_{i=1}^{k} P_{gi}\ , \tag{2.25}$$

where the number of generator on-line k is determined from (2.24).

The available power for the unit start, based on the load dependent start tables is defined as:

$$P_{av,start}(k) = P_{\text{start},g}(k) - P_g(k) = \sum_{i=1}^{k} P_{\text{start},gi}(k) - \sum_{i=1}^{k} P_{gi}\ . \tag{2.26}$$

The next generator in the sequence will be started when the available power drops below zero. In this case the following equation holds:

$$P_{\text{start},g}(k) = P_g\left(k\right) = P_g\left(k+1\right). \tag{2.27}$$

Accordingly, when *auto-stop* is initiated the following equation holds:

$$P_{\text{stop},g}\left(k\right) = P_g\left(k\right) = P_g\left(k-1\right). \tag{2.28}$$

Available power for equally rated units

For equally rated units, the maximum load step is determined from (2.19). Maximum continuous generator safe loading for equally loaded units is found after inserting (2.19) into (2.9) and assuming equal load sharing between units (2.17):

$$P^{\max}_{\text{cont},gi}(k, N_f) = P^{\max}_{\text{tran},gi}\left(a_{\max,g}, t_{FR,i}\right)\frac{k-1}{k}, \tag{2.29}$$

where $P_{gi}(k) = P^{\max}_{\text{cont},gi}(k, N_f)$ in (2.9).

2.4 Load limiting control

2.4.1 Consumer groups and limiting priority

With respect to the priority of load limiting, it is important to distinguish between the following types of loads:

- *Sheddable loads*: loads that may be used for system (network) load limiting. All non-essential consumers can be regarded as *sheddable.* However, on plants with electrical propulsion, these loads are typically electrical thrusters with frequency converters and drilling loads (May and Foss, 2000; Savoy, 2002). Due to slow responses of the vessel with respect to position and heading, thrusters can operate with reduced load in DP for some period of time. This period is typically sufficient to get the next unit on-line and increase the power generating capacity;
- *Non-sheddable loads*: consumers that have high importance of supplying the energy. These are typically loads of navigational equipment, control network load, hotel loads, auxiliary machinery loads, and similar. This depends on the vessel type and may depend on operations as well. Hotel loads will normally have higher priority in cruise vessels (passenger comfort) than it will be for other vessel types.

Load shedding can also be used for other consumers than thrusters. Traditional load shedding is based on switching off the groups of non-essential consumers when there is a deficit of generated power. When the power is available, these sheddable consumers can be switched on again. The main drawback when working with high number of sheddable consumers is difficulties in the prediction of their behavior with respect to active and reactive power during, in particular immediately after switching. Moreover, the time to restore the sheddable consumers will increase with their number, as consumers can not all be started at once. Preferable load shedding solution will include a low number of consumers. With low number of consumers, the system behavior can also be predicted up to some point.

With respect to controllability, i.e. precise control of the load, consumers can be divided into the following groups:

- *Controllable consumers*: They are capable to precisely set the load within the machine electrical/mechanical limits. These are typically consumers with frequency converters (drives). Thrusters usually belong to this group together with other controllable loads, such as the drilling loads and compressors;
- *Non-controllable consumers*: consumers that do not have the flexibility of different power settings. These are all consumers capable only for the simple switching control: ON/OFF. A great number of such consumers may be found on any vessel: various heaters and direct on-line (DOL) asynchronous motors.

With respect to the nature of the operations, the consumers can also be divided to:

- *Consumers that rely on the energy*: The best for load limiting are the consumers that rely on energy rather than power. This means that the operations will not be much affected while operating with reduced power for the limited period of time. Appliances/machines which rely on energy rather than power are: heaters, refrigerators, air conditioners (HVAC) and similar. In general, the heating processes are slower than mechanicals and electric. Thrusters also belong into this group due to the similar reasons;
- *Consumers that rely on the power*: These are consumers that require full power all the time, e.g. controllers and control equipment, navigational equipment, and similar. In

general, a limited number of consumers in the vessel really belong to this group. The reason why only some consumers can be used for load limiting is explained in Fig. 2.3.

Fig. 2.3 shows all divisions of loads with respect to load priority, energy dependence, and controllability. In order to reduce the load, the load must be *sheddable* and, if possible, also *controllable*. Then such a load can be used for temporary network power reductions when is needed from the overall blackout prevention control. Hence, the best suitable load will rely on energy rather than power.

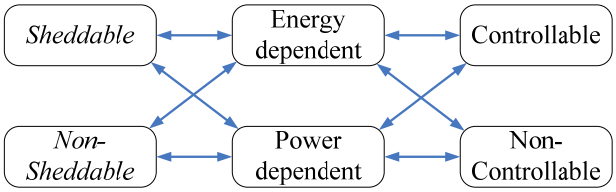

Fig. 2.3. Possibilities for shedding loads

2.4.2 Propulsion load limiting

Load limiting based on available power

The propulsion capacity will depend on the power system available power P_{av} and the total propulsion power P_{th}, according to:

$$P_{s,th}\left(P_{th},P_{av}\right)=P_{th}+w_{th}P_{av}\,, \tag{2.30}$$

where P_{th} is the total propulsion load, P_{av} is the available power, and w_{th} is the weight factor for propulsion participation in the available power control. If w_{th} = 1 then only propulsion power will be limited in order to control the available power. The propulsion load P_{th} will be limited when the available power becomes lower than zero, $P_{av} < 0$.

The propulsion load P_{th} can be directly measured or determined by subtracting the non-sheddable loads (e.g. hotel load and auxiliaries) from total power demand on generators P_g (Savoy, 2002):

$$P_{th}=P_g-P_{c-ns}\,, \tag{2.31}$$

where $P_{c\text{-}ns}$ means non-sheddable consumers, which are other consumers then propulsion. Depending on the operational PMS philosophy, the available power P_{av} can be based on the *start load tables* $P_{av,start}$ or *maximum power capacity*, $P_{r,av}$.

The propulsion load limit can be expressed as a non-dimensional ratio of total propulsion power:

$$L_{s,th}=\frac{P_{s,th}}{P_{th}},\quad L_{s,th}\le 1\ . \tag{2.32}$$

The load propulsion limit can be distributed on individual thrusters in two different ways, through:

– *Direct load limiting*, faster but not optimized i.e. proportional;
– *Indirect load limiting*, slower but optimized in DP thrust allocation algorithm.

When using the *direct load limiting*, the power can be reduced to all thrusters proportionally:

$$P_{s,thp} = w_p L_{s,th} P_{thp} \,, \tag{2.33}$$

where $P_{s,thp}$ is the power limit per thruster and w_p is the maximum loading individually set for each thruster (consumer), allowing a priority selection between the consumers.

With the *indirect load limiting*, the load propulsion limit can be distributed to all online thrusters according to:

$$P_{s,thp} = L^*_{s,thp} P_{thp} \,, \tag{2.34}$$

where $L^*_{s,thp}$ is optimized limit per thruster determined by DP controller, $0 \leq L^*_{s,thp} \leq 1$. The following constraint must be satisfied:

$$\sum_{p=1}^{N_p} L^*_{s,thp} = L_{s,th} \,. \tag{2.35}$$

Load limiting based on available power and generator individual loading

The available power is calculated from measured total power on generators P_g. However, the load may be distributed in different ways between generators. Thus, to improve the blackout prevention capabilities for the system, the load limiting may be initiated if the individual load on any of the connected generators crosses the upper limit for the safe operation, according to eq. (2.10). Then, the allowable propulsion capacity will be determined by the available power and maximum limit crossing per individual generator, according to:

– *Maximum blackout limit:*

$$P_{s,th}\left(P_{th}, P_{av,start}, P^{\max}_{\text{cont},gi}, P_{gi}, P_{rgi}\right) = P_{th} + \min\left(P_{av,start}, \min_i\left(\min\left(P^{\max}_{\text{cont},gi}\left(k, N_f\right), P_{rgi}\right) - P_{gi}\right)\right); \tag{2.36}$$

– *Unit starting limit:*

$$P_{s,th}\left(P_{th}, P_{av,start}, P_{\text{start},gi}, P_{gi}\right) = P_{th} + \min\left(P_{av,start}, \min_i\left(P_{\text{start},gi}\left(k, N_f\right) - P_{gi}\right)\right). \tag{2.37}$$

Since the starting load is lower or equal to maximum permitted, the unit starting limit is always lower than the blackout limit. Which one will be selected depends on the design preferences and operational philosophy. It may be important to notice that these constraints may not be always achievable, e.g. due to operational constraints of the intact system after a single fault: after the loss of one switchboard due to a single fault, there may pass some time

before the system is back to "normal" operation with at least two generating set on-line and blackout constraints imposed.

2.4.3 Effect of feedback filtering on propulsion limiting

Important problem with power limiting may arise related to the signal filtering.

The total power of the propulsion system P_{th} can be determined in following ways:

- From the *nominal speed* (*or thrust*) *of the propeller*, see e.g. Sørensen *et al.* (1997);
- From the *electrical power feedback* measured on the switchboard, see e.g. Savoy (2002).

Nominal speed* (*or thrust*) *of the propeller

The nominal propulsion power could be calculated from the nominal speed of the propeller ω_{0p}, see e.g. Sørensen *et al.* (1997). However, the load limiting control will rather rely on the feedback signal from the switchboard which will give higher accuracy to the control i.e. assure that the average propulsion power is really as received (Savoy, 2002). Otherwise, the speed set-point reference may not give corresponding power output due to e.g. faults or excessive thrust losses and this would increase the risk of blackout for such systems.

Electrical power feedback

As the vessel operates in harsh weather conditions and the propeller is subjected to excessive thrust losses, the electrical propulsion power output P_{th}, measured on the switchboard may fluctuate significantly about the average. These load fluctuations may be responsible for the unnecessary periodical load limiting of the propulsion, although there is sufficient power on-line.

Hence, in order to avoid unnecessary periodical load limiting of the propulsion, when there is sufficient power on-line, $P_{s,th}$ should be filtered before entering the load limiting algorithm. The following equation should be used instead of (2.30) in the load limiting algorithm:

$$P_{s,th}\left(\bar{P}_{th}, \bar{P}_{av}\right) = \bar{P}_{th} + w_{th}\bar{P}_{av}, \tag{2.38}$$

and the low pass filter (e.g. double first order) can be used:

$$\bar{P}_{th} = \left(\frac{1}{T_{f,th}s+1}\right)^2 P_{th}, \tag{2.39}$$

where, s is the Laplace operator, and $T_{f,th}$ is the filter time constant. This filter can be substituted with e.g. any other order low pass filter or similar, see e.g. Fossen (2002). The available power P_{av} can be filtered in the similar way. The described load limiting control is also called *sustained load limiting control* (Savoy, 2002).

Due to *sustained load limiting control*, in addition to computational and communication delays, the time required for the DP and PMS load limiter to calculate and transmit the thruster load limit to the Thruster PLC is typically 1 to 2 seconds (May, 2002). The thruster controller needs additional 2-3 seconds to reduce the power on thruster. This is partly due to

gain settings of PI controller. The low pass filter is required at the controller output to filter a noise introduced by the speed measurement; see Chapter 8. This filter contributes to most of the drive dynamics; see Fig. 2.4. Moreover, the communication delays between PLCs may also significantly contribute to decreased speed of response.

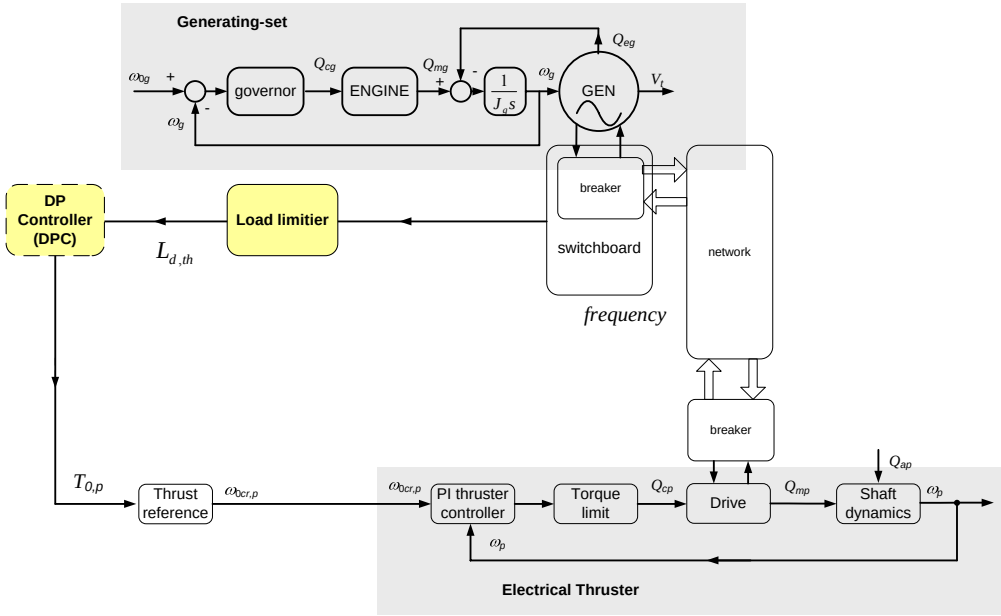

Fig. 2.4. Existing load limiting control and DP controller within power system

Load limiting mapping to thruster reference set-points

Within DP thrust allocation algorithm, the average P_{th} should be mapped to nominal propeller output $P_{0,p}$:

$$P_{0,\max p} = g_{P_{0,p}}\left(\overline{P}_{s,thp}\right), \tag{2.40}$$

which can be defined as follows:

$$P_{0,\max p} = \overline{P}_{s,thp}\eta_{dp}, \quad \text{for} \qquad \overline{P}_{s,thp} \le \overline{P}_{thp} \tag{2.41}$$

where $\eta_{pd} = \eta_{pd}\ (P_{thp})$ is the efficiency of the propulsion drive, and accounts for the mechanical and electrical transmission losses: transformer, drive, motor, mechanical. Here, it may be assumed that the thrust losses are not accounted in most of the DP thrust allocation algorithms. However, if this is the case the following mapping may be obtained:

$$P_{0,\max,p} = \overline{P}_{s,thp}\frac{\eta_{dp}}{\overline{\beta}_{loss,p}}, \quad \text{for} \qquad \overline{P}_{s,thp} \le \overline{P}_{thp} \tag{2.42}$$

where $\beta_{loss,p}$ is the torque loss factor of the propeller. This value can be estimated offline or online (in the real-time), as will be seen in Chapter 5.

The maximum allowable speed reference for each propeller can be calculated using, see e.g. Sørensen *et al.* (1997); Smogeli (2006):

$$\begin{aligned} n_{0,\max,p} &= 1.84 K_{Q0}{}^{1/3} \rho^{1/3} D^{5/3} P_{sth,p}^{1/3} \\ &= g_{n_{0\max,p}}\left(P_{sth,p}\right), \end{aligned} \tag{2.43}$$

and the maximum available nominal thrust from:

$$\begin{aligned} T_{0,\max,p} &= \frac{\rho^{1/2} D_p K_{T0p}}{2\pi K_{Q0p}} P_{sth,p}^{2/3} \\ &= g_{T_{0\max,p}}\left(P_{sth,p}\right). \end{aligned} \tag{2.44}$$

2.4.4 Propulsion load rate limiting

To reduce the excessive stress and frequency fluctuations on prime movers (engines) due to propulsion loading, the common approach in the marine industry is to set the fixed slew rate limits on the electrical thrusters, as shown in Fig. 2.5. Without load rate limits, thrusters would increase the electrical load in the system almost instantly, and this would result in a system blackout. The slew rates for thrusters are chosen in connection with the optimal prime mover load torque rates SR_g. Due to changeable power generating allocation (start/stop), the load rates on thrusters have to change with the generating power capacity. This is accomplished through constant checking the status of the generator connection breakers and the bus-tie(s). The slew rate limits are defined as the maximum values of the thruster acceleration and depend on the optimal engine load torque rates SR_g, generating capacity $P_{rg}(k)$, and the shaft speed of the thruster ω_p according to:

$$SR_p(k, P_{thp}) = \max\left(\left|\frac{d\omega_{0p}}{dt}\right|\right) = f\left(SR_g, P_{rg}(k), \omega_p\right), \tag{2.45}$$

where $f(\cdot)$ stands for the functional dependence. An increase in the ON state of the breakers indicates a higher online power generating capacity according to (2.24). With higher power generating capacity, the load rate limits for the thrusters can be increased, allowing thrusters to accelerate faster.

Different load rates have to be determined for all possible breaker i.e. generating capacity combinations. Careful tuning is required to obtain desired thruster and engine responses. In order to obtain an even power change, the load rate limits can be higher on low thruster speed and lower on higher thruster speed. The main goal is to obtain the fastest possible increase in the thrust with minimum frequency and voltage drop on generators.

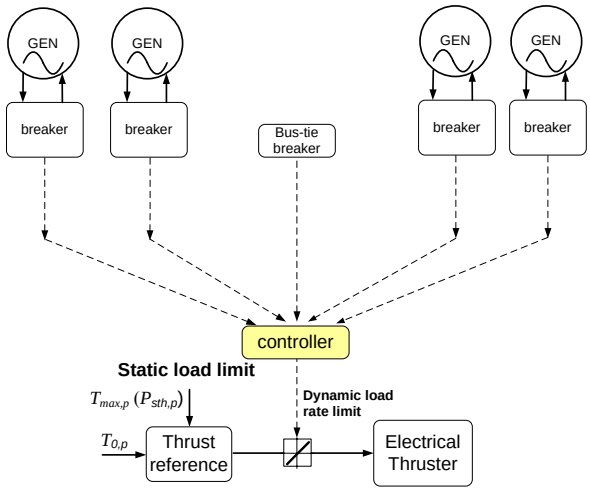

Fig. 2.5. Example of the existing load limit control system for marine thrusters

Once the fixed load rate limits have been determined for the normal vessel operations, the controller will have limited possibilities to accommodate the various detrimental effects experienced in vessel operations, such as hull and propeller fouling and decreased performance of the diesel engine. Moreover, the existing load limit control system for marine thrusters, shown in Fig. 2.5 is not robust to the number of possible faults. If the communication between switchboard (breakers) and the thruster PLC is lost, the controller will assume that the breaker is permanently disconnected (OFF). Since SR_p depends on k, the lower load rate limits will be selected and the thruster will accelerate slower than the actual engine torque can develop. The final effect is a decrease in the propeller thrust and deteriorated vessel performance in the seaway.

Chapter 3

Blackout prevention control

3.1 Blackout

Blackouts in electrical power systems are normally caused by short circuits/ground faults and overloads or by faults in the active or reactive load sharing systems. Short circuit/ground fault protection of the power system is provided by the proper selection and application of circuit breakers and protective devices. Proper selection and setting of these devices are required to obtain a *selective coordinated system*, which will isolate the faulty circuit and minimize the damage at the fault point. It should be noted that selectivity coordination is based on stationary calculations of the fault currents, applying margins in the settings of the protection relays to account for tolerances in the instrumentations and dynamic variations. It must be assumed that there may occur transient variations in the network, e.g. generator oscillations that may lead to unselective actions by the protection system.

Overload occurs when the generating power capacity is lower than the electrical power demand. The system can be overloaded in the several ways (May, 2003):

- *Circuit breaker on faulty generator is disconnected*: due to short circuit or ground fault and the system load is distributed to remaining generators on-line;
- *Generating set long-term overload*: when the engine loading exceeds its power rating $P_{gi} > P_{r,gi} \leq a_{\max,gi} P_{r,gi}$, the generator may become overheated. The generator produces excessive current and the risk of short circuit increases. This may increase the tendency to short-circuits/ground (earth) faults in the future. If the prime mover is loaded beyond the recommended limits, an increase in the rate of mechanical faults may also be expected in the near future;
- *Prime mover fault*: although, the shut-down of prime mover can be predicted within reasonable time (*pre-warning alarm*), there may be some faults that may occur unexpectedly;
- *Functionality of PMS and power system operation*: when the available power becomes low, the PMS will allocate (start) new units and/or limit the load to consumers. The overload may occur if the PMS functionality is not coordinated to an acceptable level or due to faults within the PMS.

3.2 Engine shutdown and trip of generating set

The most common types of faults, which cause a generator set to shutdown, with relatively low probability of expectance, are (May, 2003):

- *Fuel system failures*: clogged fuel lines, fuel pump failure, water in the fuel, etc;
- *Mechanical failures*: loss of oil or water pressure, over speed, high cooling medium temperature;
- *Control system failures*: false indication of low lube oil pressure, false oil mist detectors, crankcase overpressure, or loss of an I/O signal;
- *Operator / human error*: usually occurs in the set-up and synchronizing of generator sets and load balancing where engines can be tripped by the reverse power protection.

Pre-warning alarm

An important PMS function, which increases the overall blackout prevention capabilities, is called the *pre-warning alarm*. It is a function used to prevent a sudden engine loss situation. The *pre-warning alarm* should automatically initiate a start of the next available generator if any conditions which will lead to a shut down of the engine are getting critical near the shut down limit.

3.3 Blackout dynamics

In case of the generator trip, the main problem is the time aspect. Due to fast dynamics of the blackout, the control system must respond in a limited time. The events leading to blackout propagate very fast as described, see Fig. 3.1:

- *Step1*: When only a few units are on-line, a trip of one unit, $N_f = 1$, may result in a very large load step per remaining on-line units k–1, where the transient load per generator can be in the range typically $P_{tran,gi}(k, N_f=1) = 1.4\ P_{r,gi}$ to $1.8\ P_{r,gi}$. Since the engines can not be loaded higher than $P_{max,gi} = 1.1\ P_{r,gi}$ to $1.15\ P_{r,gi}$, see eq. (2.7), the load must be reduced before the frequency drops below the under-frequency limit;
- *Step2*: The generator protection system will open the circuit breaker if the frequency drops below the under-frequency limit. Due to the high synchronizing torque between paralleled generators, this will normally happen for all paralleled generators at the same time.

Fig. 3.1 shows the load step after one generator fails. The frequency drop and load reduction are also presented, and all variables are defined in accordance to the equations defined below.

After the load on the engine becomes higher than maximum permitted load given in eq. (2.7), the fuel rack hits the limit and no increase in the engine torque can be accomplished. Hence, the FLR system will typically be initiated in a situation when the limit defined in (2.8) is crossed. Thus, the available time for the load reduction will depend mainly on the inertia of the generating sets, remaining on-line, according to, see e.g. (Radan *et al.*, 2005; Radan *et al.*, 2006a):

$$t_{SL,i} = \Delta\omega_{FLR,gi}\ \frac{2H_i}{\Delta P_{FLR,gi}} P_{r,gi}\ , \tag{3.2}$$

where $\Delta\omega_{FLR,gi}$ is the permitted frequency drop during the load reduction, and $\Delta P_{FLR,gi}$ is the load to be reduced by the FLR.

According to (3.2), the time limit for the load reduction will be extended if the load to be reduced $\Delta P_{FLR,gi}$ is low. The load to be reduced by the FLR depends on the maximum transient load scenario, and is defined as follows:

$$\Delta P_{FLR,gi} = P_{\text{tran},gi}(k, N_f) - P_{gi} - \min\left(a_{\max,g} P_{r,gi} - P_{gi}, \Delta P_{\text{gi}}\right)$$
$$= \Delta P_{\text{tran},gi}(k, N_f) - \min\left(a_{\max,g} P_{r,gi} - P_{gi}, \Delta P_{\text{gi}}\right) , \quad (3.3)$$

where the maximum transient load $P_{\text{tran},gi}(k, N_f)$ depends on the scenario (worst case scenario) that may include various combinations with k on-line units and N_f units that fail. The prime mover can accept part of the transient load step. This is defined by ΔP_{gi}, and its maximum value is defined in eq. (2.8). Due to engine time-lag the frequency drops to $\Delta\omega_{en,gi}(\Delta P_{gi})$.

Fig. 3.2 shows the results of the simulation with 2 generating-sets (gen-sets), with $H_1 = H_2 = 2.5$ seconds In case a) in Fig. 3.2, the pre-fault scenario is: $P_{g1} = 0.8\ P_{r,g1}$, $P_{g2} = 0.8\ P_{r,g2}$, and $\Delta P_{FLR,g1} = 0.8\ P_{r,g2}$. In case b) in Fig. 3.2, the pre-fault scenario is: $P_{g1} = 0.57\ P_{r,g1}$, $P_{g2} = 0.57\ P_{r,g2}$, and $\Delta P_{FLR,g1} = 0.57\ P_{r,g2}$. Then, the t_{SL} is much longer than in case a). However, this is also due to gen-set is operating close to the engine load capacity of 110% $P_{r,g1}$ and due to the delayed engine response.

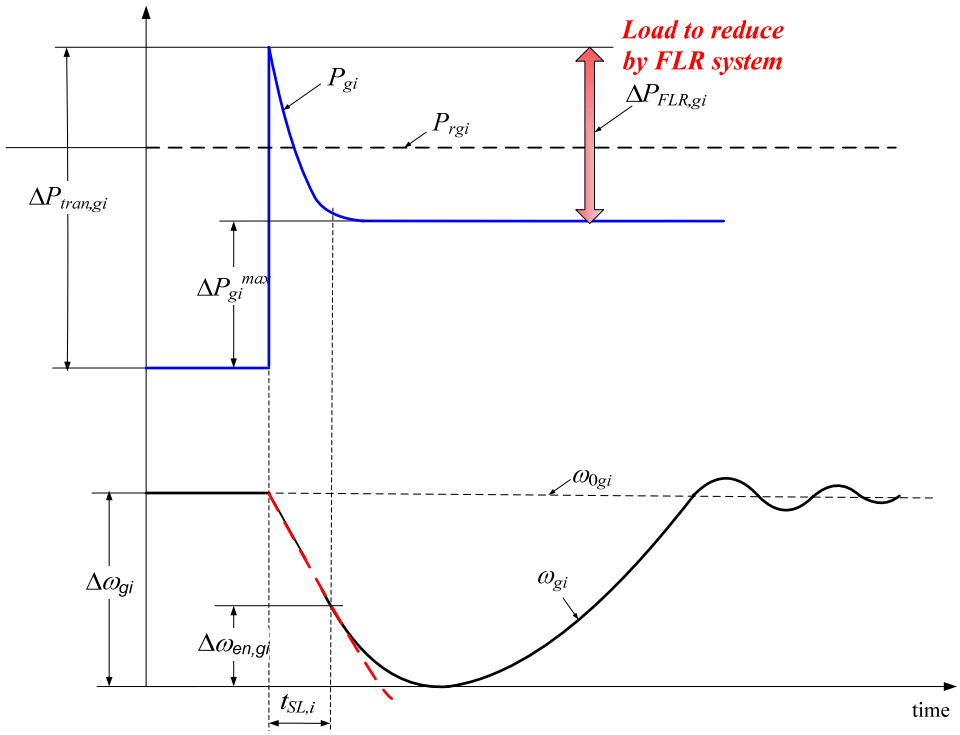

Fig. 3.1. Fast load reduction with part load accepted by the prime mover of the on-line generating set

The permitted frequency drop depends both on the frequency drop limit $\Delta\omega_{gi}^{\max}$ defined by the class society rules and the additional frequency drop that occurs when the engine takes part of the system load ΔP_{gi}, as defined:

$$\Delta\omega_{FLR,gi} = \Delta\omega_{gi}^{\max} - \Delta\omega_{en,gi}\left(\Delta P_{gi}\right). \tag{3.4}$$

An increase in the inertial time constant H_i, will provide an increase against the under-frequency trip of the generator and more resistance to blackout due to abrupt load increase. The main drawback of increased inertia on the generating sets is that the time to recover from the transient will also increase due to increased energy store in the rotating masses (Klimstra, 2004).

a) **b)**

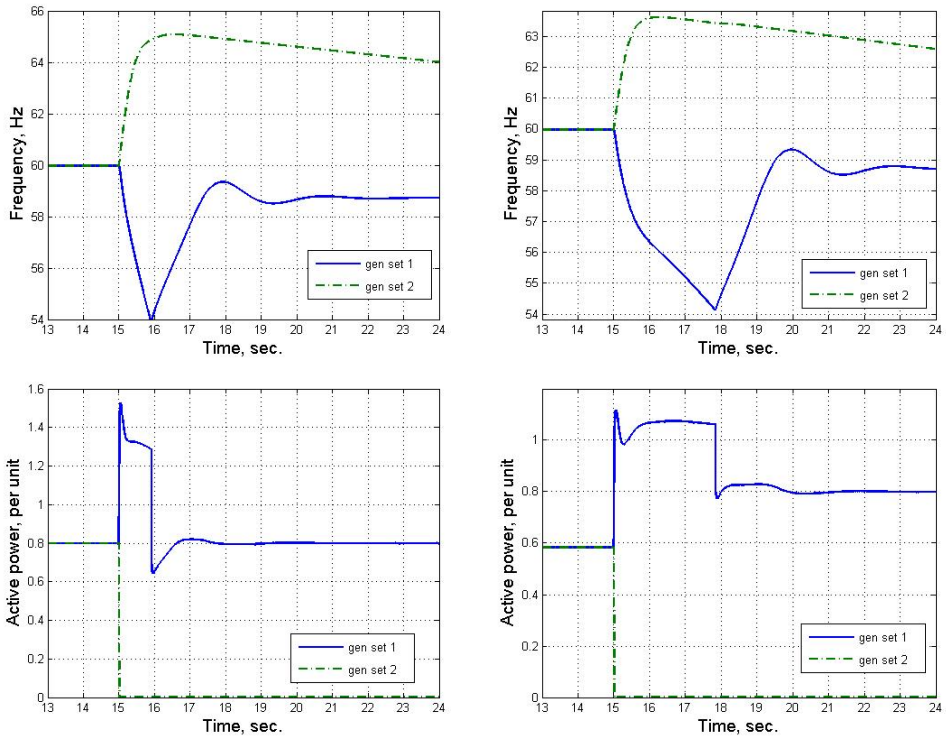

$P_{g1} = 0.8\ P_{r,g1}$, $P_{g2} = 0.8\ P_{r,g2}$, $P_{r,g1} = P_{r,g2}$

$P_{g1} = 0.57\ P_{r,g1}$, $P_{g2} = 0.57\ P_{r,g2}$, $P_{r,g1} = P_{r,g2}$

Fig. 3.2. Frequency drop when gen-set 2 is disconnected from the network in t=15 seconds, $H_1 = 2$ seconds

a) $P_{g1} = 0.8\ P_{r,g1}$, $P_{g2} = 0.8\ P_{r,g2}$,
b) $P_{g1} = 0.57\ P_{r,g1}$, $P_{g2} = 0.57\ P_{r,g2}$.

3.4 Quantity of load reduction

Modern functionality of PMS is extended to reduce the load in situations or fault scenarios than may initiate large frequency and voltage drop on the generator and cause the consequent generator trip.

With respect to the quantity of the reduced load, three main FLR methods may be used:

– *Strategy 1*: The excessive load is reduced.
The engine takes the part of the network load immediately after the fault occurred. Since the engine load step acceptance is limited, the excessive load must be reduced by the FLR;
– *Strategy 2*: Full transient load step is reduced.
The engine does not accept any additional load than initial pre-fault load. Then the engine will have the post-fault engine loading equal to pre-fault engine loading. After the fault has been cleared, the engine can be loaded slowly to the maximum permitted load;
– *Strategy 3*: A new strategy based on optimal combination of 1 and 2 is proposed.
Using the combination of methods 1 and 2, an optimal combination can be accomplished in order to maximize the time limit t_{SLi} for the load reduction. The methods can be selected depending on the instant loading of the generating set.

3.4.1 The excessive transient load step reduction (Strategy 1)

When one of the units fails, the time for the other to take a load depends on the engine inertia and the engine ability to respond to the load step. When the FLR is designed to reduce the excessive load above the maximum permitted load step, the following values are determined from (3.3) and (3.4):

$$\Delta P_{FLR,gi} = \Delta P_{\text{tran},gi}(k, N_f) - \Delta P_{\text{gi}}^{\max}, \quad \text{since } \Delta P_{\text{gi}} = \Delta P_{\text{gi}}^{\max}, \tag{3.5}$$

$$\Delta\omega_{FLR,gi} = \Delta\omega_{gi}^{\max} - \Delta\omega_{en,gi}^{\max}, \qquad \text{since } \Delta\omega_{en,gi}\left(\Delta P_{\text{gi}}^{\max}\right) = \Delta\omega_{en,gi}^{\max}.$$

Typical limits are (Westergard, 2007; MAN Diesel SE, 2006; IACS, 2006):

$$0.25P_{r,gi} \le \Delta P_{\text{gi}}^{\max}\left(P_{gi}\right) \le 0.33P_{r,gi}, \tag{3.6}$$

$$0.03\omega_{0gi} \le \Delta\omega_{en,gi}\left(0.25P_{r,gi}\right) \le 0.06\omega_{0gi},$$

$$\Delta\omega_{gi}^{\max} = 0.1\omega_{0gi},$$

where ω_{0gi} is the nominal engine speed. $\Delta\omega_{\text{gi}}$=0.1 ω_{0gi}, according to class rules. The inertial time constant H, for the marine diesel and/or gas generators, is typically between H = 0.7 to 2 seconds. (Westegard, 2007, Klimstra, 2004; MAN Diesel SE, 2006). The engine frequency respond to load step may vary from 3 to 6% nominal (Westegard, 2007).

Then, the time to reduce the load when the maximum engine load step capability is utilized can be calculated from the following equation:

$$t_{SL,i} = \left(\Delta\omega_{gi}^{\max} - \Delta\omega_{en,gi}\right) \frac{2H_i}{\Delta P_{\text{tran},gi}(k, N_f) - \min\left(a_{\max,g} P_{r,gi} - P_{gi}, \Delta P_{\text{gi}}\right)} P_{r,gi} \,. \qquad (3.7)$$

The time to reach the under frequency limit, t_{SL}, must be set higher or equal than the time necessary for the fast load reduction, $t_{SL} \geq t_{FLR}$. The speed of response of fast load reduction system t_{FLR} depends on the PMS and FLR design, as will be explained later on.

The FLR execution time may be in the range: $0.25 \leq t_{FLR} \leq 0.5$ seconds, see e.g. Lauvdal and Ådnanes (2000); May, (2003). After equalizing $t_{SL} = t_{FLR}$ and adding P_{gi} on both sides of (3.7) and rearranging, determines the maximum permitted transient load:

$$P_{\text{tran},gi}\left(t_{FLR}\right) = \left(\Delta\omega_{gi}^{\max} - \Delta\omega_{en,gi}^{\max}\right) \frac{2H_i}{t_{FLR,i}} P_{r,gi} + P_{gi} + \min\left(a_{\max,g} P_{r,gi} - P_{gi}, \Delta P_{\text{gi}}\right). \quad (3.8)$$

The maximum transient load depends on the initial loading of the generator P_{gi}, the ability of the engine to accept the load step ΔP_{gi}, and response time of fast load reduction system $t_{FLR,i}$.

3.4.2 Full transient load step reduction (Strategy 2)

If the requirement is to reduce all post-fault loads i.e. the load above the initial generator load before the failure happened, the following values are determined from (3.3) and (3.4):

$$\Delta P_{FLR,gi} = \Delta P_{\text{tran},gi}(k, N_f), \quad \text{since } \Delta P_{\text{gi}} = 0,$$

$$\Delta\omega_{FLR,gi} = \Delta\omega_{gi}^{\max}, \qquad \text{since } \Delta\omega_{en,gi}\left(\Delta P_{\text{gi}}=0\right) = 0. \qquad (3.9)$$

Then, the time to reduce the load when the full transient load step is reduced and zero engine load step capability is utilized can be calculated from the following equation:

$$t_{SL,i} = \Delta\omega_{gi}^{\max} \frac{2H_i}{\Delta P_{\text{tran},gi}(k, N_f)} P_{r,gi} \,. \qquad (3.10)$$

After equalizing $t_{SL} = t_{FLR}$ and adding P_{gi} on both sides of (3.10) and rearranging, determines the maximum permitted transient load:

$$P_{\text{tran},gi}\left(t_{FLR}\right) = \Delta\omega_{gi}^{\max} \frac{2H_i}{t_{FLR,i}} P_{r,gi} + P_{gi}, \qquad (3.11)$$

3.4.3 An optimal transient load step reduction (Strategy 3)

With regards to above, a new FLR control strategy is proposed in this thesis. The strategy is based on the combination of strategies 1 and 2 where the optimal control is based on the following:

– Select nearly optimal load step for the engine;
– Maximize the required time to reduce the load (load limit) t_{SL}.

Optimal load step

The maximum allowable load step for a supercharged diesel engine, as required from the classification societies, is defined using the following piecewise linear function (MAN B&W, 2005; IACS, 2006):

$$\frac{\Delta P_g^{\max}\left(P_g\right)}{P_{rg}} = \begin{cases} 0.33 - 0.303P_g & ,0 \le P_g < 0.33, \\ 0.3 - 0.217P_g & ,0.33 \le P_g < 0.56, \\ -0.068 + 0.444P_g & ,0.56 \le P_g < 0.74, \\ 1 - P_g & ,0.74 \le P_g \le 1. \end{cases} \tag{3.12}$$

Together with the engine manufacturer, a similar function can be obtained for the particular engine type. The nearly optimal response to load steps for the diesel engine is shown in Fig. 3.3.

In order to find the optimal engine load step responses, the following objective function is proposed in this thesis:

$$\max_{\Delta P_{gi}\left(P_g\right)} J = \max\left\{ \frac{\Delta P_{gi}\left(P_g\right)}{\Delta P_{gi}^{\max}} \frac{\Delta \omega_{en,gi}^{\max}}{\Delta \omega_{en,gi}\left(\Delta P_{\mathrm{gi}}\left(P_g\right)\right)} \right\}, \tag{3.13}$$

where the solution must be found within the following constraints:
– Maximum load step within allowable limits, $\Delta P_{gi}\left(P_g\right) \le \Delta P_{gi}^{\max}\left(P_g\right)$;
– Maximum frequency drop, $\Delta \omega_{en,gi}\left(\Delta P_{\mathrm{gi}}\left(P_g\right)\right) \le \Delta \omega_{en,gi}^{\max}$;
– Transient recovery time, $t_{\mathrm{tran,gi}} \le 5$ seconds (class rule requirement).

The load steps and frequency deviations are normalized with respect to their maximum values. The $\Delta \omega_{en,gi}\left(\Delta P_{gi}^*\right)$ and ΔP_{gi}^* are the optimal values i.e. the solution of the optimization in (3.13). The prerequisite for the optimization is available engine simulation model. This is due to $\Delta \omega_{en,gi}\left(\Delta P_{\mathrm{gi}}\left(P_g\right)\right)$ may have complex functional dependence on the engine pre-fault load and the post-fault load step. The easily build engine models are available based on the engine testing data, see e.g. Appendix A.

Real time control algorithm

Then, the following algorithm can be used in the real time control to maximize the required time limit for the load reduction t_{SL}:

$$\max\left(t_{SL,i}\right) = \max_{\Delta P_{gi}}\left\{\left(\Delta\omega_{gi}^{\max} - \Delta\omega_{en,gi}\left(\Delta P_{gi}\right)\right)\ \frac{2H_i}{\Delta P_{\text{tran},gi}(k,N_f) - \Delta P_{gi}} P_{r,gi}\right\}, \quad (3.14)$$

$$\Delta P_{gi} = \begin{cases}\Delta P_{gi}^{*}\\ 0\end{cases}, \qquad \Delta\omega_{en,gi}\left(\Delta P_{gi}\right) = \begin{cases}\Delta\omega_{en,gi}^{*}\left(\Delta P_{gi}\right)\\ 0\end{cases}$$

where the algorithm is selecting between strategy 1 and strategy 2.

The t_{SL} curves for the strategy 1 and the strategy 2 are compared in Fig. 3.3. The time to reduce the load t_{SL} is calculated for H_i=1 seconds. When using strategy 1, the engine load step is $\Delta P_{gi} = 0.33 P_{r,gi}$ and frequency drop $\Delta\omega_{gi}$ $(\Delta P_{gi}) = 0.05\ \omega_{0g}$. When the transient load $P_{tran,gi}$ is relatively low (lower than 140%), then the FLR control strategy 1 (with load step) allows to operate generators on higher load than when using strategy 2 (initial load), see Fig. 3.3. However, if the t_{FLR} = 0.5 seconds, the allowable maximum transient load step becomes very low. The curves in Fig. 3.3 show that two equally rated engines should not operate on higher load than $P_{tran,g}$ = 110% P_{rg} if strategy 1(-----) is used. Then, the maximum permitted continuous load per generator is $P_{cont,g}$ = 55% P_{rg}. In order to operate both units on full P_{rg}, i.e. $P_{tran,gi}$ = 200% P_{rg}, the load reduction must be faster than $t_{SL} = 0.2 \geq t_{FLR}$ seconds when using strategy 2, or $t_{SL} = 0.15 \geq t_{FLR}$ seconds if using strategy 1. Hence, strategy 2 is preferred when the transient load is very high, while strategy 1 is preferred when the transient load is lower, as indicated in Fig. 3.3.

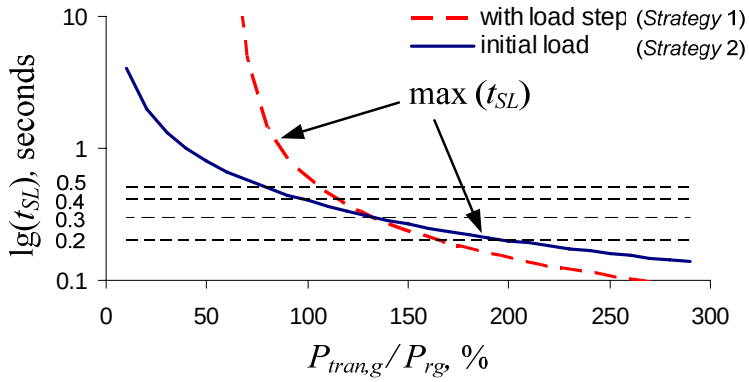

Fig. 3.3. Time to reduce the load using different fast load reduction strategies, for H=1 seconds, the load step is $\Delta P_{gi} = 0.33 P_{rg}$ and $\Delta\omega_{gi}$ $(\Delta P_{gi}) = 0.05\ \omega_{0g}$

3.5 Fast load reduction control methods

The following types of fast load reduction (FLR) algorithms have been applied on board the marine vessel:

- *Available power-based load shedding*: the load shedding, based on the available power. It will disconnect the non-essential consumers from the network in several stages;
- *Frequency-based load shedding*: Acts when the frequency is below the threshold, (May and Foss, 2000). This control is traditionally used in land-based installations for the frequency control, see e.g. Kundur, (1994);
- *Event-Based FLR* - EB-FLR (Lauvdal and Ådnanes, 2000)*:* Event based FLR system receives the signal from the switchboard transducers when protective relay opens the circuit breaker for the on-line generating set;
- *Frequency Sensitive Phased Back System* - FPBS, (May 2003): FLR system is based on the frequency drop which is as a consequence of the system protective actions.

In this Section a new *observer-based frequency sensitive FLR* (obs-FLR) is proposed. The proposed observer-based FLR is robust to communication delays and faults within the PMS control system and may execute faster than any of the existing FLR controllers. The four known FLR strategies are briefly presented, before the new *obs-FLR* is defined.

3.5.1 Available power-based load shedding

Load shedding is a fast executing function ($t_{FLR} \leq 0.25$ seconds) used to disconnect heavy consumers and groups of non-essential consumers from the network. It will trigger the circuit breaker and disconnect consumer if the available power drops below a certain level. Traditionally, a load shedding control in marine applications is based on the available power level, see Chapter 2. The level of available power may be set differently for each of the heavy consumers, as done for the propulsion in (2.33) using w_p to allow a priority selection between the consumers. It is also possible to define different time delays for each consumers group.

Depending on the available power load level, the load shedding is usually grouped in several stages where each stage represents different groups (blocks) of consumers, selected by the operational priority:

$$P_{av,start}(k,t+\tau) - \Delta\gamma_{ss} \leq 0\,, \qquad \text{for all } \tau \in \left[0, T_{ss}\right], \tag{3.15}$$

where $\Delta\gamma_{ss}$ is the load shedding limit, and s is the shedding priority, typically $s = 1$, 2, or 3.

It is important to notice that the load shedding control functionality must not interfere with *auto-start*. Less important consumers will be the first to shed if the available power continues to decrease, after the *auto-start* has been initiated.

The main drawback when working with high number of sheddable consumers is difficulties in the prediction of their behavior.

3.5.2 Frequency based load shedding

Should by any cause the load reduction system fail to work, additional safety precautions can be implemented by monitoring the network frequency, such as (May and Foss, 2000) e.g.:

- At 58.5 Hz (1.5 seconds delay) the PMS will reduce the power limit signals to 75 % of the actual consumer load;
- At 57.5 Hz (3.5 seconds delay) the drilling drives will shut down (independent of PMS);
- At 57 Hz (0.3 seconds delay) the thruster drives will be reduced to 50 % of load order (independent of PMS);
- At 57 Hz (5 seconds delay) the 11 kV bus will be split into two systems (by PMS).

The relay control settings and control actions are presented in Fig. 3.4. The speed of the frequency drop (Hz/seconds) is obtained from dividing the frequency drop, in hertz (Hz) with the time delay limit, in seconds (seconds). The *split bus* control is usually slow and acts when the frequency drops very low. The *drilling drives shut down* control acts when the frequency does not recover after 3.5 seconds, i.e. with slow rate of frequency change. The fastest rate of change for the frequency relay settings will have the control actions to reduce the load to the thruster drives.

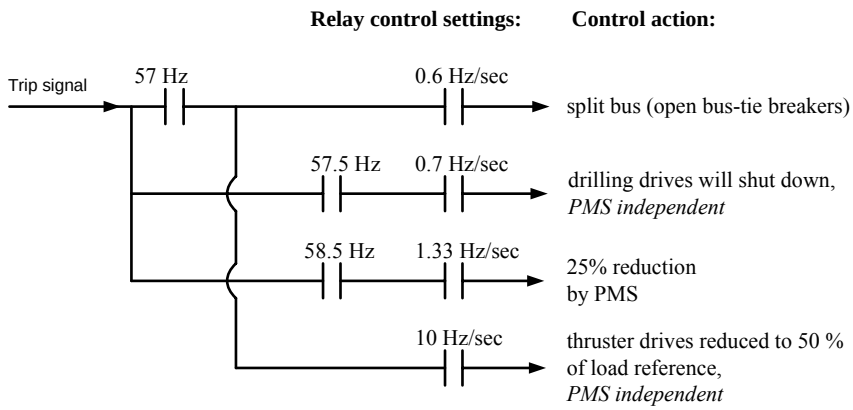

Fig. 3.4. Tripping logic for frequency based load shedding control relay

3.5.3 Event Based Fast Load Reduction System (EB-FLRS)

Event Based Fast Load Reduction System (EB-FLRS) monitors the network/generating system situation and reacts based on the event - trip of the generating-set (Lauvdal and Ådnanes, 2000). The operation of Event-based FLR is illustrated in Fig. 3.5:

- When a generator breaker is tripped in the switchboard, the signal is hardwired to the remote I/O unit located near the switchboard. Next, the signal is transmitted to the PMS controller via fieldbus and made available for the event-based load reduction program;

– The PMS program is set to perform the load reduction on thrusters in 0.05 seconds (50 milliseconds);
– Then a *reduce load* command is transmitted to the frequency converter, which reduces the load to zero. The execution time and load reduction time in the converter is approximately 50 to 100 milliseconds.

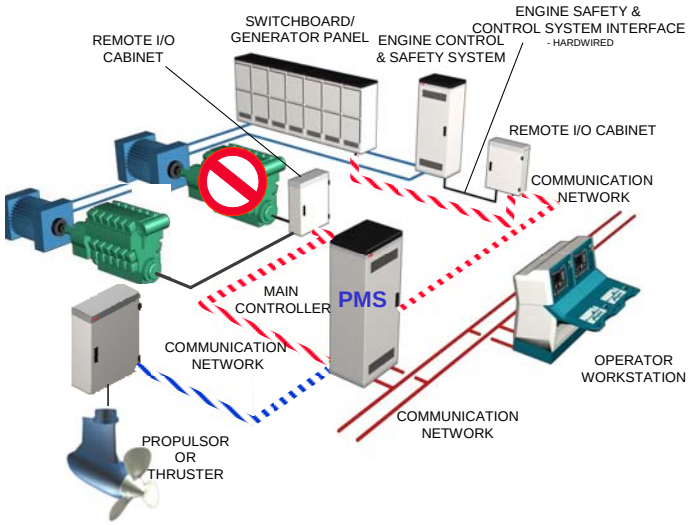

Fig. 3.5. Event-based fast load reduction (Lauvdal and Ådnanes, 2000)

The Event Based Fast Load Reduction System will typically decrease the load to the pre-fault value, so the time limit to reduce the load can be determined from (3.10).

The total time from breaker is tripped until load is reduced is theoretically $0.2 \le t_{EBFLR} \le 0.25$ seconds. Following issues may limit the effectiveness of *Event-based FLR*:

– *The communication delays*: in the communication network or PS, or PLC. The delay may also vary – especially if control software code and communication code are not synchronized;
– *The execution time of the PMS controller* (PLC);
– *Transmit of the signal to the frequency converter*;
– *Various interface/communication problems*.

The time necessary for the Event-based FLR to reduce the load depends on the known time delay to execute the load reduction t_{com}, time delay in the frequency converter t_{mp}, and the time delay due to communication problems $t_{\theta,com}$, which is uncertain and includes unknown response dynamics:

$$t_{FLR}\left(event\right) = t_{com} + t_{\theta,com} + t_{mp}\,, \tag{3.16}$$

where *event* stands for Event-based FLR.

The main constraint for the successful blackout prevention is that the FLR execution is faster than the safe time limit, according to:

$$t_{SL} \geq t_{FLR} \,. \tag{3.17}$$

The minimum load to be reduced is determined from (3.11) where t_{FLR} is determined from (3.16) and t_{SL} from (3.10).

3.5.4 Frequency Phased Back System (FPBS)

With the *Frequency Sensitive Phased Back System* **(**FPBS), the network or system frequency is sensed directly by each of the thruster PLC controllers (May, 2003). There is no lag time for computations or transmission of data. The communication problems are avoided, and each thruster contributes in blackout prevention control, as shown in Fig. 3.6. This increases the robustness against the faults within each PLC controller (FPBS). It also increases the overall blackout prevention capabilities of the system.

The FPBS system is initiated when the system frequency drops below the value allowed for normal operations. Each thruster PLC is programmed to initiate phase back of the thruster over a range of network frequencies ω_g.

When using FPBS, the maximum load limit on thruster can be defined according to:

$$P_{\max,p} = \begin{cases} P_{cp}\left(1 + k_{FLR,p}\left(\omega_g - \omega_{FLR,p}^{\max}\right)\right), & \text{for } \omega_g - \omega_{FLR,p}^{\max} < 0 \\ 0\,, & \text{for } \omega_g - \omega_{FLR,p}^{\max} \geq 0, \end{cases} \tag{3.18}$$

where P_{cp} is the commanded power on thruster, $k_{FLR,p}$ is the controller gain $k_{FLR,p} \geq 0$, ω_g is the network frequency, and $\omega_{FLR,p}^{\max}$ is the fixed maximum limit frequency below which the fast load reduction is activated, typically $\omega_{FLR,p}^{\max}$ = const = $0.966 \cdot \omega_{0g}$ or $f_{FLR,p}$ = const = $0.966 \cdot f_{0g}$ and $f_{FLR,p}^{\max}$ = 58 Hz if f_{0g} = 60 Hz.

If $\omega_g - \omega_{FLR,p}^{\max} \geq 0$, then the FPBS will not be initiated. Thus, always is $P_{max,p} \leq P_{cp}$. Each thruster's PLC will initiate the load reduction $P_{cp} - P_{max,p}$ independently from the others, depending only on the network frequency drop:

$$\Delta P_{FLR,p} = P_{cp} - P_{\max,p} = -P_{cp} k_{FLR,p}\left(\omega_g - \omega_{FLR,p}^{\max}\right). \tag{3.19}$$

When using FPBS, the total actual load reduction will be equal to the sum of all load reductions per thruster:

$$\Delta P_{FLR,g} = \sum_{p=1}^{th} \Delta P_{FLR,p} = -\sum_{p=1}^{th} P_{cp} k_{FLR,p}\left(\omega_g - \omega_{FLR,p}^{\max}\right). \tag{3.20}$$

where *th* is the number of thrusters connected on-line to the network and used for the propulsion.

The load reduction is limited to the frequency region:

$$\omega_{0g} - \Delta\omega_g^{\max} \le \omega_{FLR,p}^{\min} \le \omega_g \le \omega_{FLR,p}^{\max}. \tag{3.21}$$

So, the maximum load reduction within the maximum possible region of operation is:

$$\Delta P_{FLR,g}^{\max} = \sum_{p=1}^{th} \Delta P_{FLR,p}^{\max} = -\sum_{p=1}^{th} P_{cp} k_{FLR,p} \left(\omega_{FLR,p} - \omega_{0g} + \Delta\omega_g^{\max} \right). \tag{3.22}$$

The frequency will recover if the transient load step is lower than permitted. Hence, the feedback loop will make the FPBS to load the generators according to:

$$\Delta P_g = \sum_{i=1}^{k} \min\left(a_{\max,g} P_{r,gi} - P_{gi}, \Delta P_{\mathrm{gi}} \right). \tag{3.23}$$

With FPBS, this constraint always holds due to the control feedback from network speed (frequency) measurement, as shown in Fig. 3.6. It is important to notice that ΔP_g is inherently selected through feedback, without the need for calculating this value, in contrary to the *Event-based FLR*:

$$\Delta P_{\mathrm{tran},g} = \Delta P_{\mathrm{tran},g}\left(k, N_f\right) - \sum_{i=1}^{k} \min\left(a_{\max,g} P_{r,gi} - P_{gi}, \Delta P_{\mathrm{gi}} \right). \tag{3.24}$$

The time for the FLR execution depends on the frequency dynamics i.e. time passed before FPBS is initiated, the speed of response for FPBS, and the response time of the thruster drive t_{mp}, according to:

$$t_{FLR}\left(FPBS\right) = \left(\omega_{0g} - \omega_{FLR}^{\max} \right) \frac{2H_k}{\Delta P_{\mathrm{tran},g}^*} P_{r,g} + \frac{2H_k}{\sum_{p=1}^{th} P_{cp} k_{FLR,p}} P_{r,g} + t_{mp}, \tag{3.25}$$

where $\omega_{FLR,p}^{\max}$ is usually set equal for all *FPBS*, i.e. $\omega_{FLR}^{\max} = \omega_{FLR,p}^{\max}$. The response time for most thruster drives is known to be in the range $0.05 \le t_{mp} \le 0.1$ seconds. From (3.25) it can be noticed that increasing $k_{FLR,p}$ the time needed for FPBS to reduce the load will be reduced. However, $k_{FLR,p}$ may be limited due to other reasons, as will be explained later.

The difference between the safe time limit and the time to execute the load reduction:

$$t_{SL} - t_{FLR} = \left(\Delta\omega_g^{\max} - \Delta\omega_{en,g}^* - \omega_{0g} + \omega_{FLR}^{\max} \right) \frac{2H_k}{\Delta P_{\mathrm{tran},g}^*} P_{r,g} - \frac{2H_k}{\sum_{p=1}^{th} P_{cp} k_{FLR,p}} P_{r,g} - t_{mp}, \tag{3.26}$$

must be higher or equal to zero in order to have a blackout resistance.

The maximum possible load reduction is determined after substituting (3.26) into (3.27) and setting $t_{SL} = t_{FLR}$, in (3.26):

$$\Delta P_{\text{tran},g}^{\max}\left(t_{FLR}\right)=\max\left\{\Delta P_{FLR,g}\left(t_{FLR}\right)\right\}=\max\left\{\left(\Delta\omega_{g}^{\max}-\Delta\omega_{en,g}\right)\frac{2H_{k}}{t_{FLR}}P_{r,g}\right\}. \qquad (3.27)$$

After the FPBS has been triggered, load recovery on the individual thrusters must be slow in order to avoid frequency drop on generators due to fast loading of power network. Otherwise, the network frequency would drop again which would trigger the FPBS again. The acceptable speed of network loading will depend on the number of generators on-line and the system inertia. The speed of thruster loading is controlled by propulsion load rate limits, as described in Chapter 2.

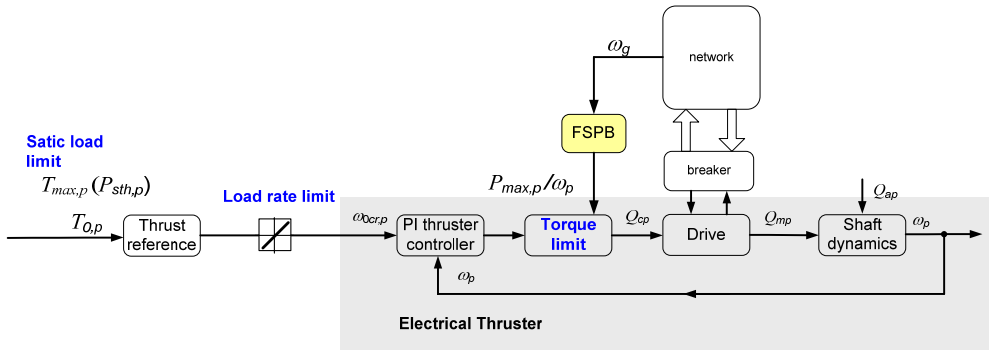

Fig. 3.6. Fast load reduction with FPBS

Blackout false detection rate

Since the FPBS is triggered by the frequency drop, it can also prevent the excessive frequency deviation in the normal faultless conditions. This means that FPBS may be triggered by any frequency drop, no matter what was the reason for frequency drop. In many cases, heavy consumers and thrusters subjected to bad weather conditions operate under fast and large variations in power.

In order to prevent too fast frequency drop and blackout, the rate of thruster limiting must be higher then the frequency decrease rate. This determines the k_{FLR} gain. Setting $\omega_{FLR,p}^{\max}$ close to ω_{0g} can increase the blackout prevention capabilities since t_{FLR} will be reduced. The drawback is possible increase in the false blackout detection rate; for fault detection, isolation and control of dynamical systems see e.g. (Blanke *et al.* 2003). The false blackout detection will initiate the fast load reduction on thrusters when this is not required from the blackout prevention functionality, and thereby possibly increase the thruster wear-out rate. With a high number of fault detections, a wear-out rate on the thrusters increases.

If the control gain of the FPBS $k_{FLR,p}$ is set high, then the load on thrusters will be decreased faster than necessary. This may induce unnecessary torque stress in the shaft and the power transmission parts of the thruster. Thus, too fast load reduction should also be avoided in order to reduce damages on the thrusters.

3.5.5 Observer-based fast load reduction

The main advantage of FPBS is that there is no lag time for computations and transmission of data. The PLC controller in each of the thrusters will sense the network frequency and react independently to the sudden drop of network frequency. The FPBS will react to any frequency drop below $f < f_{FLR}$ no matter what is the cause of the frequency drop. If the frequency drop is not caused by opening the generator breaker, then the reaction of FPBS is caused by the false blackout detection. The increase in false blackout detection rate may possibly increase the thruster wear-out rate.

The problem remains how to avoid the false fault detection of the FSPB system. A possible solution is proposed and demonstrated in this section.

Control plant model of power generating system

The motion equation for the mean acceleration of the power generating system may be expressed as follows (Anderson and Fuad, 2003; Kundur, 1994):

$$\begin{aligned} \frac{d\delta_g}{dt} &= \omega_g - \omega_{0g}, \\ \frac{d\omega_g}{dt} &= \frac{\omega_{0g}}{2H_{N_{on}}}\left[Q_{mg} - Q_{dg} - Q_{eg}\right] \\ &= \frac{\omega_{0g}}{2H_{N_{on}}}\left[Q_{mg} - \frac{D_g}{\omega_{0g}}\left(\omega_g - \omega_{0g}\right) - Q_{eg}\right], \end{aligned} \tag{3.28}$$

where ω_g is the mean rotor angular speed for all generators in the system (in per unit - pu), ω_{0g} is the nominal speed, Q_{mg} is the mechanical torque, Q_{eg} is the electrical torque, and Q_{dg} is the damping torque. The torques is expressed in per unit system (pu). The damping coefficient D_g accounts for the electrical load damping and the mechanical damping in pu. H_{Non} is the system inertial time constant in seconds. The frequency deviation between the mean and the nominal speed gives the derivative of the rotor angle $\delta_g(t)$ in radians.

The main idea for the improved blackout detection

An improved algorithm for the blackout detection is proposed in this thesis. The algorithm is used to estimate the status of the generator circuit breakers on the network i.e. to sense if there are any openings of the circuit breakers on the generators that may propagate to the blackout. The algorithm is based on the estimation of mean acceleration of the power generating system (3.28).

The proposed idea for the fast detection of circuit breaker opening is based on the comparison of network electrical and mechanical torque. Although the total network mechanical torque is not measured, it can be estimated using an observer. The mechanical torque is directly proportional to the mean acceleration of the network. Thus, the speed of blackout detection may be significantly improved.

The proposed blackout detection algorithm compares the network torque deviation with the pre-defined threshold:

$$Q_{eg} - \hat{Q}^*_{mg} - q_{FLR} \geq 0\,, \tag{3.29}$$

where $Q_{eg} - \hat{Q}^*_{mg}$ is the torque deviation sensed, and $Q^*_{mg} = Q_{mg} - Q_{dg}$ is reduced mechanical torque due to friction and damping, see eq. (3.28). The electrical torque Q_{eg} or power P_{eg} is available from the measurements. Sometimes, the torque deviations are approximated by the power deviations; see e.g. Anderson and Fuad (2003). As the mechanical torque is not known, it will be estimated using an observer. Thus, $\hat{Q}^*_{mg}$ is the estimated torque.

When the threshold q_{FLR} is crossed, the relay time $\tau_{q,FLR}$ counting is triggered:

$$\left[Q_{eg}\left(t+\tau_{q,FLR}\right) - \hat{Q}^*_{mg}\left(t+\tau_{q,FLR}\right)\right] - q_{FLR} \geq 0\,, \tag{3.30}$$

where $\tau_{q,FLR}$ is the relay time set to detect the opening of the generator breaker, $\tau_{q,FLR} \geq 0$.

The main properties of improved detection algorithm are:

- If the generator breaker is opened (by the protection relay), then the mechanical torque $\hat{Q}^*_{mg}$ will suddenly drop. The electrical torque Q_{eg} will remain almost constant in the required time interval $\tau_{q,FLR}$ if no control is used to reduce the frequency drop. Therefore, the difference between the mechanical and electrical torque $Q_{eg} - \hat{Q}^*_{mg}$ will be large.
- When the generator breaker opens, the mechanical torque drops. Then, the torque deviation is non-negative, $Q_{eg} - \hat{Q}^*_{mg} \geq q_{FLR} > 0$. The similar situation occurs if the electrical torque Q_{eg} suddenly increases – but this can not happen if load rate limiting controller functions properly. However, if this happens then the power redistribution controller (PRC), described in Chapter 6 can handle this problem;
- If $Q_{eg} - \hat{Q}^*_{mg} < 0$, then the frequency will rise. The fast load reduction system will react only if the network situation is such that the frequency drops, and the load has to be reduced. Therefore, the fast load reduction reacts only when: $Q_{eg} - \hat{Q}^*_{mg} \geq q_{FLR} > 0$.

Observers for mechanical torque estimation

The following observers are analyzed as candidates for the observer based fast load reduction:

- *Luenberger observer* (Chen, 1999);
- *Sliding mode observer* (Slotine *et al.*, 1987; Drakunov and Utkin, 1995; Utkin *et al.*, 1999).

The mechanical torque is estimated from the network frequency ω_g and the electrical torque Q_{eg} using a mechanical torque observer. Based on the control plant model in (3.28) a *Luenberger observer* is proposed:

$$\dot{\hat{\omega}}_g = \frac{\omega_{0g}}{2H_{Non}}\hat{Q}_{mg*} - \frac{\omega_{0g}}{2H_{Non}}Q_{eg} + l_{1g}\left(\omega_g - \hat{\omega}_g\right), \tag{3.31}$$

$$\dot{\hat{Q}}_{mg*} = l_{2g}\left(\omega_g - \hat{\omega}_g\right),$$

where Q_{eg} is the system electrical torque, and $\hat{Q}^*_{mg} \approx Q^*_{mg} = Q_{mg} - Q_{dg}$ is the estimated mechanical torque reduced due to friction and damping. The estimated mechanical torque is determined using the observer, where l_{1g}, l_{2g} are the observer gains used to make the correction of the state estimation.

The *sliding observer* may have significantly faster response to sudden changes in the input or measurements due to better convergence properties in the so-called "sliding mode" than the *Luenberger observer* (3.31). Based on the Slotine *et al.* (1987), the following *sliding observer* is proposed in this thesis:

$$\dot{\hat{\omega}}_g = \frac{\omega_{0g}}{2H_{Non}}\hat{Q}_{mg*} - \frac{\omega_{0g}}{2H_{Non}}Q_{eg} + l_{1g}\left(\omega_g - \hat{\omega}_g\right) + k_{1g}\,\mathrm{sgn}\left(\omega_g - \hat{\omega}_g\right), \qquad (3.32)$$

$$\dot{\hat{Q}}_{mg*} = l_{2g}\left(\omega_g - \hat{\omega}_g\right) + k_{2g}\,\mathrm{sgn}\left(\omega_g - \hat{\omega}_g\right),$$

where k_{1g} and k_{2g} are the *sliding observer* gains, while l_{1g} and l_{2g} are the *observer* gains, defined in (3.31).

3.5.6 Case study

Comparison between FPBS and proposed *observer-based fast load reduction* is presented in the case study.

The observer gains and relevant data are presented in Table 3.1. Fig. 3.7 shows the mechanical torque estimation using the *Luenberger* and *Sliding mode observer*s. The generator circuit breaker is open in t=25 seconds, and in about the same time the real mechanical torque Q_{mg} instantly drops from 0.8 to 0.4 P_{rg}. The frequency will also drop due to drop in the mechanical torque Q_{mg}, as can be seen in the lower part of Fig. 3.7. The signals of the frequency (freq) and torque measurements (Q_{eg}) are corrupted with some noise. This gives more realistic conditions for the simulation and comparison of these systems.

The FSPB will start to reduce the load on thruster when the frequency becomes lower than e.g. 58 Hz. The fast load reduction will start from about t= 25.250 seconds which is somewhat more than 250 milliseconds after the circuit breaker has opened, see Fig. 3.7.

When the torque observer is used to detect the blackout and initiate the load reduction, then the threshold q_{FLR} must be properly set. The proposed threshold value is q_{FLR} = 0.2 Q_{mg}, meaning that the FLR will be initiated if torque is suddenly changed for more than 20%. From Fig. 3.7 it can be noticed that the events leading to blackout will be detected using observers in the following time intervals:

- 50 milliseconds or less for the *Sliding mode observer*;
- 150 milliseconds for the *Luenberger observer*.

Compared to the FSPB system this means than the proposed *observer-based FLR* can have approximately 5 times faster detection rate than when using the existing *FPBS*.

Another important feature is the speed of change of the load. The measured frequency signal is changing slower than the estimated mechanical torque as can be seen in Fig. 3.11. To reduce 1/2 (half) of the load on the thrusters the following time will pass:

- 150 milliseconds or less for the *Sliding mode observer-based FLR*, as Q_{mg} hits the value of 0.4 in t=25.150 seconds;
- 300 milliseconds for *Luenberger observer-based FLR*, as Q_{mg} hits the value of 0.4 in t=25.300 seconds;
- 950 milliseconds for the *FSPB* as the *frequency* hits the value of 54 Hz in t=25.950 seconds. Usually, the FSPB system is set to reduce the 50% of the load, see May (2003).

This means that the load reduction will be commanded with much faster rate when using the proposed *observer-based FLR*.

Table 3.1. Observer and power system parameters

	Type of the observer used	**Observer gains**
1.	Real power system	H_{Non} = 3 seconds
2.	*Luenberger observer*	l_{1g} = 10; l_{2g} = 200; H_{Non} = 2 seconds
3.	*Sliding mode observer*	l_{1g} = 400; l_{2g} = 600000, k_{1g} = – 0.05; k_{2g} = 1E-5; H_{Non} = 2 seconds

Observer-based fast load reduction controller

The proposed *Observer-based fast load reduction* controller is a hybrid controller combined of:

- *Proportional action*, based on the torque deviation, $Q_{eg} - \hat{Q}^{*}_{mg} - q_{FLR}$. The similar action can be noticed in the *FPBS* which is based on the frequency deviation;
- *Switching control logic*, based on the blackout detection signal. This is similar to the *Event-based FLR*, which is using the blackout signal (breaker open) received from the switchboard and processed by the PMS controller.

When a blackout is detected i.e. torque deviation crosses the threshold $Q_{eg} - \hat{Q}^{*}_{mg} \geq q_{FLR}$, the switching logic can initiate e.g. 20% or higher load reduction on each of the thrusters. More load can be reduced if necessary by the *proportional action* based on the torque deviation, $Q_{eg} - \hat{Q}^{*}_{mg} - q_{FLR}$.

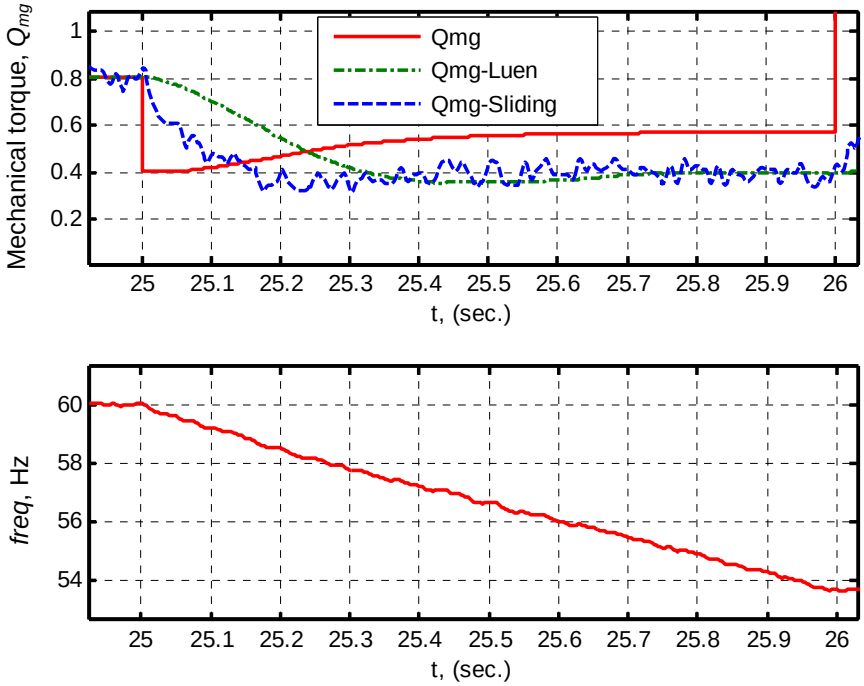

Fig. 3.7. Upper diagram: Mechanical torque estimation using *Luenberger* observer (dashed-dot) and *Sliding mode* observer (dashed,) versus real unmeasured torque (solid)
Lower diagram: system frequency in Hz

Figs. 3.8 and 3.9 show the response of the system when one of two equally rated generators is disconnected from the network. Then the load must be reduced on the consumers in order to avoid large frequency drop. The load is reduced using the *FPBS* and *Observer-based FLR*. The results of the comparison between the *FPBS* and *Observer-based FLR* with *Luenberger* type of observer is shown in Fig. 3.8, while the similar comparison when using the *Sliding mode* type observer is presented in Fig. 3.9.

The time to detect the condition leading to blackout is 70 milliseconds and after that, the *Observer-based FLR* initiates the load reduction. The *Observer-based FLR* is having 20% initial load reduction from the control logic in addition to its proportional action.

From Figs. 3.8 and 3.9 it can be noticed a lower frequency drop when using the *Observer-based FLR* compared to the *FPBS*. The frequency for each of the controllers after the control action is:

– f = 55 Hz for *FPBS*;
– f = 57 Hz for *Observer-based FLR,* with Luenberger observer;
– f = 59 Hz for *Observer-based FLR,* with Sliding mode type of observer.

Using *the Observer-based FLR* with sliding mode type of observer about 5 times lower frequency drop is accomplished than using the present FPBS technology. The main reason for the lower frequency drop is the combined action of the hybrid *Observer-based FLR controller* with very fast blackout detection, and the proportional control action based on the

mechanical torque estimation. As the mechanical torque is better estimated i.e. converge faster to the real value, the control action will be better i.e. faster. Thus, using the *Observer based FLR* with *sliding observer* significant improvements in the blackout prevention control can be accomplished. Slower speed of the *Luenberger observer* can be compensated by higher contribution of the switching control logic triggered after the blackout detection.

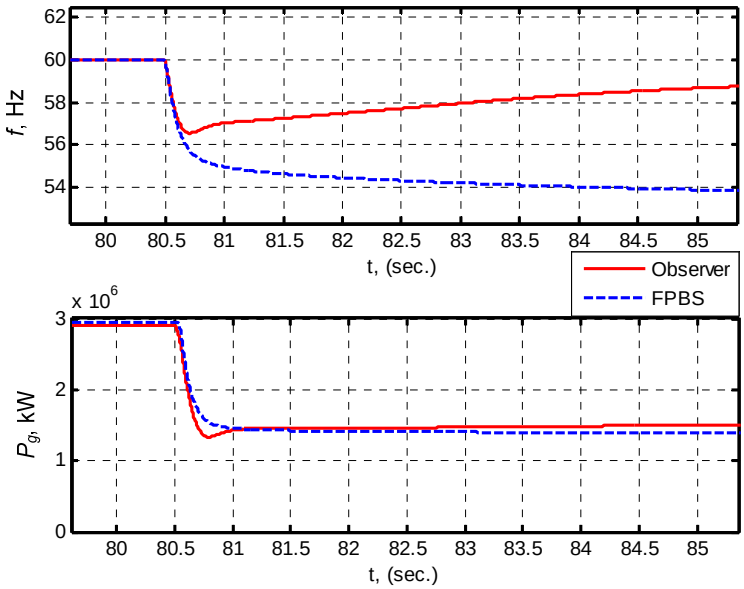

Fig. 3.8. Fast load reduction using *FPBS* and *Observer based FLR* designed with Luenberger observer

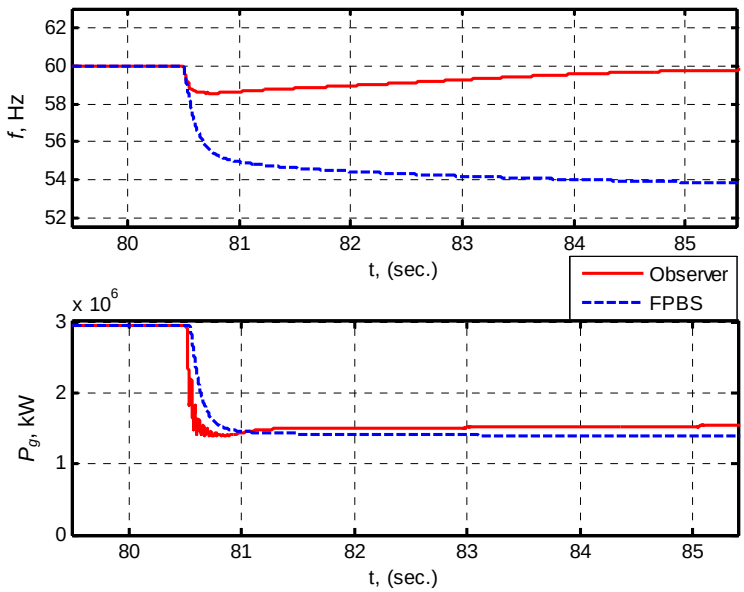

Fig. 3.9. Fast load reduction using *FPBS* and *Observer based FLR* with Sliding mode observer

3.7 An overall functionality of blackout prevention control

Fig. 3.10 presents the controller structure for the marine power system blackout prevention functionality applied on DP systems. Due to a variety of approaches and philosophies used in the PMS design, there may be some issues that require more attention. This is especially important for the load limiting functionality.

In some designs the consumer load limiting will be initiated when the generators become fully loaded e.g. 100% while it can be seen that the blackout risk limit is crossed on e.g. 80% of the load. This means that the power plant will operate in the region of increased risk of blackout as is loaded over 80% of total load.

Thus, it is proposed in this thesis to analyze the power system with respect to different levels of vulnerability to blackout. The results are summarized in Table 3.3. The proposed methodology could be used to assure safe PMS design in all operating situations.

Depending on the nature of the load, after the starting sequence is initiated the available power may still continue decreasing $dP_{av}/dt < 0$ below starting limit, $P_{av,start} < 0$ or further below zero, $P_{av,start} + \Delta\gamma_{start,g} < 0$.

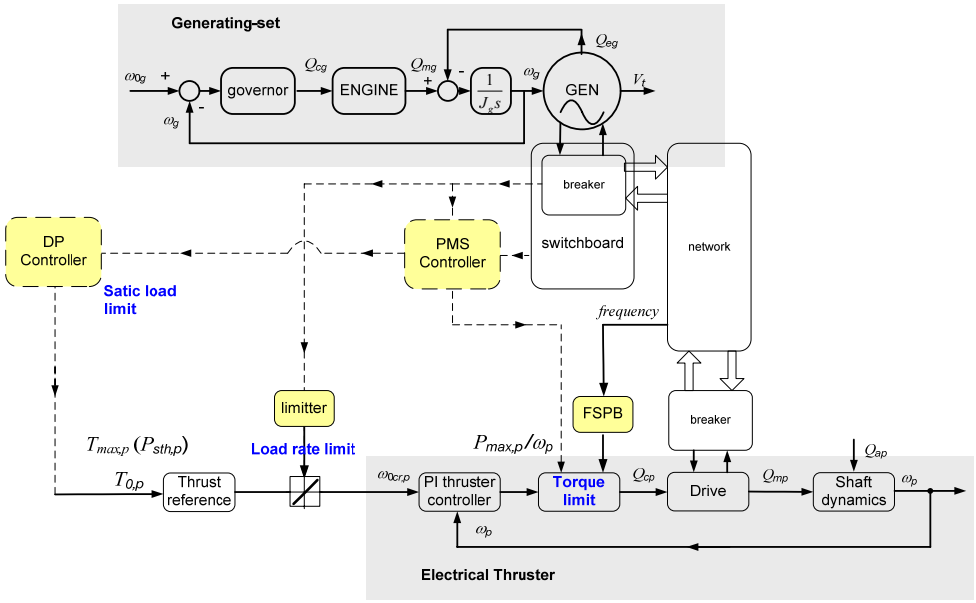

Fig. 3.10. Controller structure for the marine power system blackout prevention functionality

After the control action is initiated, the available power may continue to decrease due to the following reasons:

– The power system is not equipped with such a functionality;
– The control response time is not enough to prevent available power decrease;
– Faults in the sensors, actuators, control equipment, PMS, or elsewhere.

The actions of the PMS are based on the available power. The typical time required for the control system to perform the action is given approximately in Table 3.3. The control response time can differ depending on the system configuration, equipment manufacturers, communication between controllers, etc. The regions with different PMS response and risk levels are identified in Table 3.3. Shaded areas represent regions of increased blackout risk.

Table 3.3. Proposed levels of blackout vulnerability for the marine power system

Available power:	PMS action:	Control response time, T_{cr}:	Available capacity:	Consequences (blackout risk levels):
$P_{av,start} > 0$	*None*		$P_{r,av} > P_{av,start} > 0$ $P_{gi} < P_{start,gi}$	*Blackout-proof*
$P_{av,start} = 0$ $P_{av,start} > 0$	*Starting next unit*	≈ 30 to 40 seconds	$P_{r,av} > 0$ $P_{gi} < P_{start,gi}$	*Blackout-proof*
$P_{av,start} < 0$ $P_{av,start} > 0$	*Waiting for unit(s) to share the load*		$P_{r,av} > 0$ $P_{gi} < P_{start,gi}$	*Blackout-proof* - Unit that is just connected on-line can not be considered in the online capacity calculation
$P_{av,start} < 0$ $P_{av,start} = 0$	*Load limiting (direct)*	≈ 2 to 3 seconds	$P_{r,av} > 0$ $P_{gi} = P_{start,gi}$	*The risk of blackout* - Blackout prevention capability is lost but - no blackout occurs in faultless situation
	Load limiting (indirect)	≈ 3 to 6 seconds		
$P_{av,start} < 0$	*Load limiting fault*		$P_{r,av} > 0$ $P_{start,gi} < P_{gi} < P_{r,gi}$	*The risk of blackout further increases* if the load limiting can not be performed
$P_{av,start} < 0$	*Load limiting fault*		$P_{r,av} < 0$ $P_{start,gi} < P_{gi} < a_{max,gi}P_{r,gi}$	*The risk of blackout further increases* if the load limiting can not be performed
$P_{av,start} < 0$	*Fast load reduction*	< 0.5 seconds	$P_{r,av} < 0$ $P_{gi} = a_{max,gi}P_{r,gi}$	*Load reduction* - due to frequency drop below threshold for the FPBS
	None			*Blackout* - due to frequency drop below limit for the system without FPBS
$P_{av,start} < 0$	*Blackout restoration*	≈ 1 to 2 minutes	$P_{r,av} = P_{r,g}$ $P_g = 0$ $k = 0$	*- e.g. drilling operations stopped,* *- vessel unable to perform maneuvering,* *- possible loss of heading and position,* *- severe risk for vessel and environment*

$P_{av,start} = P_{av,start}(\Delta\gamma_{start,g}=0)$; $P_{r,av} = P_{r,av}(\Delta\gamma_{start,g}=0)$

As can be seen from Table 3.3, the system is *blackout-proof* until $P_{av,start} + \Delta\gamma_{start,g}=0$. Then the load limiting must be performed in order to maintain the blackout resistance of the system. If $P_{av,start}+\Delta\gamma_{start,g}<0$, and $P_{r,av} > 0$, the blackout will not occur under the condition of faultless system operation. However, a blackout would occur in case of generator trip. If the load is not limited, due to e.g. an actuator fault, the available power may continue to

decrease. When the load on generators becomes higher than the maximum load $P_{gi} > a_{max,gi}P_{r,gi}$, the frequency will start to drop. Systems equipped with frequency sensitive phased back system (FPBS) are capable to prevent the blackout in such a case. The indirect load limiting is performed through combined action of PMS/DP controllers. The DP controller receives the available power signal from the PMS load limiter and re-calculates new speed settings for the thrusters. As explained in the Chapter 2, the indirect load limiting is slower than direct load limiting.

Chapter 4

Minimization of fuel consumption and operational costs

4.1 Background and motivations

Ship versus on-land power generation

When optimizing the costs in the marine vessel operations, the comparison with the on-land power generation system is of interest. These two similar but different optimization problems are summarized in Table 4.1.

Traditionally, the on-land power generation is centralized, and electrical power is produced within large centralized power plants. The power at these plants is typically natural (hydro), combustion (coal, gas, oil), and nuclear generated. The units are committed (started) in order to satisfy the load demand, see Wood and Wollenberg (1996), Bansal (2005), Bansal (2006) and the references therein.

As apparent in Table 4.1, the important difference between centralized on-land power generation and the vessel power generation is the variation in the load demand. The load demand in the vessel may change from the full power to almost none nearly instantaneous, due to changeable operational conditions; e.g. operations of offshore supply vessels (ABB AS, 2003). Besides, a large number of consumers in the vessel are susceptible to weather conditions, e.g. Radan *et al.* (2006b). In dynamic positioning (DP) of the vessel, the propeller loadings will change depending on the various factors, among the most important are: the controller modes, weather conditions, vessel performance and the tuning of the DP controller, see e.g. Fossen (2002), and Fossen and Johansen (2006) and the references therein. Fast load fluctuations on thrusters, continuously present during a storm, are mainly responsible for the network frequency fluctuations. These are also generated by the propeller thrust losses, see e.g. Sørensen *et al.* (2005), Sørensen *et al.* (1997) and Smogeli (2006), Radan *et al.* (2006b) and the references therein.

Due to relatively low number of units installed and low variety of prime mover types and fuels used, the energy control found today in the marine vessel is fairly simple, see Hansen (2000), Arntsen (2005), Davey (2005), and Levander (2006). The generators are committed according to pre-set load dependent start and stop tables. In addition, the blackout constraint is imposed for the power management systems (PMS) with the blackout prevention capabilities see e.g. Radan *et al.* (2005) and the references therein. The load dependent start/stop tables, as presented in Chapter 2, are usually fixed and do not change with the dynamics of the vessel operations. The extensive knowledge contained in the literature for the on-land power generation and distribution has limited use in the marine application. However, these methods may provide potentially significant operational cost savings together with the improvements in planning and intelligent handling of the marine power plant. Therefore, the main aim of this Chapter is to make a contribution towards decreasing

operational costs of the marine vessel and to increase the level of automatic control in the marine power plant.

Table 4.1. Comparison of the on-land power generation and the power generation on marine vessel

	On-land power generation (centralized)	**Power generation in the isolated marine vessel**
Power demand *certainty*:	*High*, depends on large consumer groups-can hardly be controlled but is very predictable.	*Low*, although depends on smaller consumer groups.
Power demand *control*:	*Low*, difficult to control but possible e.g. through pricing and in extreme cases by disconnection.	*High*, can be controlled using load limiting PMS functionality.
Power demand *importance*:	*Very High*, must be served, and outages must be avoided.	*Depend on the operations* *Medium*, - if vessel operations may adapt temporarily to power unavailability (e.g. decrease DP capability or vessel speed). *Very High* - if the risk for loss of vessel is high (e.g. risk of collision or grounding).
Power demand *variations* due to operational conditions:	*Low*, but depend on the service.	*High*, depend on the vessel type and service (high for Supply Vessel, low for Cruise Vessel).
Power demand *variations* due to weather conditions (*long-time periods*):	*High*, -storms periods: due to increased number of faults, - year periods: depend on the season (summer/winter) - day periods: high consumption in the afternoon, low in the night.	*High*, due to changes in the operational modes and weather conditions; these may change several times every hour.
Power demand *variations* due to weather conditions (*short-time periods*):	*Low* - hour and minute periods: the load variations are relatively low.	*High* consumers are susceptible to weather conditions that may change every approx. 6 to 20 seconds (wave periods) (e.g. propeller loads, drilling loads, active heave compensation, etc.).
Number of generating units in the system:	*High*	*Low*, typically from 4 to 8 units.
Variety of types of generating units in the system:	*High*, (e.g. centralized: nuclear, thermal, hydro + distributed: solar, micro-turbines, fuel-cells, etc.).	*Low*, but increasing, (typically diesel engine, DF engine, but combined plants are also used: COGES, CODAG, etc.).
Fuel cost variance:	*High*, (e.g. nuclear, coal, gas, oil, bio-diesel, etc.).	*Low*, but may increase (typically heavy fuel oil or gas).
Criteria which units to commit (start/stop):	*Optimized every hour*, depending on the load demand, operational costs, fuel market price, etc.	*Fixed* (pre-selected), depending on the expected load demand, expected operational costs, and maintenance/operational practices.

Operational costs and constraints

The limits defined in Chapter 3 define the region of blackout-proof (resistant) operation of the power system. The optimization problem is to find the load dependent start/stop tables and the ratings of the generating sets in order to:

- *Minimize the fuel consumption* in the vessel operational life;
- *Minimize other operational costs* of the power generating system,

subject to the following constraints:

- *Given installed power* or selected rating of the units;
- *Blackout-proof operation*;
- *Class societies rules*, e.g. DNV;
- *Pre-defined design limits*, e.g. power system configuration, design preferences, and operational philosophy and constraints.

The power system configuration and design preferences will determine the number of generators per engine-room (compartment) and the total number of the engine-rooms in the vessel, as described in the Chapter 2. The optimization procedures proposed in this Chapter assume that the generators operate connected at the same bus. For vessels with split bus configurations, the optimization procedure can be repeated for each bus.

4.1.1 Economic dispatch problem

It might be important to emphasize the essential difference between the economic dispatch, the unit commitment and operational planning.

As defined in Wood and Wollenberg (1996), the economic dispatch problem assumes that there are k units already connected on-line to the same bus. Then the purpose of the optimization is to find the load participation of each unit – the load sharing factor S_{gi}.

The optimization study is particularly important if the unequally rated units will be installed and even more if these units will have a different fuel costs, see e.g. Olsbu *et al.* (1988), Hansen (2000), Davey (2005) and Levander (2006). Then the load sharing may be included in the optimization.

As shown in Hansen (2000), the optimal economic dispatch for unequally rated units may be found using appropriate optimization methods. For equally rated units operating in high power demand, nearly-minimum fuel consumption can be obtained using equal load sharing on units. For lower load demand P_g the minimum fuel cost is obtained by running as many units as possible at their maximum, and one unit take the rest load. This has been confirmed in the Arntsen (2005) and by the results shown in Fig. 4.2.

4.1.2 Unit commitment problem

In the on-land unit commitment problem, the challenge is to forecast the demand to be served. The question that is asked can be summarized as follows, Wood and Wollenberg (1996):

Given that there are a number of subsets of the complete set of k generating units that would satisfy the expected demand, which of these subsets should be used in order to provide the minimum costs?

The time interval between updates of a plan is called the *planning interval.* The number of intervals into the future, over which the plan is specified, is called the *planning horizon*. With respect to the length of the *planning horizon* (the time of forecasting), two types of the unit commitment optimization methods will be distinguished in this thesis:

- *Long term unit commitment optimization* for marine vessel is proposed in this thesis. The goal of the optimization is to find the best design parameters of the power plant, such as unit ratings and power plant configuration, see e.g. Olsbu *et al.* (1988). The planning horizon is typically one year of the vessel operation. In this thesis, the proposed unit commitment method aims to decrease the risk of committing (starting) and decommitting (stopping) another unit in the specific vessel operations and weather conditions, while keeping the minimum operational costs, Radan *et al.* (2005), Radan *et al.* (2006a). Another contribution in the thesis is the definition of operational costs of the marine power plant. These costs are used in the trade-off optimization case studies provided at the end of each Section;
- *Short-term unit commitment optimization* for marine vessel is also proposed in this thesis. It is based on the real-time load demand P_g feedback. The *planning interval* (measured time interval) and the *planning horizon* (predicted time interval) may extend from several hours to several days. This will depend on the type of the vessel and the load demand variations. The proposed method can be used as a very convenient way to re-adjust the load dependent start/stop tables continuously in the vessel operations. This is demonstrated in the case study for offshore supply vessel (OSV). Thus, the vessel may change the route, area of the operation, the operational policy, weather conditions (summer/winter), along with a number of other factors, while keeping the optimum performance.

The unit commitment problem for the marine power system with the blackout prevention capabilities has been presented in Radan *et al.* (2005). In the long term unit commitment, a probability is typically used to forecast the load demand. The long term unit commitment based on the operational profile of the vessel has been proposed in Radan *et al.* (2006a). The optimization of unit commitment takes into account the expected load demand with calculated probability dependant on the changeable weather conditions of the vessel and the specific types of operations. It is proposed to start and stop units when the vessel changes the distinguishable modes of operations. The distinguishable operational modes will have a load demand for which high probability of occurrence is expected. The convex optimization methods can be mostly used to solve such problems, see e.g. Fletcher (2000), Rao (1996), Stephen and Vandenberghe (2004).

The short term unit commitment problem is more complex and is much more difficult to solve (Wood and Wollenberg, 1996). The solution may also involve the economic dispatch problem as a sub-problem. Due to changeable load demand and switching of units, the cost functions may become non-smooth (discontinuous) and non-convex, as will be seen later in this Chapter and demonstrated in the case study. Due to unit starting/stopping, the problem involves integer variables, that is, the generating units must be either on or off. For the short-term unit commitment the solution is provided in this thesis using *Evolutionary based methods*, see e.g. Bansal (2006), Michalewicz *et al.* (1996) and the references therein.

Other methods to solve the unit commitment problem can be used. In Olsbu *et al.* (1988) and Karnavas and Papadopoulos (1999) the *mixed-integer programming* model is used for the optimization of economic operation of autonomous diesel–electric station.

The short time unit commitment problem is usually extended over some period of time, such as 24 hours or the 168 hours of a week. It remains a challenge to determine the suitable planning interval/horizon for the marine vessels. The sensitivity of changing planning interval and planning horizons with changes in the cost functions has not been performed in this thesis due to lack of practical data.

The application of short term unit commitment problem has been proposed in this thesis and the results for the *Viking Energy* offshore supply vessel are presented. The fuel savings of more than 6% are obtained using the optimized PMS load dependent start/stop tables and more than 8% fuel savings if the rating of the engines is changed – e.g. for another new built vessel of same type, similar dimensions and bollard pull force. The optimization procedure that takes into account a variety of aspects of vessel operation is established, and the performance successfully demonstrated.

4.2 General optimization problem

4.2.1 Instantaneous fuel consumption

The instantaneous fuel consumption for each of the generating sets is calculated according to, Wood and Wollenberg (1996):

$$FC_{gi}\left(P_{gi}\right) = b_{e,gi}\left(P_{gi}\right)P_{gi}\,, \tag{4.1}$$

where P_{gi} is the generated power on unit *i,* and $b_{e,gi}$ is the specific brake fuel consumption (SBFC) for each unit, usually indicated in g/kWh, see e.g. MAN B&W (2005). For medium speed diesel engines b_e is typically a convex curve with a minimum value at about 80% rated power, 0.8 $P_{r,gi}$. The SBFC, $b_{e,gi}$ is to be defined from the values given by the engine manufacturer using polynomial approximation as follows:

$$b_{e,gi}\left(P_{gi}\right) = \sum_{j=0}^{M_a} a_{j,gi} \cdot \left(\frac{P_{gi}}{P_{r,gi}}\right)^j\,, \tag{4.2}$$

where $a_{j,gi}$ are approximation constants for each generating set *i*. The unit power load is dimensionless, as can be seen from the term in the brackets. The 3rd or 4th degree polynomial (M_a = 3, or M_a = 4) is usually sufficient for the adequate approximation.

The load sharing factor depends on *k*, as defined in (2.11) is repeated here for the convenience:

$$P_{gi}(k) = S_{gi}(k)P_g\,, \tag{4.3}$$

where it is important to notice that the load demand P_g comprises the load of the consumers and the power transmission losses. The power transmission losses are in general very low for marine vessels, as they are operating in the islanding conditions; see e.g. Kundur, P. (1994).

After (4.3) is substituted into (4.2), the instantaneous SBFC dependant on the load sharing is obtained:

$$b_{e,gi}\left(S_{gi}\left(k\right),P_g\right)=\sum_{j=0}^{M_a}a_{j,gi}\cdot\left(\frac{S_{gi}(k)P_g}{P_{r,gi}}\right)^j, \tag{4.4}$$

and the total instantaneous fuel consumption is determined as a summation of the individual fuel consumptions:

$$FC_g\left(P_g\left(k\right)\right)=\sum_{i=1}^{k}FC_{gi}\left(S_{gi}\left(k\right),P_g\right)=\sum_{i=1}^{k}b_{e,gi}\left(S_{gi}\left(k\right),P_g\right)S_{gi}\left(k\right)P_g\ . \tag{4.5}$$

The challenge is to minimize the total fuel consumption subject to the various constraints and operational costs.

4.2.2 Unit start/stop effect on the fuel consumption

The highest operational cost on marine vessels is typically the fuel cost; see e.g. Watson (2002), Tupper (1996). Thus, the fuel cost should be always minimized, along with some other costs that depend on the particular case, as will be explained later in this Chapter.

One of the important assumptions in the fuel minimization problem is that the power load demand P_g is not affected by the system i.e. the consumer operation is completely independent from the operation of the power generating system. This is in general true, for the most of the vessel operational life. However, in order to prevent a blackout, the PMS functions defined in Chapter 2 and Chapter 3 may decrease the load demand P_g. This will happen only occasionally and can be disregarded in the operational costs optimization study.

Based on this assumption, the load demand will remain the same when the unit starts:

$$P_g=P_g\left(k\right)=P_g\left(k+1\right)=\ldots=P_g\left(N_g\right). \tag{4.6}$$

When the unit starts, the load per unit and the total load are determined from:

$$k\rightarrow k{+}1:\qquad P_{\text{start},gi}\left(k\right)=P_{gi}\left(k\ \rightarrow\ k+1\right),\quad P_{\text{start},g}\left(k\right)=\sum_{i=1}^{k}P_{gi}\left(k\ \rightarrow\ k+1\right). \tag{4.7}$$

It is important to notice that the generated power must always equal the load demand, as defined in (2.12). Thus, when one of the units starts the percentage of loading on the individual units will usually decrease:

$$\frac{P_{gi}\left(k\right)}{P_{r,gi}}\geq\frac{P_{gi}\left(k+1\right)}{P_{r,gi}}, \tag{4.8}$$

as can be easily noticed for equally rated units with equal load sharing S_{gi} where:

$$k \rightarrow k+1: \qquad P_{\text{start},gi}(k) = \frac{P_g(k \rightarrow k+1)}{k}, \qquad P_{gi}(k+1) = \frac{P_g(k \rightarrow k+1)}{k+1}. \tag{4.9}$$

This will affect the specific fuel consumption $b_{e,gi}(P_{gi})$ in (4.4) and the total fuel consumption in (4.5).

4.2.3 Constraints of the optimization

The cost function has to be minimized subject to the number of constraints. Most of these constraints are defined in Chapter 2 but have to be listed here.

Power balance
As defined in (2.12), the power balance assures that all consumed capacity is generated.

The blackout constraint
The blackout constraint defines the maximum allowable continuous loading of the generator where the system is blackout-proof, according to (2.20).

The low load maintenance constraint
The engine should not be loaded lower than a certain value specified by the engine manufacturer in order to reduce the maintenance costs and downtime. This is defined in (2.20) and (2.21).

Stopping unit constraint-start/stop strategy
The load dependent stop must not coincide with the load dependent start, according to (2.22).

The installed power constraint
The installed power P_{rg} is determined from the maximum power in the vessel operational profile. The installed power must equal to the total ratings of all units:

$$P_{rg} = \sum_{i=1}^{N_g} P_{r,gi} = \sum_{i=1}^{N_g} w_{r,gi} P_{r,g}, \qquad w_{r,gi} > 0, \ \sum_{i=1}^{N_g} w_{r,gi} = 1. \tag{4.10}$$

Load sharing constraint
According to (2.12) and (2.13), the load sharing constraint can be used to distribute the exact amount of load sharing on generators. If the equal proportion of rated power on generators is required, then the load sharing is determined from:

$$S_{gi}(k) = \frac{P_{rgi}(k)}{P_{r,g}(k)} = P_{rgi}(k) \ \frac{1}{\sum_{i=1}^{k} P_{r,gi}}. \tag{4.11}$$

4.3 Operational costs and constraints

The operational costs of the power generating system are to be minimized within the optimization constraints. As the engine performance decreases, the risk for the pre-warning alarm will increase. Then the blackout prevention capability of the system will decrease. Gentle equipment handling will assure lower system susceptibility to faults. Lower the system faults, lower is the risk of blackout.

In order to minimize the fault susceptibility and the maintenance costs of the power generating system, the following control and design objectives for generating sets are proposed in this thesis (e.g. Matt *et al.*, 2005; Karnavas and Papadopoulos, 1999, Klimstra, 2004b, Klimstra, 2004c):

- Avoid engine high load running;
- Avoid engine low load running;
- Avoid high and frequent load variations;
- Avoid excessive starting and stopping;
- Decrease the stand-by costs when the engine is stopped;
- Decrease the exhaust gas emissions;
- Control the running hours on the units.

4.3.1 High load cost

The high engine loading should be avoided due to following reasons:

- As the system operates closer to the blackout constraint, the available power becomes lower and the blackout capability decreases. Then, the possible $\Delta P_{tran,gi}(k, N_f)$ increases and the permitted time to reduce the load t_{SL} deceases. Another reason is the response time of fast load reduction system t_{FLR}, obtained from testing, will not always be exactly matched in the real applications, as explained in the Chapter 3. Thus, it may be advisable to set the limits based on somewhat higher t_{FLR} than obtained from the FLR testing;
- The thermal and mechanical loading of the engine. To reduce the engine susceptibility to faults, operators usually prefer running the prime mover on somewhat lower load than maximum permitted. The optimal engine loading for the minimum downtime, as given from the manufacturers, is found between 50% to 85% engine rated load, $0.5 \le P_{gi} \le 0.85\ P_{r,gi}$, (Matt *et al.*, 2005; Karnavas and Papadopoulos, 1999).

Therefore, the high load cost can be defined as a penalizing factor when running the engines close to the blackout limit i.e. low available power, (Michalewicz *et al.*, 1996):

$$C_{HL}^{t}(k) = e^{1-\frac{c_0}{P_{r,gi}(k)}\left[\min\left(P_{\mathrm{cont},gi}^{\max}(k,N_f),P_{r,gi}\right)-P_{\mathrm{start},gi}(k)\right]}, \qquad (4.12)$$

where t is the number of new record, as shown in Table 4.5. c_0 is the constant to determine the sensitivity when approaching the constraint.

4.3.2 Low load cost

To reduce the soot accumulation inside the engine and consequent maintenance costs, the continuous low load engine operation has to be avoided, as defined by the constant $a_{\min,gi}$ in (2.21).

Running at a reduced load increases the specific maintenance costs linearly (Klimstra, 2004b). Therefore, the low load cost can be defined to linearly penalize running the engine below 50% of the rated load:

$$C_{LL}^{t} = \begin{cases} m_0 - m_1 \dfrac{P_{gi}}{P_{r,gi}} & \text{for } 0 \le \dfrac{P_{gi}}{P_{r,gi}} \le 0.5 \\ m_2 & \text{for } 0.5 \le \dfrac{P_{gi}}{P_{r,gi}} \le 1, \end{cases} \tag{4.13}$$

where m_0 is the maintenance cost when the unit is unloaded, the m_1 is the linear constant between m_0 and m_2, and m_2 is the specified maintenance cost in an ideal case, i.e. when the unit does not operate in the low load conditions.

Relieving operation method

Some vessels operate the same number of engines k for low and high load demands. Then the engine load P_g may become low in e.g. DP conditions, e.g. $P_{gi} \le 0.2\ P_{r,gi}$. It is critical to have sufficient power after a single point failure, which is defined in the blackout limit (2.20). When the mode changes to e.g. transit mode, the operator increases the vessel speed and the load on the engines, typically in the range $0.7\ P_{r,gi} \le P_{gi} \le 1.0\ P_{r,gi}$. The engines may be loaded up to the maximum load in order to blow-out the soot accumulated inside during the low load running.

The diagrams in Fig. 4.1 show the time limits for part load operation on heavy fuel oil, on the left and duration of "relieving operation" on the right side (MAN diesel SE, 2006). According to these diagrams, the engine is allowed to operate for example on $P_{gi} \le 0.1\ P_{r,gi}$ for $t_{LL} \le 19$ hours (arrow *a* in Fig.4.1) if the "*relieving operation*" necessary to blow-out the soot accumulated during the low load running is longer than $t_{rel,LL} \ge 1.2$ hours on $P_{gi} \ge 0.7\ P_{r,gi}$ (arrow *b* in Fig.4.1).

The main advantage of the *relieving operation method* is permanent availability of selected units. The main drawbacks are increased fuel costs and environmental costs due to running engines on low load. Other drawbacks may include an increase in high load costs when engines are highly loaded in the "relieving operation" and an increase in the load variation costs due to frequent change in the load demand.

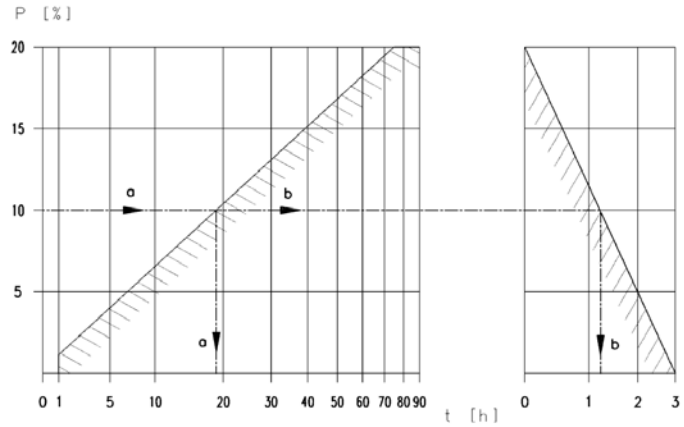

Fig. 4.1. Time limits for part load operation on heavy fuel oil (left) and duration of "relieving operation" (right) (MAN diesel SE, 2006)

4.3.3 The load variation cost

The load variation cost will usually oppose to the low load cost. As the engines are running on low load, the necessity for the *relieving operation method* increases the load variation cost. The load variation cost increases as the load variation per unit between two successive steps t and t -1 is higher:

$$C_v^t = \frac{v_0}{P_{r,gi}}\left(P_{gi}^t - P_{gi}^{t-1}\right), \tag{4.14}$$

where v_0 is a parameter to be set. The value of v_0 wil depend on the engine resistance to variations in load. It may also depend on the state of the engine maintenance or similar.

The load variation cost is typically opposing to the load switching cost, meaning that the load variation per individual unit decreases if more units are connected on-line, as can be seen from Fig. 4.10 in the results of simulation of short term unit commitment optimization.

4.3.4 Unit switching cost and unit availability

If the load is expected to change from a high value to low and back again, it may not be optimal to shut down one unit even for the price of increased fuel cost, as noticed in Hansen (2000). This is defined here as the starting and stopping cost or the unit switching cost. When the unit is stopped, the availability of the generated power is decreased along with the response of the power plant to fast load demand variations.

If the number of unit switching is too high, the maintenance costs may increase. It may be important to note that, along with maintenance costs, the engine susceptibility to faults will also increase. The reciprocating engines show hardly additional wear from stopping and starting if the switching frequency is not excessive (Klimstra, 2004b).

Stand-by cost

The cold engine start should be avoided as this is regarded as one of the worst engine transients. Hence, a usual practice is to keep the engines preheated and lubricated, see e.g. MAN diesel SE, (2006). However, this increases the unit stand-by cost.

The stand-by cost refers to the cost of keeping the engine in the stand-by mode of the operation, where the engine is not running but should be pre-heated, pre-lubricated and in some occasions in the "slow-turning" mode. The stand-by engine mode can consume some amount of energy that can be determined from:

$$C^t_{\text{stand-by}} = \begin{cases} P_{\text{stand-by}}\begin{pmatrix}\text{pre-heating}\\ \text{pre-lubricating}\\ \text{slow-turning}\end{pmatrix}\cdot OP^t & \text{, the unit is stopped} \\ 0 & \text{, the unit is running.} \end{cases} \tag{4.15}$$

Definition of unit switching cost

It is important to notice that the risk of unit unavailability and the reliability of the control system (*risk costs*), are the costs that may be very difficult to express in the cost units, i.e. \$, or €. Although the *start-up cost*, *shut-down cost* and the *stand-by cost* can be quantified, these costs may be low for the diesel-generator power plant, and hence of less importance than the *risk costs*.

Therefore, the switching unit cost proposed in this thesis depends on the following: the total number of unit switching in the selected time period (planning horizon), the time needed to start-up the unit $T_{start\text{-}up,gi}$ and the time spent within the power demand $OP^t(P_g)$:

$$C^t_{sw} = 1 - e^{\frac{-1}{OP^t\left(P^t_g\right)}\, T_{start-up,gi}\left[k\left(P^t_g\right)-k\left(P^{t-1}_g\right)\right]}. \tag{4.16}$$

Similar reasoning can be found in Lee and Chen (2007). As the time spend in certain load demand increases $OP^t(P_g)$, the switching of units becomes more justified. The switching cost is increasing with the number of units to switch $k\left(P^t_g\right)-k\left(P^{t-1}_g\right)$.

4.3.5 Environmental cost

Legislation has been developed for e.g. greenhouse gas emissions, transboundary emissions such as NOx and SOx, particulates as well as noise. The exhaust gas emissions are generally proportional to reductions in the fuel consumption, see e.g. White D. (2004).

In order to achieve low gas emissions costs, typically the operation below 0.5 $P_{r,gi}$ should be avoided, and the following aproximation can be used if more accurate equation is not avilable:

$$C^t_e = 1 - e^{-e_0 \frac{1}{P_{gi}/P_{r,gi}}}, \tag{4.17}$$

where e_0 is the coefficient used to approximate the emission cost.

4.3.6 Running hours

The sequence of unit starting and stopping can be selected according to the maintenance schedule and program. This may depend on the availability of spare parts, time planed to spend in port available for the maintenance operations, etc, see e.g. Murry and Mitchell (1994).

Maintenance of reciprocating engines is normally carried out in a schedule based on the amount of running hours (Klimstra, 2004b).

4.4 Long term unit commitment and relative fuel cost

4.4.1 Classification of optimization variables

It is useful first to classify the optimization variables into the following groups:
- *Decision variables*, i.e. the output of the optimization that defines the solution;
- *Parameters*, i.e. the input data to the optimization problems;
- *Auxiliary variables*, "internal" variables that are introduced for convenience when there are model equations that link the parameters and decision variables.

Then for each optimization problem, all these variables will be described and how they are linked with model equations and constraints.

4.4.2 Definition of fuel cost function

In order to define the cost or objective function, an example of different fuel optimization strategies is given in Fig. 4.2. The break specific fuel consumption (BSFC) for equally rated units with N_g=4 are compared for the following cases:
1. *All units operate*;
2. *PMS start table*: low load unit start with equal load sharing;
3. *Optimal economic dispatch*: low load unit start with optimal economic dispatch (class rule constraint relaxed);
4. *Optimal unit commitment*: optimal unit start with class rule constraint imposed.

The highest fuel consumption is obtained when *all units operate*– units behave like one large engine, and the load dependent start/stop strategy is not utilized. This case is given just for the comparison.

For the *PMS start table* case the units are started on low load, at about $P_{start,gi}(k) = 0.5\ P_{r,gi}$ but having equal load sharing.

The *optimal economic dispatch* is an operation where as many units as possible operate at their maximum loads, and one unit take the rest of the load demand, Hansen (2000). In the *optimal economic dispatch* case presented in Fig. 4.2, the load sharing is optimal (and unequal), and the units are committed (started) at low load, as is the case for the *PMS start table*, i.e. at about $P_{start,gi}(k) = 0.5\ P_{r,gi}$.

When the units start, the load demand remains the same, $P_g(k+1) = P_g(k)$. However, the load per individual unit decreases $P_{gi}(k+1) < P_{gi}(k)$ and the total fuel consumption may increase with $k+1$ units on-line $FC_g(P_g(k+1)) > FC_g(P_g(k))$.

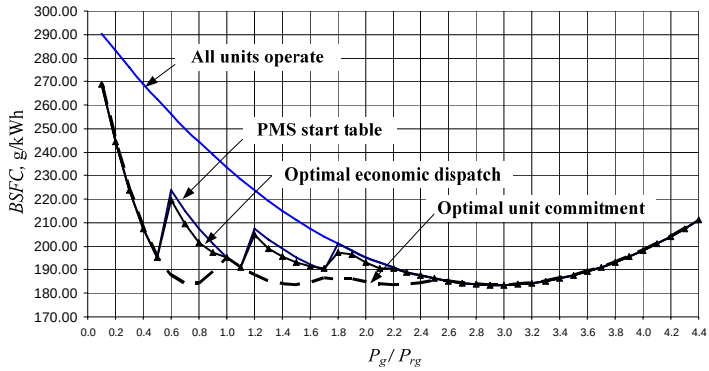

Fig. 4.2. BSFC for different load dependent start tables, Arntsen, T. (2005)

Fuel cost function based on specific fuel consumption

Based on the results of Arntsen, T. (2005) and considerations presented in Fig. 4.2, the following cost function can be used to find the optimal load demand when the unit starts $P_{g,start}(k)=P_g(k \rightarrow k+1)$ in order to minimize the fuel consumption FC_g for the long-term, as defined in Radan *et al.* (2005), Radan *et al.* (2006a):

$$\min_{P_{\text{start},g}(k)} J_{FC} = \min_{P_{\text{start},g}(k)} \left(\sum_{i=1}^{k+1} FC_{gi}\left(P_{gi}(k+1)\right) w_g(k) - \sum_{i=1}^{k} FC_{gi}\left(P_{gi}(k)\right) w_g\left((k)\right) \right), \quad (4.18)$$

$$k \in [1, N_g], \; J_{FC} \geq 0,$$

$$P_{\text{start},g}(k) = P_g(k \rightarrow k+1) \text{ for minimum } J_{FC},$$

$$P_g(k) = \sum_{i=1}^{k} P_{gi}, \qquad P_g(k+1) = \sum_{i=1}^{k+1} P_{gi},$$

where k is the number of units on-line, N_g is the number of installed units, and $w_g(k)$ are the weighting terms. $FC_{gi}(P_{gi}(k))$ is the instantaneous specific fuel consumption (tons/hour) for each unit with k units on-line. $P_{gi}(k)$ is the load on the individual unit when the next unit in the sequence starts.

The optimal cost J_{FC*} (4.18) is determined when the optimal decision variables $P_{start,g}$ are found. The following properties of the optimal cost J_{FC*}, may be noticed:

– The cost function J_{FC} is non-convex. It is concave, as can be noticed in Fig. 4.3. It should be noticed that 2 minima exist for the concave cost function. The easiest solution to this problem, when using classic convex optimization techniques, is to commit units when they operate in the upper operating region;

- The optimal cost J_{FC*} will give the optimal solution $P_{start,g}$ for minimum total fuel consumption $FC_{gi}(P_{gi})$. Thus, the fuel consumption is minimized by minimizing the difference in the instantaneous fuel consumptions for all units with k and k+1 units on-line;
- For the unconstrained problem, the optimal solution is found when $J_{FC*} = 0$. Sometimes, due to constraints imposed (blackout limits), $J_{FC*} = 0$ can not be obtained;
- The cost function should be constraint non-negative, $J_{FC} \geq 0$. This is due to the available power $P_{r,av}(k)$ will be higher when $J_{FC} \geq 0$: $P_{r,av}(J_{FC} < 0) < P_{r,av}(J_{FC} \geq 0)$, for possibly equal fuel consumption, and $FC_{gi}(J_{FC} < 0) \approx FC_{gi}$ $(J_{FC} \geq 0)$;
- The weighting terms $w_g(k)$ can be used to increase the importance of fuel minimization in some preferable situations e.g. when heaving low number of units on-line and/or to avoid optimization for e.g. k=1, when only one unit is on-line.

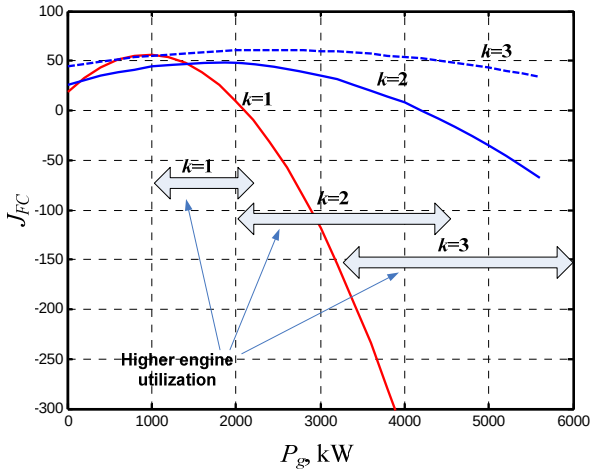

Fig. 4.3. Instantaneous fuel cost function

Fuel cost function based on vessel operational profile

Another cost function can be used to minimize the fuel consumption, (Radan *et al.*, 2006a). The fuel consumption per year is based on the operational profile of the vessel and defines the probability based fuel minimization according to:

$$J_{FCyear} = \int_0^{P_{r,g}} \left(FC(P_g)\ OP(P_g) \right) dP_g \,, \tag{4.19}$$

where $OP(P_g)$ is the operational profile of the vessel.

The following properties of cost function J_{FCyear} defined in (4.19) can be noticed:
- J_{FCyear} gives more flexibility in optimizing the fuel consumption since the fuel can be distributed in a way that more fuel will be spent in modes where the vessel will operate for a very short time per year;
- The main drawback when using J_{FCyear} is the optimization dependence on the load demand probability. As the probability may change, the optimization would become incorrect. Thus, the optimization certainty will be higher if J_{FC} in (4.18) is used.

Combined cost function

A cost function for a long-term optimization is proposed in this thesis. It is a combination of cost functions defined previously:

$$\min\left(J_{comb}\right) = \min\left(\gamma_1 J_{FC} + \gamma_2 C_{HL} + \gamma_3 J_{FCyear}\right)$$
$$= \min\left\{\gamma_1\left[\sum_{i=1}^{k+1} FC_{gi}\left(P_{gi}(k+1)\right)w_g(k) - \sum_{i=1}^{k} FC_{gi}\left(P_{gi}(k)\right)w_g\left((k)\right)\right]\right.$$
$$\left. + \gamma_2 e^{\sum_{k=1}^{N_g}\sum_{i=1}^{k} 1 - \frac{c_{0i}}{P_{r,gi}(k)}\left[\min\left(P_{\mathrm{cont},gi}^{\max}(k,N_f),P_{r,gi}\right) - P_{\mathrm{start},gi}(k)\right]} + \gamma_3 \int_0^{P_{r,g}} \left(FC(P_g)\ OP(P_g)\right)dP_g\right\}$$

$k \in [1, N_g]$, (4.20)

where γ_1, γ_2, γ_3 are the weighting terms and $J_{comb} = \gamma_1 J_{FC} + \gamma_2 C_{HL} + \gamma_3 J_{FCyear}$.

The *decision variables* of the optimization are:

1. *Load demand* when starting the next unit $P_{start,g}(k) = P_g(k \rightarrow k+1)$;
2. *Installed power* ratio $w_{r,gi} = P_{r,gi}/P_{rg}$ (4.10): it may be pre-selected according to design preferences and practices, maintenance practices, engine availability, or similar;
3. *Allocated units* (units selected to be committed for each k), $K \in G$, where $G = \{1, 2,..., i, i+1,.., N_g\}$. Generators selected to be committed will belong to sub-set $K \in G$. For each k generators operating on-line, only one of these combinations will be optimal in given conditions. This determines the decision variable, the sub-set $K \in G$.

Solution to non-convex problem

As the problem is actually concave, 2 solutions (minimums) may exist for every unit committing situation, $k \rightarrow k + 1$. Thus, the solution may converge to lower $P_g(k)$ where the fuel consumption $FC(P_g)$ is actually higher. To prevent this, the $P_{start,gi}(k)$ should be limited, e.g. $P_{start,gi}(k) \geq 0.5\ P_{r,gi}$. The proposed area is indicated in Fig. 4.3. This is well in accordance to the low load and the high load costs. This method will assure that the unit will be optimally committed when classic convex optimization techniques are used, (Wood and Wollenberg, 1996; Fletcher, 2000; Rao, 1996; Stephen and Vandenberghe, 2004).

4.4.3 Equal percentage of load sharing

The class rule (2.14) imposes the constraint where equal percentage of load sharing must be used for all units operating on-line. When *equal percentage of load sharing constraint* is imposed, the load sharing factor S_{gi} is not being optimized, and the economic dispatch problem is disregarded. Then, only the unit commitment problem have to be solved and optimal start/stop determined.

The class society rule constraint is imposed in the proposed optimization, due to the following reasons:

– Unequal load sharing may increase the *high load costs* and the *low load costs*;

- The optimal load sharing may decrease the load on some units to minimum permitted. Then, the blackout limit may decrease for these units;
- The *equal percentage of load sharing constraint* gives nearly-optimal load sharing, as can be noticed in Fig. 4.2 (Arntsen, 2005);
- The *load sharing constraint* simplifies the general optimization problem since the number of decision variables becomes significantly reduced.

4.4.4 Optimization procedure

The goal of the optimization procedure is to find the optimal ratings of the installed units, to allocate units in different operating conditions, and to find the load dependent start tables for the minimum fuel consumption in the whole operational region $0 \leq P_g \leq P_{rg}$.

The *decision variables* of the long-term optimization are defined as in (4.20).

All load demand information is not available in the vessel design, e.g. the load demand variability, change of the vessel operational modes, and similar. Thus, some of the costs including the load switching cost and load variation cost can be excluded from the optimization.

All decision variables can be optimized at once, using the combined cost function J_{comb}, (4.20). If the unit ratings $w_{r,gi} = P_{r,gi}/P_{rg}$ and the unit allocation K are pre-selected manually, then $P_{start,g}(k)$ is the only decision variable in the cost function (4.20). As solutions are determined for various K allocation combinations and $w_{r,gi}$, they may all be compared using the per year fuel consumption $J_{FC,year}$. The optimal solution will be the one that gives the lowest fuel consumption per year of operation $J_{FC,year}$ with adequate design configuration and philosophy (Radan *et al.*, 2006a). With manually selected combinations, the designer may have the best overview of the optimization problem and the greatest flexibility in the design. This will be demonstrated in the case study in this Section.

ALGORITHM – manually selected combinations

The sequence of optimization procedure can be followed in this order:

1. Select the total installed power for the power system P_{rg};
2. Select the initial ratio of the rated power, $w_{r,gi} = P_{r,gi}/P_{rg}$;
3. Select the unit allocation candidate K for each k and selected $w_{r,gi}$;
4. Using the numerical optimization, find the starting load demand $P_{start,g}(k \rightarrow k+1)$ using the cost function (4.18) or (4.20). Other decision variables, K and $w_{r,gi}$ will be held fixed in the numerical optimization;
5. Repeat the procedure from the step 3 for another unit allocation candidate K and provide solutions for several candidates;
6. Repeat the procedure from the step 2 for another installed power ratios $w_{r,gi}$ and provide solutions for all selected $w_{r,gi}$ and unit allocation candidates K;
7. Compare the fuel consumption per year of operations using $J_{FC,year}$ (4.19) and select the preferred solution that gives:
   - Nearly-lowest fuel consumption $J_{FC,year}$;
   - Adequate power plant configuration and design philosophy;
   - Starting load demand $P_{start,gi}(k)$, possibly further from the blackout limit;
   - In general, explore the sensitivity to various operational costs between the solutions.

4.4.5 Case study

The case study is used to demonstrate the application of the optimization strategy.

A case study of a small size Anchor Handling and Tug Support Vessel (AHTS) with diesel electric propulsion will be used to explain the proposed method. The basic configuration is similar as for many offshore support vessels. It is assumed to have approximately 100 metric tons bollard pull.

Optimization parameters

– All prime movers are medium speed diesel engines burning the same type of fuel (heavy fuel oil). Break specific fuel consumption, BSFC (4.2):

$$b_{e,gi}\left(P_{gi}\right) = 298.015 - 310.54\frac{P_{gi}}{P_{r,gi}} + 210.65\left(\frac{P_{gi}}{P_{r,gi}}\right)^2 \qquad \text{for } i \in [1, N_g]; \tag{4.21}$$

– Number of engine rooms (compartments): N_{comp}=2;

– Number of installed units is selected, N_g=4;

– Inertial time constant for unit: H_i=1 seconds for all units;

– Time to reduce the load: t_{FLR} (*event*) = 0.3 seconds;

– $w_{r,gi} = P_{r,gi}/P_{rg}$ is manually pre-selected and listed in the table;

– Total installed power P_{rg} = 7 000 kW.

Decision variables

The *decision variables* of the long-term optimization are:
1. *Load demand* when starting next unit $P_{start,g}(k) = P_g(k \rightarrow k+1)$;
2. *Installed power* ratio $w_{r,gi} = P_{r,gi}/P_{rg}$ (4.15);
3. *Allocated units*, $K \in G$, where $G = \{1, 2,..., i, i+1,.., N_g\}$. .

In Table 4.3, K and $w_{r,gi}$ are manually selected for the design solutions 1 to 7. For the design solutions 8 to 9, they are outputs of the numerical minimization with J_{comb}.

Constraints of the optimization

The following constraints are included:

– Real power balance:

$$P_g = \sum_{i=1}^{k} S_{gi}(k) P_g = \sum_{i=1}^{k} P_{gi}\ ; \tag{4.22}$$

– The low load maintenance constraint:

$$a_{\min,g} P_{r,gi} \le P_{\text{stop},gi}(k) \le P_{gi}(k)\,, \tag{4.23}$$

The low load constraint is used instead of the *low load cost*;

– Blackout constraint:

$$P_{gi}(k) \le P_{\text{start},gi}(k) \le \min\left(P^{\max}_{\text{cont},gi}(k, N_f), P_{r,gi}\right), \tag{4.24}$$

The blackout constraint is based on the unit failure anticipated scenario and performance of the FLR, as will be defined more detailed later;

– Installed power constraints:

$$\begin{aligned} P_{rg} - \sum_{i=1}^{N_g} w_{r,gi} P_{r,g} &= 0\,, \\ w_{r,gi} &\ge 0.1\,; \end{aligned} \tag{4.25}$$

– Equal percentage of load sharing constraint:

$$S_{gi}(k) = \frac{P_{rgi}(k)}{P_{r,g}(k)} = P_{rgi}(k)\ \frac{1}{\sum_{i=1}^{k} P_{r,gi}}\,; \tag{4.26}$$

– Increasing load operations unit start strategy constraint:

$$P_{\text{start},g}(k) < P_{\text{start},g}(k+1)\,; \tag{4.27}$$

– Identical engine-rooms constraint:
The installed power per unit ratio $w_{r,gi}$ is fixed due to the design preference (constraint) that units in all engine rooms must have the same ratings:

$$w_{r,gi} = w_{r,gj} \qquad i \in [1, N_g(c=1)], \quad j \in [1, N_g(c=2)], \quad c \in [1, N_c], \tag{4.28}$$

where c is the engine compartment index. The installed power per unit ratio will be different for different cases. For the solutions 8 and 9 this constraint is relaxed, see Table 4.2;

– Auxiliary constraint:
In addition to the problem constraints, defined above, the auxiliary variable is introduced in order to provide comparable results for the fuel consumption per year J_{FCyear}:

$$P_{start,gi}(k=1) = P_{start,gi}(k=2) - 0.05 P_{r,gi}, \tag{4.29}$$

This constraint is imposed on all solutions except 9 in Table 4.2.

Blackout limit calculation

The blackout limit is based on the fault scenario and the FLR system performance. The load scenario is defined as the worst case scenario i.e. the unit with the highest power rating fails as defined in (2.3). Then, the transient load step on the remaining units (2.4) is determined from:

$$\Delta P_{\text{tran},gi}(k,N_f)=\frac{H_i P_{r,gi}(k)}{\sum_{i=1}^{k} H_i P_{r,gi}-\max_i P_{r,gi}(k)}\max_i P_{gi}(k). \tag{4.30}$$

The maximum possible load reduction will depend on the selected FLR design method and the selected load reduction strategy.

In this case study the following design is used:
1. FLR method: Event-based FLR system;
2. FLR control strategy: Strategy 2 in Section 3.4.2 *Full transient load step reduction*.

Then, the following equations determine the capabilities of the FLR system:

$$\begin{aligned}&\Delta P^{\max}_{\text{tran},gi}\left(a_{\max,g},t_{FLR,i}\right)=\Delta\omega^{\max}_{gi}\ \frac{2H_i}{t_{SL,i}}P_{r,gi},\\ &t_{FLR}\left(event\right)=t_{com}+t_{\theta,com}+t_{mp}.\end{aligned} \tag{4.31}$$

Finally, the maximum continuous safe load limit (2.9) is determined from the anticipated scenario and the fast load reduction system capabilities (4.31):

$$\begin{aligned}P^{\max}_{\text{cont},gi}(k,N_f)&=P_{\text{tran},gi}(k,N_f)-\Delta P^{\max}_{\text{tran},gi}\left(a_{\max,g},t_{FLR,i}\right)\\ &=P_{gi}(k,N_f)+\Delta P_{\text{tran},gi}(k,N_f)-\Delta P^{\max}_{\text{tran},gi}\left(a_{\max,g},t_{FLR,i}\right)\\ &=P_{gi}(k,N_f)+\frac{H_i P_{r,gi}(k)}{\sum_{i=1}^{k} H_i P_{r,gi}-\max_i P_{r,gi}(k)}\max_i P_{gi}(k)-\Delta\omega^{\max}_{gi}\ \frac{2H_i}{t_{SL,i}}P_{r,gi}.\end{aligned} \tag{4.32}$$

Optimization results for case 1

Results of the optimization for case 1 with t_{FLR} = 0.5 seconds are compared in Table 4.2. Due to relatively slow response of load reduction with respect to inertia dependant time limits, the maximum allowable power load step $\Delta P^{\max}_{\text{tran},gi}\left(a_{\max,g},t_{FLR,i}\right)$ will be relatively low and the units will have to operate further from the optimum operational point – in all 6 design solutions the $P^{\max}_{\text{cont},gi}(k,N_f)\le 0.4\ P_{r,gi}$, as can be seen in Table 4.2. Case 1 is the *highest fuel consumption case*.

Optimization results for case 2

The solutions for case 2, namely solutions: 2, 3 and 4 with t_{FLR} = 0.3 seconds are given in Table 4.2. If the fast load reduction can operate faster, i.e. with $t_{FLR} \leq 0.3$ seconds, then the fuel consumption will be reduced, compared to case 1. In this case the maximum allowable power load step $\Delta P_{\text{tran},gi}^{\max}\left(a_{\max,g}, t_{FLR,i}\right)$ will be higher, so the engines can be loaded more than in case 1, meaning that the engines can operate closer to the optimum operating point and more fuel can be saved.

Optimization results for case 3

The solutions for case 3, namely solutions: 5 to 9 with t_{FLR} = 0.1 seconds are given in Table 4.2. In this case the fast load reduction system acts extremely fast (this may be considered as a hypothetical case with the present available CPU capacity of PLC controllers) and the allowable power load step $\Delta P_{\text{tran},gi}^{\max}\left(a_{\max,g}, t_{FLR,i}\right)$ will be considerably higher than in cases 1 and 2. The blackout constraint is not active for the whole operational region, meaning that the units operate far from the blackout constraint.

The instantaneous fuel consumption $FC_g(P_g)$ for various design solutions has been compared in Fig. 4.4. The break specific fuel consumption (BSFC) for various design solutions has been compared in Fig. 4.5. It can be easily noticed from Figs. 4.4 and 4.5 that lower fuel consumption is obtained with the design solutions 7 and 8 than with the solutions 1 and 2, for the whole region of operation.

4.4.6 Conclusion

From the case study (last raw in Table 4.2), it can be noticed that more than 6% of fuel can be saved if the fast load reduction technology is improved (t_{FLR} =0.1 seconds instead t_{FLR} =0.5 seconds) and the proposed optimization method is used. The exhaust gas emissions will also reduce along with the fuel consumption.

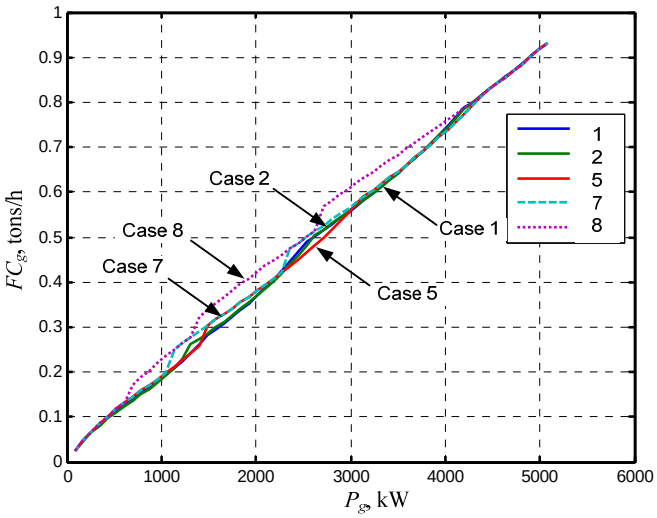

Fig. 4.4. Instantaneous fuel consumption for various design solutions

Table 4.2. Results of fuel consumption optimization for case 1

Cases:	**1**	**2**			**3**				
Solutions:	**1**	**2**	**3**	**4**	**5**	**6**	**7**	**8**	**9**
Algorithm:	**2**	**2**			**2**			**1**	
	<========== H_i = 1 seconds ==========>								
Time to reduce the load, t_{FLR}:	t_{FLR} = 0.5 seconds	t_{FLR} =0.3 seconds			t_{FLR} =0.1 seconds				
Installed power ratio, $w_{r,gi}$:	$w_{r,gi}$= same eng. rooms							$w_{r,gi}$= optimal	
	$w_{r,gi}$	$w_{r,gi}$	$w_{r,gi}$	$w_{r,gi}$	$w_{r,gi}$	$w_{r,gi}$	$w_{r,gi}$	$w_{r,gi}$	$w_{r,gi}$
***i*= 1**	0.250	0.250	0.300	0.2	0.25	0.300	0.200	0.236	0.212
***i* = 2**	0.250	0.250	0.200	0.2	0.25	0.200	0.200	0.139	0.223
***i* = 3**	0.250	0.250	0.300	0.3	0.25	0.300	0.300	0.314	0.237
***i* = 4**	0.250	0.250	0.200	0.3	0.25	0.200	0.300	0.311	0.327
	$P_{start,gi}/P_{r,gi}$, %								
	For all solutions except 9: $P_{start,gi}(k=1) = P_{start,gi}(k=2) - 0.05P_{r,gi}$								
***i* = 1; *k* = 1**	35.03	61.67	35.00	61.67	83.45	85.72	88.81	90.49	95.99
***i* = 1, 2; *k* = 2**	40.00	66.67	40.00	66.67	88.45	90.72	93.81	95.49	89.49
***i* = 1, 2, 3; *k* = 3**	50.48	84.24	81.90	86.72	84.24	81.90	86.72	87.28	88.14
	P_g, kW								
starting no 2:	613.0	1079.2	735.0	863.3	1460.4	1800.1	1243.4	1492.3	1424.8
starting no 3:	1400.0	2333.3	1400.0	1866.7	3095.8	3175.2	2626.7	2503.5	2727.6
starting no 4:	2650.0	4422.6	4586.4	4249.2	4422.6	4586.4	4249.2	4208.0	4149.7
	J_{FCyear}								
Fuel saved (START), % 1st solution	**0.00**	**4.64**	**1.16**	**4.61**	**6.14**	**6.34**	**6.41**	**6.41**	**6.47**

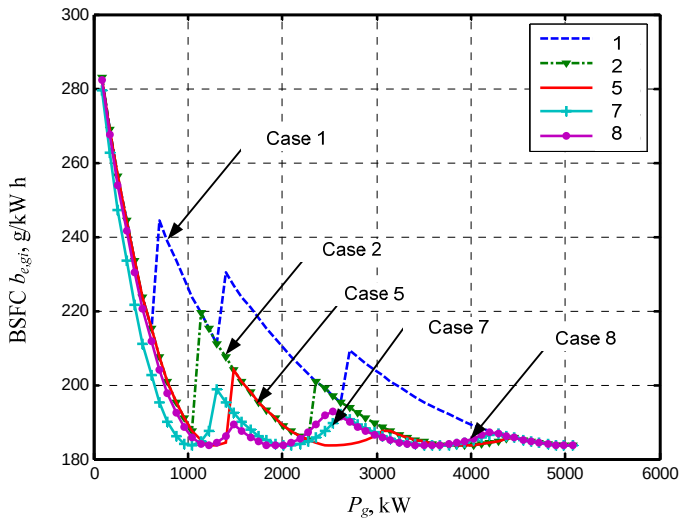

Fig. 4.5. BSFC $b_{e,gi}$ for various design solutions

4.5. Probability based unit commitment

4.5.1 Load dependent stop

In load increasing operations, the units will be started and connected on-line, gradually one at the time. The fuel consumption will be minimized for the optimum starting load, the installed unit ratings and the starting sequence combination, as proposed in Section 4.4.

In load decreasing operations, these on-line units can be disconnected and stopped (de-committed) in order to save fuel and decrease the unit wear-out and the maintenance costs. The available criterion (2.22) is that the load dependent stop tables must not coincide with the load dependent start tables, which corresponds to the following constraint:

$$P_{g,stop}(k+1) = P_{g,start}(k) + \nu \cdot \left(P_{g,start}(k+1) - P_{g,start}(k) \right), \text{ for } \nu \in [0, 1], \qquad (4.33)$$

where $P_{g,start}(k)$ is determined using the load dependent start optimization algorithm, defined in Section 4.4. Fig. 4.6 shows the corresponding hysteresis due to the load dependent stop table. Two extreme situations when stopping units can be distinguished in the (4.33):

– If $\nu = 0$ in (4.33), then $P_{g,stop}(k+1)=P_{g,start}(k)$. By stopping the units near the lower limit, $P_{g,start}(k)$, the blackout prevention capability will be increased due to high spinning reserve and low possible $\Delta P_{tran,gi}$ (k, N_f). However, the engines will operate on low load, with increased fuel consumption and maintenance costs. An increase in the specific fuel consumption due to unit stop on low load can be noticed in Fig. 4.6;
– If $\nu = 1$ in (4.33), then $P_{g,stop}(k+1)=P_{g,start}(k+1)$. The unit is stopped immediately after the load becomes lower then the staring load, in the load decreasing operations. Then the fuel consumption for unit stopping will be equal to the fuel consumption for the unit starting, defined in the optimized load dependent start tables, $P_{start,gi}(k)$. Then, the overall fuel consumption may be the lowest. However, it may be uncertain how long the load P_g (k) will be lower than the stopping load $P_{g,stop}(k)$. If this is short, than a high number of unit starting and stopping can be expected, and the unit switching cost will increase.

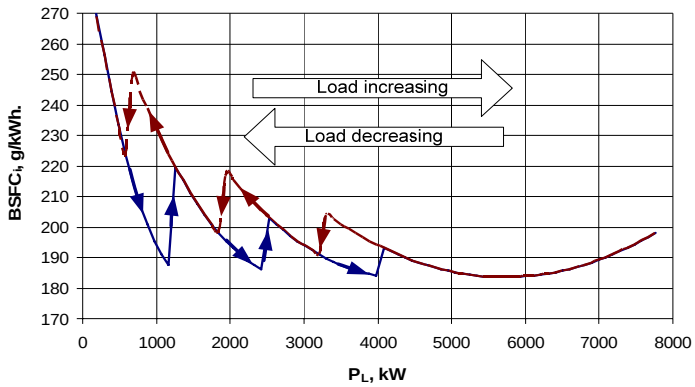

Fig. 4.6. BSFC hysteresis when starting and stopping units

In the *long-term unit commitment*, the unit switching cost may be difficult to estimate. Thus, in order to trade-off between the excessive unit switching and the large load variation, the

$P_{g,stop}(k+1)$ may be set about the middle between $P_{g,start}(k)$ and $P_{g,start}(k+1)$, as shown in Fig. 4.6. This is done in real applications as well.

4.5.2 Switching units between modes

If there exists significant difference in the load demand between two modes, than the units may be selected in order to switch (start/stop) between these modes (Radan *et al.*, 2006a). The idea to switch units between preferable modes is illustrated in Fig. 4.7.

Based on the proposed idea, the following constraint is introduced in the optimization in order to force the unit starting between the selected modes:

$$P_{g,start}(k) = P_{gm}, \quad m \in [0, M_g], m \in I, \tag{4.34}$$

$$P_g(OP, m) \le P_{gm} \le P_g(OP, m+1),$$

$$M_g \le N_g - 1,$$

where P_{gm} is the selected load demand between 2 distinct modes: m and m+1. The m+1 mode is a higher power consuming mode than the m mode.

Since the units can be started and stopped between the switching modes m, the fuel consumption for stopping units can be minimized. When a low number of units operate on-line, the blackout risk decreases if the units switch-off when the vessel change the operation to lower load demanding mode.

It is important to notice that the proposed idea will not affect the existing PMS unit start/stop philosophy. The units can still be stopped at lower received load P_g than started, as explained in (2.22). Then the PMS unit start/stop algorithm will be defined with hysteresis, as shown in Fig. 4.6. The difference is that the proposed *probability based load switching* can be used to select the size of the units and the starting load per unit $P_{g,start}$ in order to achieve load based start/stop between the switching modes m in (4.34). Then, the units will behave as $P_{g,start}$ is equal to $P_{g,stop}$ for most of the time although the PMS start/stop tables may be set according to (2.22), i.e. $P_{g,stop}(k+1) < P_{g,start}(k+1)$.

Example of the proposed idea

The summary of electric load analysis for the drilling vessel *Nereus* is presented in Table 4.3, for more details see Design Team (2003). The load demand P_g in kW is estimated for the PORT, DP and TRANSIT mode of operation. The vessel is required to operate in weather conditions of sea state 7 (SS7). Hence, the load demand is determined for DP mode and three distinguished weather conditions: SS3, SS5 and SS7.

From Table 4.3 it can be noticed that the highest load demand in DP mode is close to P_g(DP-SS7)≈16 000 kW, is still significantly lower than the load demand in the *Transit* mode, which is P_g(TRAN)≈26 000 kW. This is 10 000 kW difference of consumed load when the vessel change the mode of operation, and well enough to be distinguished by the PMS algorithm, as proposed above.

The probability of time spent in operating modes for drilling vessel *Nereus* is presented in Fig. 4.7. If the units are required to switch between selected modes, a low number of units switching may be achieved. For instance, one may want to commit 1 or 2 additional units only when the vessel is in the transit mode. If the same units are always committed, then the units would operate only 10% of the time per year, or about 8760 hours · 0.1 ≈ 876 hours/year. Then, these units may have possibly higher ratings than those used in a DP mode.

Table 4.3. Electric load analysis for drilling vessel *Nereus* (Design Team, 2003)

			Normal drilling			
Description	**capacity**	**PORT**	**DP-SS3**	**DP-SS5**	**DP-SS7**	**TRAN**
	kW	kW	kW	kW	kW	kW
thrusters(6 x 5500 kW)	33000		1254.2	2065	3485	19540
drilling drives			5140	5140	5430	
480V distribution	23125	2234.6	7046	7046	7046	6340
Total load:	**56125**	**2234.6**	**13440.2**	**14251**	**15961**	**25880**
Consumer capacity utilization, %		**3.98**	**23.95**	**25.39**	**28.44**	**46.11**
Per engine capacity:	**7780**					
Number of units:	**6**					
Total generating capacity:	**46680**					
Generating capacity utilization, %:		4.79	28.79	30.53	34.19	55.44

DP=dynamic positioning mode, PORT=port mode, TRAN=transit mode, SS=sea state.

The maximum number of preferable modes is M_g which is lower than the number of installed units N_g, since at least one unit must always operate. $P_g(OP, m)$ defines the load demand per hours of operations OP in the m mode. The load demands $P_g(OP, m)$ and $P_g(OP, m+1)$ should be distinguished, meaning that the difference must be larger than some value: $P_g(OP, m+1) - P_g(OP, m) \geq \Delta P_{g,sw}$.

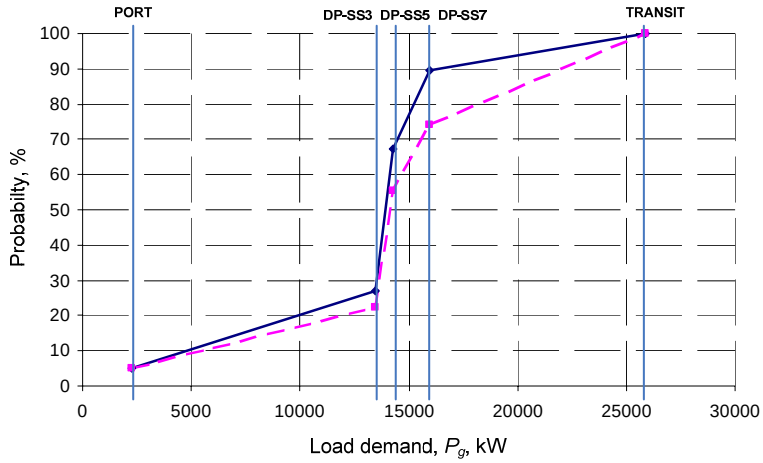

Fig. 4.7. Probability of time in operating modes for drilling vessel *Nereus* estimated for following scenarios: SCENARIO 1 (full line): PORT=1%, DP=90%, TRAN=9%; SCENARIO 2 (dotted line): PORT=5%, DP=70%, TRAN=25%

4.5.3 Optimization procedure

ALGORITHM – probability based mode switching

The sequence of optimization procedure should be followed in this order:

1. Select the total installed power for the power system P_{rg};
2. Select one of the preferable mode switching combinations and select m;
3. The bus load demand when the unit starts $P_{g,start}(k)$ is determined from the constraint $P_{g,start}(k)=P_{gm}$;
4. Find the optimal power ratio $w_{r,gi}$ and starting combination using the cost function (4.18) or (4.20);
5. Repeat the procedure from the step 3 for another switching mode combinations;
6. Compare the fuel consumption per year of operations for various combinations using $J_{FC,year}$ and select the preferred solution that gives:
   - Nearly-lowest fuel consumption $J_{FC,year}$;
   - Adequate power plant configuration and design philosophy;
   - Starting load demand $P_{start,gi}$ (k) possibly further from the blackout limit with low k;
   - In general, explore the sensitivity to various operational costs between the solutions.

4.6 Short-term unit commitment and real time generator allocation control

The time the vessel will spend in each mode and the corresponding load demand can be obtained from the operational profile of the vessel, as proposed in the proceeding section. However, the operational profile may not be fully accurate.

When using the operational profile to predict the vessel behavior, the following problems may be encountered:

- The vessel route, the weather conditions, and the vessel operations may change in the life of the vessel, and the operational profile may become different from the time when the vessel was designed;
- The operational profile may have frequent variations e.g. due to changes in the weather conditions per season (summer/winter) or hull and propeller fouling, etc;
- The operational profile is obtained from the statistics of the vessel operations, meaning that the number of mode switching and the load demand variations are not known.

Due to described reasons, most of the operational costs previously defined may have limited use in the long-term planning.

In order to minimize operational costs and have increased flexibility in operations planning, the continuous update of the load dependent start/stop tables can be based on the feedback measurements of the vessel load demand. Based on the load demand feedback (*planning interval*) the load demand is forecasted for about the same time interval (*planning horizon*). This real-time control is defined as the *short-term unit commitment optimization* and is proposed in this Section.

4.6.1 Short-term unit commitment costs

Short-term unit commitment cost function

All defined costs can be used in the *short-term* (real-time) *optimization* where the data will be available from the load demand measurements. The proposed short-term unit commitment cost function is a combination of operational costs defined in Section 4.3.

The same *decision variables* are used as in the *long-term* unit commitment optimization.

Two main purposes of the optimization may exist:
1. The *long-term unit commitment optimization* to design the power plant and find the optimal unit ratings $P_{r,gi}$ based on the typical daily operations recorded in the short time interval (few days);
2. The *short-term unit commitment optimization* to continuously update the load demand information, provide a short-term forecast and re-calculate the load dependent start/stop tables.

The *short-term cost function* will change due to vessel operations. Then the start tables $P_{start,gi}(k)$ can be recalculated for a new $OP^t(P_g)$. The optimization procedure can be repeated in a short time periods of days, or weeks depending on the vessel operational plan, route, weather conditions, etc.

Two methods of short-term optimization are proposed:
- *Method 1*: The operational costs are defined and a combined cost function is used to obtain the optimal solution;
- *Method 2*: The fuel cost and the number of unit switching is defined. Other costs are represented as constraints.

Method 2 is more intuitive and practical than *Method 1* if the costs are difficult to estimate. Therefore, *Method 2* can be used for the optimization of the operational costs on the vessel until enough data are collected for *Method 1* to become feasible.

Method 1

The fuel cost function depends on the fuel consumption in the selected *planning interval* (measurement time interval) T_{EM}:

$$J_{FC}^t = \sum_{t=1}^{T_{EM}} FC(P_g)\ OP^t(P_g) = \sum_{t=1}^{T_{EM}} \sum_{i=1}^{k} FC(P_{gi})\ OP^t(P_g), \tag{4.35}$$

where the $OP^t(P_g)$ is the time the vessel spend in the particular load demand P_g, given in minutes or hours. The *planning interval* can be selected from hours to days or weeks depending on how fast the *planning horizon* should change i.e. how fast the PMS load dependent start-stop tables will be optimized.

The following combined cost function is defined in the short term optimization:

$$J_{comb}^t = J_{FC}^t + \gamma_{HL} C_{HL}^t + \gamma_{LL} C_{LL}^t + \gamma_v C_v^t + \gamma_{sw} C_{sw}^t, \tag{4.36}$$

where the γ 's are the weighting terms. The gas emission cost is contained within the low load cost.

Method 2

As operational costs may be difficult to estimate, the constraints may be defined in order to explore the sensitivity of fuel costs to other operational cost in an intuitive manner.

Then, only the fuel cost is contained within the combined cost function (4.36):

$$J_{comb}^{t} = J_{FC}^{t}, \tag{4.37}$$

where other costs can be controlled by setting different constraints:

– *High load constraints:*

$$\frac{1}{P_{r,gi}(k)}\left[\min\left(P_{\text{cont},gi}^{\max}(k,N_f),P_{r,gi}\right)-P_{\text{start},gi}(k)\right]\geq L_{HL,i}, \tag{4.38}$$
$$L_{HL,i}\geq 0;$$

– *Low load constraints*:

$$\frac{1}{P_{r,gi}(k)}\left(P_{\text{start},gi}(k)-a_{\min,gi}P_{r,gi}\right)\geq L_{LL,i}, \tag{4.39}$$
$$L_{LL,i}\geq 0;$$

– *Load variation constraints*:

$$\frac{1}{P_{rg,i}}\left|P_{gi}^{t}-P_{gi}^{t-1}\right|\leq L_{v,i}, \tag{4.40}$$
$$L_{v,i}\geq 0;$$

– *Number of unit switching constraint*:

$$N_{k,sw}^{t}=\sum_{t=1}^{T_{EM}}k\left(P_{g}^{t}\right)-k\left(P_{g}^{t-1}\right)\leq L_{k,sw}. \tag{4.41}$$

The non-smooth cost functions arise in economic dispatch studies due to valve point loading effects, prohibited operational zones, and fuel switching effects, see e.g. Perez-Guerrero and Cedenio-Maldonado (2005).

The *short-term fuel cost function* for the *Viking Energy* vessel is shown in Fig. 4.8. It can be noticed that the cost function is not smooth since sharp transitions from one state to another can be noticed. As can be noticed from Fig. 4.9, the switching cost is a non-convex function i.e. concave and discontinuous. The low cost switching areas are indicated in Fig. 4.9 for

k=1, 2 and 3, suggesting the load demand $P_g(k)$ for which the units should switch in order to have a low switching cost.

4.6.2 Results of short-term optimization

The results of the short-term optimization are obtained using *Method 2*.

The real measurements of power demand P_g for the *Viking Energy*, offshore supply vessel (OSV) are shown in Table 4.5. The units will be started depending on the match between the load demand P_g and the $P_{start,g}(k)$ determined from the PMS load dependent start tables $P_{start,gi}(k)$. The units will be stopped at the same received load P_g as when started, with $\nu = 1$ in (4.33).

Solutions including various constraints and additional operational costs are given in Table 4.4. First four solutions (*design solutions*) are given for the design, with $P_{r,gi}$ are optimized. Other six solutions are calculated for the real time generator allocation (*PMS solutions*), with $P_{r,gi}$ fixed.

Design solution 3 in Table 4.4 would require somewhat smaller size of the generator, in order to accomplish more than 8% fuel savings compared to original. The solutions with high and low switching costs are also given. The PMS solutions are easier to accomplish once the units have been installed in the vessel. The highest fuel savings are accomplished in the PMS solution 5, with more that 6% fuel savings. However, this solution requires very high loading on the generators which increases the blackout risk and maintenance costs. Hence, PMS solutions 6 and 4 can give lower engine loading for the price of 1 to 2% of additional fuel.

Results of load variations per engine are shown in the time for the *real time solutions*: 1, 2, 4, 5. in Fig. 4.10. Fig. 4.10 clearly demonstrates the ability of the optimization to deal with the load variations. While the solution 1 has the highest load variations, the solution 4 would have the lowest load variations in addition to load that is never lower than 0.3 $P_{r,gi}$. Solution 5 would give a higher load in average with acceptable variations and the lowest fuel consumption.

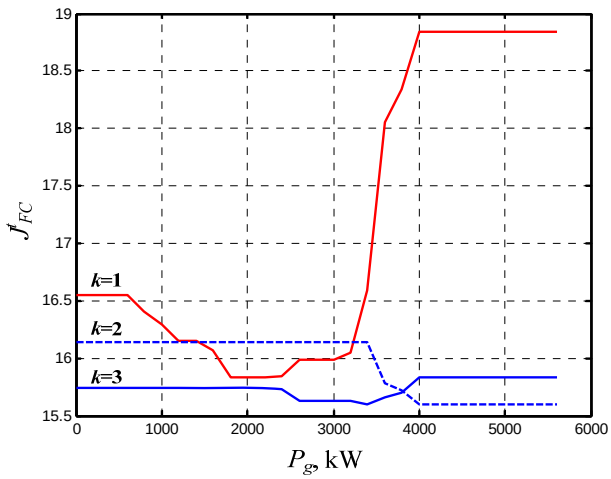

Fig. 4.8. Short-term fuel cost function

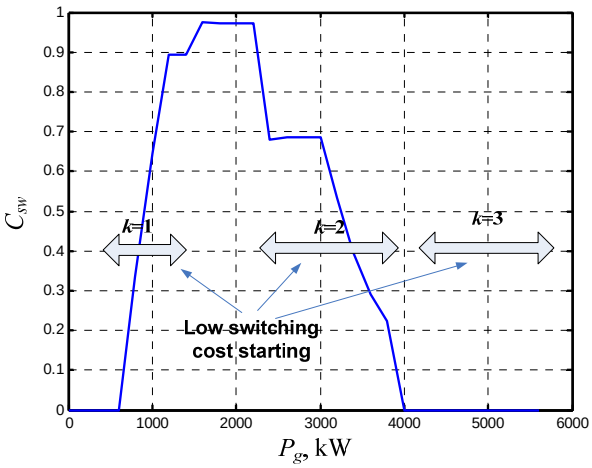

Fig. 4.9. Switching cost, showing the function non-convexity and low cost switching areas for unit start

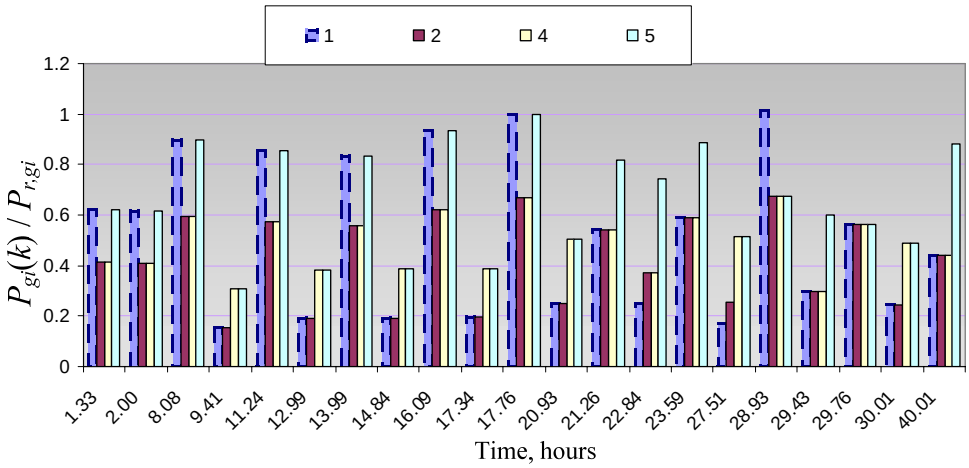

Fig. 4.10. Time results of load variations per engine for real time solutions: 1, 2, 4, 5

Table 4.4. Results of fuel optimization study for OSV *Viking Energy* using the real time generator allocation control (*Method 2*)

	Design solutions				***PMS solutions - real time generator allocation,*** $P_{r,gi}$ = fixed					
	original	**Low switch**	**High switch**	**Low switch**	**original**	**Low switch**		**High load cost**	**Constr. higher load**	**Constr. blackout**
			Min fuel			**k >=2**			**Min fuel**	
Solution:	**1**	**2**	**3**	**4**	**1**	**2**	**3**	**4**	**5**	**6**
$P_{r,gi}$, **kW =**	1950	1950	1437.5	1454	1950	1950	1950	1950	**1950**	1950
	$P_{start,gi}(k) / P_{r,gi}$									
***k*=1**		0.30	0.75	0.41		0.31	0.43	0.52	0.98	0.80
***k*=2**		0.61	0.70	0.83		0.62	0.60	0.60	0.88	0.76
***k*=3**		0.68	0.81	0.92		0.68	0.68	0.68	0.84	0.68
	$P_{start,g}(k)$, kW									
***k*=1**	NA	**600**	1075	**600**	NA	600	840	1008	1916	1560
***k*=2**	NA	**2400**	2000	**2400**	NA	2400	2340	2340	3449	2964
***k*=3**	NA	**4000**	3500	**4000**	NA	4000	4000	4000	4928	3971
total FC, tons=	16.62	16.34	15.29	15.63	16.62	16.34	16.21	15.93	**15.6**	15.76
% orig.	**0.00**	**1.66**	**8.03**	**5.95**	**0.00**	**1.66**	**2.44**	**4.14**	**6.17**	**5.19**
$N_{k,sw}$ =	2.00	**15**	**37**	**15**	2	15	23	29	27	34
aver (P_{gi} = P_g/*k*)=	0.52	0.42	0.62	0.56	0.52	0.42	0.45	0.49	0.60	0.54
STD(P_{gi} = P_g/*k*)=	0.31	0.18	0.12	0.24	0.31	0.18	0.14	0.11	0.16	0.11
Average(*k*) =	2.19	2.48	2.33	2.48	2.19	2.48	2.29	2.14	1.76	1.95
STD (*k*) =	0.40	0.51	1.11	0.51	0.40	0.51	0.78	0.91	0.83	0.92

Aver = average, STD=standard deviation

Table 4.5. The real time optimization for the PMS solution 4 defined in Table 4.4 (*Method 2*)

Time record	**Mode**	**Operat. profile**	**Time passed**	**Total Load demand**	**Prop. Load demand**	**Numb. units on-line**	**Power on unit**	**Spec. fuel consump.**	**Fuel consump.**	**Number of unit switching**
t -	**Mode** -	OP^t **hours**	OP^t (*t*=*t*+1) **hours**	$P_g(t)$ **kW**	P_{th}, **kW**	$k\ (P_g(t))$ -	P_{gi} **p.u.**	$b_{e,g1}$ **g/kWh**	**FC, tons**	$k\ (P_g(t))$- $k\ (P_g(t\text{-}1))$
1	TRAN	1.33	1.33	2420	1670	3	0.41	205.85	0.662544	-
2	TRAN	0.67	2	2400	1600	3	0.41	206.26	0.331669	0
3	TRAN	6.08	8.08	3490	2700	3	0.60	183.73	3.898572	0
4	DP	1.33	9.41	600	0	1	0.31	222.23	0.177342	2
5	TRAN	1.83	11.24	3340	2590	3	0.57	186.83	1.141939	2
6	DP	1.75	12.99	750	0	1	0.38	206.45	0.270964	2
7	TRAN	1	13.99	3250	2340	3	0.56	188.69	0.613242	2
8	DP	0.85	14.84	755	0	1	0.39	205.92	0.132151	2
9	TRAN	1.25	16.09	3640	2840	3	0.62	186.71	0.849527	2
10	DP	1.25	17.34	760	0	1	0.39	205.40	0.195126	2
11	TRAN	0.42	17.76	3900	2850	3	0.67	185.08	0.30316	2
12	DP	3.17	20.93	980	0	1	0.50	195.10	0.606093	2
13	TRAN	0.33	21.26	3180	2460	3	0.54	190.14	0.19953	2
14	DP	1.58	22.84	1450	0	2	0.37	209.08	0.479001	1
15	TRAN	0.75	23.59	3450	2620	3	0.59	184.56	0.477537	1
16	DP	3.92	27.51	1000	0	1	0.51	193.86	0.759924	2
17	TRAN	1.42	28.93	3950	2720	3	0.68	184.77	1.036353	2
18	DP	0.5	29.43	1170	0	2	0.30	223.81	0.13093	1
19	TRAN	0.33	29.76	2200	1620	2	0.56	187.66	0.136239	0
20	DP	0.25	30.01	950	0	1	0.49	196.96	0.046778	1
21	TRAN	10	40.01	1720	1100	2	0.44	202.54	3.483702	1

4.6.3 Discussions and conclusions

It has been demonstrated that the short-term unit commitment optimization can provide a practical and efficient method to reduce the operational costs of the marine power plant, including the reduction in the risk of blackout.

Clear indication of regions where these costs can be minimized is provided. In the case study for *Viking Energy* offshore supply vessel, it has been demonstrated that about 1.0 ton of fuel can be saved per 40 hours operation. This is equivalent to 6% savings (PMS solution 5 in Table 4.4) or about 2 000 NOK per 40 hours operation.

The PSV may be in the operation 60 to 90% of the time, which is equivalent to about 5200 to 7800 hours per year, see e.g. Ådnanes (2005). Thus, there is a potential for about 130 to 200 tons of fuel saved per year of operation for this vessel, or about 260 000 to 400 000 NOK/year. In the 20 year period, this is equivalent to 5 to 8 millions of NOK per vessel.

Chapter 5

Propulsion load limiting control

5.1. Motivations

Depending on the consumer type, operation and susceptibility to weather conditions, consumers might draw different levels of load from the network and thus induce load fluctuations with different oscillation frequencies. For some of these load fluctuations, the generators may not be able to keep steady frequency. This is demonstrated through the simulations. Higher frequency load fluctuations, not considered in the optimization of operational costs in Chapter 4, may make high frequency and voltage fluctuations in the marine network. These fluctuations may have detrimental effect on the consumers supplied from the network. Moreover, the power fluctuations may increase the mechanical and thermal stress on prime movers, in addition to an increase in the fuel consumption.

A *quasi-static load limiting control strategy* is proposed in this thesis. The proposed controller can be used to reduce the frequency and power fluctuations in the power electrical network and to prevent excessive mechanical stress on the individual thrusters. The proposed *quasi-static load limiting controller* is based on the measurement of the frequency fluctuations on the network, thruster shaft accelerations, and off-line prediction and on-line real time estimation of propeller thrust losses.

5.1.1. Risk of the blackout

The risk of the blackout will increase with the level of frequency fluctuations in normal faultless conditions. Since the vessel may be subjected to harsh weather conditions, the blackout prevention control must be regarded to the dynamic environmental conditions as well. However, the *quantity of load reduction* in Chapter 3 is determined assuming steady network load, i.e. nearly constant frequency and voltage. If the frequency drops below the nominal in the pre-fault conditions, this will shorten the control action response time limits for the FLR. The permitted frequency drop defined in (3.4) will be changed due to frequency fluctuations in the following way:

$$\Delta\omega_{FLR,gi} = \Delta\omega_{gi}^{\max} - \Delta\omega_{en,gi}\left(\Delta P_{gi}\right) - \Delta\omega_{gi}^{\mathrm{osc}}, \tag{5.1}$$

where $\Delta\omega_{gi}^{\mathrm{osc}}$ is the oscillating frequency deviation from the nominal ω_{0gi} in the normal (i.e. pre-fault) conditions, initiated only by the load variations due to external disturbances.

When network load and frequency fluctuations are present, t_{SL} and $P_{tran,gi}(t_{FLR})$ defined in (3.7) and (3.8), together with the equations defined later on in Chapter 3 will be reduced due to the oscillating frequency deviation $\Delta\omega_{gi}^{\mathrm{osc}}$. If $\Delta\omega_{gi}^{\mathrm{osc}}$ is not introduced into the calculations, as is the typical practice today, the limits determined in Chapter 2 and Chapter 3 would be

correct only for the steady (static) network loading.

Thus, the risk of blackout will increase with limited ability of the generating sets to respond to a variable power demand. Having more generators operating online will lower the load variations sensed by the generators, decrease $\Delta\omega_{gi}^{osc}$ and thus decrease the risk of blackout due to:

– Increase in the system inertia H_k;
– Disturbance distribution on generators i.e. lower load participation per generator.

However, the fuel consumption may increase as the engines are required to operate further from their optimal operating regions. Moreover, an increase in the fuel consumption may be generated by large load fluctuations on the engines. In addition, load fluctuations on diesel engines are directly responsible for increased thermal and mechanical stress.

5.1.2 Diesel engine transient fuel consumption

According to (5.1) the fuel consumption depends on the break specific fuel consumption (BSFC) $b_{e,gi}$, equivalent to the efficiency of prime mover. For diesel engines operating in steady state conditions, $b_{e,gi}$ is typically as calculated in Chapter 4.

Large load fluctuations on the network may affect the fuel consumption for the prime movers of the generating sets. According to Lindgren (2005), Hansson *et al.* (2003) and He and Jang (2006), a correction factor is added to accommodate the changes in diesel engine speed and torque during transients:

$$FC_{gi}^{tran}\left(P_{gi}\right) = FC_{gi}^{stat}\left(1 + CR_{gi}^{tran}\right), \tag{5.2}$$

where *FC* is the fuel consumption, superscript *tran* in (5.2) is used for engine transient conditions and *stat* for static i.e. steady state conditions, as determined in Chapter 4. *CR* is the correction factor for transient operations.

In Lindgren (2005), the effects of transient loads on the fuel consumption were investigated in the full scale. The additional fuel consumption due to transients on engines for agriculture tractors varied from 0.3% for the fairly static transport operation up to approximately 13% during front end loading. The two other operations studied, resulted in a decreased fuel efficiency of approximately 3 and 7% respectively. One can notice that the real fuel savings will be even higher than calculated here, as demonstrated in Lindgren (2005) on the full scale engine trials.

The simplified model that accounts for the load dynamics, taken from He and Jang (2006), is defined:

$$\begin{aligned} b_{e,gi}\left(P_{gi}\right) &= b_{e,gi}^{s}\left(P_{gi}\right) + b_{e,gi}^{d}\left(P_{gi}\right) \\ &= b_{e,gi}^{s}\left(P_{gi}\right) + b_{e,gi}^{s}\left(P_{gi}\right)\frac{k}{3600}\left(\frac{d}{dt}P_{gi}\right)^{2} \end{aligned} \tag{5.3}$$

$$b_{e,gi}^{s}\left(P_{gi}\right)=c_0+c_1\frac{P_{gi}}{P_{r,gi}}+c_2\left(\frac{P_{gi}}{P_{r,gi}}\right)^2,$$

where the transient correction coefficient is $k = 7\cdot10^{-4}$ $(\mathrm{kW/s})^{-2}$.

5.2 Classification of network load disturbances

Depending on the level of increased blackout risk, the dynamic power disturbances on the generators caused by the consumers can be separated in the following main groups (Radan *et al.*, 2006b):

1. *Static disturbances* due to ship operations and service functions such as:
   - Servo-motors for the various hydraulic systems: winches, steering gear, etc.;
   - Pumping, compressing, ventilation;
   - Heating, air-conditioning, etc;
2. *Low-frequency disturbances*:
   - Disturbances due to thruster loadings;
   - Crane operations;
   - Drilling loads (dependent on sediments)
   - Other systems;
3. *Medium-frequency fluctuations*:
   - Fluctuations due to the propeller thrust/torque loss effects, transmitted through electrical thrusters;
   - Active heave compensation fluctuations;
   - Fluctuations from impact from the first order wave loads acting on the vessel both during DP operations and in transit;
4. *High-frequency fluctuations*:
   - Fluctuations in the range of the cylinder combustion frequency, affecting the engine torque;
   - Fluctuations in the range of propeller-blade frequency, affecting the mechanical torque on the electrical thrusters;
   - Various fast changing electric effects in the network, e.g. current and voltage harmonic distortions;
   - Noise, measurement error.

These considerations are important in order to separate the quasi-static or slowly varying power disturbances from the dynamic disturbances. The dynamic power level primarily can be estimated from the weather conditions.

Static disturbances

Disturbances due to the ship operations and service functions are usually slowly varying, i.e. they may be considered as static. They mainly depend on the required operations but may also be affected by the weather conditions. For deteriorating weather conditions, the static disturbances may increase the level but the frequency usually does not change significantly.

Low-frequency disturbances

Low-frequency disturbances are typically disturbances due to thruster loadings. Thruster loading is commanded from the thrust allocation system in the DP control system or from the navigating bridge to set speed of the vessel.

The DP system keeps the vessel heading and position where the heading and position are affected by 2nd order wave loads, wind and current loads, with periods higher than about 15 seconds. The level and frequency of these disturbances are mainly determined by the DP controller response to vessel disturbances and the load rate limits set on the thrusters. The load rate limits can decrease the load variations to an acceptable level, as described in Chapter 2.

Medium-frequency fluctuations

Medium-frequency fluctuations or wave encounter frequency fluctuations are caused by the vessel motions in waves. Medium frequency fluctuations are in the range of the vessel wave encounter frequency; typical motion periods are 4 to 12 seconds.

For a vessel operating in harsh seas, these fluctuations may result in fatigue and failure of the mechanical parts, while the mean available thrust may be considerably reduced (Koushan, 2004). These disturbances may also cause large frequency variations on generators and affect the blackout resistance. Typically, the proportional-integral (PI) controller is used to keep propeller speed on thrusters close to the reference, see Sørensen et al. (1997); Smogeli (2006) and the references therein.

High-frequency fluctuations

High-frequency fluctuations in the range of the propeller-blade frequency will be mostly filtered by the power system due to the motor and generator inductances and inertia of the rotating parts. Therefore, high-frequency fluctuations will not be part of the network load analysis scheme since they do not affect the blackout risk or the fuel consumption. However, these fluctuations induce vibrations and increase the wear-out rate on transmission components on thrusters, engines and generating-sets. In this way, high frequency fluctuations may increase the risk of component failure. Problems related to speed control of thrusters with regards to high frequency and medium frequency torque fluctuations will be described more in detail in Chapter 8.

5.2.1 Propeller loads and losses

As described above, the propeller load variations are affecting the power system on two important levels:

- Thruster loadings – controllable from DP control system or vessel speed setting;
- Thruster losses – non-controllable if standard PI speed controller is used on thrusters. The same applies for controllable pitch propellers operated with constant or varying speed

The propeller load variations will be further analyzed in Section 5.3.

5.2.2 Other loads

Other loads typically include hotel load (accommodation), drilling loads, compressors, deck equipment e.g. winches, auxiliary equipment (pumps and compressors for prime movers) cranes, and similar. Most of these loads can be considered as static or low frequent if not affected by the vessel motion in waves.

5.2.3 Active heave compensation

Heave compensation is a system for increasing the control over a suspended object when it is moved to and from the seabed by a ship. It relies on eliminating the vessel vertical movement, so that the object itself moves much more controlled.

The frequency of load fluctuations with active heave compensation control will be in the range of the heave motion frequency of the local point in the vessel from where the module is lowered. Therefore, the crane with active heave compensation control will generate the medium-frequency disturbances on the power network.

5.3 Propeller loads

5.3.1 Propeller loads and power system dynamics

The power consumption for most of the consumers mainly depends on the vessel's operational conditions. However, for the propulsion system it will be strongly influenced by the weather conditions as well. Thrusters are the largest consumers, and they can consume up to 80 to 90% of the total installed power. Hence, the power fluctuations on the generators are mainly due to the power variations of the propulsion system. These variations can be determined from the thruster loading and losses. Thrust loss effects and the design of propulsion control strategies for electrically driven propellers in normal and extreme conditions have been dealt with in Sørensen *et al*. (1997); Smogeli *et al*. (2004), Bakkeheim *et al*. (2006), Radan *et al*., (2007a), Pivano *et al*. (2007), and Smogeli (2006).

The following thruster control plant model is used for the control (Smogeli *et al*., 2004):

$$\frac{d}{dt}\omega_p = \frac{1}{J_p}\left(Q_{mp} - Q_{ap} - Q_{fp}\right), \tag{5.4}$$

where J_p is the moment of inertia of the shaft, motor, gear, propeller, and added mass of the propeller, Q_{mp} is the motor torque, Q_{ap} is the load torque, and Q_{fp} is the friction torque. The following propeller load torque model, as given in Smogeli (2006), is used for the analysis:

$$\begin{aligned} Q_{ap} &= Q_{0p}\beta_{loss,p}\left(V_{ap}, \omega_p, h_p\right) \\ &= \frac{1}{4\pi^2} K_{Q0p}\rho D_p^5\ \omega_{0p}^2 \beta_{loss,p}\left(V_{ap}, \omega_p, h_p\right), \end{aligned} \tag{5.5}$$

where β_{loss} is the torque loss factor for the ventilation, in-and-out-of-water effects, and inline water inflow losses. The torque loss factor can also be denoted as $\beta_{loss} = Q_a/Q_0$. Different notation is used to distinguish a modeled real value of torque loss from its statistics-based expectation. It is important to notice that β_{loss} will not be influenced by the change in Q_{0p} if the vessel speed does not change significantly, as is the case in DP.

With torque loss substituted, (5.4) is written:

$$\frac{d}{dt}\omega_p = \frac{1}{J_p}\left(Q_{mp} - \frac{1}{4\pi^2}K_{Q0p}\rho D_p^5\ \omega_{0p}^2\beta_{loss,p} - Q_{fp}\right). \tag{5.6}$$

If perfect shaft speed control on thruster is assumed, $d\omega_p/dt = 0$, and the friction is assumed to be insignificant $Q_{fp} = 0$, the following equation holds:

$$P_{mp} = \frac{1}{4\pi^2}K_{Q0p}\rho D_p^5\ \omega_{0p}^3\beta_{loss,p} = k_1\omega_{0p}^3\beta_{loss,p}\,, \tag{5.7}$$

$$k_1 = \frac{1}{4\pi^2}K_{Q0p}\rho D_p^5\ .$$

The change in power can be expressed as:

$$\Delta P_{mp} = k_1\omega_{0p}^3\left(1-\beta_{loss,p}\right). \tag{5.8}$$

It can be noticed that the power fluctuations on the network will increase with third potential of the propeller nominal (desired) speed ω_{0p}. In other words, as thruster operates on higher load, it will have a higher potential to "pollute" the network with large load fluctuations. These fluctuations will be generated when the propeller is subjected to thrust losses operating in harsh waves.

5.3.2 Propeller thrust and torque losses

The thrust and torque losses can be determined on-line in real time, as proposed in Smogeli (2006). These losses can also be predicted using the generic approximate model derived from model tests. Such model was used in Smogeli (2006) to verify the thruster control strategies. In this thesis, the model is readjusted in order to become suitable for the probability studies, and allow the predicting thrust losses of-line, as proposed:

$$\left(Q_a/Q_0\right)_v = \begin{cases} 0, & h_p/R < -1, \\ a_1 + b_1\left(h_p/R\right), & -1 \le h_p/R < 1.1, \\ a_2 + b_2\left(h_p/R\right), & 1.1 \le h_p/R \le 1.3, \\ 1, & h_p/R > 1.3. \end{cases} \tag{5.9}$$

where Q_{0p} is the nominal torque on the propeller, and $Q_a/Q_0 = \beta_{loss,p}$ is the torque loss factor that, when multiplied with nominal torque Q_0, will give the estimated (predicted) torque amplitude peak during the ventilation.

The coefficients for an open propeller are: $a_1 = 0.143 = b_1$, $a_2 = -3.55$, $b_2 = 3.5$ if $n = n_{max}$ ($Q_0/Q_a = 0.3$ if $h_p/R = 1.1$) and $a_1 = 0.17 = b_1$, $a_2 = -3.226$, $b_2 = 3.255$ if $n \approx n_{crit}$ ($Q_0/Q_a = 0.36$, $h_p/R = 1.1$).

The vessel in DP operations and maneuvering will be subjected to strong ventilation propeller loss effects due to low propeller advance number J_a, i.e. low vessel speed and high propeller shaft speed, $n > n_{crit}$, where typically $n_{crit} = 0.4 - 0.5\ n_{max}$.

When the vessel is in the transit mode, the propeller will have mostly high J_a and in-and-out-of-water torque loss effects will become more pronounced. With high J_a, the propellers will be in the *partially ventilated regime* or sub-critical regime (Young & Kinnas 2003, Koushan, 2004). Based on the representation of thrust loss effects given in Minsaas *et al.* (1983) a simplified piecewise linear approximation is given:

$$\left(Q_a / Q_0\right)_{pv} = \begin{cases} 0, & h_p / R < -0.48, \\ 0.32 + 0.523 h_p / R, & -0.48 \le h_p / R \le 1.3, \\ 1, & h_p / R > 1.3. \end{cases} \tag{5.10}$$

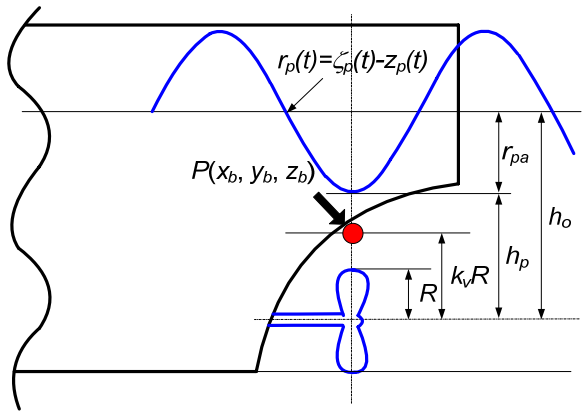

Fig. 5.1. Propeller submergence h_p on vessel fixed point $P(x_b, y_b, z_b)$

5.4 Probability of propeller torque losses

In this section, the method to determine the probability of torque losses per thruster is proposed. The probability of thrust losses will determine the expected number and intensity of torque losses on the propeller when the vessel is in harsh weather conditions. The main influencing factors on thrust losses are:

- Weather conditions, wind speed i.e. sea state;
- Position of the propeller with respect to vessel center of gravity;
- Speed of the vessel;
- Vessel-wave encounter angle.

The proposed concept is based on the marine hydrodynamic theory used to determine the vessel motion in waves. The proposed idea is demonstrated through use of linear strip-theory, see e.g. Price and Bishop (1974), Faltinsen (1990), Journee (2000), and Faltinsen (2005).

5.4.1 Torque loss occurrences

The probability of propeller emergence can be used to estimate the number of propeller thrust losses due to in-and-out-of-water or ventilation effects in one hour or in one storm lasting several hours.

When calculating the power system and thruster limits, it may be sufficient to determine the responses when e.g. the azimuthing thruster is in the position in which produces the largest thrust and torque losses. Accordingly, for the main aft propellers the azimuth angle is aligned with the central line of the vessel, and the propeller disk is positioned to the aft, in order to maximize the distance to center of gravity of the vessel x_b in (5.12). For the azimuth bow thruster the position of the propeller disk is perpendicular to the central line.

The absolute wave displacement at point P is determined by:

$$\zeta_p = \zeta_a \cos(\omega_e t - \frac{\omega^2}{g} x_b \cos\mu) , \tag{5.11}$$

where ζ_a is the wave amplitude, ω is the wave frequency, ω_e is vessel-wave encounter frequency, μ is the relative vesselwave heading angle, and g is the acceleration of gravity. The harmonic vertical relative displacement r_p, of the point $P(x_b, y_b, z_b)$ fixed to the ship coordinate system, with respect to the undisturbed wave surface, can be obtained from:

$$r_p = \zeta_p - z_p = \zeta_p - z + x_b\theta - y_b\phi = r_{pa}\cos(\omega_e t + \varepsilon_{r_p\zeta}) , \tag{5.12}$$

where z_p is the absolute vertical displacement of the point P. The spectral density of the vertical relative displacement at the point P is given by:

$$S_{r_p}(\omega) = \left(\frac{r_{pa}}{\zeta_a}\right)^2 \cdot S_\zeta(\omega) , \tag{5.13}$$

where $S_\zeta(\omega)$ is the wave power spectrum. The spectral moments are:

$$m_{nr_p}(\omega) = \int_0^\infty S_{r_p}(\omega) \cdot \omega_e^n d\omega \text{, with: } n = 0,1,2,\ldots \tag{5.14}$$

Using the Rayleigh distribution, the short term probability of propeller thrust loss in a given storm condition is:

$$\Pr\left\{r_{pa} > h_0 - k_v R\right\} = \exp\left(-\frac{\left(h_0 - k_v R\right)^2}{2m_{0r_p}}\right), \tag{5.15}$$

where h_0 is the nominal propeller shaft immersion, measured in still water, as shown in Fig. 5.1. The expected number of times per hour $N_{p,loss}$ that the thrust loss will occur due to water surface proximity in a certain sea state can be determined from the short term probability (Price and Bishop, 1974):

$$N_{p,loss} = N_p \cdot \Pr\left\{r_{pa} > h_0 - k_v R\right\}, \tag{5.16}$$

where N_p is the total number of zero-crossings per hour:

$$N_p = \frac{3600}{2\pi}\sqrt{\frac{m_{2r_p}}{m_{0r_p}}}. \tag{5.17}$$

The mean period for the total number of zero-crossings in one hour can be calculated using:

$$\overline{T}_{zp} = \frac{3600}{N_p} = 2\pi\sqrt{\frac{m_{0r_p}}{m_{2r_p}}}. \tag{5.18}$$

The significant amplitude is defined as:

$$r_{pa1/3} = 2 \cdot \sqrt{m_{0r_p}} = 2 \cdot RMS. \tag{5.19}$$

The relative torque is a function of propeller relative submergence:

$$\left(Q_a / Q_0\right) = f\left(h_p / R\right). \tag{5.20}$$

In (5.15) $k_v \in [-1,1.3]$ is the selected value of h_p/R. The relative submergence can be expressed as the inverse of relative torque:

$$h_p / R = \left(Q_a / Q_0\right)^{-1}\left(h_p / R\right), \tag{5.21}$$

and the relative propeller submergence can be directly related to the relative torque in the probability:

$$\Pr\left\{\left(Q_a / Q_0\right) < q_h\right\} = \exp\left(-\frac{\left(h_0 - \left(Q_a / Q_0\right)^{-1} R\right)^2}{2m_{0_{r_p}}} \right). \tag{5.22}$$

This is the probability that the relative torque Q_a/Q_0 will be lower than a certain threshold $q_h \in [0, 1]$.

Using the inverse functions in the probability allows using the thresholds expressed through the relative torque values q_h instead of $h_0 - k_v R$ as in (5.15). The inverse function for the partial ventilation torque loss effects in (5.10) is:

$$\left(h_p / R\right)_{pv} = \begin{cases} -1, & \left(Q_a / Q_0\right) < 0, \\ 1.91\left(Q_a / Q_0\right) - 0.61, & 0 \le \left(Q_a / Q_0\right) \le 1, \\ 1, & \left(Q_a / Q_0\right) > 1. \end{cases} \tag{5.23}$$

The inverse functions for other torque loss effects can be derived in a similar way. The expected number of thrust loss incidents is calculated by:

$$N_{p,loss} = N_p \cdot \Pr\left\{\left(Q_a / Q_0\right) < q_h\right\}. \tag{5.24}$$

5.4.2 Results and discussion

In Figs. 5.2 and 5.3, the following case studies for standard size L=70 meters offshore supply vessel (OSV) operating in DP with zero speed V_s=0 knots are presented:

- $Q_a / Q_0 < 0.3(Q_a / Q_0)_{\max}$ for the two nearby main aft propellers, in Fig. 5.2;
- $Q_a / Q_0 < 0.3(Q_a / Q_0)_{\max}$ for the stern propeller and bow tunnel thruster, in Fig. 5.3.

From Fig. 5.2 it can be noticed that the motions for the two nearby propellers are very correlated, especially in head waves, μ = 120 to 240 deg. Contrary, the motions between the aft and bow thrusters are not correlated, as can be seen in Fig. 5.3. While the aft thruster may have very large number of thrust and torque losses the bow thruster will have a very low number. This number is directly proportional to the vessel slamming occurrence, see e.g. Price and Bishop (1974), Faltinsen (1990), Journee (2000), and Faltinsen (2005).

The correlation between thruster motions indicates the nature of the power transient transfer from the propulsion system to the power network. For highly correlated thrusters, the power transients will mainly appear at the same time on the network, and thus will superimpose as a joint disturbances. On the other hand, uncorrelated motions, such as those between the aft and bow thrusters will appear more or less independently on the network. In other words, uncorrelated transients will be most of the time out-of-phase while the correlated transients will be in-phase. Then, it can be assumed that uncorrelated transients will not superimpose as joint disturbances on the network, and the majority of disturbances will appear separately in time. The frequency of disturbance occurrence generated by the thrust losses will be higher in this case but the level will be lower.

The number of torque loss occurrences N_{loss} per hour, in the whole region $0 \le (Q_a/Q_o)_p \le 1.0$, is compared for two different operating modes of the OSV:

– DP mode, zero speed V_s =0 knots, presented in Fig. 5.4;
– Transit mode, V_s =13 knots, presented in Fig. 5.5.

Fig 5.4 presents the mappings for the number of all torque loss occurrences N_{loss} for aft propeller, with respect to ship's heading and torque loss factor Q_a/Q_0, for the offshore supply vessel in transit operation, speed V_s =13 knots, waves H_w=4.9 m. Fig 5.5 presents the N_{loss} mappings for the same propeller and the same weather conditions, but for DP operations with zero vessel speed, V_s =0 knots. It can be noticed from Fig. 5.4 that the most of torque losses will have low torque loss factor Q_a/Q_0, i.e. about N_{loss} = 35 torque losses will occur per hour, where each will be higher than Q_a/Q_0 > 0.9, meaning that 35 fluctuations cannot be higher than 10% nominal torque. About N_{loss} = 15 per hour torque losses will have Q_a/Q_0 > 0.8, i.e. the load fluctuations lower than 20% nominal torque. In Fig. 5.5 it can be noticed that about 150 torque loss occurrences per hour will have Q_a/Q_0 > 0.3, i.e. the load fluctuations lower than 70% nominal torque. This is due to special effect of ventilation where the abrupt torque loss of more than 70% happens with every ventilation occurrence.

When the vessel is in DP operations, subjected to following waves, μ = 300 to 60 deg, significant increase in number of torque loss occurrences N_{loss} can be noticed from Figs. 5.4 and 5.5. In addition, the torque losses are more pronounced, and the expected torque loss factor Q_a / Q_0 = $\beta_{loss,p}$ for the ventilation occurrence may be higher than 70% nominal. It appears that most of the thrust losses in DP are generated when the vessel is in the following waves (i.e. μ = 270 to 90 deg,). However, when the vessel is in transit operation, then the head waves will transfer more thrust loss effects, as expected.

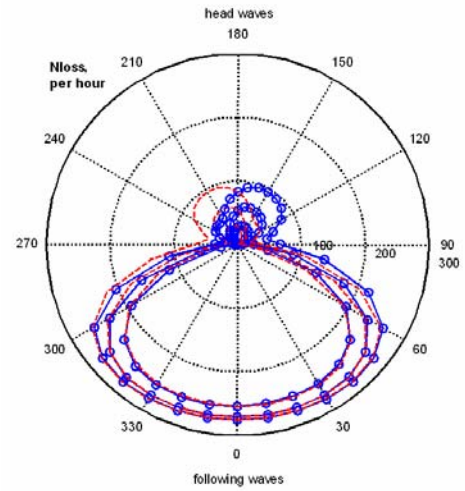

Fig. 5.2. Number of ventilation occurrences per hour with Q_a/Q_0<0.3$(Q_a/Q_0)_{max}$ for the two nearby main aft propellers, OSV, L=70 m, speed V_s=0 knots

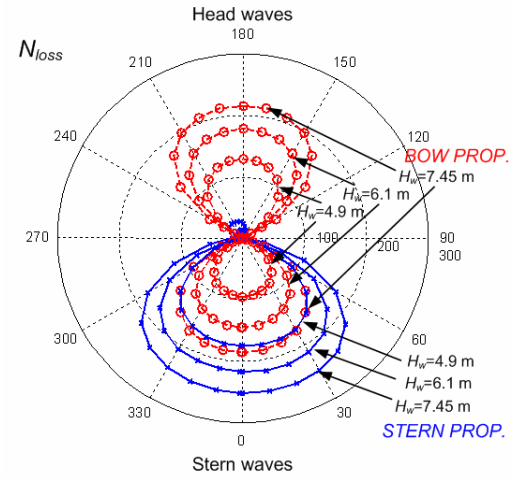

Fig. 5.3. Number of ventilation occurrences per hour with Q_a/Q_0<0.3$(Q_a/Q_0)_{max}$ for stern propeller (—) and bow tunnel thruster (-o-), OSV, L=70 m, speed V_s =0 knots

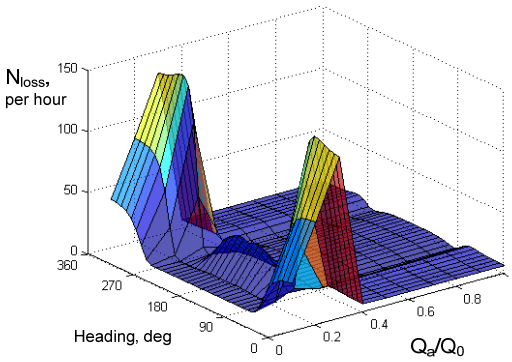

Fig. 5.4. Number of all torque loss occurrences N_{loss} for aft propeller, with respect to ship's heading and relative torque loss Q_a/Q_0, for OSV in DP operations, L=70 m, speed V_s =0 knots, waves H_w=4.9 m

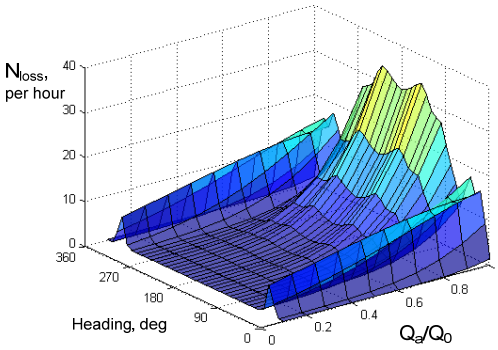

Fig. 5.5. Number of all torque loss occurrences N_{loss} for aft propeller, with respect to ship's heading and relative torque loss Q_a/Q_0, for OSV in transit, L=70 m, speed V_s =13 knots, waves H_w=4.9 m

5.5 Quasi-static thruster load limiting control (real-time)

In this section, a controller for propulsion load limiting based on the network load fluctuations is proposed. When the propellers are subject to large thrust losses, the proposed controller can reduce the load fluctuations on the thrusters and the network, and thereby prevent excessive wear-out and damage of thruster power transmission parts.

5.5.1 Load fluctuations sensitivity to thrust

The dependence of nominal power on nominal thrust is expressed through the following equation (Sørensen *et al.*, 1997):

$$P_{0,p} = \frac{2\pi K_{Q0p}}{\rho^{1/2} D_p K_{T0p}} T_{0,p}{}^{3/2} = \text{const. } T_{0,p}{}^{3/2}. \tag{5.25}$$

The dependence of power load fluctuations to thruster speed in found from (5.8). Thus, the sensitivity of the power fluctuation amplitude to changes in the propeller speed is expressed:

$$\frac{\partial \Delta P_{mp}}{\partial \omega_p} \approx 3\ k_1 \omega_{0p}^2 \left(1 - \beta_{loss,p}\right), \tag{5.26}$$

where the changes in the friction torque may be disregarded. The nominal propeller thrust is expressed as (Sørensen *et al.*, 1997):

$$T_{0,p} = \frac{1}{4\pi^2} \rho D_p^4 K_{T0p} n_{0,p}^2 = k_2 \omega_{0,p}^2, \tag{5.27}$$

$$k_2 = \rho D_p^4 K_{T0p},$$

and the thrust sensitivity to changes in the speed can be compared through:

$$\frac{\partial T_{0,p}}{\partial \omega_p} = 2k_2\omega_{0,p}\,. \tag{5.28}$$

From the above equations, it can be noticed that the power load fluctuations on the network will drop with the square of propeller nominal speed ω_{0p}, while the thrust will drop linearly with ω_{0p}. Comparing the changes in the power fluctuations (5.26) with the changes in the nominal thrust (5.28) the following equation is obtained:

$$\frac{\partial \Delta P_{mp}}{\partial T_{0,p}} \approx \frac{3k_1}{2k_2}\omega_{0p}\left(1-\beta_{loss,p}\right) \approx \frac{3D_pK_{Q0p}}{8\pi^2K_{T0p}}\omega_{0p}\left(1-\beta_{loss,p}\right). \tag{5.29}$$

Thus, the sensitivity of decreasing thrust to reduce the load fluctuations on the network will linearly increase with the nominal speed of the propeller.

5.5.2 Thruster load limiting controllers

The propulsion capacity is typically limited based on the static level of the available power and blackout prevention capabilities, see e.g. (2.48) in Chapter 2. The propulsion must be limited if the available power becomes negative, i.e. $P_{s,th} < P_{th} \rightarrow P_{av,start} < 0$ or $P_{start,gi}\left(k, N_f\right) - P_{gi} < 0$. As explained in Chapter 2, P_{av} and P_{gi} have to be filtered in order to determine the average values and reject the load fluctuations. Thus, the load limiting control will have steady, smooth and relatively slow responses.

In this section, a new modified allowable propulsion control limit is proposed. It consists of a static (existing) and a dynamic (proposed) part:

$$\begin{aligned} &P_{s,thp}\left(P_{th}, P_{av,start}, P^{\max}_{\text{cont},gi}, P_{gi}, P_{rgi}, \partial\Delta P_{pm}/\partial T_{0p}, \Delta\omega_g, \Delta\omega_p, \beta_{loss,p}\right) \\ &= P_{s,thp}\left(P_{th}, P_{av,start}, P^{\max}_{\text{cont},gi}, P_{gi}, P_{rgi}\right) + P_{d,thp}\left(\partial\Delta P_{pm}/\partial T_{0p}, \Delta\omega_g, \Delta\omega_p, \beta_{loss,p}\right), \end{aligned} \tag{5.30}$$

where the dynamic part depends on the sensitivity of the power load fluctuations to nominal thrust $\partial\Delta P_{pm}/\partial T_{0p}$, network frequency fluctuations $\Delta\omega_g$, and torque losses $\beta_{loss,p}$ or propeller shaft speed fluctuations $\Delta\omega_p$. The static part is determined in the (2.30).

The dynamic part of load limiting control law will be determined for each propeller independently:

$$P_{d,thp} = L_{d,thp}P_{thp}\,. \tag{5.31}$$

All proposed controllers will be based on the network frequency fluctuations. Although the frequency is easily available to measure, the problem may be to know which thruster is injecting more disturbances to the network and requires higher load reduction than the others. Thus, the controller design will be based on the analysis conducted in the proceeding section as:

$$L_{d,th} = L_{d,th}\left(\Delta E_{pm}, \delta E_{p,loss}, \partial \Delta P_{pm} / \partial T_{pm}\right)$$
$$= -k_{thp1}\left(\partial \Delta P_{pm} / \partial T_{p}\right)\frac{1}{t}\int_{0}^{t}\left(Q_{mg} - Q_{eg}\right)^{2} dt. \tag{5.32}$$

where k_{thp1} is the controller gain, and Q_{mg} and Q_{eg} are the mechanical and electrical torque on the generators, respectively, defined in Chapter 3. The proposed controller theoretically accounts for a variety of important effects, as depends on the following:

- Sensitivity of power fluctuations to developed thrust;
- Propeller shaft accelerations;
- Energy loss in the network due to network frequency fluctuations.

In the following sub-sections, these effects will be quantified i.e. available from the measurements. The energy loss in the network can be directly obtained from the generator torque balance i.e. shaft acceleration.

5.5.3 Load limiting controller based on the probability of torque loss

Based on the (5.29), the torque loss occurrences below the threshold are proportional to the average torque losses and the following applies:

$$\frac{\partial \Delta P_{mp}}{\partial T_{0,p}}\left(q_{h,p}\right) \approx \text{const.}\ \omega_{0p}\left(q_{h,p} - \beta_{loss,p}\right) = \omega_{0p} f\left(N_{loss,p}\left(\beta_{loss,p} < q_{h,p}\right)\right), \tag{5.33}$$
$$N_{p,loss}\left(\beta_{loss,p} < q_{h,p}\right) = N_{p}\ \Pr\left\{\left(Q_{a} / Q_{0}\right) < q_{h,p}\right\}.$$

The proposed load limiting control law is based on the probability of torque loss:

$$L_{d,th} = -k_{thp1}\left|\omega_{0p}\right|\ N_{p,loss}\left(q_{h}, V_{s}, H_{w}, \mu\right)\frac{1}{t}\int_{0}^{t}\left(Q_{mg} - Q_{eg}\right)^{2} dt, \tag{5.34}$$

where $q_{h,p}$ is the threshold to account for high intensity fluctuations and disregard low intensity fluctuations. The vessel speed V_s, observed wave height H_w, and heading to the waves μ, are to be provided from the vessel management system (VMS). A high accuracy of the required information is not necessary for the controller. The H_w can be related to the wind speed assuming wind generated waves, see e.g. Journee (2001).

In the proposed control law, the sensitivity of power fluctuations to changes in propeller thrust is expressed using the probability of thrust loss occurrence, i.e. parameter $N_{loss,p}$, derived in Section 5.4 (Radan *et al.*, 2006b).

5.5.4 Load limiting controller based on the real-time torque loss

In (5.33) the probability based $N_{loss,p}$ is substituted for $q_{h,p} - \beta_{loss,p}$. The proposed control law accounts for the average value of $q_{h,p} - \beta_{loss,p}$ as proposed in Fig. 5.6:

$$\begin{aligned} L_{d,th} &= -k_{thp1} \left|\omega_{0p}\right| \Delta\overline{\beta}_{loss,p} \frac{1}{t}\int_0^t \left(Q_{mg} - Q_{eg}\right)^2 dt \\ &= -k_{thp1} \left|\omega_{0p}\right| \Delta\overline{\beta}_{loss,p} \frac{1}{t}\int_0^t \left(\frac{d}{dt}\omega_g\right)^2 dt, \\ \Delta\overline{\beta}_{loss,p} &= \left(\overline{q_{h,p} - \beta_{loss,p}}\right). \end{aligned} \tag{5.35}$$

The average relative torque loss $\Delta\overline{\beta}_{loss,p}$ can be calculated knowing only the propeller speed ω_p and the thruster torque Q_{mp}.

The average relative torque loss is obtained using low pass filtering of the estimated load torque:

$$\begin{aligned} &\Delta\overline{\beta}_{loss,p} = \Delta\hat{\beta}_{loss,p} - T_{Qf}\Delta\dot{\overline{\beta}}_{loss,p}, \\ &\Delta\hat{\beta}_{loss,p} = q_{h,p} - \hat{\beta}_{loss,p}, \\ &\hat{\beta}_{loss,p} = \frac{\hat{Q}_{ap*}}{\hat{Q}_{0p}} = \frac{4\pi^2}{K_{Q0,p}\rho D_p^5\ \omega_p^2}\hat{Q}_{ap*}, \qquad \omega_p \neq 0, \end{aligned} \tag{5.36}$$

where T_{Qf} is the low pass filter time constant, $\hat{Q}_{ap*}$ is to extended load torque estimate obtained from the propeller load torque observer:

$$\begin{aligned} \dot{\hat{\omega}}_p &= \frac{1}{J_p}\left(Q_{mp} - \hat{Q}_{ap*}\right) + l_{1p}\left(\omega_p - \hat{\omega}_p\right), \\ \dot{\hat{Q}}_{a,p*} &= l_{2p}\left(\omega_p - \hat{\omega}_p\right), \end{aligned} \tag{5.37}$$

where and l_{1p}, l_{2p} are the observer gains, and $\hat{Q}_{ap*}$ is the extended load torque that includes the friction:

$$\hat{Q}_{ap*} \approx Q_{ap*} = Q_{ap} + Q_{fp}. \tag{5.38}$$

The equilibrium point of the observer error dynamics can be shown to be globally exponentially stable (GES) in the case of a constant load torque if the observer gains l_{1p} and l_{2p} are chosen according to:

$$l_{1p} > -l_{2p}/J_p, \qquad l_{2p} > 0. \tag{5.39}$$

5.5.5 Load limiting controller based on the thruster acceleration

It has been indicated that the influence of torque losses to the propeller and the network fluctuations can be quantified using the average relative torque loss. Similar approach can be obtained using the propeller real-time measurements of the shaft speed i.e. shaft acceleration. The acceleration measurement can be used as an indication of thrust loss severity on the propeller and consequent transmission of load fluctuations to the network.

The propeller speed and load fluctuations will be in general low in low speed operation regime and significantly higher in a high speed operation regime. This can be seen from (5.6).

Propeller low speed regime

In the propeller low speed regime the standard PI speed controller should not have any problems to keep the desired speed, thus:

$$\frac{\mathrm{d}}{\mathrm{dt}}\omega_p \approx 0 \qquad \rightarrow \qquad Q_{mp} \approx \frac{1}{4\pi^2} K_{Q0p} \rho D_p^5 \, \omega_{0p}^2 \beta_{loss,p} + Q_{fp} \,. \tag{5.40}$$

Propeller high speed regime

As ω_{0p} increases, the load torque also increases, and the standard PI shaft speed controller may have problems to keep the speed ω_p close to desired ω_{0p}. In this case, the shaft acceleration $\mathrm{d}\omega_p/\mathrm{dt}$ increases proportionally with the torque unbalance $Q_{mp} - Q_{ap}$, which is more pronounced for low inertia propellers, with low J_p:

$$\left|\frac{\mathrm{d}}{\mathrm{dt}}\omega_p\right| > 0 \qquad \rightarrow \qquad \left|Q_{mp} - Q_{ap} - Q_{fp}\right| > 0 \,. \tag{5.41}$$

The torque unbalance in (5.41) is responsible for the propeller wear and tear indicating that the propeller load torque is not completely balanced by the motor torque. Thus, the shaft is subjected to fluctuations of torque. These fluctuations can induce shaft vibrations and potentially increase the fatigue and wear-out rate of power transmission parts.

One very useful property for the load limiting controller can be noticed from the above analysis. As the load torque fluctuations on the propeller become more pronounced, the shaft acceleration increases and load fluctuations with higher magnitude are transferred to the network. Thus, the load limiting controller can be based on the shaft acceleration, as an indication of large propeller load and generator torque fluctuations:

$$\begin{aligned} L_{d,th} &= -k_{thp1}\left|\omega_{0p}\right| \frac{1}{t}\int_0^t \left(Q_{mp} - Q_{ap}\right)^2 dt \, \frac{1}{t}\int_0^t \left(Q_{mg} - Q_{eg}\right) dt \\ &= -k_{thp1}\left|\omega_{0p}\right| \frac{1}{t}\int_0^t \left(\frac{d}{dt}\omega_p\right)^2 dt \, \frac{1}{t}\int_0^t \left(\frac{d}{dt}\omega_g\right)^2 dt. \end{aligned} \tag{5.42}$$

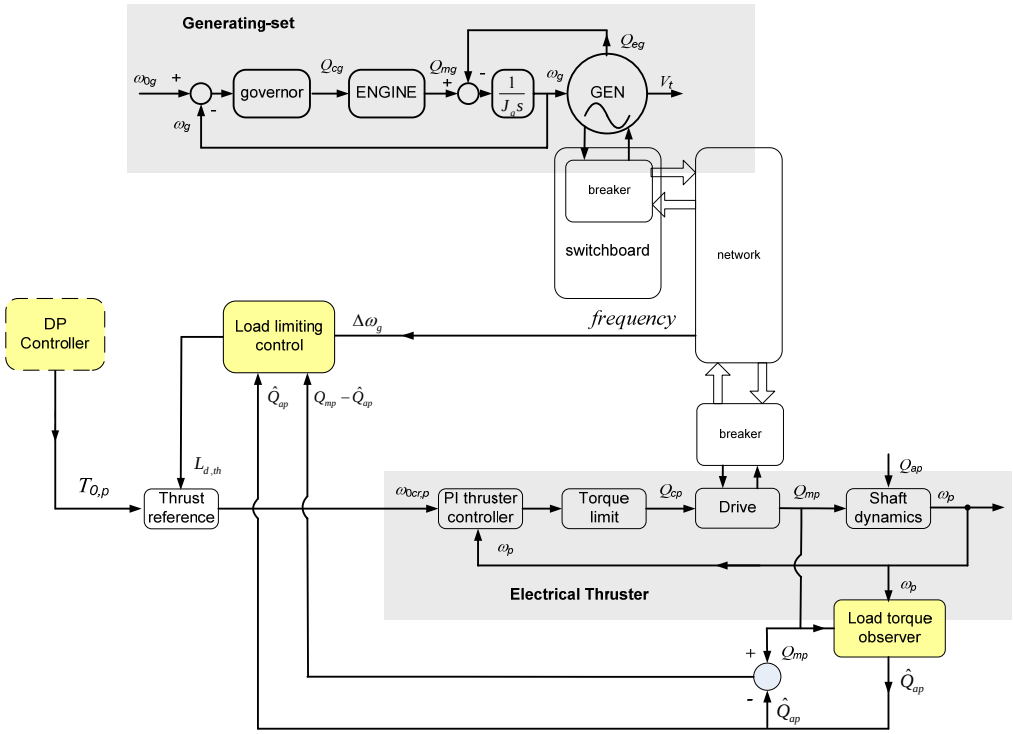

Fig. 5.6. Real-time based propulsion load limiting controllers

5.5.6 Simulation results

A case study with an offshore supply vessel has been carried out to demonstrate the proposed ideas.

A case study for the typical platform supply vessel (PSV) is presented in Figs. 5.7 to 5.12. Two 1.6 MW aft thrusters are in the operation. Two gen-sets, each 1.5 MW are online, so 3.0 MW is the power generating capacity in the system. Generators are operating in the isochronous mode, aiming to keep constant ω_{0g} and with H_k=2 seconds.

The following cases are compared:
- *Load limiting controller based on the real-time torque loss*;
- *Load limiting controller based on the thruster acceleration*;
- *No load limiting controller* – the signal from DP thrust allocation algorithm is directly fed to thruster speed reference (set-point).

Fig. 5.7 shows the speed reference on thruster 1 (upper) and thruster 2 (lower). As can be seen in Fig. 5.8, the thrust losses produce thrust and torque fluctuations on thruster 1. The thruster 2 does not have such thrust and torque fluctuations. Thus, the *load limiting controller based on the real-time torque loss* and *controller based on the thruster acceleration* will reduce the load only on bad performing thruster – the one which injects large power fluctuations to the network and having excessive shaft accelerations, and this

one is Thruster 1. Then, the frequency fluctuations will reduce as can be seen in Fig. 5.9. The propeller shaft accelerations are also controlled with these controllers, as can be seen in Fig. 5.10. The benefit of *controller based on the thruster acceleration* is that the excessive acceleration threshold can be set for the controller. This safes the thrusters extending their operating life and reducing the maintenance costs.

As the engine load fluctuations decrease, the fuel consumption will proportionally decrease. This is demonstrated in Figs. 5.11 and 5.12 where the reductions in the fuel consumption of 9 kg per hour on 2.72 MW engine is accomplished – this is equivalent to 226 – 217 / 226 ≈ 4% fuel savings. For 10 MW power plant the savings would be 33 kg per hour, or nearly 800 kg per day, or 80 tons saved fuel for 100 days/year of bad weather conditions. Assuming the cost of one ton of heavy fuel oil (HFO, 380 cSt) to be about 2100 NOK or about 350 USD this would bring the cost reductions of 80 2100 = 168 000 NOK per year of operations with one 10 MW propulsion vessel.

It is very important to notice that the set-point reference correction is much larger when the thruster is highly loaded and subjected to large thrust losses than when the thruster is on the low load and/or with low thrust losses. This is consistent with the analysis provided in this section. Moreover, it is demonstrated that the set-point correction signal can be properly filtered, preventing introduction of additional dynamics in to the control loop, see Fig. 5.7.

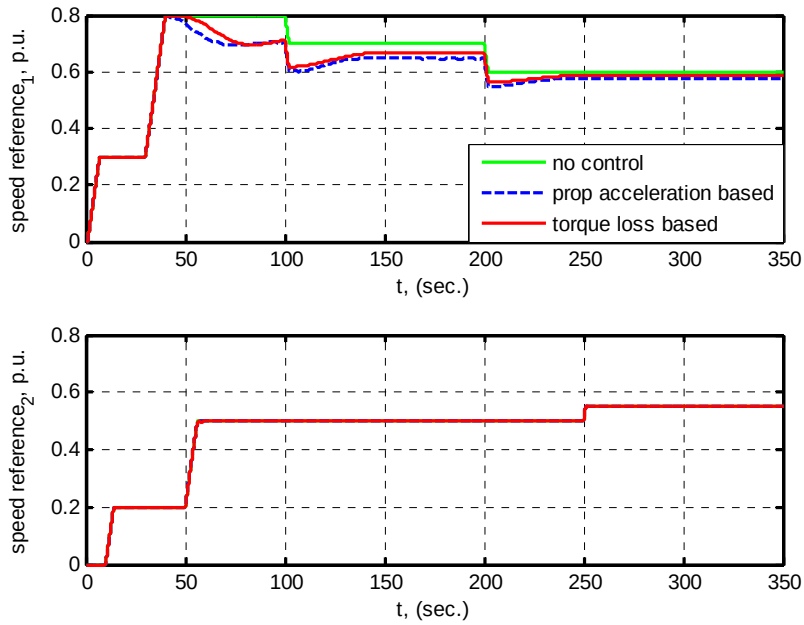

Fig. 5.7. Thruster speed reference on thruster 1 (upper) and thruster 2 (lower)

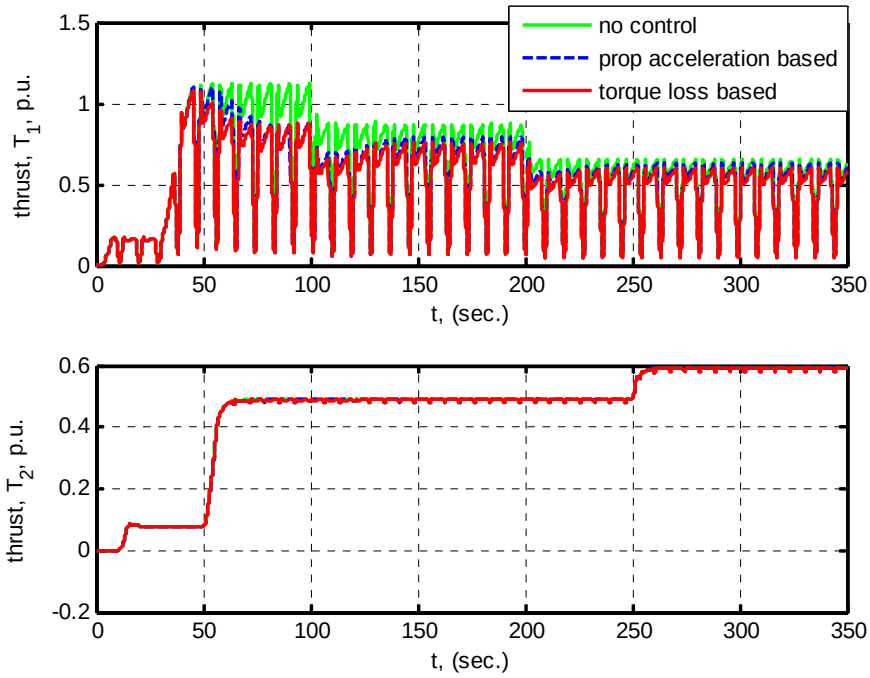

Fig. 5.8. Thrust on thruster 1 (upper, T_1) and on thruster 2 (lower, T_2)

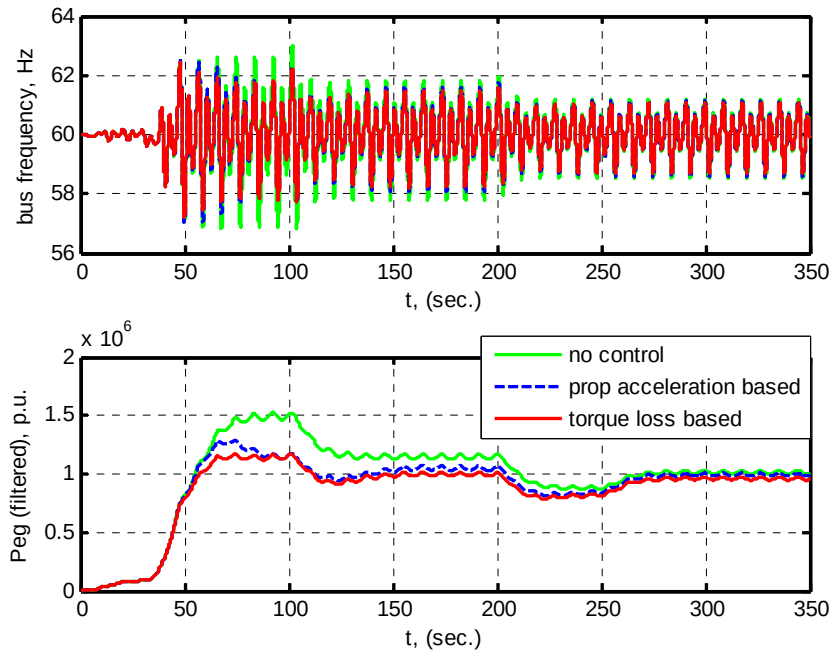

Fig. 5.9. Network (bus) frequency (upper) and network active power – filtered (lower)

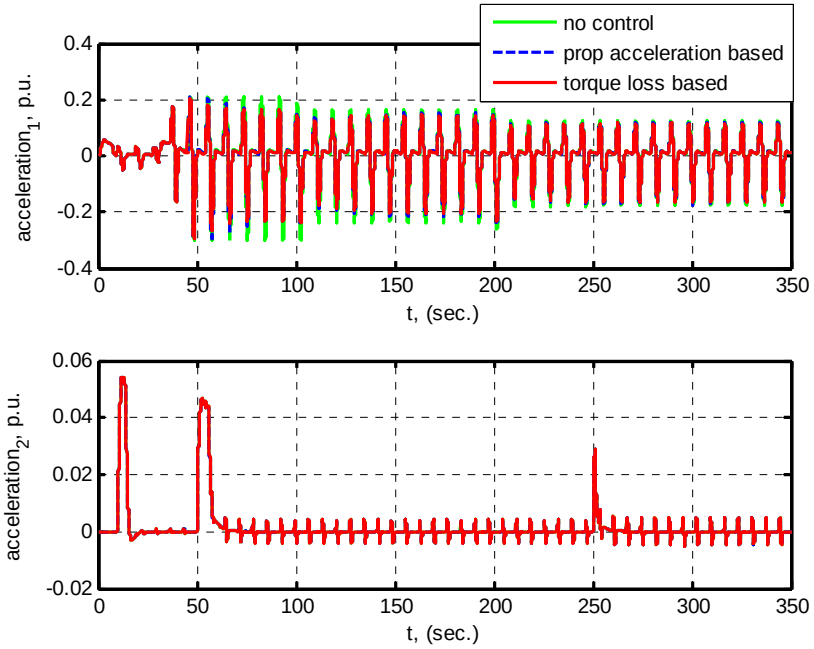

Fig. 5.10. Shaft acceleration on thruster 1 (upper) and thruster 2 (lower)

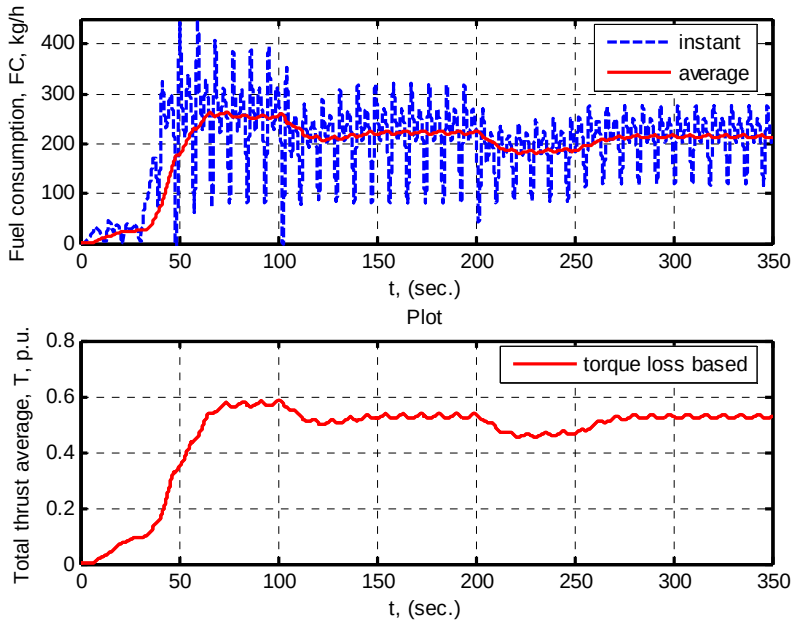

Fig. 5.11. Fuel consumption for torque loss based controller and average thrust

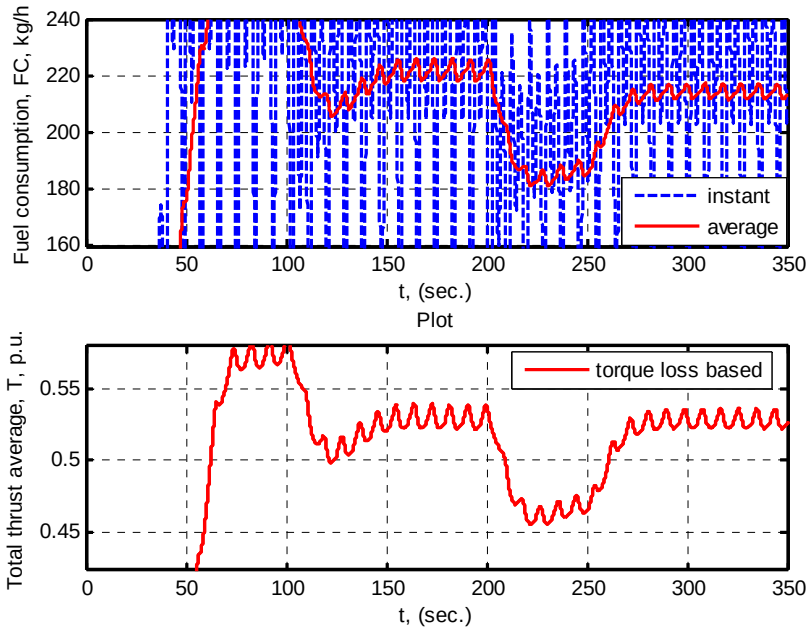

Fig. 5.12. Detail of fuel consumption for torque loss based controller and average thrust

5.6 Discussion and conclusions

In this Chapter, a *quasi-static load limiting controller* of marine propulsion is proposed. The most important advantages of the proposed control concepts are stated as follows:

- The load limiting controller is reducing the network frequency fluctuations, and propeller shaft accelerations for simulated real-time based solutions;
- With an acceleration based controller it is possible to keep the shaft accelerations within the prescribed threshold limit. This may increase the operating life of thrusters and reduce the maintenance cost;
- The fuel consumption is reduced by 4% when the load is limited on the thruster operating with excessive thrust losses and compensating with the thruster operating with low thrust losses. These savings would bring extra 3.36 mill. NOK per 20 years of operations with 10 MW engines of half load, assuming 100 days/year of bad weather operations in the North Sea;
- The potential for fuel savings may be up to 13% of fuel or 3 times more than demonstrated, according to Lindgren (2005) results with full scale on-land engine trials;
- The quasi-static propulsion load limiting controller is distributed among thrusters, i.e. the controller could be programmed within the thruster PLC as the control does not depend on the communication with other thrusters, generators or consumers. This increases the robustness of the controller;
- The load limiting controller will re-adjust the speed reference signal fed from the DP thrust allocation algorithm. Thus, the feedback about the altered set-point reference should be provided to the DP thrust allocation. Then the thrust allocation algorithm can compensate the reduced thrust by increasing the thrust on non-fluctuating thruster.

Chapter 6

Power Redistribution Control (PRC)

6.1 Motivations

In Chapter 5, the proposed *quasi-static load limiting control* is based on the measurement of frequency fluctuations on generators and thrusters and thruster torque/thrust losses. These strategies aim to limit the bad performing thrusters from injecting fluctuating loads to network and from increase in wear and tear due to excessive propeller shaft torque fluctuations. The *quasi-static load limiting control* strategies allow the use of non-fluctuating thrusters with standard PMS available power based static limits, described in Chapter 2. These slowly changing limits are fed back to DP thrust allocation algorithm which recalculates new set-points within the prescribed limits. It has been demonstrated in the simulations in Chapter 5 that the proposed strategy can reduce the load fluctuations on thrusters and network with limited success.

In this chapter, a new strategy to *completely attenuate* the frequency and voltage fluctuations on the network is proposed. The main idea is that the frequency control on marine vessel can be improved by using the dynamic feedback from the power system to the electrical thrusters. The proposed control is termed the *Power Redistribution Control* (PRC) as the control will redistribute power around nominal on individual thrusters, depending on the network frequency fluctuations.

6.2 Possibilities for reducing network power load fluctuations

In this section, possibilities for the power control on the network aiming to attenuate the frequency fluctuations on the generators will be given.

Among different solutions used in different areas of application, these are highly considered for application in the control of the network power in the marine vessel:

– *Local thruster control concepts*: independent speed/torque/power and anti-spin control with combined control for the control of marine thrusters and propellers. These control strategies have been applied or considered for the application in the marine systems, see e.g. Sørensen *et al*. (1997); Smogeli *et al*. (2004), Bakkeheim *et al.* (2006), Pivano *et al.* (2007), Radan *et al.* (2007a), and Smogeli (2006) and references therein. These control methods can provide smooth power output from thrusters subjected to large torque losses such as propeller ventilation. However, the thruster loadings and effects of multiple thrusters operating in the system are not dealt within the low level control algorithms. The local thruster controller considers only local power oscillations for each individual thruster, and the effect of multiple thrusters and other power consumers in the system is not known;

– *DP thrust allocation algorithms*: optimization algorithms capable to find optimal distribution of power (thrust) on marine thrusters, usually reducing the total power consumption on thrusters and proportionally reduce the fuel consumption. These control strategies have been applied or considered for the application in the marine systems, see e.g. Johansen (2004), Johansen *et al.* (2004a), Johansen *et al.* (2004b), Fossen and Johansen (2006), Ruth *et al.* (2007) and the references therein. The thrust allocation algorithm implies that the smooth change in the thrust references will provide smooth power transients on the power system. However, this may not be the case when propellers are subjected to large thrust and torque losses. The algorithm is limited to propulsion loads while other loads that may produce significant load fluctuations on the network have not been considered. Besides, faults and malfunctions that may affect the overall vessel response are not handled by thrust allocation algorithm.
– *Energy storage*: some form of energy storage devices such as batteries, capacitors, flywheels, etc. are used to compensate for fluctuating energy demand in the network. The optimization-based energy management systems are typically proposed to control hybrid electric (automotive) vehicles, see e.g. He and Jang (2006), Aoyagi *et al.* (2001), *Koot et al.* (2006) and references therein. The energy storage technology has not been widely applied on the marine vessels, mainly due to large size and weight considerations involved although this technology can provide energy savings and significant improvements in frequency and voltage regulation;
– *Frequency demand switching control*: utilizes control devices which will turn off and on the machine/appliance in response to frequency deviations in order to restore the supply/demand balance (Black and Ilic, 2002).

A new *power redistribution controller* (PRC) is proposed in the thesis. PRC is reducing the load fluctuations on the vessel's network generated by vessel's consumers. It is based on the *demand-based frequency control,* and *fast load reduction*. The main idea is that the frequency control on marine vessel can be improved by using the dynamic feedback from the power system to the electrical thrusters. Due to relatively large inertia of the vessel, fast power modification on the thrusters, introduced by PRC will not have a significant effect on vessel responses. Other consumers which rely on energy can be used for the control as well.

6.2.1 Thrust allocation algorithms

Thrust allocation algorithms to make a smooth transition of thrust references, have successfully been applied on board vessel, see Fossen (2002), Johansen (2004), Johansen *et al.* (2004a), Johansen *et al.* (2004b), Fossen and Johansen (2006), Ruth *et al.* (2007) and the references therein.

The thrust allocation algorithm implies that the smooth change in the thrust references will provide smooth power transients on the power system. However, this may not be the case when propellers are subjected to large thrust and torque losses. The algorithm is also limited to propulsion loads while other loads that may produce significant load fluctuations on the network have not been considered.

The performance of the vessel, sub-systems and controllers is illustrated in Fig. 6.1. Based on the measured vessel potion i.e. drift from the position and heading, the DP controller will set demanded thrust forces in horizontal directions τ_x, τ_y and the moment around z axis, ψ_z. Then, the thrust allocation algorithm will, based on the defined cost function, find the optimal thruster set-points, T_{0p}. In the local thruster controller the desired thrust will be

mapped to desired speed (*speed control*) or desired power (*power control*) and control error will be minimized. Depending on the design of controllers and tuning, the power load will be transmitted to power plant where the load fluctuations may make problems for the generators to keep the required frequency and voltage.

The *standard conventional PMS static load controller,* widely used on the installations today, is based on the slowly changing signal of low pass filtered available power, measured from the switchboard, as explained in the Chapter 2.

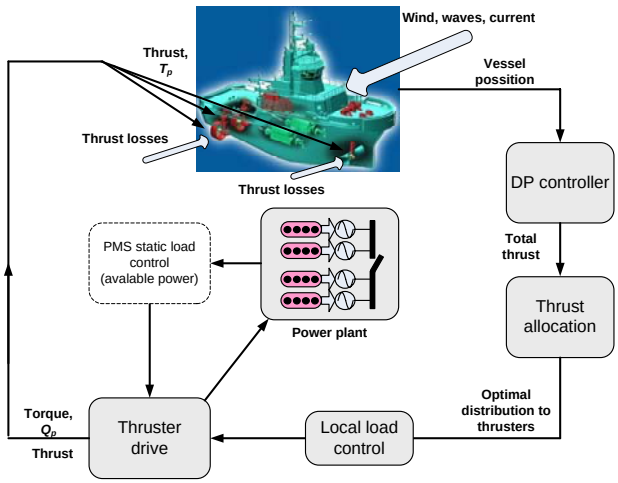

Fig. 6.1. Propulsion control structure

6.2.2 Frequency demand switching control

In Black and Ilic (2002), the authors studied the characteristics of *demand based frequency control* (DBFC) for distributed power generation. It utilizes control devices which will turn off (on) the machine/appliance in response to frequency deviations in order to restore the supply/demand balance, and will turn them back on (off) at a time when the frequency deviations are in the acceptable range. Appliances/machines which rely on energy rather than power, such as heaters, refrigerators, and air conditioners, will regulate their consumption to minimize the frequency deviations.

The following challenges are related to application of DBFC onboard the marine vessel:
- The load variations in marine vessel may be very fast, as described in Chapter 5;
- The load switching of consumers may not be allowed due to necessity of having uninterruptible power supply of consumers.

Thus, the frequency demand switching or consumer switching control proposed in Black and Ilic (2002) may not be fully applicable for the marine vessel. However, depending on the vessel type and operations, the DBFC could be applicable for the limited power.

6.3 Local thruster control effects

6.3.1 Effects of local thruster speed control

The control plant model for thruster is presented in (5.4) and Appendix B. If standard thruster PI speed controller is used:

$$Q_{cp} = k_{Pp} e_p + k_{Ip} \int_0^t e_p d\tau \,,\; e_p = \omega_{0p} - \omega_p \tag{6.1}$$

where ω_{0p} is the thruster speed reference, and k_{Pp} and k_{Ip} are the nonnegative proportional and integral control gains, respectively. Assuming the frequency deviation is produced by only one thruster and, for the simplicity, the speed controller is only proportional, the following controller output is obtained:

$$Q_{cp} = k_{Pp} e_p = k_{Pp} \left(\omega_{0p} - \omega_p \right), \tag{6.2}$$

and the motor torque:

$$Q_{mp} = Q_{cp} - T_{mp} \dot{Q}_{mp} = k_{Pp} \left(\omega_{0p} - \omega_p \right) - T_{mp} \dot{Q}_{mp} \,. \tag{6.3}$$

Due to small value of T_{mp}, the thruster dynamics may be disregarded to simplify the analysis, then $T_{mp} \dot{Q}_{mp} = 0$.

The electrical torque on the power generating system is generated when supplying current to all consumers, including thrusters:

$$Q_{eg} = \frac{1}{\omega_g} \left(\sum_{p=1}^{T_{on}} Q_{mp} \omega_p + P_{c-p} \right), \tag{6.4}$$

where Q_{mp} is the electrical motor torque and ω_p is the shaft speed on each of the running thrusters in the system and $P_{c\text{-}p}$ is power summation for all other consumers then thrusters.

Network load effects with propeller speed controller

The motion equation for the mean acceleration of the power generating system is presented in (3.28).

In present simplified closed-loop analysis it is assumed that the thruster is the only one consumer in the system. Since Q_{eg} is expressed in per unit, in equation (6.4), the following equation to map Q_{mp} to Q_{eg} follows:

$$Q_{eg} = \frac{\omega_p}{P_{rg} \omega_g} Q_{mp} \,, \tag{6.5}$$

After inserting (6.2) into (6.3) and disregarding the thruster dynamics i.e. Q_{cp}=Q_{mp}, and then into (3.28) the following closed-loop equation is obtained:

for $\omega_p \neq \omega_{0p}$:

$$\frac{d}{dt}\omega_g = \frac{\omega_{0g}}{2H_{N_{on}}}\left[Q_{mg} - \frac{D_g}{\omega_{0g}}\left(\omega_g - \omega_{0g}\right) - \underbrace{\frac{k_{pp}\omega_p}{P_{rg}\omega_g}\left(\omega_{0p} - \omega_p\right)}_{Q_{eg}} \right], \tag{6.6}$$

From the generator motion closed-loop equation (6.6) the following control properties can be noticed:

- The thruster loading is opposing the engine mechanical torque. The generator speed deviations are produced when the electrical load torque Q_{eg} is high and can not be balanced fast enough by the engine torque Q_{mg};
- For fixed pitch propellers (FPP), the load torque increases with thruster shaft speed ω_p and shaft speed deviations $\omega_{0p} - \omega_p$ are more sensed by the network when ω_p is high. The disturbances on generators Q_{eg} will increase proportionally with the propeller speed ω_p for the same error $\omega_{0p} - \omega_p$ and k_{Pp}. This also shows that the FPP thruster can not produce large load torque on the generators when operates on low speed;
- The response of power system will depend on tuning of propeller shaft speed controller on thruster. This is easy to see as the proportional term in PI speed controller k_{Pp} is decreased in (6.2) the generator shaft acceleration will tend to diminish, $\mathrm{d}\omega_g/\mathrm{d}t \rightarrow 0$ in (6.6). The drawback is decreased thruster shaft speed control performance, as the error of $\omega_{0p} - \omega_p$ will increase;

Network load effects with perfect propeller speed controller

Assuming perfect speed control on thruster with very high value of k_{Pp} (and no measurement noise) may completely diminish the propeller shaft accelerations $\mathrm{d}\omega_p/\mathrm{d}t \rightarrow 0$. Disregarding the friction torque Q_{fp} = 0 and assuming $\mathrm{d}\omega_p/\mathrm{d}t$ = 0 in (6.6), the following closed-loop equation is obtained:

for $\omega_p = \omega_{0p}$:

$$\dot{\omega}_g = \frac{\omega_{0g}}{2H_{N_{on}}}\left[Q_{mg} - \frac{D_g}{\omega_{0g}}\left(\omega_g - \omega_{0g}\right) - \underbrace{\frac{k_1}{P_{rg}\omega_g}\omega_{0p}^3\beta_{loss,p}}_{Q_{eg}} \right]. \tag{6.7}$$

As can be seen from (6.7), propeller load torque will be almost directly transferred to the electrical network i.e. generators. This means that the sensitivity of the network to propeller thrust losses $\beta_{loss,p}$ will increase with the 3rd degree of the propeller speed. This may induce large disturbances on the generators, and potential problems with excessive frequency fluctuations.

6.3.2 Effects of local thruster power control

Thruster power control

The use of power control for marine thrusters to reduce the network load fluctuations has been proposed in Sørensen *et al.*, (1997). In this Chapter, the effect of thruster power control to propeller shaft speed fluctuations is also considered.

In (6.7) the propeller load torque depends on the torque loss factor. Then, the load power is:

$$P_{ap} = \frac{1}{4\pi^2} K_{Q0p} \rho D_p^5 \ \omega_p^3 \beta_{loss,p} = k_1 \omega_p^3 \beta_{loss,p} \ . \tag{6.8}$$

When using the power control, the load power is equal to the desired power (Sørensen *et al.*, 1997):

$$P_{ap} = P_{0p} \ , \tag{6.9}$$

and the actual speed, dependant on desired power is obtained from (6.8):

$$\omega_p = \frac{1}{k_1^{1/3}} \left(\frac{P_{0p}}{\beta_{loss,p}} \right)^{1/3} \ . \tag{6.10}$$

Thus, as the power increases, the shaft speed fluctuations will also increase, depending on the torque losses – more if torque losses are higher, i.e. torque loss factor $\beta_{loss,p}$ is low.

Considering $\overline{\beta}_{loss,p}$ as average torque loss factor, the average shaft speed fluctuations can be determined from:

$$\Delta \overline{\omega}_p = \frac{1}{k_1^{1/3}} \left[\left(\frac{P_{0p}}{\overline{\beta}_{loss,p}} \right)^{1/3} - P_{0p}^{1/3} \right] . \tag{6.11}$$

The sensitivity of shaft speed fluctuations to desired propeller power with various $\overline{\beta}_{loss,p}$ is shown in diagram in Fig. 6.3. It is important to notice that the slope of the curve in diagram in Fig. 6.3 will decrease with the propeller power (thrust), e.g. for higher power, the sensitivity to speed fluctuations will become lower. This means that thruster load increase for highly loaded thruster will have much less effect on shaft speed fluctuations (and accelerations) than load increase for low loaded thruster. Diagram shows that the sensitivity to speed fluctuations is higher on low load. Moreover, the intensity of speed fluctuations and the sensitivity will increase with thrust losses. As average torque loss factor $\overline{\beta}_{loss,p}$ is lower, indicating higher thrust losses, the sensitivity to propeller shaft speed fluctuations will increase. Then, an increase of the load for propeller subjected to high thrust losses ($\overline{\beta}_{loss,p}$ is low) can be penalized in the control low.

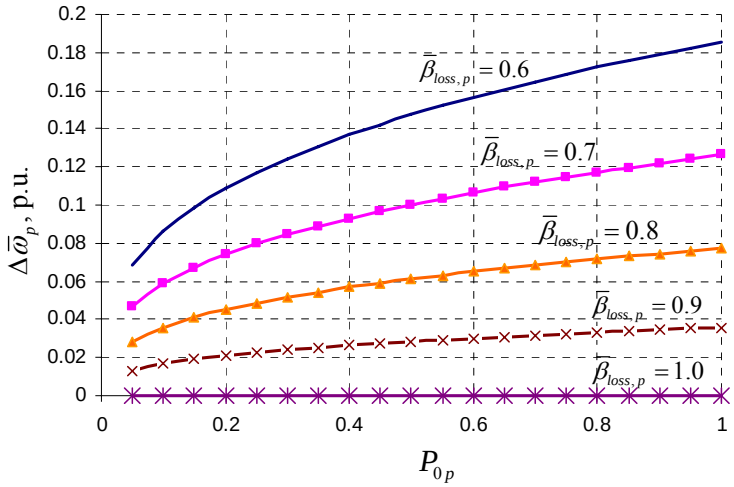

Fig. 6.3. Sensitivity of propeller shaft speed fluctuations to desired power and average torque loss factor

Network load effects with propeller power controller

For the power control the $P_{mp} = Q_{mp}\ \omega_p$ and the close-loop equation of motion for the network load effects is obtained:

$$\frac{d}{dt}\omega_g = \frac{\omega_{0g}}{2H_{N_{on}}}\left[Q_{mg} - \frac{D_g}{\omega_{0g}}\left(\omega_g - \omega_{0g}\right) - \frac{1}{P_{rg}\omega_g}P_{mp}\right]. \qquad (6.12)$$

The network accelerations will be significantly diminished if the P_{0p} = const. → P_{mp} = const. i.e. $dP_{0p}/dt = 0 \rightarrow dP_{mp}/dt = 0$. This means that the generator shaft accelerations will not be suppressed if the set-point references P_{0p} change fast (from DP thrust allocation), i.e. $dP_{0p}/dt >> 0$. This, among other factors, initiated the development of advanced thrust allocation algorithms, see e.g. Johansen (2004), Fossen and Johansen (2006), and the references therein.

6.3.3 Combined control concepts for thruster control

The ultimate goal of the thruster control is to provide the thrust that is requested from the supervisory control system, while:

1. *Decrease propeller shaft speed and torque fluctuations* – decrease wear and tear of thrusters;
2. *Decrease power load fluctuations on the network* – decrease wear and tear/faults of prime movers, electrical equipment and machines;
3. *Increase thrust capacity and thrust availability* – increase DP capability and maneuvering of the vessel.

These goals are to some extent in mutual contradiction. The challenge is how to efficiently achieve the opposing goals in order to reduce damages to onboard machines and equipment and to reduce the fuel consumption.

The effects of speed, power and combined speed/power control concepts are considered with regards to wear and tear effects on thrusters and generators in addition to providing the required thrust, as shown in Tables 6.1 and 6.2. Table 6.1 is based on the quantitative analysis of proceeding sub-sections, and Table 6.2 is just a qualitative overview.

The speed control on thrusters will transfer a significant part of propeller load torque fluctuations to the network and will increase the frequency fluctuations on the generators. However, good propeller shaft speed control will increase the life of the thruster, as will reduce the torque fluctuations on the power transmission parts and reduce the potential thruster wear and tear.

Table 6.1. Effect of various control concepts on thruster control and generators – quantitative overview

	Prop. speed	**Load power**	**Gen. torque balance**
Speed control	$\omega_p = \omega_{0p} = \text{const.}$ $\lvert\omega_p - \omega_{0p}\rvert = 0$	$P_{mp} = k_1 \lvert\omega_{0p}\rvert \omega_{0p}^2 \beta_{loss,p} + P_{fp}$ $P_{mp} \neq \text{const.}$	$\left\lvert Q_{mg} - \frac{k_1}{P_{rg}\omega_g} \omega_{0p}^3 \beta_{loss,p} \right\rvert >> 0$
Power control	$\omega_p = \frac{1}{k_1^{1/3}} \left(\frac{P_{0p}}{\beta_{loss,p}} \right)^{1/3}$ $\lvert\omega_p - \omega_{0p}\rvert >> 0$	$\lvert P_{ap} - P_{0p}\rvert = 0$ $P_{mp} = \text{const.}$	$Q_{mg} - \frac{1}{P_{rg}\omega_g} P_{0p} = 0$
Combined speed/power (trade-off)	$\lvert\omega_p - \omega_{0p}\rvert \neq 0$	$P_{mp} \neq \text{const.}$	$Q_{mg} - \frac{k_{pp}\omega_p}{P_{rg}\omega_g} (\omega_{0p} - \omega_p) \neq 0$

Table 6.2. Benefits for thrusters and generators of various control concepts with local thruster control – qualitative overview

	<=== Existing ===>			<======== **proposed** ========>	
Thruster control =>	Speed control	Power control	Power/speed control potential	Load limiting control, (Chapter 5)	Combined power/speed/load limiting control
Effect to:					
Thrusters	*Good*	*Bad*	*Medium*	*Good*	*Good*
Generators	*Bad*	*Good*	*Good*	*Medium*	*Good*
Thrust capacity	*Good*	*Good*	*Good*	*Medium*	*Good*

Contrary, the thruster power control, as shown in Sørensen *et al.* (1997) will be very beneficial for the network, as the network load fluctuations will be minimized if thruster set-points are changed slowly. However, the thruster power control will increase the speed and torque fluctuations on thrusters and thus increase thruster wear and tear.

The desired features of thruster speed and power control can be obtained, as will be presented later in this Chapter.

6.4 Network loading problems with existing control technology

To reduce the frequency deviations due to propulsion loading the common approach in the marine industry is to set the fixed load rate limits on the electrical thrusters, as described in Chapter 2. Without load rate limits, the electrical load in the system would depend on reference settings commanded from the DP thrust allocation algorithm or manually changed by the operator. The consequence of such system would be that the load demand per thruster may increase instantly, e.g. during maneuvering of the vessel, shallow water and passage operation, station-keeping, etc.

The response of modern electric motor drives on fixed pitch propellers (FPP) thrusters is very fast, e.g. within 100 milliseconds (Ådnanes, *et al.*, 1997; English, 2001). The gains on the speed controller i.e. proportional-integral (PI) terms are usually set very high in order to provide good speed control and reduce speed and torque fluctuations when propellers are subjected to excessive thrust loss and harsh weather conditions. Thus, the motor torque will be very sensitive to small speed drift from the nominal.

As the generators are not capable to withstand very high increase of load, the network frequency may drop below low-frequency limit. Thus the slew rates for thrusters are chosen in connection with the engine torque load rates and will depend on the number of generators operating on-line. The following issues should be considered:

- Increasing the load on one thruster or several thrusters together is not the same. With fixed slew rates on the thrusters, the change in the load must be determined for the worst case of loading, e.g. all thrusters in the system loaded together. This gives unnecessary slow loading when the reference is changed on only one thruster. Therefore it is difficult to find the optimal engine loadings for every load-generator combination using fixed slew rates on thrusters;
- Changes to other loads are not considered in the control algorithms for thrusters although all consumers have an affect on the power system responses. The thrusters can be loaded together with some other consumers where the loading may increase the frequency deviation;
- If an engine fault occurs, the fast load reduction system will reduce the load on the propulsion system preventing blackout. The responses of the fast load reduction system are calculated assuming the nominal speed on the engine i.e. nominal frequency on the network. However, the engine speed may fluctuate due to the network disturbances, and the risk of the blackout will increase in proportion of the speed fluctuations. This makes the ship the most vulnerable to blackout during maneuvering and station-keeping when the load changes on the propulsion system are large and rapid, and when the system ideally should have the highest resistance to blackout;
- On some applications, the load ramp limits on thrusters depend on the power generating capacity. The number of load ramp functions to select for each thruster can be set equal to the number of the gen-sets. The information on the power generating capacity is obtained from the status of the generator breakers that is fed to each thruster reference; see Chapter 2 on load rate limit control. By the time, the faults start to occur in the lines fed from the breaker status. Then the controller selects the lowest rate limits assuming the lowest number of gen-sets online. The consequence is slow thruster loading and low propeller acceleration in all network conditions, even when the generating power capacity is high.

6.5 Power redistribution control (PRC)

6.5.1 Concept of Power redistribution control (PRC)

A new controller reducing the load fluctuations on the vessel's network generated by the consumers is proposed. The controller is termed the *power redistribution controller* (PRC) and is based on the combination of ideas in *demand-based frequency control* (Section 6.2) and *fast load reduction-FPBS* (Chapter 3) described in this thesis (Radan *et al.*, 2008). The main idea is that the frequency control on marine vessel can be improved by using the dynamic feedback from the power system to the electrical thrusters. Due to relatively large inertia of the vessel, fast power modification on the thrusters, introduced by PRC will not have a significant effect on vessel responses. Moreover, other consumers which rely on energy can be used for the control as well.

The proposed *power redistribution control* is a *network-based combined thruster speed/power control*. It can be used to decrease the load fluctuations on bad performing thrusters and redistribute the excessive energy on the network to other thrusters and consumers providing significant improvements in the network stability and intelligent equipment handling. The PRC will limit load fluctuations on thruster subject to large thrust losses. It may also limit the thrust on the same thruster, but only if the thruster injects high level of load fluctuations in to the network.

The proposed control law

The proposed control law is based on the correction of the propeller shaft speed deviations $\omega_{0p} - \omega_p$ using two different control strategies (Radan *et al.*, 2008):

– *Strategy 1: the feedback from the network frequency deviation*:

$$e_p = \omega_{0p} - \omega_p + k_{gp}\left(\omega_g - \omega_{0g}\right); \tag{6.13}$$

– *Strategy 2: the feedback from the generating system torque deviation*:

$$e_p = \omega_{0p} - \omega_p + k_{gp}\left(\hat{Q}_{mg*} - Q_{eg}\right), \tag{6.14}$$

where k_{gp} is the feedback gain.

The reduced mechanical motor torque accounts for the generator damping, as can be seen from (3.28). The state estimator i.e. the observer in (3.31) is used to provide the noise filtering of the frequency and torque measurements.

The PRC concept for the *Strategy 2* is presented in Fig. 6.4.

Closed-loop analysis and network load effects

***Strategy 1*:** Using the feedback from the network frequency deviation in (6.13), the thruster motor torque becomes:

$$Q_{mp} = k_{pp}\left(\omega_{0p} - \omega_p\right) + k_{pp}k_{gp}\left(\omega_g - \omega_{0g}\right). \tag{6.15}$$

with the thruster dynamics disregarded. After inserting (6.15) into (6.5) and then into (3.28), the closed loop equation is obtained:

$$\frac{d}{dt}\omega_g = \frac{\omega_{0g}}{2H_{Non}}\left[Q_{mg} - \frac{D_g}{\omega_{0g}}\left(\omega_g - \omega_{0g}\right) - \frac{k_{pp}\omega_p}{P_{rg}\omega_g}\left(\omega_{0p} - \omega_p\right) - k_{gp}\frac{k_{pp}\omega_p}{P_{rg}\omega_g}\left(\omega_g - \omega_{0g}\right)\right]. \tag{6.16}$$

It can be noticed that the thruster feedback from the generator frequency deviation increases the damping in the closed-loop frequency equation. The frequency fluctuations will be reduced due to cancellation of the load i.e. increased stability. If the generator frequency increases, the thrust reference will temporarily increase and dump the excessive system energy. If the frequency decreases, the thrust reference will decrease, therefore decrease the system load. The change in the load reference will occur temporally until the mechanical torque Q_{mg} becomes available from the engines and new load balance is obtained.

***Strategy 2*:** Using the feedback from the generating system torque deviation in (6.14), the thruster motor torque becomes:

$$Q_{mp} = k_{pp}\left(\omega_{0p} - \omega_p\right) + k_{pp}k_{gp}\left(\hat{Q}_{mg*} - Q_{eg}\right), \tag{6.17}$$

with the thruster dynamics disregarded. The disregarded dynamics is all included in the simulation model, used to demonstrate the applicability of the proposed PRC concept. Using eq. (6.14) and (3.28) the second term in eq. (6.17) can be rearranged:

$$Q_{mp} = k_{pp}\left(\omega_{0p} - \omega_p\right) + k_{pp}k_{gp}\frac{2H_{Non}}{\omega_{0g}}\frac{d}{dt}\omega_g\,. \tag{6.18}$$

This makes the thruster controller dependent on the generating system acceleration. After inserting (6.18) into (6.5) and then into (3.28) the closed loop equation is obtained:

$$\frac{d}{dt}\omega_g = \frac{\omega_{0g}}{2H_{Non}\left(1 + \dfrac{\omega_p}{P_{rg}\omega_g}k_{pp}k_{gp}\right)}\left[Q_{mg} - \frac{D_g}{\omega_{0g}}\left(\omega_g - \omega_{0g}\right) - \frac{\omega_p}{P_{rg}\omega_g}k_{pp}\left(\omega_{0p} - \omega_p\right)\right]. \tag{6.19}$$

The frequency fluctuations will be reduced due to virtual increase in the system inertia. This control method has been known as the acceleration feedback (Fossen, 2002) or inertial response control (Morren *et al.*, 2006).

Network load effects with multiple thrusters operating in the system

For two or more thrusters operating in the same system, the following closed loop equations are obtained:

***Strategy 1*:** With the feedback from the network frequency deviation:

$$\dot{\omega}_g = \frac{\omega_{0g}}{2H_{Non}}\left[Q_{mg} - \frac{D_g}{\omega_{0g}}\left(\omega_g - \omega_{0g}\right) - \frac{1}{P_{rg}\omega_g}\sum_{p=1}^{Ton} k_{pp}\omega_p\left(\omega_{0p} - \omega_p\right) - \frac{1}{P_{rg}\omega_g}\left(\omega_g - \omega_{0g}\right)\sum_{p=1}^{Ton} k_{gp}k_{pp}\omega_p \right] \tag{6.20}$$

***Strategy 2*:** With the feedback from the generating system torque deviation:

$$\frac{d\omega_g}{dt} = \frac{\omega_{0g}}{2H_{Non}\left(1 + \frac{1}{P_{rg}\omega_g}\sum_{p=1}^{Ton}\omega_p k_{pp}k_{gp}\right)}\left[Q_{mg} - \frac{D_g}{\omega_{0g}}\left(\omega_g - \omega_{0g}\right) - \frac{1}{P_{rg}\omega_g}\sum_{p=1}^{Ton}\omega_p k_{pp}\left(\omega_{0p} - \omega_p\right)\right] \tag{6.21}$$

where $Q_{eg} = \frac{1}{P_{rg}\omega_g}\sum_{p=1}^{Ton} Q_{mp}\omega_p = \frac{1}{P_{rg}\omega_g}\sum_{p=1}^{Ton} Q_{cp}\omega_p$ and $k_{pp} = k_{p1} = k_{p2}$. For $p = 1$, $\omega_p = \omega_1$, for $p = 2$ $\omega_p = \omega_2$, etc.

If ω_1 decreases due to propeller load increase and $\omega_{01} - \omega_1 > 0$, then the controller will act to balance the load by increasing ω_{02} and making $\omega_{02} - \omega_2 < 0$.

Discussion on PRC control strategies

While *strategy 1* is very easy to implement and can offer immediate improvements in the frequency regulation, the *strategy 2* implements faster correction of the speed setting signals and thus better frequency regulation with less control effort. Moreover, *strategy 2* provides the ability to set fixed load rate limits directly on the engines. For both of these strategies, improved frequency filtering using the state estimation observer is proposed.

Another problem is the droop control of the generating system. If the system operates in the droop mode, i.e. the steady state frequency depends on the steady state load, the ω_{0g} can vary by ±2.5%, i.e. from 58.5 to 61.5 Hz on 60 Hz system. This may introduce the steady state error in the control and the thrust may be decreased more than necessary. It might be difficult to estimate the exact value of the droop for the distributed power systems, as described in Black and Ilic (2002). Although the ω_{0g} can be accurately determined in the isolated power system such as marine vessel, using *strategy 2* another feedback (steady state droop) is avoided and robustness of the controller is increased.

Hence, due to improved robustness properties the *strategy 2*: *feedback from the generating system torque deviation* will be further analyzed in the thesis and case study. For the *strategy 2*, the observer is needed. It will be shown through the simulation that the observer is robust to parameter data inaccuracies and suitable for the control.

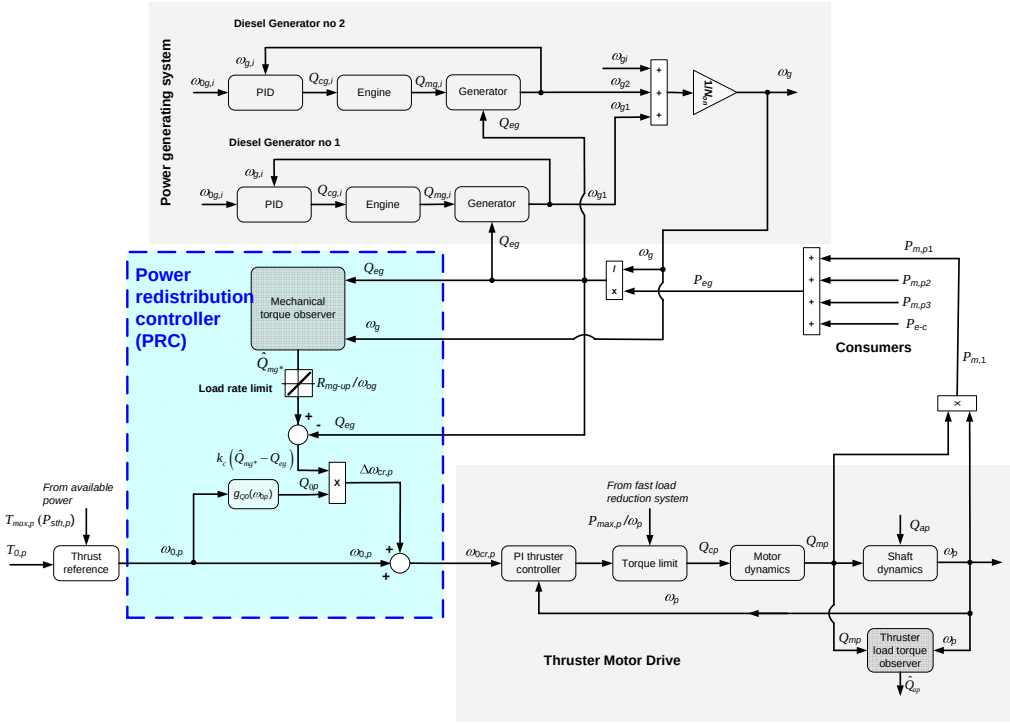

Fig. 6.4. Power redistribution controller within the marine power plant (Radan *et al.*, 2008)

6.5.2 Load dependent PRC gains

The thruster can not contribute significantly to the frequency fluctuations when operated on low load or low speed for thrusters with the fixed pitch. In order to prevent high frequency drop during loading, the load gains can increase faster than the thruster load. Thus, the gain should depend on the expected thruster loading according to (Radan *et al.*, 2008):

$$k_{gp} = k_c \, Q_{0p} \,, \tag{6.22}$$

where k_c is the proportional gain, and Q_{0p} is the expected nominal torque (or desired torque reference) for each propeller p:

$$Q_{0p} = \frac{1}{4\pi^2} K_{Q0p} \rho D_p^5 \, \omega_{0p}^2 = g_{Q0p}\left(\omega_{0p}\right). \tag{6.23}$$

The torque reference for each propeller p can be calculated directly from the thrust reference (Sorensen *et al.*, 1997):

$$Q_{0p} = \frac{D_p K_{Q0p}}{K_{T0p}} \, T_{0p} = g_{Q0p}\left(T_{0p}\right), \tag{6.24}$$

where K_{T0p} and K_{Q0p} are the thrust and torque coefficients, as previously defined, but for zero advance coefficient, i.e. J_a=0, where J_a=V_a / n D.

If the nominal torque increases, the gain will also increase, therefore providing stiffer protection for the power fluctuations. When the nominal torque decreases, the PI controller will have a higher proportion of control, since the reference correction will become low.

6.5.3 The mechanical torque limits

Using the proposed PRC, the load rate limits can be selected directly on engines. This is in contrast to present practice where the load rate limits must be pre-determined and will depend on the number of thrusters and generators on-line, as explained in Chapter 2. When using the proposed PRC controller, the measurements of individual load and speed on generators as well as propulsion loading are not necessary for the successful engine load rate limiting. As the total mechanical torque is estimated, all engines with generators on-line will have the same load rate limit. Using mechanical torque rate limit, the engines are completely safe of turbocharger surging; for turbocharger surging see e.g. Gravdahl and Egeland (1999) and Theotokatos and Kyrtatos (2001).

The engine operational region can shrink according to the recommended load rate limits (*) given by an engine vendor:

$$\frac{R_{mg-un}}{\omega_{0g}} < \frac{R^*_{mg-un}}{\omega_{0g}} \leq \frac{d}{dt}\hat{Q}_{mg^*} \leq \frac{R^*_{mg-up}}{\omega_{0g}} < \frac{R_{mg-up}}{\omega_{0g}}, \qquad (6.25)$$

where the power slew rate magnitudes are divided by the nominal gen-set speed ω_{0g} obtaining the torque slew rate magnitudes.

6.5.4 Case Studies – PRC vs. standard thruster speed control

The simulator is made in SIMULINK/MATLAB. Diesel generating system consists of two generating-sets, operating in the isochronous mode with constant ω_{0g} and H_{Non}=2 seconds. Diesel generators are modeled with frequency control through PID governors and modeled fuel actuators. Based on the results presented in Appendix A, the network voltage is assumed constant and hence only the active power is considered in the model. The main motion is governed by equation (3.28) and the responses of the power system are affected only by the responses of the diesel engines. Thrusters are modeled as the active power consumers where the power consumption depends on thruster shaft speed. This is due to PWM-VSI operates with high power factor, PF ≈ 0.95 for all loadings. The drive time constant is very low, T_{mp} = 0.05, since the drive has very fast response to commanded torque. The response in the real system will be slower then in this simulator due to the additional low pass filtering of commanded torque Q_{cp}. The diode rectifier is installed on the network side of the frequency converter and thus the energy flows only in the network-converter direction, but not in the opposite. The energy excess on DC link is dissipated in the water-cooled resistor bank.

The mechanical torque observer: l_{1g} = 20, l_{2g}= 200, H_{Non}=1.5 seconds, so the parameter error in H_{Non} is included in the simulation. PRC gain k_c = 20, and is dependent on thruster loadings and losses. A signal will pass through the low pass filter before being fed to the thruster speed controller, so k_{gp} / (0.01 s +1).

A case study for the typical platform supply vessel (PSV) presented in Table 6.3 has been made. The system is shown in Fig. 6.5. One side of the two split system is simulated. Two thrusters are in the operation, the 2.3 MW aft thruster and the 1 MW bow thruster together with auxiliary loads. Two gen-sets, each 1.5 MW are online, so 3.0 MW is the power generating capacity in the system.

The simulation scenario is as follows:
t=0 second:

The speed reference for the aft thruster is set to 30% rated speed, $\omega_{0p1}=0.3\omega_{r1}$ and for the bow thruster $\omega_{0p2}=0.2\omega_{r2}$, where ω_{rp} is the thruster rated power;

t=30 second: $\omega_{0p1}=0.65\omega_{r1}$;
t=50 second: $\omega_{0p2}=0.60\omega_{r2}$;
t=100 second: $\omega_{0p1}=0.3\omega_{r1}$ while the $\omega_{0p2}=0.60\omega_{r2}$, remains constant.

Table 6.3. Main characteristics of the vessel and power plant

Vessel main particulars:	L=69.7 m, B=16.8 m, T=6.1 m, $Vol.$.=3950 m^3, max speed 16 knots, service speed 13 knots
Thrusters:	Aft thrusters: 2 x 2 300 kW Bow thrusters: 2 x 1 000 kW
Auxiliaries and winch loads:	400 kW
Generators:	4 x 1 500 kW

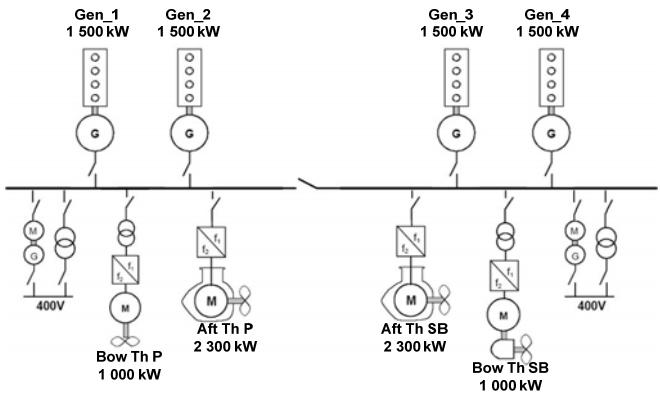

Fig. 6.5. Single line diagram for the vessel

The following control systems are compared:

1. *Power redistribution control*, based on the system mechanical torque observer with fixed slew rates on the system mechanical torque (PRC).
2. *Local speed control* on thrusters and fixed slew rates on thrust references (LSC).

CASE 1 - Both thrusters compensate for the load fluctuations

Using the proposed PRC, significant reductions in frequency and power fluctuations can be noticed from Fig. 6.6. The frequency deviations with PRC are mainly within ±0.2 Hz, while when using conventional LSC are more than ±2 Hz. The reduced load fluctuations indicate that is possible to increase the engine load without risking the fuel actuator to hit the torque limiter. Thus, the thrust capacity can be increased with improved blackout prevention capabilities.

The speed, power and thrust are compared in Figs. 6.7, 6.8, and 6.9 respectively. The main characteristic of the proposed PRC are presented in Fig. 6.7. The power redistribution among the consumers, namely thrusters, provides the smoother power output sensed by the generators and engines.

When the thrust allocation algorithm command the thruster to be loaded, then the PRC will use the excess of energy on the network to load the thruster in order to minimize the frequency fluctuations on the network. The excess of energy on the network can be produced by other consumers or thrusters subject to thrust losses. The benefit of having PRC is e.g. the thrust loss on one thruster may speed-up the loading of the other thruster. Thus, a fast loading of the thruster is achieved with low frequency deviation on the power network. This can be noticed in Figs. 6.6 and 6.7 at about t = 50 second.

Reducing the power transients may increase the shaft speed fluctuations on thrusters, as explained in this Chapter. The proposed PRC will increase the network stability with low increase in the propeller shaft speed fluctuations. Moreover, the power fluctuations are compensated by several thrusters, and hence, the speed fluctuations on individual thrusters may be slightly increased. This can be noticed in Fig. 6.8. Before t = 50 second, only one thruster operates and the speed fluctuations are somewhat higher than after t = 50 second when both thrusters compensate for the network load fluctuations.

CASE 2 - One of two thrusters compensates for the load fluctuations

In Figs. 6.10 and 6.11 the results of simulation for the same system are presented, but in this case the aft thruster is not controlled by the proposed PRC. Somewhat higher fluctuations in the frequency and electrical load can be noticed in Fig. 6.10, compared with the system presented in Fig. 6.6 where both thrusters compensate for the load fluctuations.

From these observations, it can be concluded that the success in the reduction of network load fluctuations with proposed PRC will depend on the power used for redistribution, i.e. number of controllable consumers used to compensate for the network load fluctuations and their nominal load. In Figs. 6.10 and 6.11 it can be noticed that the frequency fluctuations are still high in t = 30 second, due to low load i.e. low nominal speed of the bow thruster. When the nominal load on bow thruster increases in t = 50 second, the network stability increases and the frequency fluctuations become compensated.

When the nominal speed on bow thruster is increased, the load also increases and, after t=50 second, the frequency fluctuations are reduced. PRC is using bow thruster to redistribute the excess of energy in the system generated by aft thruster subject to large thrust losses. The success in reduction of fluctuations is limited since the bow thruster has low power output compared to aft thruster.

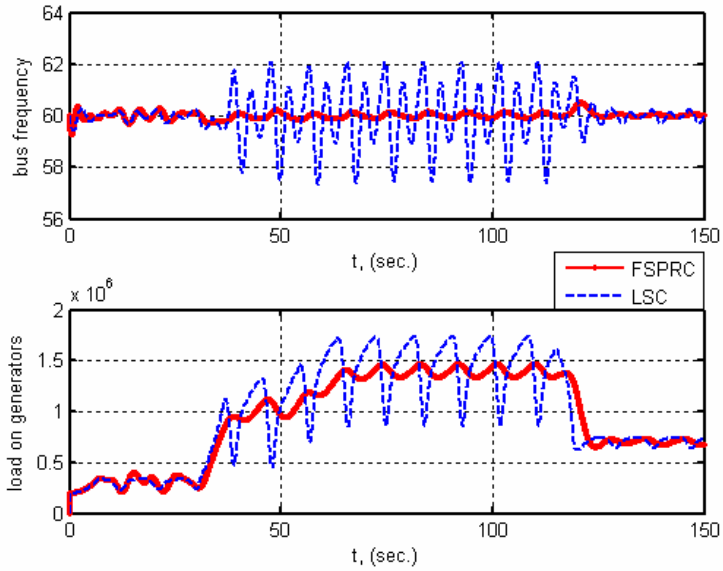

Fig. 6.6. Bus frequency (higher) and electrical power load on generating system (lower) for proposed PRC (FSPRC) and standard LSC, with 2 fast power controllable consumers

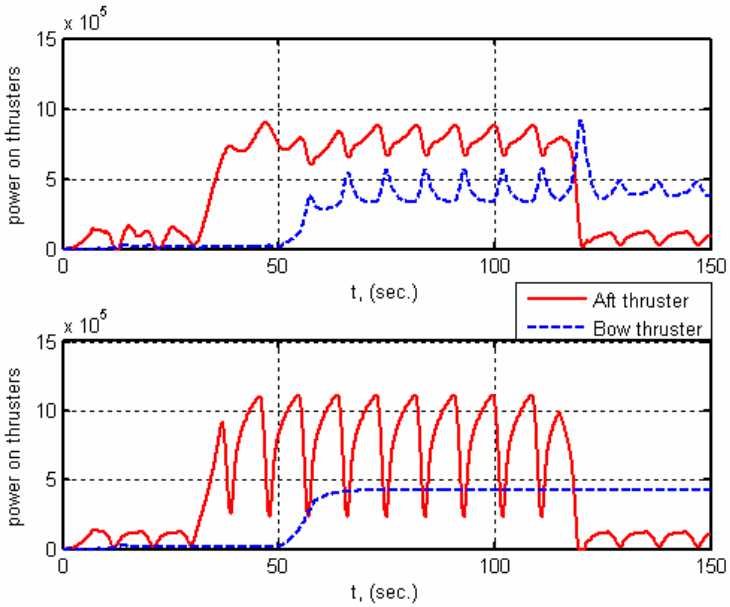

Fig. 6.7. Thruster power output with proposed PRC (higher) and with LSC (lower), with 2 fast power controllable consumers

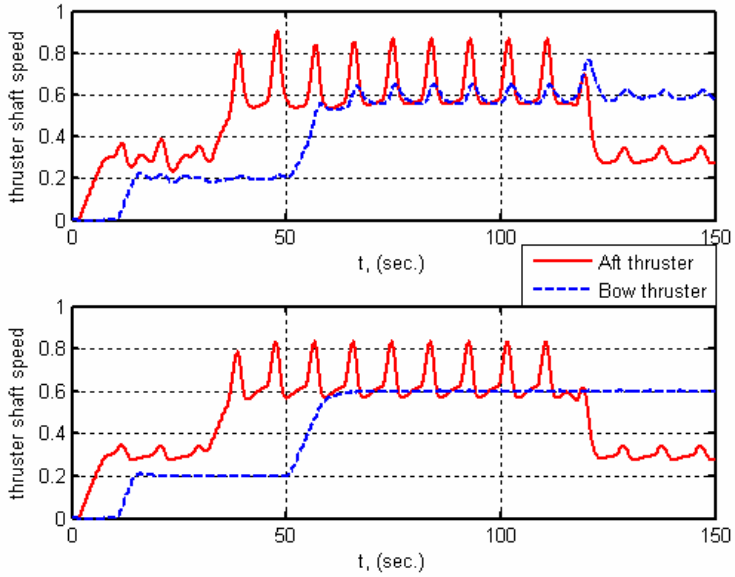

Fig. 6.8. Thruster shaft speed (in per unit) with proposed PRC (higher) and with conventional LSC (lower), with 2 fast power controllable consumers

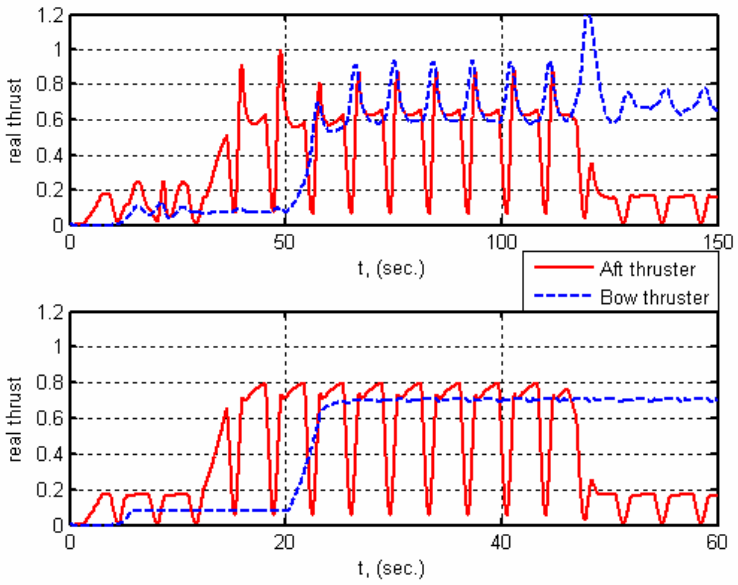

Fig. 6.9. Real thrust (in per unit) with proposed PRC (higher) and with conventional LSC (lower), with 2 fast power controllable consumers

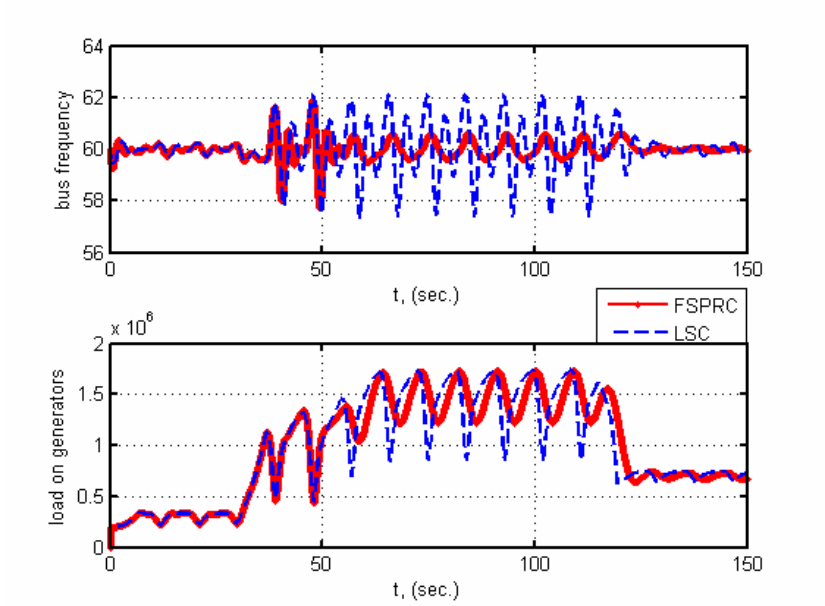

Fig. 6.10. Bus frequency (higher) and electrical power load on generating system (lower) using PRC on bow thruster without PRC interference to the LSC of aft thruster

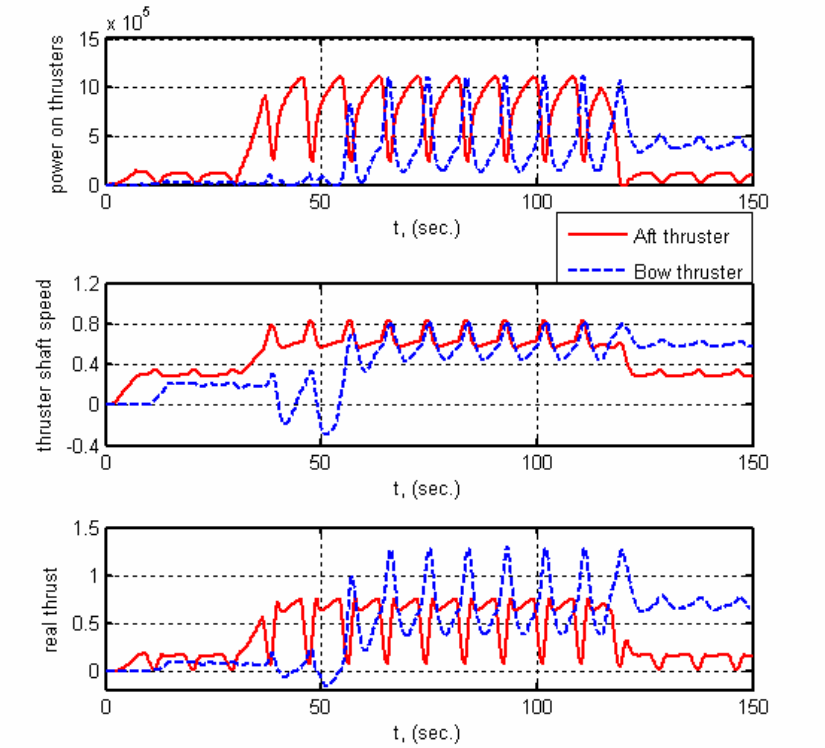

Fig. 6.11. Thruster power, shaft speed (pu) and thrust (pu) using PRC control on bow thruster without PRC interference to the LSC controller of aft thruster

6.5.5 Case Studies: PRC vs. quasi-static load limiting controllers

The following controllers have been compared in the case study:
- *Local speed controller* (LSC) or equivalently: without load limiting control (*no control*);
- *Propeller acceleration based quasi-static controller*, described in Chapter 5;
- *Torque loss bases quasi-static controller*, described in Chapter 5;
- Proposed *power redistribution controller* (PRC).

In this case study, both thrusters compensate for the load fluctuations.

Using the proposed PRC, significant reductions in frequency and power fluctuations can be noticed from Fig. 6.12. While quasi-static load limiting controllers can reduce the frequency fluctuations only to some limit, the PRC proposed in this Chapter can almost completely attenuate the frequency fluctuations.

The thrust, propeller shaft accelerations, thruster speed references, and fuel consumption have been compared for all listed controllers in Figs. 6.13, 6.14, and 6.15 respectively. As can be noticed from the detailed view of thrust per thruster in Fig. 6.13.b, the modifications of thrust when using the proposed PRC versus the local thruster speed control (*LSC* or *no control*) is too small to be able to affect the DP and maneuverability of the vessel. This can be also confirmed from Fig. 6.16.a for the vessel thrust average.

Fig. 6.14.b shows detailed view of propeller shaft acceleration on propeller 1 (upper) and propeller 2 (lower). When using standard *LSC* (*no load limit control*), the shaft accelerations on the propeller 2 are very low as the propeller is not subject to any thrust losses. However, as the *PRC* is using thruster 2 to compensate the load fluctuations in the network (in addition to thruster 1 that is subject to thrust losses), the shaft acceleration on the propeller 2 must increase, accordingly. This value is about 0.04 as can be seen from the lower part of Fig. 6.14. The acceleration on thruster 2 is probably well below the threshold for the increased wear and tear potential, since the shaft accelerations on the propeller, subject to high thrust losses are about 4 to 5 times higher, i.e. around 0.2 in the upper part of Fig. 6.14.

A very good potential for improving the fuel economy in the systems equipped with PRC controller can be seen from Fig. 6.16.a. There, the low pass filtered values of fuel consumption in kg/hour are compared for all listed controllers. It can be noticed that around t = 150 to 200 seconds, the fuel savings using PRC compared to standard LSC (no control) is about 260 – 235 / 260 ≈ 9.6 % or around 25 kg/hour fuel. This is due to the fuel consumption being function of derivative of electrical network load dP_{eg}/dt (Lindgren, 2005; He and Jang, 2006).

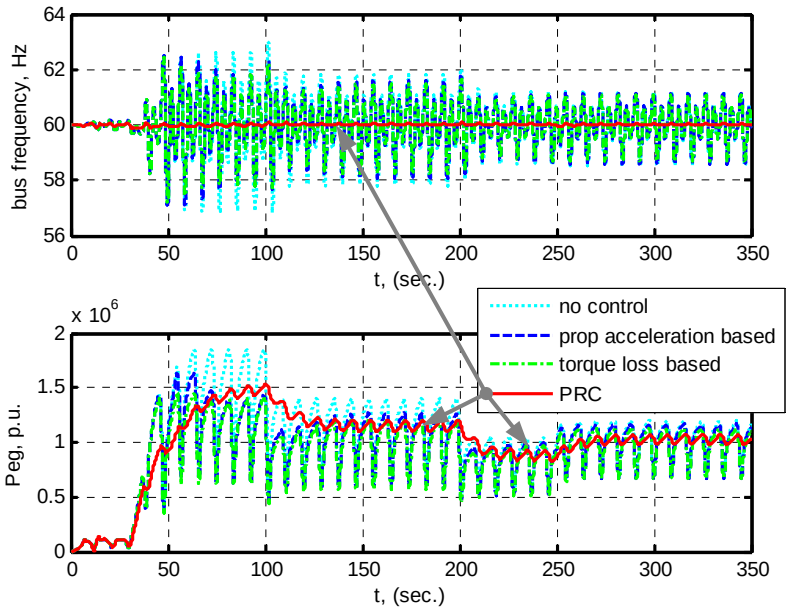

Fig. 6.12. Network frequency (upper) and total electrical active power (lower) with various controllers: no control (….), propeller acceleration based quasi-static controller (------), torque loss bases quasi-static controller (-.-.-.), and power redistribution controller (_____, PRC)

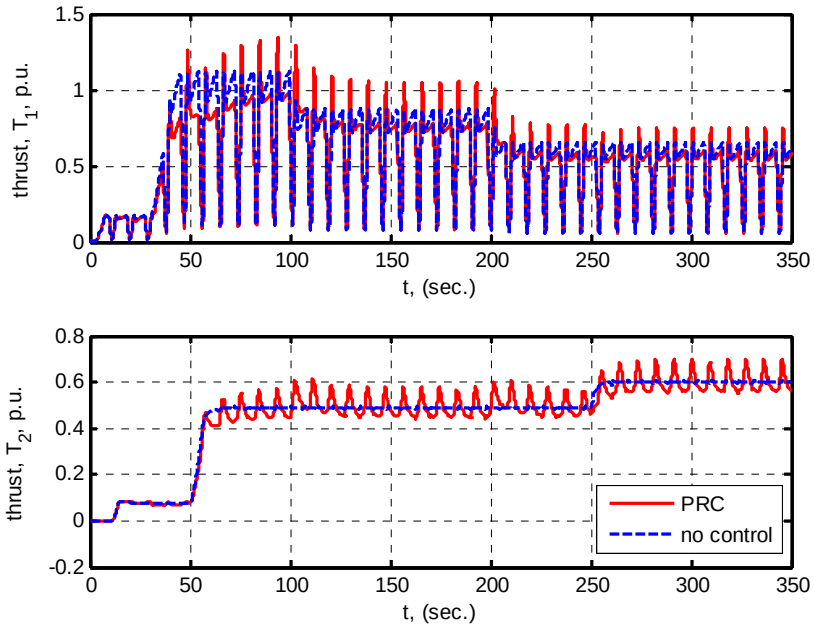

Fig. 6.13.a) Thrust on propeller 1 (upper) and propeller 2 (lower) with PRC controller (_____) and without controlling network load fluctuations (-------)

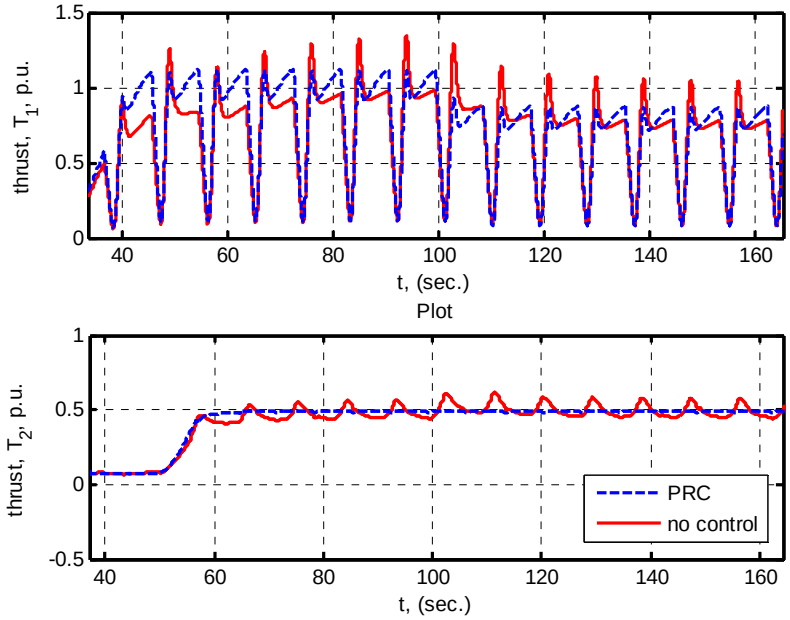

Fig. 6.13.b) Detailed view of thrust on propeller 1 (upper) and propeller 2 (lower) with PRC controller (_____) and without controlling network load fluctuations (-------)

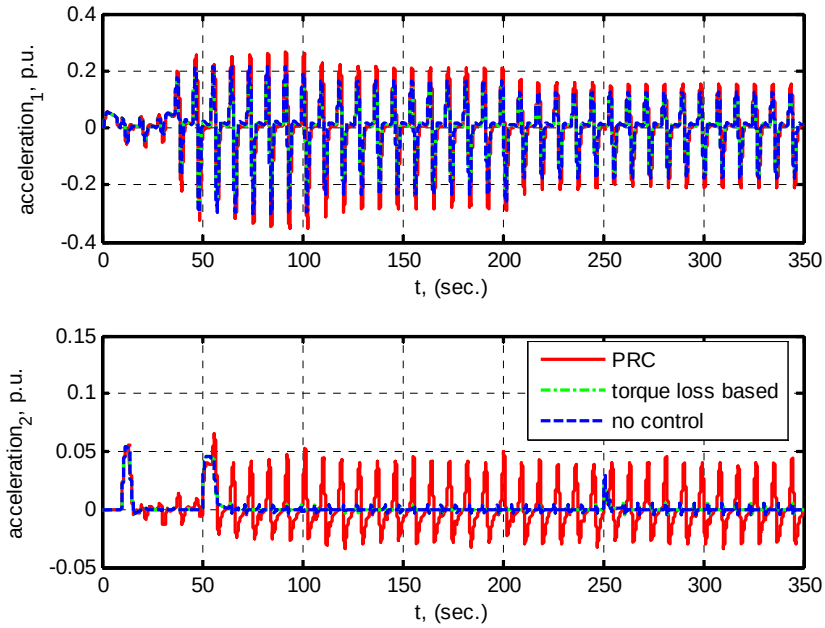

Fig. 6.14.a) Propeller shaft acceleration on propeller 1 (upper) and propeller 2 (lower) with PRC controller (_____), with quasi-static torque loss based controller (-.-.-.-.-), and without controlling network load fluctuations (-------)

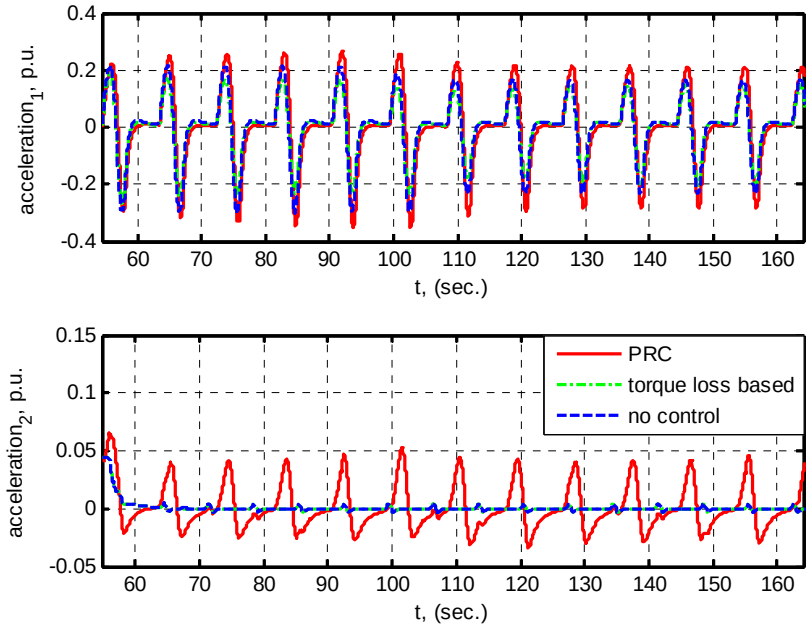

Fig. 6.14.b) Detailed view of propeller shaft acceleration on propeller 1 (upper) and propeller 2 (lower) with PRC controller (_____), with quasi-static torque loss based controller (-.-.-.-.-), and without controlling network load fluctuations (-------)

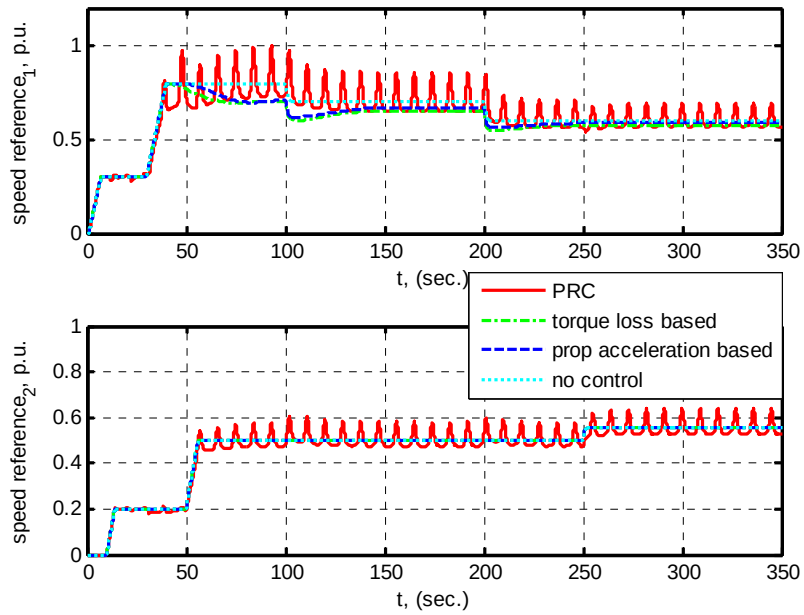

Fig. 6.15. Speed references on thruster 1 (upper) and thruster 2 (lower): PRC controller (_____), with quasi-static torque loss based controllers (-------, -.-.-.-.-), without controlling network load fluctuations (……..)

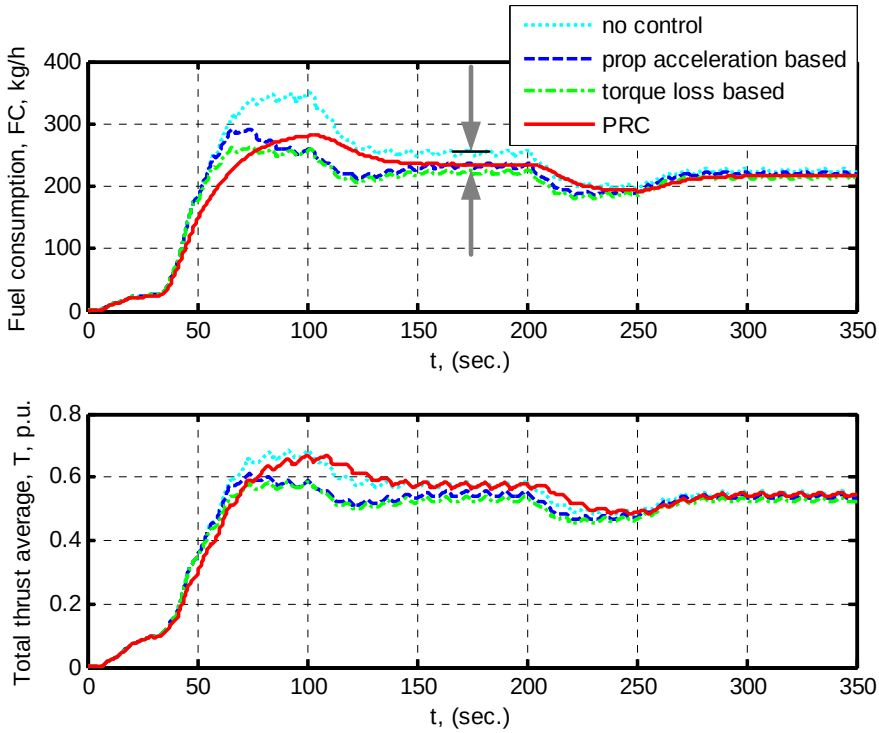

Fig. 6.16.a) Fuel consumption in kg/hour (upper) and total thrust average-low pass filtered (lower)

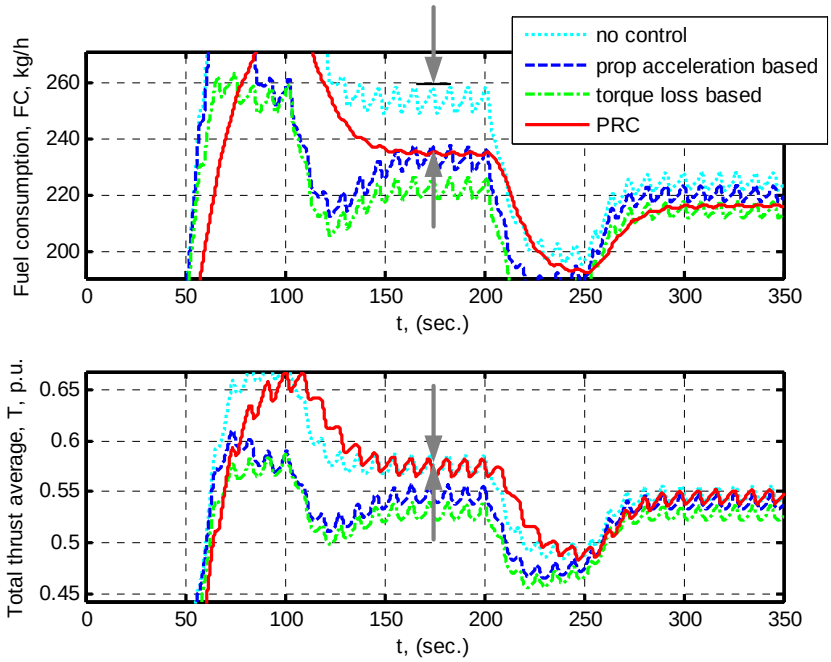

Fig. 6.16.b) Detailed view of fuel consumption in kg/hour (upper) and total thrust average-low pass filtered (lower)

6.5.6 Discussions and limitations

Minimum load limitations

Thrusters used for the compensation of disturbances generated by other consumers will provide a limited success in the frequency regulation if operating at low load. When FPP thruster is operated on low load, i.e. low speed, the change in the speed must be very high in order to obtain sufficient power change, see Fig. 6.17 for a typical propeller load curve. When the propeller speed is lower than about 60% rated speed, the power change will be very low due to small value of the slope $dP_{mp}/d\omega$. This is the reason why the load compensation was inefficient in Figs. 6.10 and 6.11 for t = 30 to 50 second. However, if thrusters that produce load fluctuations are variable speed, fixed pitch propellers (FPP), each will provide a self-compensation for the loads and thus significantly improve the network stability.

The load on the individual thrusters can be increased using increased *zero thrust*. This requires the coordination with the thrust allocation algorithm; see e.g. Fossen (2002). However, the load compensation may be inherently provided in most of the cases. The network load fluctuations depend on the vessel operations and the sea states. When the sea state increases the required thrust will also increase due to increase in the forces of external disturbances, i.e. 2nd order waves, wind and current. Then the thrusters will be highly loaded and increase in *zero thrust* may not be necessary. If *zero thrust* is used, the total load and fuel consumption would increase. The *zero thrust* can be minimized if using strategies and concepts proposed in the Sections that follow, e.g. concerning integration of DP with the power system and thrusters.

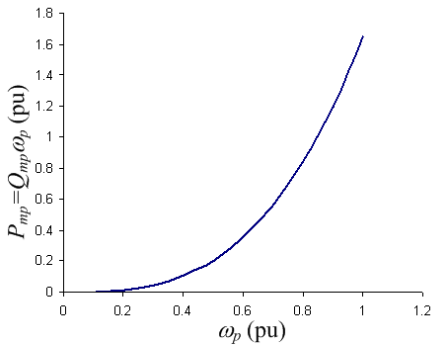

Fig. 6.17. Power curve for the thruster operating with zero vessel speed (J_a=0)

Maximum load limitations

Another limitation that should be mention is the reduced ability to compensate for the network load fluctuations when the thruster operates close to the maximum load. Since the thruster load can not be increased above the maximum load limit, the load compensation with PRC is reduced. However, as can be noticed from Fig. 6.17, thruster load P_{mp} is very sensitive to the speed change ω_p when thruster is highly loaded. Thus, the thruster speed reference can be slightly reduced ω_{0p} in order to provide a non-constraint region for the thruster load compensation. The reduction in the nominal thrust will be very small in this

case, e.g. 5%. This behavior will be implemented in the thrust allocation algorithm, as proposed later in this Chapter.

Chapter 7

Integrated network power control

7.1 Improved propeller shaft acceleration control for PRC

The PRC described in Chapter 6 can be integrated with *quasi-static load limiting control*, described in Chapter 5. This may provide an increased robustness to the faults in the control system as the *quasi-static load limiting controller* is contained within the thruster PLC, operate based on the measurements, and does not depend on the communication with other controllers, such as DP thrust allocation.

The concept of the proposed integration of *PRC* with *quasi-static load limiting controllers* is shown in Fig. 7.1. The signal from the *load limiting controller* $L_{d,th}$ is fed to *power redistribution controller* (PRC) where the dynamic correction to thrust speed reference is calculated for the individual thruster.

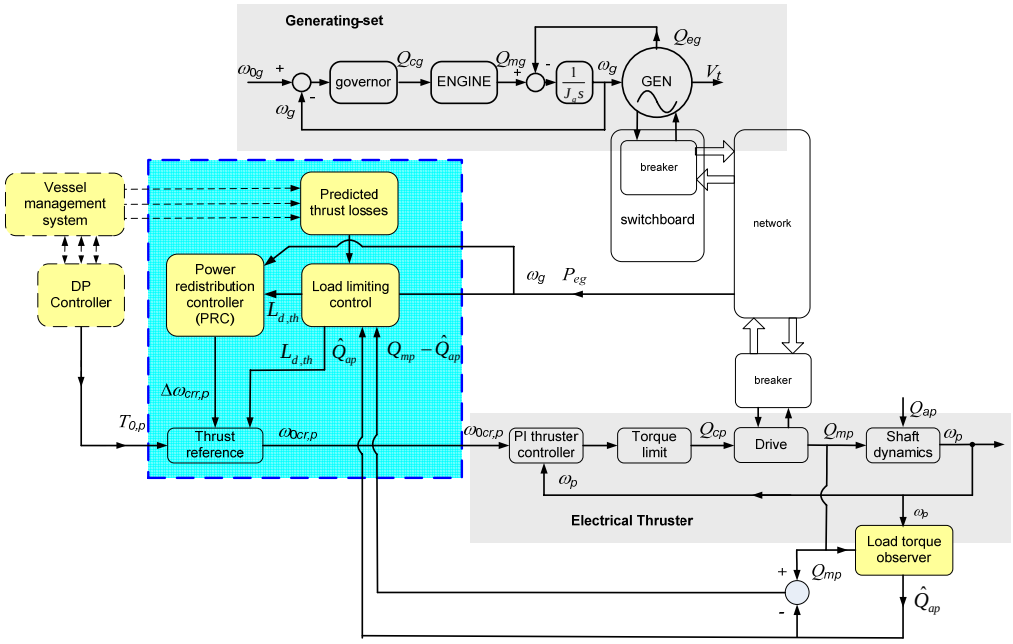

Fig. 7.1. The concept of integrated PRC with quasi-static load limiting control

7.1.1 Controller gains dependent on thruster load and thrust losses

Each thruster may be subjected to different torque (thrust) losses where the thrusters with higher losses produce higher frequency fluctuations. When using power redistribution control (PRC) the network frequency fluctuations will be almost completely suppressed which will result to having $L_{d,th} \approx 0$, as shown:

– In (5.34):

$$L_{d,th} = -k_{thp1}\left|\omega_{0p}\right| \; N_{p,loss}\left(q_h, V_s, H_w, \mu\right) \underbrace{\frac{1}{t}\int_0^t \left(\frac{d}{dt}\omega_g\right)^2 dt}_{\approx 0} \approx 0\,; \tag{7.1}$$

– In (5.35):

$$L_{d,th} - k_{thp1}\left|\omega_{0p}\right| \Delta\bar{\beta}_{loss,p} \underbrace{\frac{1}{t}\int_0^t \left(\frac{d}{dt}\omega_g\right)^2 dt}_{\approx 0} \approx 0\,; \tag{7.2}$$

– In (5.42):

$$L_{d,th} = -k_{thp1}\left|\omega_{0p}\right| \frac{1}{t}\int_0^t \left(\frac{d}{dt}\omega_p\right)^2 dt \underbrace{\frac{1}{t}\int_0^t \left(\frac{d}{dt}\omega_g\right)^2 dt}_{\approx 0} \approx 0\,. \tag{7.3}$$

PRC controller gains dependent on average load torque

Thus, the following control law is proposed to be used with PRC (Radan *et al.*, 2008):

$$k_{gp} = k_c \; Q_{0p}\bar{\beta}_{loss,p}\,, \tag{7.4}$$

where $\bar{\beta}_{loss,p}$ is the average relative load torque, $0 < \bar{\beta}_{loss,p} \le 1$. The average relative load torque is obtained using low pass filtering of the estimated load torque in a similar way as described in (5.36) of Chapter 5:

$$\bar{\beta}_{loss,p} = \hat{\beta}_{loss,p} - T_{Qf}\dot{\bar{\beta}}_{loss,p}\,, \tag{7.5}$$

$$\hat{\beta}_{loss,p} = \frac{\hat{Q}_{ap*}}{\hat{Q}_{0p}} = \frac{4\pi^2}{K_{Q0p}\rho D_p^5\;\hat{\omega}_p^2}\hat{Q}_{ap*}\,, \qquad \hat{\omega}_p \neq 0\,,$$

where T_{Qf} is the low pass filter time constant, and $\hat{Q}_{ap*}$ is to extended load torque estimate obtained from the propeller load torque observer, stated in (5.37).

After inserting (7.5) into (7.4), the final equation for the dynamic gain is obtained:

$$k_{gp} = \frac{k_c}{4\pi^2}\frac{\omega_{0p}^2}{\omega_p^2}\left(4\pi^2\hat{Q}_{ap} - T_{Qf}\dot{\bar{\beta}}_{Q,p}K_{Q0,p}\rho D_p^5\;\omega_p^2\right). \tag{7.6}$$

In (7.6) it can be noticed that the factor $\omega_{0p}^2 / \omega_p^2$ will amplify the fluctuations in the k_{gp} gain proportionally with the thruster shaft speed fluctuations i.e. it will introduce the dynamics of the shaft speed fluctuations into the control low. The k_{gp} gain will decrease when the ω_p increases. This is desirable behavior of the controller since less power will be distributed to the thruster as the propeller shaft speed fluctuations increase i.e. $\omega_{0p}^2 / \omega_p^2$ is high (the opposite holds as well). Based on the analysis in the Section 6.3, the speed fluctuations on thruster may indicate decreased thruster performance, both for the cases of the limited ability to control the shaft speed or having increased thrust losses. If the PRC is used on thruster, speed fluctuations may only indicate that the thruster is having high thrust losses. This gives "natural" sense of the thrust losses for the PRC controller and consequent load fluctuation injections to the network. Thus, the following dynamic PRC control gain is proposed:

$$k_{gp} = k_c \, Q_{0p} \left[\bar{\beta}_{loss,p}^{n} - T_{Qf} \dot{\bar{\beta}}_{loss,p} \right], \tag{7.7}$$

where $n = 2, 4, 6, \ldots$

7.1.2 Thruster gain dependent on sensitivity of shaft speed fluctuations

The average shaft speed fluctuations are determined from (6.11). The sensitivity for the shaft fluctuations is determined as differentiate of (6.11) with respect to the propeller load:

$$\frac{\partial \Delta \bar{\omega}_p}{\partial P_{0p}} = \frac{1}{k_1^{1/3}} \frac{1}{3} \left[\frac{1}{\bar{\beta}_{loss,p}} \left(\frac{P_{0p}}{\bar{\beta}_{loss,p}} \right)^{-2/3} - P_{0p}^{-2/3} \right]. \tag{7.8}$$

If the sensitivity to shaft speed fluctuations increases, the load increase on this propeller can be penalized. Then, the thrust would be re-distributed to other propellers.

PRC controller gains dependent on sensitivity of shaft speed fluctuations

The following control law is proposed for PRC gains:

$$k_{gp} = k_c \left[\frac{1}{\bar{\beta}_{loss,p}} \left(\frac{P_{0p}}{\bar{\beta}_{loss,p}} \right)^{-2/3} - P_{0p}^{-2/3} + 1 \right] Q_{0p}, \tag{7.9}$$

$$k_{gp} \geq k_c Q_{0p}, \quad P_{0p} \text{ is in p.u. (percentage of total)},$$

where the last term in (7.9) is used to neutralize the load compensation for thrusters that have very low thrust losses, $\beta_{loss,p} \approx 1$. Thus, the thrusters that do not experience thrust losses will depend on Q_{0p} only.

7.1.3 Results of simulation

The results of the simulation when using both of these control laws are presented in Figs. 7.2 to 7.5. The following PRC controller gains have been compared:

1. *No loss sensitive*: PRC average load torque without thrust losses included (6.22);
2. *Torque loss based*: PRC controller gains dependent on average load torque (7.4);
3. *Speed fluctuation based*: PRC Thruster gains dependent on the sensitivity of shaft speed fluctuations (7.9).

The same load scenario is used as previously in this Chapter.

The propeller shaft accelerations with *torque loss based* PRC gains and with *shaft speed fluctuations* based PRC gains are compared to nominal torque Q_{0p} dependant PRC gains (i.e. non sensitive to thrust losses) and presented in Figs. 7.2 and 7.3 respectively.

The main control goal is to keep the propeller shaft accelerations as low as possible while keeping the network frequency within prescribed limits.

It can be noticed from Fig. 7.2 that when using *torque loss based* PRC controller gains the control will not be improved with respect to propeller shaft accelerations – in fact, in this case they become somewhat worse as the values of the acceleration on thruster 2 in the lower part of Fig. 7.2 increase.

The shaft accelerations for the PRC controller gains based on *shaft speed fluctuations*, are presented in Fig. 7.3. The shaft speed results of simulation on both thrusters, for both controllers are shown in Fig. 7.4.

From Fig. 7.3, it can be noticed that the accelerations on the thruster 2 are lower than as for the *no loss sensitive* case, while on the thruster 1 are nearly the same. It may be important to see from Fig. 7.5 that with PRC controller gains based on *shaft speed fluctuations* the network frequency control improves while at the same time the propeller shaft accelerations decrease. The price of the reduction of shaft accelerations on thrusters will not be high for the network frequency control. Thus, the trade-offs are not necessary as both goals can be accomplished. The simulation results show that this controller has all desired features.

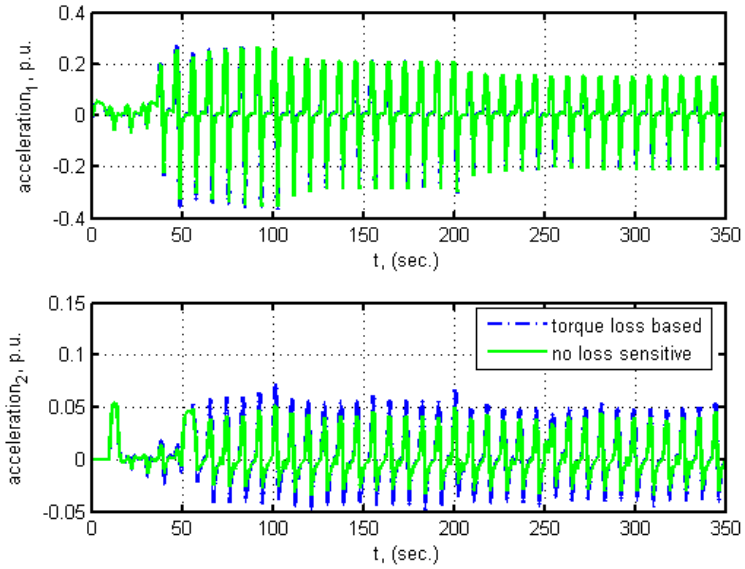

Fig. 7.2. Propeller shaft accelerations with PRC when
using *PRC controller gains dependent on average load torque*

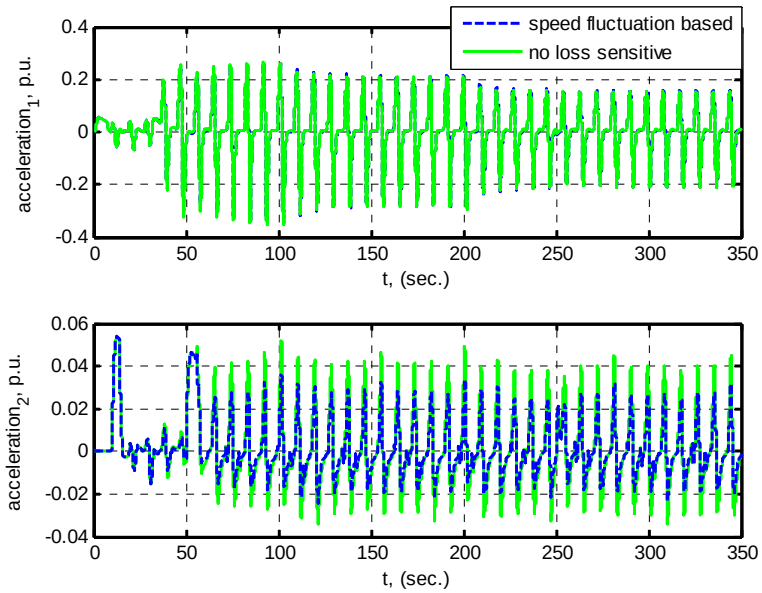

Fig. 7.3. Propeller shaft accelerations with PRC when
using *thruster gain dependent on sensitivity of shaft speed fluctuations*

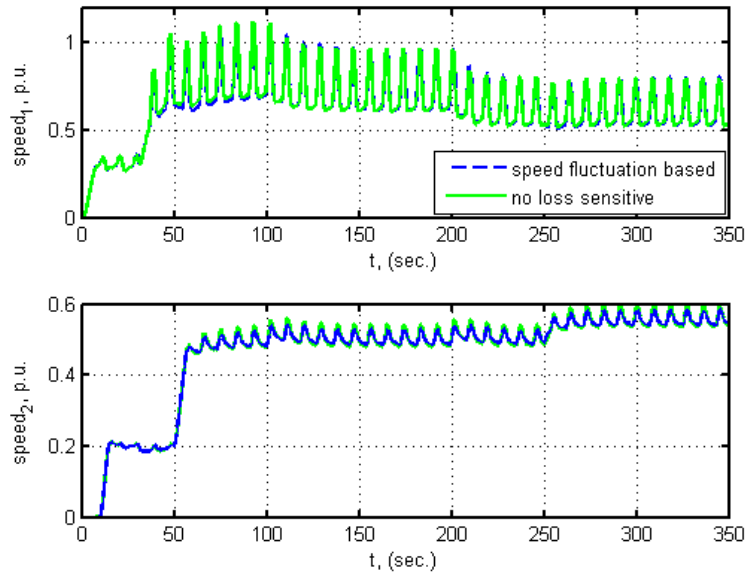

Fig. 7.4. Propeller shaft speed with PRC when
using *thruster gain dependent on sensitivity of shaft speed fluctuations*

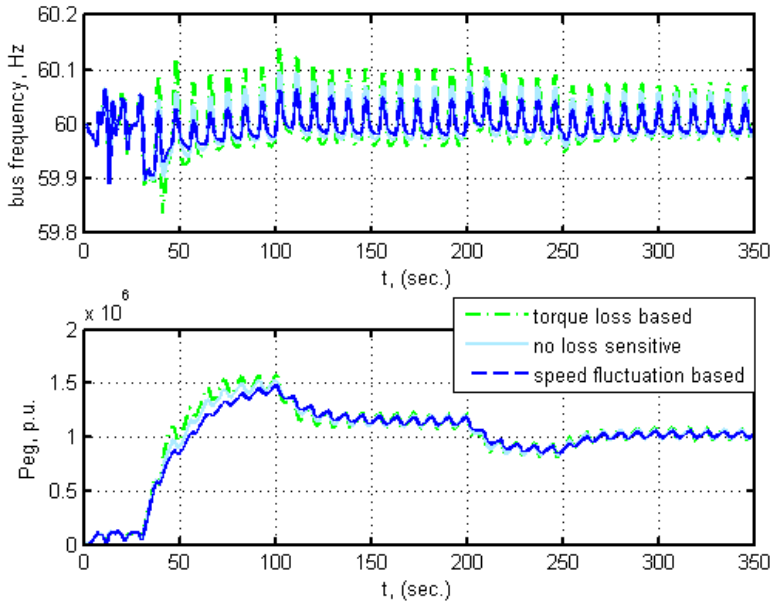

Fig. 7.5. Frequency and electrical network power when using proposed PRC controller gains

7.2 Frequency-based load limiting control

The frequency based load limiting control is part of the *Power Redistribution Control* (*PRC*), presented in Chapter 6. In order to have highly accurate frequency-based load limiting, the proposed control law is based on the PRC, in addition to the integrating term (low pass filtered term) feedback as follows:

$$e_p = \omega_{0p} - \omega_p + k_{gP}\frac{2H_{Non}}{\omega_{0g}}\frac{d\hat{\omega}_g}{dt} + k_{gI}\frac{1}{\tau_{gI}s+1}\frac{d\hat{\omega}_g}{dt}. \tag{7.10}$$

The propeller speed control is obtained using PI controller (6.1). Hence, when using the feedback from the generating system torque deviation in e_p (7.10), the thruster commanded torque becomes:

$$\begin{aligned} Q_{cp} &= k_{pP}\left(\omega_{0p} - \omega_p\right) + k_{pP}k_{gP}\frac{2H_{Non}}{\omega_{0g}}\frac{d\hat{\omega}_g}{dt} + k_{pP}k_{gI}\frac{1}{\tau_{gI}s+1}\frac{d\hat{\omega}_g}{dt} \\ &+ k_{pI}\int_0^t\left(\omega_{0p} - \omega_p\right)d\tau + k_{pI}k_{gP}\hat{\omega}_g\frac{2H_{Non}}{\omega_{0g}} + k_{pI}k_{gI}\int_0^t\frac{1}{\tau_{gI}s+1}\frac{d\hat{\omega}_g}{dt}d\tau. \end{aligned} \tag{7.11}$$

Taking the average network frequency as:

$$\bar{\hat{\omega}}_g = \frac{1}{\tau_{gI}s+1}\frac{d\hat{\omega}_g}{dt} = \hat{\omega}_g - \tau_{gI}\frac{d\hat{\omega}_g}{dt}, \tag{7.12}$$

the commanded torque is obtained:

$$\begin{aligned} Q_{cp} &= k_{pP}\left(\omega_{0p} - \omega_p\right) + \left(k_{pP}k_{gP}\frac{2H_{Non}}{\omega_{0g}} - k_{pP}k_{gI}\tau_{gI}\right)\frac{d\hat{\omega}_g}{dt} + k_{pP}k_{gI}\hat{\omega}_g \\ &+ k_{pI}\int_0^t\left(\omega_{0p} - \omega_p\right)d\tau + \left(k_{pI}k_{gP}\frac{2H_{Non}}{\omega_{0g}} - k_{pI}k_{gI}\tau_{gI}\right)\hat{\omega}_g + k_{pI}k_{gI}\int_0^t\hat{\omega}_g d\tau. \end{aligned} \tag{7.13}$$

Thus, if $k_{pI}k_{gP}\frac{2H_{Non}}{\omega_{0g}} = k_{pI}k_{gI}\tau_{gI}$, then the 2nd and 5th terms in the brackets will diminish and the commanded torque would become:

$$Q_{cp} = k_{pP}\left(\omega_{0p} - \omega_p\right) + k_{pP}k_{gI}\hat{\omega}_g + k_{pI}\int_0^t\left(\omega_{0p} - \omega_p\right)d\tau + k_{pI}k_{gI}\int_0^t\hat{\omega}_g d\tau, \tag{7.14}$$

for $\tau_{gI} = \frac{k_{gP}}{k_{gI}}\frac{2H_{Non}}{\omega_{0g}}$.

In (7.14) the thruster commanded torque does not depend on the mean acceleration of the power generating system, as suppose when using PRC control strategy 2 (6.14) on thruster PI speed controller, i.e.:

$$Q_{cp} = k_{pP}\left(\omega_{0p} - \omega_p\right) + k_{pP}k_{gp}\frac{2H_{Non}}{\omega_{0g}}\frac{d\hat{\omega}_g}{dt} + k_{pI}\int_0^t\left(\omega_{0p} - \omega_p\right)d\tau + k_{pI}k_{gp}\frac{2H_{Non}}{\omega_{0g}}\hat{\omega}_g \,, \quad (7.15)$$

This means that as long as $\tau_{gI} < \frac{k_{gP}}{k_{gI}}\frac{2H_{Non}}{\omega_{0g}}$ the control law will have the feedback acceleration and consequent behavior of increased system inertia. As τ_{gI} is increasing, the thruster controller becomes more dependent on the generating system speed than the acceleration.

Assuming that one thruster is the only consumer in the system the motion equation for the mean acceleration of the power generating system may be expressed as:

$$\begin{aligned}\frac{d\omega_g}{dt} = \frac{\omega_{0g}}{2H_{N_{on}}}\Bigg[& Q_{mg} - \frac{D_g}{\omega_{0g}}\left(\omega_g - \omega_{0g}\right) - \frac{\omega_p}{P_{rg}\omega_g}k_{pP}\left(\omega_{0p} - \omega_p\right) - \frac{\omega_p}{P_{rg}\omega_g}\frac{d\hat{\omega}_g}{dt}\left(k_{pP}k_{gP}\frac{2H_{Non}}{\omega_{0g}} - k_{pP}k_{gI}\tau_{gI}\right) \\ & - \frac{\omega_p}{P_{rg}\omega_g}k_{pP}k_{gI}\hat{\omega}_g - \frac{\omega_p}{P_{rg}\omega_g}k_{pI}\int_0^t\left(\omega_{0p} - \omega_p\right)d\tau \\ & - \frac{\omega_p}{P_{rg}\omega_g}\left(k_{pI}k_{gP}\frac{2H_{Non}}{\omega_{0g}} - k_{pI}k_{gI}\tau_{gI}\right)\hat{\omega}_g - \frac{\omega_p}{P_{rg}\omega_g}k_{pI}k_{gI}\int_0^t\hat{\omega}_g d\tau\Bigg]\end{aligned} \quad (7.16)$$

where the feedback acceleration term will be responsible for the increase in the system inertia, as shown when assuming $Q_{cp} = Q_{mp}$ and $\dot{\hat{\omega}}_g = \dot{\omega}_g$:

$$\begin{aligned}\left(1 + \frac{\omega_p}{P_{rg}\omega_g}k_{pP}k_{gP} - \frac{\omega_{0g}\tau_{gI}}{2H_{N_{on}}}\frac{\omega_p}{P_{rg}\omega_g}k_{pP}k_{gI}\right)\frac{d\hat{\omega}_g}{dt} = \frac{\omega_{0g}}{2H_{N_{on}}}\Bigg[& Q_{mg} - \frac{D_g}{\omega_{0g}}\left(\omega_g - \omega_{0g}\right) \\ & - \frac{\omega_p}{P_{rg}\omega_g}k_{pP}\left(\omega_{0p} - \omega_p\right) - \frac{\omega_p}{P_{rg}\omega_g}k_{pP}k_{gI}\hat{\omega}_g - \frac{\omega_p}{P_{rg}\omega_g}k_{pI}\int_0^t\left(\omega_{0p} - \omega_p\right)d\tau \\ & - \frac{\omega_p}{P_{rg}\omega_g}\left(k_{pI}k_{gP}\frac{2H_{Non}}{\omega_{0g}} - k_{pI}k_{gI}\tau_{gI}\right)\hat{\omega}_g - \frac{\omega_p}{P_{rg}\omega_g}k_{pI}k_{gI}\int_0^t\hat{\omega}_g d\tau\Bigg]\end{aligned} \quad (7.17)$$

Thus, if $k_{gP} < \frac{\omega_{0g}}{2H_{N_{on}}}k_{gI}\tau_{gI}$, the system inertia will become lower than without the PRC controller, and the overall control performance will deteriorate. This equation indicates the value limits for tuning the PRC controller with respect to accuracy in the control responses.

7.3 Integration aspects of PRC with DP thrust allocation

7.3.1 Real thrust estimation and thrust fluctuations

The thrust reference is the output from the DP thrust allocation algorithm. When the vessel is in waves, the real torque will oscillate about the nominal value due to vessel-wave interaction at the propeller disk. The main purpose of PRC is to slightly alter the required thrust reference in order to obtain smooth power output sensed by the generators on the network. Therefore, it may be of importance for the DP system to estimate the actual thrust.

The propeller load torque can be estimated using an observer. A real-time estimated thrust can be determined from the real-time load torque (5.37):

$$\hat{T}_{a,p} = \frac{K_{T0,p}}{D_p K_{Q0,p}} \hat{Q}_{a,p} . \tag{7.18}$$

Alternate mappings are also possible, for details see Smogeli (2006) and references therein. The altered expected nominal thrust can be fed back to the thrust allocation algorithm, as proposed in Fig. 7.6. The estimated thrust can be filtered using a low pass filter as proposed:

$$\hat{T}_{a,p} = h_{Tp}(s) \frac{K_{T0,p}}{D_p K_{Q0,p}} \hat{Q}_{a,p} .$$

$$h_{Tp}(s) = \frac{1}{\tau_{Tp} s + 1} , \tag{7.19}$$

where low pass filter may have many alternative designs, see e.g. Fossen (2002).

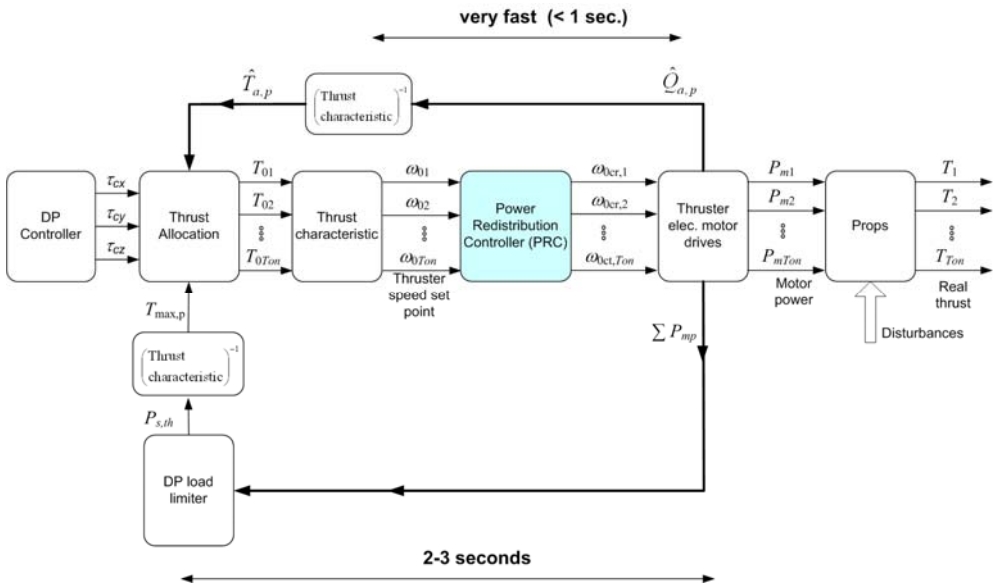

Fig. 7.6. Structure of proposed PRC with DP and thrust allocation

7.3.2 Constrained control allocation with sensitivity to propeller speed fluctuations

The proposed *propeller shaft speed fluctuation sensitivity* can be implemented in most of the thrust allocation algorithms proposed in e.g. Fossen (2002), Fossen and Johansen (2006), Johansen, (2004) and the references therein.

Typical thrust allocation algorithm will find an optimal distribution of control forces to thrusters in order to keep the vessel in the position with minimum energy or power, see e.g. (Fossen, 2002). The minimum energy solution referees to the hydrodynamic disturbances as the thrust allocation algorithm attempt to keep the vessel in the position with minimum forces on thrusters subject to various constraints (azimuth angle, thrust force, etc.).

The cost function proposed in this section can be used to distribute the thrust between thrusters, set by thrust allocation algorithm, in order to *reduce the speed fluctuations on thrusters*. This can be done in two ways:

- The proposed *propeller shaft speed fluctuation sensitivity* is directly included in the total cost function of the thrust allocation algorithm, and minimized together with the power consumption;
- The proposed *propeller shaft speed fluctuation sensitivity* can be implemented in thrust allocation as the constraint. Within the allowed constraint, the individual thrusters are allowed to fluctuate. Then, crossing the predefined threshold would be penalized in the cost function.

Strategy 1 *- propeller shaft speed fluctuation sensitivity included in thrust allocation cost function*

The *sensitivity to shaft speed fluctuations* shown in Fig. 7.7, is proposed in this thesis to be implemented in the DP thrust allocation algorithm developed by Johansen *et al.* (2004b) for constrained control allocation with azimuthing thrusters. Then the following DP thrust allocation cost function is proposed to be used with the proposed *power redistribution controller* (PRC):

$$J = \min_{f,\alpha,s} \left\{ \sum_{p=1}^{N_p} \Pi_p \left| T_{0p} \right|^{3/2} + s^T Q\, s + \left(\alpha - \alpha_0\right)^T \Omega \left(\alpha - \alpha_0\right) + \frac{\rho}{\varepsilon + \det\left(T(\alpha) W^{-1} T^T(\alpha)\right)} + \sum_{p=1}^{N_p} \Psi_p \left[\frac{T_{0p}^{1/2}}{\overline{\beta}_{loss,p}^{1/3}} - T_{0p}^{1/2} \right] \right\}, \tag{7.20}$$

subject to following constraints:

- $T(\alpha) F = \tau + s$;
- $T_{0p,\min} \le T_{0p} \le T_{0p,\max}$;
- $\alpha_{p,\min} \le \alpha_p \le \alpha_{p,\max}$;
- $\Delta\alpha_{p,\min} \le \alpha_p - \alpha_{p0} \le \Delta\alpha_{p,\max}$,

where:

- $\sum_{p=1}^{N_p} \Pi_p \left| T_{0p} \right|^{3/2}$ represents the total power consumption, as the power is function of thrust on degree of 3/2, see (5.25) where: $P_{0p} = \text{const.}\ T_{0p}{}^{3/2}$, Π_p are positive weights $\Pi_p > 0$;
- $\sum_{p=1}^{N_p} \Psi_p \left[\frac{T_{0p}{}^{1/2}}{\bar{\beta}_{loss,p}^{1/3}} - T_{0p}{}^{1/2} \right]$ represents the proposed speed fluctuation included in the last term of the cost function when $P_{0p} = \text{const.}\ T_{0p}{}^{3/2}$ is substituted in (6.11), ψ_p are positive weights $\psi_p > 0$;
- $s^T Q\, s$ penalizes the error of the constraint $T(\alpha)F = \tau + s$. The weight matrix Q is chosen so large that the optimal solution $s \approx 0$ is whenever possible;
- $T(\alpha)F = \tau + s$, where τ is the total required thrust, s is the slack variable of the optimization, $T(\alpha)$ is the thrust configuration matrix and F is the vector of thrust forces, as defined later (Fossen, 2002);
- $T_{0p,\min} \le T_{0p} \le T_{0p,\max}$ is used to limit the thrust force;
- $\alpha_{p,\min} \le \alpha_p \le \alpha_{p,\max}$ is used to limit the feasible sectors of azimuth angle;
- $\Delta\alpha_{p,\min} \le \alpha_p - \alpha_{p0} \le \Delta\alpha_{p,\max}$ is used to limit the rate of change of azimuth angle;
- $\frac{\rho}{\varepsilon + \det\left(T(\alpha)W^{-1}T^T(\alpha)\right)}$ is used to avoid singular solution with $\det\left(T(\alpha)W^{-1}T^T(\alpha)\right) = 0$ as this would will be strongly penalized in the cost function J in (7.20). W is the positive definite cost matrix and ρ is the penalty constant.

$T(\alpha)$ is the thrust configuration matrix and F is the vector of thrust forces as define below:

$$T(\alpha)F = \begin{bmatrix} t_1 & t_2 & \dots & t_{N_p} \end{bmatrix} \begin{bmatrix} T_{01} \\ T_{02} \\ \vdots \\ T_{0N_p} \end{bmatrix}, \tag{7.21}$$

where t_p is the thust configuration vector and $T(\alpha)$ is the thrust configuration matrix (Fossen, 2002) and F is the vector of thrust forces. Inside F, the T_{0p} is thrust force per thruster.

The thrust force T_{0p} is used in most of the thrust allocation algorithms, e.g. Fossen (2002), Fossen and Johansen (2006), Johansen, (2004) and the references therein.

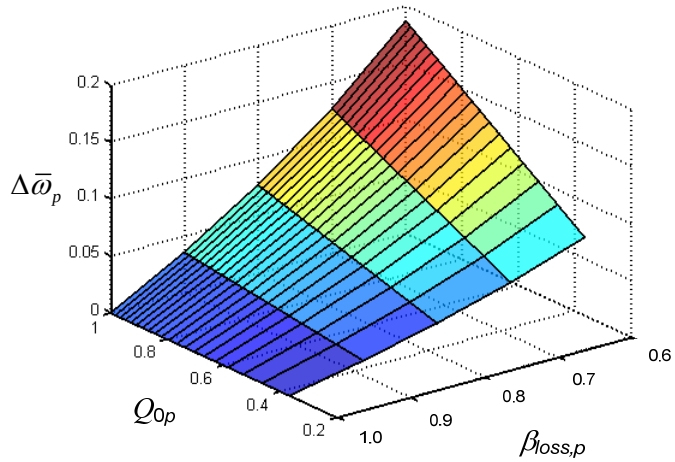

Fig. 7.7. Control sensitivity map to shaft speed fluctuations when using PRC with DP and thrust allocation

Strategy 2 - *propeller shaft speed fluctuation sensitivity included as the constraint in thrust allocation*

The proposed *propeller shaft speed fluctuation sensitivity* is implemented in thrust allocation as the constraint. Within the allowed constraint, the individual thrusters are allowed to fluctuate. Then, crossing the predefined threshold is penalized in the thrust allocation cost function as shown:

$$J = \min_{f,\alpha,s}\left\{\sum_{p=1}^{N_p}\Pi_p\left|T_{0p}\right|^{3/2} + s^T Q\, s + (\alpha-\alpha_0)^T\,\Omega(\alpha-\alpha_0) \;+\frac{\rho}{\varepsilon+\det\left(T(\alpha)W^{-1}T^T(\alpha)\right)} + p_s{}^T R_\omega p_s\right\}, \tag{7.22}$$

subject to the same constraints as in (7.20) and the following additional constraint:

– $\Delta\bar{\omega}_{th} = p_{\Delta\omega} + p_s$;

where $p_s{}^T R_\omega p_s$ is used to penalize the error of the constraint $\Delta\bar{\omega}_{th} = p_{\Delta\omega} + p_s$. The weight matrix R_ω is chosen so large that the optimal solution $p_s \approx 0$ is whenever possible.

The vectors in the constraint are defined as:

$$\Delta\bar{\omega}_{th} = \left(\Delta\bar{\omega}_1 \quad \Delta\bar{\omega}_2 \quad \ldots \quad \Delta\bar{\omega}_{N_p}\right)^T \text{ and } p_{\Delta\omega} = \left(p_{\Delta\omega 1} \quad p_{\Delta\omega 1} \quad \ldots \quad p_{\Delta\omega N_p}\right)^T, \tag{7.23}$$

where:

$$\Delta\bar{\omega}_p = \frac{1}{k_1^{1/3}}\left[\left(\frac{P_{0p}}{\bar{\beta}_{loss,p}}\right)^{1/3} - P_{0p}^{1/3}\right] = \frac{1}{k_1^{1/3}}\left[\frac{T_{0p}{}^{1/2}}{\bar{\beta}_{loss,p}^{1/3}} - T_{0p}{}^{1/2}\right]. \tag{7.24}$$

7.4 Integrated network control concept for increased robustness to faults and blackout

When using the power redistribution controller (PRC), a number of other controllers are not necessary. This can be seen by comparing the PRC presented in Fig. 7.8 with the existing controller structure presented in Fig. 3.10.

The PRC utilizes a low number of sensors and communication feedbacks and is using distributed controllers, as shown in Fig. 7.8. This increases the robustness of power plant to faults and blackout. The following aspects of the integrated power network control are proposed in this Chapter:

1. ***Power Redistribution Control*** (*PRC*) proposed in Chapter 6: The control redistributes the power among consumers that generate load fluctuations and thrusters that generate and compensate for the fluctuations. Significant improvements in the network frequency and voltage control are achieved;
2. ***Frequency-based load limiting control*** proposed in this Chapter: It is based on the extended functionality of *PRC* with fast control adaptation to changes in the structure of the power plant, e.g. open/closed generator circuit breaker, open/closed bus-tie, new consumers start/stop. The controller is independent of the communication and information share about the circuit breaker status;
3. ***Quasi-static load limiting control*** proposed in Chapter 5: It is based on the estimated thrust losses on the propeller and implicative indications of network load fluctuations generated by individual consumers. The controller is independent of the communication. The integration with DP thrust allocation is accomplished simply by providing a new limits for thrust allocation algorithm;
4. ***DP thrust allocation control*** proposed in this Chapter: It implements the existing thrust allocation algorithms with the sensitivity to propeller speed fluctuations. In this way, the commanded thrust on bad performing thruster will be reduced and the thrust will be reallocated to other thrusters.
5. ***Observer-based fast load reduction*** (*Obs-FLR*) proposed in Chapter 3: It is capable to recognize the generator trip from the network frequency and power (current, voltage) measurements. There is no dependence on communication with PMS controller and the switchboard about the breaker status. The blackout detection algorithm, within the controller, is capable to sense the breaker status without heaving communication links from the switchboard. Although similar to controller under 2, it will react much faster in order to prevent the blackout. *Obs-FLR* is based on the hybrid control concept consisted of the network frequency sensing and detection of breaker switching.

The main feature of integrated control concept is that the problems with communication delays and faults are avoided and the number of sensors and communication between controllers is minimized. Moreover, as the control is distributed in the power system, high level of redundancy and reliability is achieved i.e. robustness to faults and blackouts.

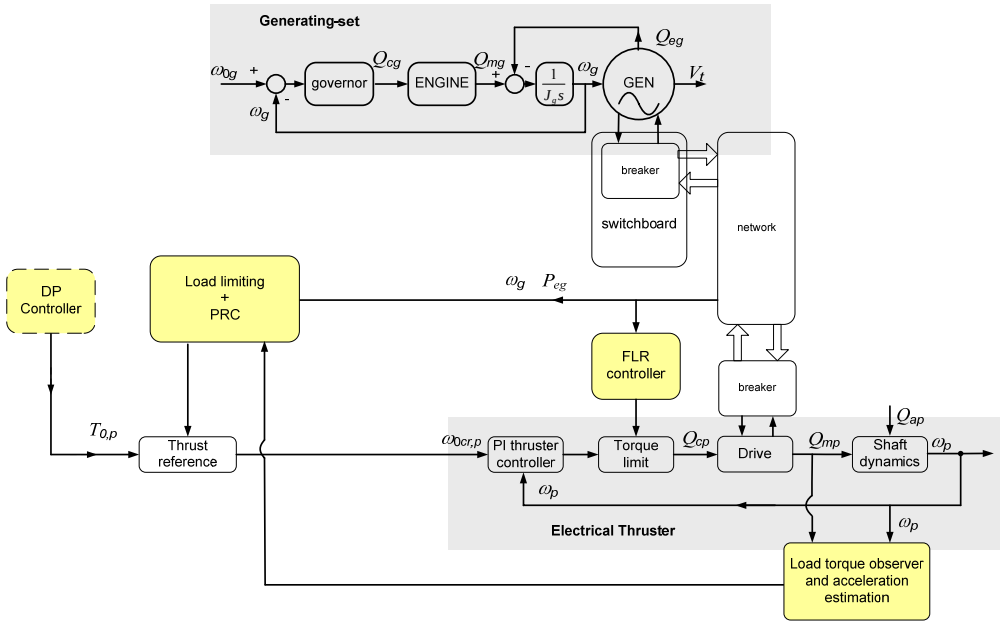

Fig. 7.8. Integrated power network control with low number of feedbacks, and with distributed controllers

Chapter 8

Speed control of generators and thrusters

8.1 Motivations

Propeller torque losses

When vessel operates in harsh weather conditions, the propellers may be subjected to large thrust and torque fluctuations. These fluctuations are generated by the propeller periodic change of submergence condition which leads to ventilation (air suction) and partial or full propeller emergence, see Sørensen *et al.* (1997), Smogeli *et al.* (2004a), Smogeli *et al.* (2004b), Smogeli (2006), Ruth (2005), Ruth and Smogeli (2006), Bakkeheim *et al.* (2006), Bakkeheim *et al.* (2007a), Bakkeheim *et al.* (2007b), Radan *et al.* (2006b), Radan *et al.* (2007a), Pivano *et al.* (2007a), and Pivano *et al.* (2007b).

Wear and tear

Large torque variations on propulsion engines are known to produce high frequency torsional vibrations in the stern shaft which transmits to the engine bearings, gears and vessel structure. The guidelines for preventing vibrations caused by the engine combustion and interaction with propeller are given by the engine vendors, see e.g. MAN B&W, Wartsila and classification societies, see e.g. Tienhaara (2004), Carlton and Vlasic (2005), and Dahler *et al.* (2006).

The propeller interations on electrical thrusters and causes for the increased wear-out rate of thrusters operating in hash offshore conditions have been identified using model experiments, see e.g. Koushan (2004), Koushan (2006), and references therein. Large variations in the shaft speed may be the cause of mechanical failures of the power transmission parts such as shaft bearings, gears and increased wear-out of shaft seals.

Speed encoders

Typically, the shaft encoder used for the shaft speed measurement produces the noise in the speed signal. If the signal is fed back to the controller, the noise will be interpreted as the disturbance, and the commanded torque may induce undesired torsional vibrations in the power transmission. These vibrations can increase the fatigue of the mechanical components and increase the risk of component failure. To obtain robustness and noise suppression in the commanded torque, speed controllers for electric machines are typically proportional-integral (PI), while the derivative term (D) is typically set to zero. Avoiding the noise amplification in high bandwidth actuators, such as electric drives, requires special attention.

For diesel engines, gas- and steam turbines, the actuator dynamics of the speed governor acts typically as a low pass filter, and the responses of the engine itself are relatively slow compared to the electrical variable speed thruster. Thus, the D-term in the controller may have low positive values improving the speed of response to large disturbances. Since the D-

term can not be set high, large diesel engines are typically equipped with fast-acting over-speed cut-out devices used to cut the fuel supply when over-speed occurs preventing possibly serious damages of the engine and stern-shaft components, see e.g. Nikolaos *et al.* (2000). The problems involved in speed control of large diesel engines (2 stroke) are extensively analyzed and tested in the full scale in Nikolaos *et al.* (2000), where the authors proposed using accelerometers and sensors to determine the proximity of the water surface to the propeller blade.

D-term

As the D-term can improve the control, the problem remains how to suppress the sensor noise amplified in the D-term. Moreover, the noise will also be amplified as undesired disturbance in the PI terms as well. Typically, low pass filters are used to suppress the noise in the measurements. The problem arises due to relatively large phase shift that may have detrimental effect on the control – the feedback signal is filtered but delayed.

Speed encoder observers

One approach to improve the performance of speed control of electric machines is to use the observer (state estimator) to filter the noise from the measurement. The observers may include the machine and encoder dynamics, as proposed in e.g. Kweon and Hyun (1999), Tilli and Montanari (2001), Wang *et al.* (2004), Comes Sanz *et al.* (2004), Kovudhikulrungsri and Koseki (2006).

In this thesis, several types of observers (state estimators) and controllers are proposed. The proposed observers are capable to reduce the noise from any measurement and/or estimation, including speed and electrical torque, while having low detrimental impact on the control.

Noise handling separation principle

In this thesis, the observers are designed and tuned with respect to controller performance, so the overall closed-loop performance is considered (Radan *et al.*, 2007a). This is found contrary to separation principle used in the design of linear (but also some class of non-linear) observers. Thus, semi-global stabilization under output feedback is assumed (Atassi and Khalil, 1999). The semi-global stabilization and various robustness issues will be considered in order to obtain good suppression of noise and modeling error. This Chapter demonstrates how the design and tuning of the controller will depend on the design and tuning of the observer and how non-linear controllers may provide better overall control performance with respect to mechanical stress and constraints of the cascaded control structure.

Noise suppression observers - proposed

Based on the Radan *et al.* (2007a), one of the proposed observers is termed the *inertial observer*, as it is used to calculate the shaft acceleration from the measured or the estimated speed with low level of noise transmitted.

Other observer types are also considered for the control of electric machines and engines, namely *proportional-integral observers* (PIO), proposed by Shafai and Carroll (1985), Beale and Shafai (1989), Shafai and Nork (2002), and Busawon and Kabore (2001). The proposed observers are used to improve the speed control performance of electric machines and

engines by improving the robustness to noise and faults in the sensors. One of the important benefits of PIO observer is that it can handle the noise in the states and input, rather than only output signal - as is the case when using the *speed encoder observers*. The proposed observers are compared with *low pass filter* when used with standard PI(D) controllers.

The enhanced speed control performance is accomplished when combined (hybrid) of *speed and torque observers* and the *inertial observer* (PIDO) are used with controllers.

Noise suppression controllers

The following controllers, used to attenuate the noise in the measurements and states, are proposed in the thesis. These are namely:

- *PI(D) controller with dynamic gains*;
- *Inertial controller* (Radan *et al.*, 2007a);
- *Combined inertial controller with damping*;
- *Direct torque-loss controller or soft-anti spin controller*. The anti spin controller for the marine thrusters is first proposed in Smogeli *et al.* (2004a), and improvements in the control performance can be found in Smogeli (2006), Bakkeheim *et al.* (2006), Bakkeheim *et al.* (2007a), Bakkeheim *et al.* (2007b). In this thesis a modified anti-spin control is proposed.

The proposed controllers combined with the PIDO observers can improve the speed control of electrical thrusters, and potentially improve the speed control of propulsion engines and generating-sets. The proposed control strategies do not require any additional sensors. The application for the thrusters is demonstrated in the case studies although the potential applicability is provided also for all electrical machines and engines.

8.2 Effect of noise on shaft speed control

Assume that the speed controller is affected by some measurement noise $d_\omega(t)$. Then, the speed variation e_p is:

$$e_p = \omega_{0p} - \left(\omega_p + d_\omega\right). \tag{8.1}$$

If the standard PI controller is used $Q_{cp} = k_{Pp} e_p + k_{Ip} \int_0^t e_p d\tau$ then the measurement noise will be transmitted into the commanded torque:

$$\begin{aligned} Q_{cp} = {} & k_{Pp}\omega_{0p} - k_{Pp}\omega_p - k_{Pp} d_\omega + \\ & \int_0^t k_{Ip}\omega_{0p} d\tau + \int_0^t -k_{Ip}\omega_p d\tau + \int_0^t -k_{Ip} d_\omega d\tau \\ & k_{Dp}\frac{d}{dt}\omega_{0p} - k_{Dp}\frac{d}{dt}\omega_p - k_{Dp}\frac{d}{dt} d_\omega \end{aligned} \tag{8.2}$$

The noise entering the control loop is highly undesirable due to high bandwidth of the current controller which will interpret the noise as fast changing disturbance, see Appendix B:

$$Q_{cp} = Q_{cp,s} + Q_{cp,d}\,, \tag{8.3}$$

where:

- $Q_{cp} = k_{Pp}\left(\omega_{0p} - \omega_p\right) + k_{Ip}\int_0^t \left(\omega_{0p} - \omega_p\right) d\tau + k_{Dp}\frac{d}{dt}\left(\omega_{0p} - \omega_p\right)$ is the noiseless part of commanded torque;
- $Q_{cp,d} = -k_{Pp} d_\omega - \int_0^t k_{Ip} d_\omega d\tau - k_{Dp}\frac{d}{dt} d_\omega$ is additional undesirable torque due to measurement noise d_ω.

Neglecting the thruster dynamics Q_{mp}=Q_{cp}, and inserting (8.2) into (5.4) the following closed-loop equation of the propeller shaft motion is obtained:

$$\frac{d}{dt}\omega_p = \frac{1}{J_p}\left[k_{Pp}\left(\omega_{0p} - \omega_p\right) + k_{Ip}\int_0^t \left(\omega_{0p} - \omega_p\right) d\tau + k_{Dp}\frac{d}{dt}\left(\omega_{0p} - \omega_p\right) \right.$$
$$\left. \underbrace{-k_{Pp} d_\omega - \int_0^t k_{Ip} d_\omega d\tau - k_{Dp}\frac{d}{dt} d_\omega}_{Q_{cp,d}} - Q_{ap} - Q_{fp} \right]. \tag{8.4}$$

As can be seen from (8.4), the undesired measurement noise $d_\omega(t)$, is transferred to the shaft motion through the control action $Q_{cp,d}$. Due to noise amplification in the controller, the shaft torque vibrations will increase. Therefore, as the noise will be amplified in the controller, the speed variations e_p may not be reduced to the desired level. This may result in the increased wear-out rate of the power transmission system on the thruster.

The closed-loop equation of motion (8.4) clearly explains why the D-term in PID control is usually diminished or set to zero in electro-mechanical rotating machinery. By setting k_{Dp} = 0, the term that differentiates the noise $d_\omega(t)$, in (8.4) will be canceled. The drawback is that the derivative term in the k_{Dp}d/dt($\omega_{0p} - \omega_p$) noiseless part of commanded torque (8.4) will also be canceled, and the shaft speed control, for ideal noiseless control system may deteriorate. This may be partly compensated by increasing the gains in PI-terms. When PI-terms are high, the thruster acceleration/deceleration must be limited using the load rate limits described in Chapter 2.

As long as the propeller is subject to moderate weather conditions, standard PI controller may cope well with the propeller disturbances. Thus, the described problems are more pronounced in the harsh environmental conditions. As the shaft torsional vibrations are induced by the torque variations, the controller gains of PI(D) controller are actually bounded with a function of torque deviation (Radan *et al.*, 2007a):

$$k_{Pp}, k_{Ip}, k_{Dp} \le f\left(\left\| Q_{mp}\left(\omega_s\right) - Q_{ap}^*\left(\omega_s\right)\right\|\right), \tag{8.5}$$

where $Q_{mp} - Q_{ap}^{*}$ is the torque deviation sensed on the shaft, $Q_{ap}^{*} = Q_{ap} + Q_{fp}$ is the extended load torque that includes friction and ω_s is the noise frequency. The torque fluctuations are to be suppressed above certain frequency ω_s range.

Thus, the main goal, with any shaft speed control is to reduce torque deviations on the propeller shaft, which is in fact the same as reducing the shaft accelerations in (8.4).

8.3 State estimation for improved noise filtering

8.3.1 Proportional observer

The proportional observer is usually regarded to be classical Luenberger form for linear systems or a high gain observer for non-linear systems, see e.g. Gauthier *et al.* (1992), Shafai (1985), and Busawon and Kabore (2001).

Luenberger observer

Consider the time invariant system described by:

$$\frac{d}{dt}x = Ax + Bu \tag{8.6}$$

$$y = Cx\,,$$

where $x \in R^n$ is the state vector, $u \in R^m$ is the control vector, $y \in R^p$ is the output of the system, and *A*, *B*, *C* are corresponding matrices and vectors.

The proportional (P) observer is:

$$\frac{d}{dt}\hat{x} = A\hat{x} + Bu + L\left(y - C\hat{x}\right), \tag{8.7}$$

where L is the observer gain vector. The estimation error is defined as $\tilde{x} = x - \hat{x}$, and differentiation of estimation error $\dot{\tilde{x}} = \dot{x} - \dot{\hat{x}}$, thus the error dynamics would have the expression:

$$\dot{\tilde{x}} = \dot{x} - \dot{\hat{x}} = \left(A - LC\right)\tilde{x}\,, \tag{8.8}$$

Where *A*–*LC* should be *Hurwitz* matrix in order to guarantee the asymptotic stability (Chen, 1999).

Measurement noise d_y

Now, consider the measurement noise present at the output signal. The model would be:

$$\frac{d}{dt}x = Ax + Bu \tag{8.9}$$

$$y = Cx + Ed_y,$$

where the disturbance vector $d_y \in R^q$ represents the measurement noise vector. Using the proportional observer in (8.7), the following error dynamics is obtained:

$$\dot{\tilde{x}} = \dot{x} - \dot{\hat{x}} = (A - LC)\tilde{x} - LEd_y, \tag{8.10}$$

where *A–LC* should be *Hurwitz*. Now, the problem arises due to LEd_y present in the error dynamics. As the observer gain L increases, the error dynamics converges faster to zero for the price of amplifying the measurement noise in the error dynamics.

Thruster performance with proportional observer

If the proportional observer form in (8.7) is used to estimate ω_p then the following observer is obtained:

$$\frac{d}{dt}\hat{\omega}_p = \frac{1}{J_p}\left(Q_{mp} - \hat{Q}^*_{ap}\right) + l_{1p}\left(\omega_p - \hat{\omega}_p\right), \tag{8.11}$$

$$\frac{d}{dt}\hat{Q}^*_{ap} = l_{2p}\left(\omega_p - \hat{\omega}_p\right),$$

Now, investigate how the proportional observer may filter the noise. When the estimated measurement is used in the control, then:

$$e_p = \omega_{0p} - \hat{\omega}_p, \tag{8.12}$$

and the observer will contain the noise in the estimated signal as well:

$$\frac{d}{dt}\hat{\omega}_p = \frac{1}{J_p}\left(Q_{mp} - \hat{Q}^*_{ap}\right) + l_{1p}\left(\omega_p + d_\omega - \hat{\omega}_p\right), \tag{8.13}$$

$$\frac{d}{dt}\hat{Q}^*_{ap} = l_{2p}\left(\omega_p + d_\omega - \hat{\omega}_p\right),$$

where the sensor noise d_ω is proportional to the observer gain l_{1p}, used to stabilize the error dynamics. As l_{1p} increases, the noise will be more amplified. The same holds for l_{2p}. However, a second state Q_{ap} will be integrated before entering the first state equation ω_p. Contrary to time differentiation, the time integration of Q_{ap} will suppress some of the noise amplified by l_{2p}.

8.3.2 Proportional-integral observer

Consider the time invariant system described in (8.9). Then, the original structure of proportional-integral observer (PIO) in Beale and Shafai (1989) is defined as:

$$\frac{d}{dt}\hat{x} = A\hat{x} + Bu + L_p\left(y - C\hat{x}\right) + L_I\hat{d}_y, \tag{8.14}$$
$$\frac{d}{dt}\hat{d}_y = y - C\hat{x},$$

where L_p and L_I terms are the observer proportional and integral term, respectively. If $L_I = 0$, $L_p = L$, then PIO observer in (8.14) would be the same as P observer in (8.7). As can be seen from (8.14) the integral is called due to L_I term where:

$$\hat{d}_y = \int_0^t \left(y - C\hat{x}\right) d\tau. \tag{8.15}$$

The observer error dynamics would have the expression:

$$\begin{bmatrix} \dot{\tilde{x}} \\ \dot{\hat{d}}_y \end{bmatrix} = \begin{bmatrix} A - L_pC & -L_I \\ C & 0 \end{bmatrix}\begin{bmatrix} \tilde{x} \\ \hat{d}_y \end{bmatrix} + \begin{bmatrix} -L_pE \\ E \end{bmatrix} d_y, \tag{8.16}$$

which may give more flexibility than P observer in (8.10) in selecting the observer gains for adequate state convergence versus output noise d_y attenuation. However, the noise d_y will not be completely attenuated in the observer as will be multiplied by the proportional gain L_p.

PIO for thruster

If the PIO observer form in (8.14) is used to estimate the states for the thruster, then the following observer is proposed:

$$\frac{d}{dt}\hat{\omega}_p = \frac{1}{J_p}\left(Q_{mp} - \hat{Q}^*_{ap}\right) + l_{1Pp}\left(\omega_p - \hat{\omega}_p\right) + l_{1Ip}\hat{d}_y,$$
$$\frac{d}{dt}\hat{Q}^*_{ap} = l_{2p}\left(\omega_p - \hat{\omega}_p\right) + l_{2Ip}\hat{d}_y,$$
$$\frac{d}{dt}\hat{d}_y = \omega_p - \hat{\omega}_p \tag{8.17}$$

This linear proportional-integral observer is shown to be globally asymptotically stable (GAS) for:

$$l_{1Pp} > 0,\ \ l_{2Pp} < 0,\ l_{1Ip} > 0,\ \ l_{2Ip} < 0. \tag{8.18}$$

8.3.3 Modified proportional-integral observer

Now consider the system:

$$\begin{aligned} \frac{d}{dt}x &= Ax + Bu + Fd_x \\ y &= Cx + Ed_y, \end{aligned} \tag{8.19}$$

where d_x and d_y represent faults or disturbances appearing in state and output equations and E and F are corresponding gain vectors. In this analysis, it will be assumed that they are modeled as identical disturbances, i.e. $d_y = d_x = d$.

The modified proportional-integral observer (PIOM) has been proposed in Shafai and Nork (2002):

$$\begin{aligned} \frac{d}{dt}\hat{x} &= A\hat{x} + Bu + L_p\left(y - C\hat{x} - E\hat{d}\right) + F\hat{d}, \\ \frac{d}{dt}\hat{d} &= L_I\left(y - C\hat{x} - E\hat{d}\right). \end{aligned} \tag{8.20}$$

Setting the estimation error as $\tilde{x} = x - \hat{x}$, the following estimation error dynamics is obtained:

$$\begin{bmatrix} \dot{\tilde{x}} \\ \dot{\hat{d}}_y \end{bmatrix} = \begin{bmatrix} A - L_pC & L_pE - F \\ L_IC & -L_IE \end{bmatrix}\begin{bmatrix} \tilde{x} \\ \hat{d} \end{bmatrix} + \begin{bmatrix} -L_pE + F \\ L_IE \end{bmatrix} d \tag{8.21}$$

where the $\left(L_pE - F\right)\hat{d} - \left(L_pE - F\right)d = \left(L_pE - F\right)\left(\hat{d} - d\right)$, and the noise/fault term d will be decoupled from the state estimate. This means that the observer gains will not amplify the noise (or error or fault), as was the case with the last term $-L_pEd_y$ in the original PIO design (8.14). The freedom of selecting E and F parameters allows one to choose low observer gains L_P and L_I for reducing noise amplification and at the same time to guarantee the stability of the error dynamics.

Thruster PIOM

If the PIOM observer form in (8.20) is used to estimate the states for the thruster, then the following observer is proposed:

$$\begin{aligned} \frac{d}{dt}\hat{\omega}_p &= \frac{1}{J_p}\left(Q_{mp} - \hat{Q}^*_{ap}\right) + l_{1Pp}\left(\omega_p - \hat{\omega}_p - e_1\hat{d}_y\right) + f_1\hat{d}_y, \\ \frac{d}{dt}\hat{Q}^*_{ap} &= l_{2Pp}\left(\omega_p - \hat{\omega}_p - e_1\hat{d}_y\right) + f_2\hat{d}_y, \\ \frac{d}{dt}\hat{d}_1 &= l_{1Ip}\left(\omega_p - \hat{\omega}_p - e_1\hat{d}_y\right), \end{aligned} \tag{8.22}$$

,

where E and F in (8.20) are selected as $E = (e_1, 0)^T$ and $F = (f_1, f_2)^T$.

The PIOM is GAS for:

$$l_{1Pp} > 0\,,\ \ l_{2Pp} < 0\,,\ \ f_{1p} > 0\,,\ \ \ f_{2p} < 0\,,\ e > 0\,. \tag{8.23}$$

8.3.4 Noise trade-off possibilities

If the observer is used mainly for the noise suppression, then it should provide improvements over the low pass filter. In this thesis, the two main objectives for the observer design are distinguished:
- Obtain low phase shift between estimated and real signal, i.e. stabilize error dynamics, by increasing the observer gains L;
- Suppress the noise.

However, these objectives are usually conflicting, and trade-offs must be made, see e.g. Busawon and Kabore (2001).

As the A–LC eigenvalues are more to the left-hand side of the imaginary plane, the error dynamics will faster converge to zero (Chen, 1999). Fast convergence of the observer is required in order to obtain fast control response – but for the price of amplified noise in the signal. Increased noise amplification may be acceptable (even more) in some cases e.g. when having large propeller disturbances such as propeller ventilation.

A slow converting estimation signal can be beneficial when there are no disturbances in the system or, the disturbances are small, small thrust variations in moderate weather conditions. However, when large disturbances are present, the slowly converting observer would lag behind the real signal and the control response will be delayed for the price of large shaft over-speed and risk of damages to the power transmission parts.

8.3.5 Case study simulations

A case study simulation of electrical thruster operating in harsh environmental conditions is performed using MATLAB/SIMULINK and results are presented in Figs. 8.2 to 8.6 and Tables 8.1 to 8.4. The simulated thrust loss peak is 95% nominal, which corresponds to almost full propeller emergence. The filters/observers are tested with standard PI controller.

The following filters/observers are compared in this study:
- *Non-filtered* – non-filtered case;
- *Low pass* – Butterworth second order low pass filter;
- *PO* – proportional observer;
- *PIO* – proportional-integral observer;
- *PIOM* – modified proportional-integral observer.

The noisy measurements in shaft speed ω_p and electrical torque Q_{mp} are simulated by adding the signal perturbations, uniformly distributed, with min/max relative error of ± 1 to 2% and 3% respectively. All variables, as well as the controller gains, are normalized. The nominal

speed of the thruster is $\omega_{0p} = 0.3\ \omega_{p,rated}$ and after $t = 30$ seconds it becomes $\omega_{0p} = 0.9\ \omega_{p,rated}$, so the controllers can be compared with different thruster loadings i.e. regimes: low speed vs. high speed regime. The total inertial time constant for the thruster rotating parts is $H = 0.5$ seconds, where $J = 2\ H$ in p.u., see e.g. Kundur (1994).

A low pass filter is filtering the commanded torque Q_{cp} signal at the controller output. A low pass filter is carefully tuned in order to obtain good control response with adequate noise filtering, as follows:

– For the low pass filter: $Q_c^f = \frac{1}{T_{1fp}s+1}\frac{1}{T_{2fp}s+1}Q_c$;

– Low pass filtering when observers are used: $Q_c^f = \frac{1}{T_{fp}s+1}Q_c$.

Observer and controller gains are given in Table 8.1.

Table 8.1. Observer, filter and controller parameters

	Type of the filter used	**Filter and observer gains**	**Controller gains**
1.	PI controller with noiseless output and states	-	standard PI controller: k_{Pp}= 10 p.u., k_{Ip} = 1 p.u., k_{Dp} = 0 p.u.
2.	PI controller with low pass filter	$T_{1fp} = 0.1$, $T_{2fp} = 0.2$	
3.	PI controller with PO – observer	$l_{1Pp} = 20$; $l_{2Pp} = -150$; $H = 0.5$ seconds; $T_{fp} = 0.15$	
4.	PI controller with PIO – observer	$l_{1Pp} = 10$; $l_{2Pp} = -50$; $l_{1Ip} = 10$; $l_{2Ip} = -100$; $H = 0.5$ seconds; $T_{fp} = 0.1$	
5.	PI controller with PIOM – observer	$l_{1Pp} = 50$; $l_{2Pp} = -300$; $l_{Ip} = 3$; $f_{1p} = 5$; $f_{2p} = -20$; $e_p = 0.5$ $H = 0.5$ seconds; $T_{fp} = 0.05$	

CASE 1 – noise reduction

The noise disturbance is presented in Table 8.2.

The commanded torque Q_{cp} in all PI controllers is low pass filtered. The low pass filter constant is selected lower if the observers are used for the shaft speed filtering (estimation), as shown in Table 8.1.

The results of simulation for the shaft torque fluctuations and shaft speed for thruster operating in various load regimes, namely 30% to 90% of the rated speed, are presented in Figs. 8.2 to 8.4 and Tables 8.2 to 8.4.

As explained in Section 8.2 *Effect of noise on shaft speed control*, the shaft torque fluctuations $\|\Delta Q_p\| = \|Q_{mp} - Q_{ap}^*\|$ are defined as the main cause of increased thruster wear and tear, as they may cause increased fatigue of power transmission components in addition to increased excitation of torsional vibrations. A controller could be tuned in a way to decrease a shaft torque fluctuations for the price of increased shaft speed fluctuations $\|\Delta\omega_p\| = \|\omega_p - \omega_{0p}\|$ - up to some point. Although the torque deviations are directly proportional to speed deviations, the presence of noise may introduce such nonlinearity i.e. non-separation. In order to obtain good comparisons, the standard deviation of shaft torque fluctuations are compared to the standard deviation of speed fluctuations, as shown in Tables 8.3 and 8.4.

Table 8.2. Noise parameters

Noise signal:	**Speed**	**Motor torque**
Noise sampling rate	10 milliseconds	1 milliseconds
Amplitude	± 2 %	± 3 %

Table 8.3. Standard deviation in shaft torque deviations (accelerations) for various noise filtering types

	Noise filtering	**Standard deviation of overall torque fluctuations**	**increase fluctuations w.r.t. noiseless**
1.	Noiseless	0.0400	-
2.	Low pass filter	0. 0561	40%
3.	PO – observer	0. 0461	15.2%
4.	**PIO – observer**	**0. 0430**	**7.5%**
5.	PIOM – observer	0. 0443	10.7%

Table 8.4. Standard deviation in shaft speed for various noise filtering types

	Noise filtering	**Standard deviation of overall shaft speed fluctuations**	**increase fluctuations w.r.t. noiseless**
1.	Noiseless	0. 0328	-
2.	Low pass filter	0. 0366	11.5%
3.	PO – observer	0. 0348	6%
4.	**PIO – observer**	0. 0321	**2%**
5.	PIOM – observer	0. 0338	3%

From Figs. 8.2 to 8.4, and Tables 8.3 and 8.4 following conclusions can be made:

- The overall shaft torque fluctuations will be lower with proportional observer (PO) than the low pass filter, shown in Fig. 8.2;
- More complex observers (PIO and PIOM) may further decrease the torque fluctuations, however for the price of increased complexity of tuning, as shown in Tables 8.3 and 8.4;
- Although the shaft torque fluctuations are about 28% higher with low pass filter than PO, this can hardly be noticed from the shaft speed estimation, in the lower part of Fig. 8.2. Thus, small differences in the speed estimation error will be amplified with the high gain (PI) controller and transmitted to the shaft as undesired torque fluctuations;

– The PI controller is selected with high gains (k_{Pp}=10 in p.u.) in order to enhance the speed control performance and compensate for the phase-shift introduced by the low pass filtering. This would make the thruster to respond very fast to the changes in the speed reference signal;
– Fig. 8.3 shows the detailed view of torque fluctuations and speed for all filters when thruster is operating on a high load. The quantitative comparison of filters is available in Tables 8.3 and 8.4 where it can be noticed that an increase in the torque fluctuations due to noise with PIO filter will be just 7.5% while the increase in the shaft speed fluctuations due to noise will be 2%. This is much lower than when using standard low pass filtering with 40% increase in the torque fluctuations and 11.5% increase in the speed fluctuations compared to noiseless case;

The proportional integral observer (PIO) may give the best performance with respect to shaft speed and torque fluctuations when used with standard PI controller. The PIO is easy to tune as the absolute values of the observer integral gains should be somewhat higher than their proportional (PO) values.

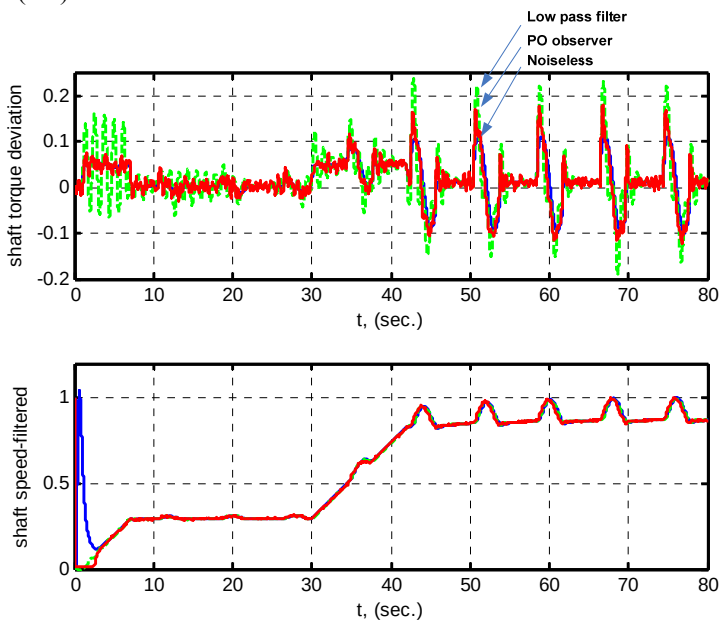

Fig. 8.2. Shaft torque fluctuations and shaft speed for thruster operating in various load regimes and using following filters: *ideal noiseless* (_____, blue), *PO filtered* (-.-.-.-, red), *Low pass filter* (------, green)

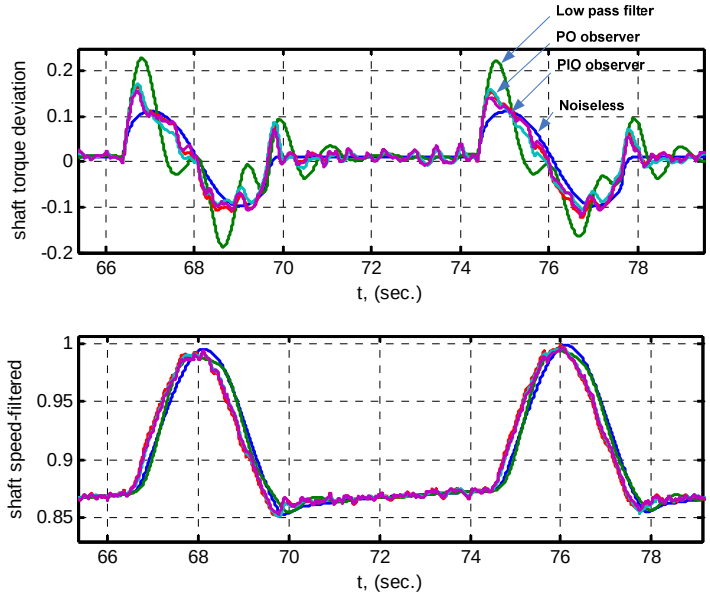

Fig. 8.3. Shaft torque fluctuations and shaft speed for thruster operating in various load regimes and using all filters: *ideal noiseless*, *low pass filter*, *PO*, *PIO*, *PIOM*

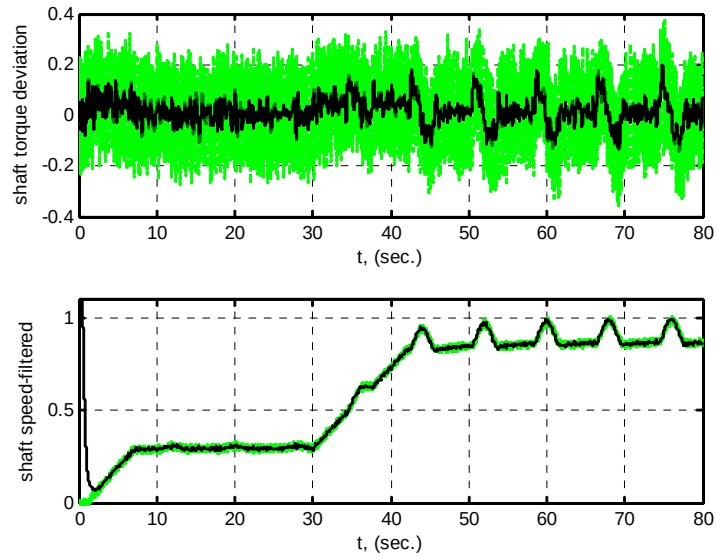

Fig. 8.4. Shaft torque (upper) and shaft speed (lower) fluctuations for thruster operating in various load regimes when using following filters: *non-filtered* (----, green), *Low pass filter* (——, black)

8.4 Dynamic gains for noise-control tradeoff strategy

With respect to possible noise-control tradeoffs, the following strategy is proposed:
- Increase the controller gains when large disturbances are present;
- Decrease the controller gains when the disturbances are low.

With the standard observer at low speed, the behaviour related to the speed and disturbance torque estimates may become oscillatory due to encoder quantization, see e.g. Kweon and Hyun (1999).

As the disturbances are increasing with nominal torque Q_{0p}, the following modification to standard PI controller is proposed (Radan *et al.*, 2007a):

$$Q_{cp} = \left(k_{Pp} e_p + k_{Ip} \int_0^t e_p d\tau \right) \; k_1 \; \omega_{0p}^2 \,, \tag{8.24}$$

where k_1 is the controller gain and ω_{0p} is in p.u.

8.5 Inertial control

The proposed *inertial control* concept is applied to improve the speed control of rotating machinery drive systems. In this group belong: marine electric thrusters, engines connected to propellers and generating-sets.

8.5.1 Inertial control concept

The inertial control concept is proposed to improve the shaft speed control by improving the virtual inertia of the drive, as proposed in Morren *et al.* (2006) for the application in wind electricity generation:

$$Q_{iner,p} = k_{iner,p} \frac{d}{dt} \omega_p \,, \tag{8.25}$$

where $k_{iner,p}$ is the control gain. With the inertial control included, the following shaft speed controller is obtained, as presented in Fig. 8.5:

$$\begin{aligned} Q_{cp} &= k_{Pp} e_p + k_{Ip} \int_0^t e_p d\tau \,, \\ e_p &= \omega_{0p} - \omega_p - k_{iner,p} \frac{d}{dt} \omega_p \,. \end{aligned} \tag{8.26}$$

Then, the inertial controller is obtained:

$$Q_{cp} = k_{Pp} \left(\omega_{0p} - \omega_p \right) + k_{Ip} \int_0^t \left(\omega_{0p} - \omega_p \right) d\tau - k_{Pp} k_{iner,p} \frac{d}{dt} \omega_p - k_{Ip} k_{iner,p} \omega_p \,, \tag{8.27}$$

where it may be noticed that last two terms in (8.27) are due to inertial control. Neglecting the thruster motor and frequency converter dynamics Q_{mp}=Q_{cp}, and inserting (8.27) into (5.4) the following closed-loop equation of motion is obtained:

$$\frac{d}{dt}\omega_p = \frac{1}{J_p + k_{Pp}k_{iner,p}}\left(k_{Pp}\left(\omega_{0p} - \omega_p\right) + k_{Ip}\int_0^t\left(\omega_{0p} - \omega_p\right)d\tau - k_{Ip}k_{iner,p}\omega_p - Q_{ap} - Q_{fp}\right), \tag{8.28}$$

where it can be noticed that the proportional term of the PI controller will increase the virtual inertia due to feedback acceleration controller action (Fossen, 2002), while the inertial term will increase the virtual damping in the system.

The inertial control concept is presented in Fig. 8.5. From (8.25) it can be noticed that the inertial control strategy can be obtained using direct differentiation of the shaft speed ω_p, if an accurate shaft speed can be measured. The measurement noise in the speed ω_p will limit the performance of the controller as the derivation of noisy measurement $d\omega_p/dt$ may cause the increased wear of thruster components.

8.5.2 Inertial observer

The inertial observer is designed and proposed for the output derivative estimation (Radan *et al*. 2007a). As the output derivative is proportional to the rotating system inertia, the observer is termed the *inertial torque observer* (ITO). The ITO is used for the noise suppression i.e. disturbance attenuation in the output derivative.

The inertia can be estimated from the following equation:

$$\hat{Q}_{iner,p} = k_{iner,p}\left(Q_{mp} - \hat{Q}^*_{ap}\right), \tag{8.29}$$

where the extended estimated load torque includes friction:

$$\hat{Q}^*_{ap} \approx Q^*_{ap} = Q_{ap} + Q_{fp}\,, \tag{8.30}$$

and is calculated using one of the previously proposed observers (PO, PIO, PIOM).

Then, the inertial torque observer is used to estimate the speed differentiation. The estimated shaft acceleration is obtained from the inertial torque considering the following equation:

$$\frac{d}{dt}\hat{\omega}^*_p = \frac{1}{J_p}\left(Q_{mp} - \hat{Q}^*_{ap}\right) = \hat{Q}_{iner,p} / J_p k_{iner,p}\,. \tag{8.31}$$

The inertial torque observer (8.29) is used for the estimation of the inertial torque $Q_{iner,p}$ which is equivalent to the shaft acceleration. Thus, D-term of the controller is estimated through the estimation of the inertial torque, as proposed in Fig. 8.6.

Then the following controller output is obtained:

$$Q_{cp} = k_{Pp}e_p + k_{Ip}\int_0^t e_p d\tau\,, \tag{8.32}$$

$$e_p = \omega_{0p} - \omega_p - k_{iner,p}\frac{1}{J_p}\left(Q_{mp} - \hat{Q}^*_{ap}\right).$$

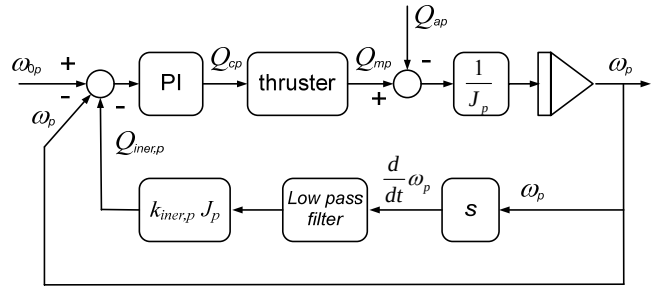

Fig. 8.5. Acceleration based inertial control of electrical thruster

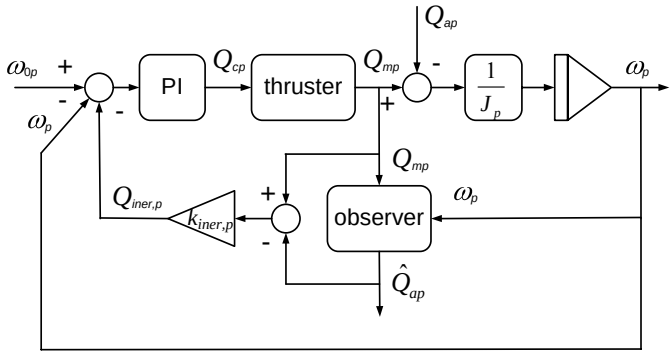

Fig. 8.6. Proposed inertial torque observer used to suppress the noise in the *D*-term

8.5.3 Response to noise

Controller noise suppressing

With output noise present i.e. the noise at the shaft speed measurement, the error to the *inertial controller* is obtained:

$$e_p = \omega_{0p} - \left(\omega_p + d_\omega\right) - k_{iner,p}\frac{d}{dt}\left(\omega_p + d_\omega\right). \tag{8.33}$$

The inertial controller output becomes:

$$Q_{cp} = Q_{cp,s} + Q_{cp,d}, \tag{8.34}$$

where:

– $Q_{cp,s} = k_{Pp}\left(\omega_{0p} - \omega_p\right) + k_{Ip}\int_0^t\left(\omega_{0p} - \omega_p\right)d\tau - k_{Ip}k_{iner,p}\omega_p - k_{Pp}k_{iner,p}\frac{d}{dt}\omega_p$ is the noiseless part of the inertial controller;

– $Q_{cp,d} = -k_{Pp} d_\omega - k_{Ip} \int_0^t d_\omega d\tau - k_{iner,p} \frac{d}{dt} d_\omega$ is the additional undesirable torque due to measurement noise d_ω.

Neglecting the thruster motor and frequency converter dynamics Q_{mp}=Q_{cp}, and inserting (8.34) into (5.4) the following closed-loop equation of motion is obtained:

$$\frac{d}{dt}\omega_p = \frac{1}{J_p + k_{Pp} k_{iner,p}} \Big[k_{Pp}\left(\omega_{0p} - \omega_p\right) + k_{Ip} \int_0^t \left(\omega_{0p} - \omega_p\right) d\tau - k_{Ip} k_{iner,p} \omega_p - Q_{ap} - Q_{fp} - k_{Pp} d_\omega - k_{Ip} \int_0^t d_\omega d\tau - k_{iner,p} \frac{d}{dt} d_\omega \Big]. \tag{8.35}$$

Although, the undesirable part of the inertial controller $Q_{cp,d}$ (8.34) is similar to $Q_{cp,d}$ of the PID controller (8.3), the noiseless part $Q_{cp,s}$ of the inertial controller (8.35) is enhanced. It can be noticed that $Q_{cp,s}$ in (8.35) increases the damping(k_{Ip} part) in addition to the virtual inertia. This indicates that the damping may be increased if the I-term (k_{Ip} gain) in the PI controller is increased. Such features may give more flexibility in handling noise i.e. "dirty derivatives" and provide enhancements in the overall control system.

Observer output noise suppressing

In order to reduce the "dirty derivatives" introduced in the control loop when differentiate the speed output, the inertial observer is used:

$$\frac{d}{dt}\hat{\omega}_p^* = \frac{1}{J_p}\left(Q_{mp} - \hat{Q}_{ap}^*\right) = \hat{Q}_{iner,p} / J_p k_{iner,p} \,. \tag{8.36}$$

It can be noticed that the time derivative in (8.36) will contain less noise than if the standard observer is used in the controller.

Observer suppressing the motor torque noise

Moreover, a noise is also present in the Q_{mp} as the motor torque is estimated within the frequency drive by e.g. current observer for permanent magnet synchronous machines and rotor flux observer for the induction motor (Utkin *et al.*, 1999).

Considering the proportional observer, as given in (8.7) with noise in the motor torque:

$$\begin{aligned} \frac{d}{dt}\hat{\omega}_p &= \frac{1}{J_p}\left(Q_{mp} + d_Q - \hat{Q}_{ap}^*\right) + l_{1p}\left(\omega_p + d_\omega - \hat{\omega}_p\right) \\ \frac{d}{dt}\hat{Q}_{ap}^* &= l_{2p}\left(\omega_p + d_\omega - \hat{\omega}_p\right), \end{aligned} \tag{8.37}$$

the following time derivative of the speed is obtained:

$$\frac{d}{dt}\hat{\omega}_p^* = \frac{1}{J_p}\left(Q_{mp} - \hat{Q}_{ap}^*\right) = \frac{1}{J_p}\left[Q_{mp} - l_{2p}\int_0^t\left(\omega_p - \hat{\omega}_p\right)d\tau + d_Q - l_{2p}\int_0^t d_\omega d\tau\right]. \quad (8.38)$$

It can be noticed that the noise in the time derivative of the speed can be suppressed by adjusting the l_{2p} observer gain. Then a cancellation of the noise in $d_Q - l_{2p}\int_0^t d_\omega d\tau \to 0$ can be achieved.

The error to the *inertial controller* is obtained:

$$\begin{aligned} Q_{cp} &= k_{Pp}e_p + k_{Ip}\int_0^t e_p d\tau\,, \\ e_p &= \omega_{0p} - \left(\omega_p + d_\omega\right) - k_{iner,p}\frac{1}{J_p}\left(Q_{mp} - \hat{Q}_{ap}^*\right). \end{aligned} \quad (8.39)$$

Then the following inertial controller with the observer estimated time derivative is obtained:

$$\begin{aligned} Q_{cp} = {} & k_{Pp}\left(\omega_{0p} - \omega_p\right) + k_{Ip}\int_0^t\left(\omega_{0p} - \omega_p\right)d\tau \\ & - k_{Pp}k_{iner,p}\frac{1}{J_p}\left(Q_{mp} - \hat{Q}_{ap}^*\right) - k_{Ip}k_{iner,p}\frac{1}{J_p}\int_0^t\left(Q_{mp} - \hat{Q}_{ap}^*\right)d\tau \\ & - k_{Pp}d_\omega - k_{Ip}\int_0^t d_\omega d\tau \end{aligned} \quad (8.40)$$

When the P-term (k_{Pp}) is reduced this may directly suppress the noise transmission to the controller and the closed-loop and the control behavior improved due to increased virtual inertia and damping increased by increased $k_{iner,p}$.

8.5.4 Simulations

A simulation study of electrical thruster operating in harsh environmental conditions is performed using MATLAB/SIMULINK and results are presented in Figs. 8.7 to 8.9. The simulated thrust loss peak is 95% nominal, which corresponds to almost full propeller emergence.

The following filters/observers are compared in this study:
- *Low pass*: Butterworth second order low pass filter based PI controller;
- *Inertial*: Observer-based inertial controller.

The noisy measurements in shaft speed ω_p and electrical torque Q_{mp} are simulated by adding the signal perturbations, uniformly distributed, with min/max relative error of ± 1 to 2% and 5% respectively. All variables, as well as the controller gains, are normalized. The nominal speed of the thruster is $\omega_{0p} = 0.3\ \omega_{p,rated}$ and after $t = 30$ seconds it becomes $\omega_{0p} = 0.9\ \omega_{p,rated}$, so the controllers can be compared with different thruster loadings i.e. regimes: low speed vs. high speed regime. The total inertial time constant for the thruster rotating parts is $H = 0.5$ seconds, where $J = 2\ H$ in p.u., see e.g. Kundur (1994).

The observer gains and filter time constants are given in Table 8.5. The k_{Pp}= 3 p.u. which is more than 3 times lower then the P-gain of PI controller compared in this study.

The selected inertial time constant for the observer is H = 0.8 seconds although the real H=0.5 seconds This demonstrates the robustness of the observer-based inertial controller to the parameters and data.

One very interesting feature of the proposed controller is that the inertial controller gain $k_{iner,p}$ can be selected very high and in this case study is $k_{iner,p}$ = 80. This is due to good noise suppression ability of the inertial observer and cancellation of the noise term in (8.38).

The results are presented in Figs. 8.7 to 8.9. It can be noticed that the inertial control can decrease the torque shaft fluctuations in all regimes, especially when discontinuous change in the thrust references are present, as can be noticed from t = 30 to 45 seconds

It can be noticed from Fig. 8.9 that the inertial controller will inject into the closed-loop less high frequency component noise than the low pass filter and thus may improve the inner-loop control performance of the cascade control structure.

Table 8.5. Observer, filter and controller parameters

	Type of the filter used	**Filter and observer gains**	**Controller gains**
1.	PI controller with Low pass filter	T_{1fp} = 0.1, T_{2fp} = 0.2	standard PI controller: k_{Pp}= 10 p.u., k_{Ip} = 1 p.u., k_{Dp} = 0 p.u.
2.	PI controller with PIO – observer	l_{1Pp} = 10; l_{2Pp} = –50; l_{1Ip} = 10; l_{2Ip} = –100; H = 0.5 seconds; T_{fp} = 0.1	same as in 1.
3.	Inertial controller with PO – observer	l_{1Pp} = 20; l_{2Pp} = –200; H = 0.8 seconds, T_{fp} = 0;	Inertial controller: k_{Pp} = 3 p.u., k_{Ip} = 1 p.u., $k_{iner,p}$ = 80;

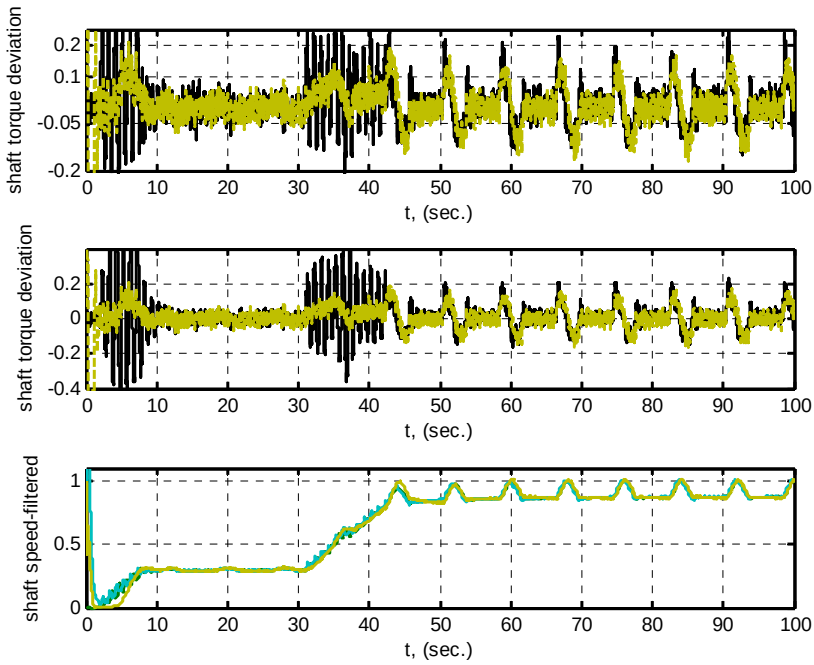

Fig. 8.7. Shaft torque (top and middle) and shaft speed (lowest) fluctuations with regards to discontinuous speed reference for thruster operating in various load regimes and using filters: *low pass filter PI controller* (——, black), *PO based inertial controller* (------, yellow)

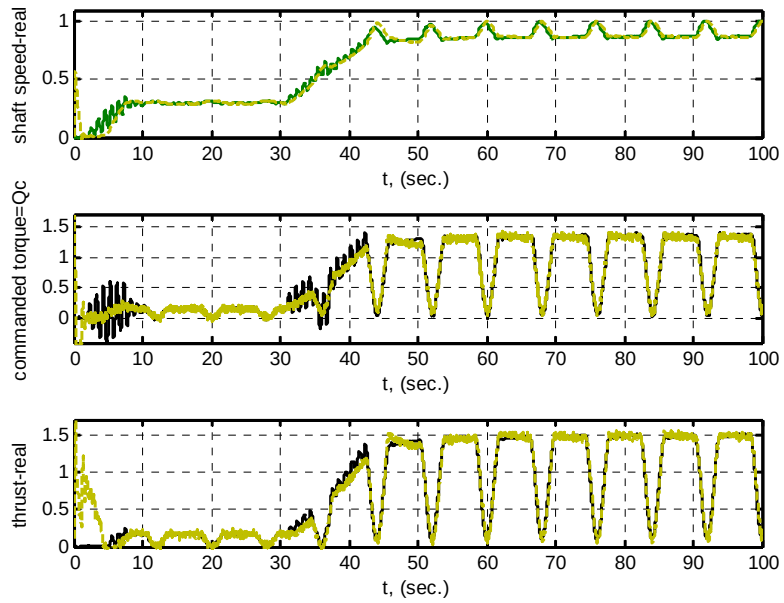

Fig. 8.8. Real shaft speed (top), command (middle) and real thrust (lowest) when using: *Low pass filter* (——, black), PIO (------, yellow)

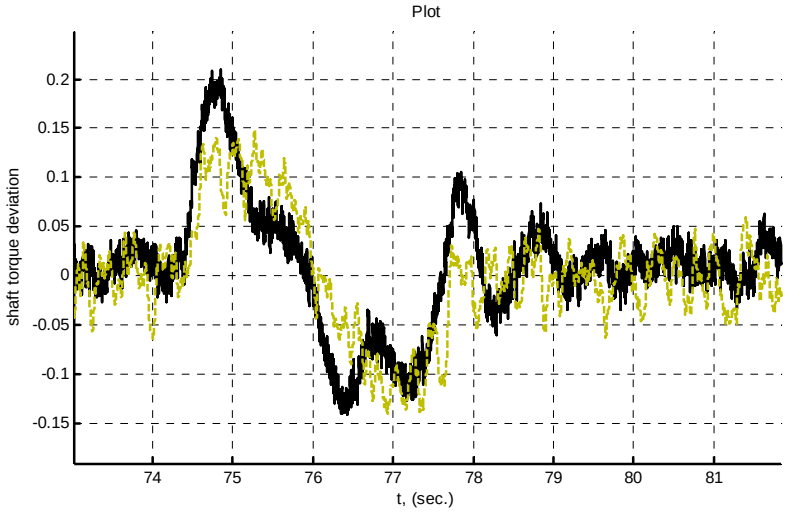

Fig. 8.9. Shaft torque fluctuations using filters:
low pass filter PI controller (——, black), *PO based inertial controller* (------, yellow)

8.6 Direct torque-loss controller

8.6.1 Motivation

In this thesis another version of inertial controller is proposed. The proposed controller is termed the *direct torque-loss controller* or *soft anti-spin controller* as is used to improve the shaft speed control and reduce the speed and torque fluctuations on the propeller. The main idea is based on including the sensitivity to the disturbances directly in to the control law, in a somewhat different way than with the inertial control, previously explained.

The idea motivation is based on the anti-spin control. The anti spin controller for the marine thrusters is first proposed in Smogeli *et al.* (2004a), and improvements in the control performance can be found in Smogeli (2006), Bakkeheim *et al.* (2006), Bakkeheim *et al.* (2007a), and Bakkeheim *et al.* (2007b). In these papers, authors use a switching control to reduce the thrust reference every time when the thrust loss occurs. The control rely on the thrust loss detection logic based on the estimate of the thrust loss factor $\beta_{loss,p}$. The problems that have been considered when using switching control logic may be stated as follows:

- Due to noise in the measurements, it may be difficult to set the "optimal" thresholds, so the anti-spin will switch (ON/OFF) every time when the significant thrust loss occurs, whereas small thrust losses should be ignored;
- The bumpless switching should be achieved in order to reduce the torque imbalance on the shaft and consequent wear and tear;
- The quantity of the thrust reduction may be a problem. This is evident when the various propeller regimes are considered: if the load reduction is too high, there may be not enough time for the thruster to recover from the transient before the next thrust loss transient occurs - this would make thruster to operate with reduced average thrust;
- The speed of the thrust recovery when switching back to nominal thrust – same problems as explained above.

8.6.2 Estimation of the thrust loss factor

The thrust loss factor is estimated using the following equation (Smogeli *et al.*, 2004a):

$$\hat{\beta}^*_{loss,p} = \frac{\hat{Q}^*_{ap}}{\hat{Q}_{0p}} = \frac{\hat{Q}^*_{ap}}{\frac{1}{4\pi^2}\hat{K}_{Q0p}\rho\hat{D}_p^5\omega_p^2}, \tag{8.41}$$

$$\text{where } \hat{\beta}^*_{oss,p} \text{ should have: } 0 \le \hat{\beta}^*_{loss,p} \le 1 \rightarrow \left(1-\hat{\beta}^*_{loss,p}\right) \ge 0,$$

where $\hat{\beta}^*_{oss,p}$ is the estimated thrust loss factor, $\hat{Q}^*_{ap}$ is estimated load torque (using state observer), $\hat{Q}_{0p}$ is calculated nominal torque from measured speed ω_p, $\hat{K}_{Q0p}$ is pre-determined propeller torque coefficient, $\hat{D}_p$ is the propeller diameter. The parameters $\hat{K}_{Q0p}$ and $\hat{D}_p$ must be known. Problems with regards to robustness to the parameter inaccuracy will arise due to real value of $\hat{K}_{Q0p}$ may be difficult to know for the whole operating region as:

- If the $\hat{K}_{Q0p} < K_{Q0p}$ then $\hat{\beta}^*_{oss,p} > 1$ in steady state;
- If the $\hat{K}_{Q0p} > K_{Q0p}$ then $\hat{\beta}^*_{oss,p} < 1$ in steady state;
- If $\hat{K}_{Q0p} = K_{Q0p}$ then $\hat{\beta}^*_{oss,p} = 1$ in steady state.

If $\hat{\beta}^*_{loss,p}$ is used directly in the control law and $\hat{\beta}^*_{loss,p} \neq 1$ then the steady state error will be introduced in the control, i.e. the equilibrium point of the system will change in the operating regime.

In order to avoid problems with steady state error, the anti-spin control switching logic proposed in Smogeli *et al.* (2004a) is mainly based on the threshold limits set on the $\hat{\beta}^*_{loss,p}$ as the anti-spin will be initiated when $\hat{\beta}^*_{loss,p} \le \beta_{loss,p,ON}$.

In this thesis, the *washout filters* are proposed as a method to remove the steady state error and reduce the dependence on the parameters of the control; for washout filters and lead compensators see e.g. Hassouneh *et al.* (2004), Franklin *et al.* (2006) and the references therein. The background for the proposed idea can be found in the controller structure of classical automatic voltage regulator (AVR), see e.g. Kundur (1994), Anderson and Fuad (2003), and references therein.

Thus, the proposed estimation of the thrust loss factor is as follows:

$$\hat{\beta}^*_{loss,p} = h_{\beta w}(s)\frac{\hat{Q}^*_{ap}}{\hat{k}_{1p}\omega_p^2} + 1, \tag{8.42}$$

$$h_{\beta w}(s) = \frac{s}{\tau_\beta s + 1}.$$

where s term is the Laplace operator and $\tau_{\beta s}$ is the time constant. The $\hat{Q}_{0p} = \hat{k}_{1p}\omega_p^2$ and $\hat{k}_{1p} = \frac{1}{4\pi^2}\hat{K}_{Q0p}\rho\hat{D}_p^5$ can be roughly estimated as the *washout filter* $h_{\beta w}(s)$ will guarantee the steady state error will converge to zero for any reasonable value of $k_{1p} > 0$. This is demonstrated in Fig.8.10, where it can be noticed that washout filtered $\hat{\beta}^*_{loss,p}$ signal will not have large phase-lag compared to non-filtered estimation.

8.6.3 Direct torque-loss controller

Using the benefits of the *washout filters* the proposed control is based on the inclusion of the thrust loss factor $\hat{\beta}^*_{loss,p}$ directly into the control law, avoiding the switching logic. Thus, the following control strategy is proposed:

$$
\begin{aligned}
& e_p = \omega_{0p} - \omega_p - k_{\beta,p}\omega_{0p}^2\left(1-\hat{\beta}^*_{loss,p}\right)^g, \\
& g > 0,\ g \in R, \\
& \hat{\beta}^*_{loss,p} = h_{\beta w}(s)\frac{\hat{Q}^*_{ap}}{\hat{k}_{1p}\omega_p^2} + 1, \\
& h_{\beta w}(s) = \frac{s}{\tau_\beta s + 1}, \\
& 0 \le \hat{\beta}^*_{loss,p} \le 1 \ \rightarrow \left(1-\hat{\beta}^*_{loss,p}\right) \ge 0,
\end{aligned}
\tag{8.43}
$$

where the $k_{\beta,p}$ is the controller gain for the $\beta_{loss,p}$ terms. In steady state, when the thrust loss is not present the $\hat{\beta}^*_{loss,p} = 1$ and $k_{\beta,p}\left(1-\hat{\beta}^*_{loss,p}\right)^g = 0$.

When the noise is present, the speed reference will become:

$$
e_p = \omega_{0p} - \omega_p - d_\omega - k_{\beta,p}\omega_{0p}^2\left(1-\hat{\beta}^*_{loss,p}\right)^g. \tag{8.44}
$$

If PI controller is used $Q_{cp} = k_{Pp}e_p + k_{Ip}\int_0^t e_p d\tau$, then the following commanded torque is obtained:

$$
\begin{aligned}
Q_{cp} = {} & k_{Pp}\left(\omega_{0p} - \omega_p\right) + k_{Ip}\int_0^t\left(\omega_{0p} - \omega_p\right)d\tau - k_{Pp}d_\omega - k_{Ip}\int_0^t d_\omega d\tau \\
& - k_{Pp}k_{\beta,p}\omega_{0p}^2\left(1-\hat{\beta}^*_{loss,p}\right)^g - k_{Ip}k_{\beta,p}\int_0^t\omega_{0p}^2\left(1-\hat{\beta}^*_{loss,p}\right)^g d\tau.
\end{aligned}
\tag{8.45}
$$

The last two terms with $k_{\beta,p}$ in (8.45) will increase the controller stability dependent on the disturbance $\hat{\beta}^*_{loss,p}$. The $\hat{\beta}^*_{loss,p}$ is estimated using an observer and may contain some noise. However, the noise in the $\hat{\beta}^*_{loss,p}$ can be significantly suppressed as the *washout filter*

introduces the phase-lead and the low pass filter (phase-lag) constants could be increased in order to attenuate noise in the wider range of frequencies.

If $k_{\beta,p} = \hat{k}_{1p}$, then the following commanded torque is obtained:

$$Q_{cp} = k_{Pp}\left(\omega_{0p} - \omega_p\right) + k_{Ip}\int_0^t\left(\omega_{0p} - \omega_p\right)d\tau - k_{Pp}d_\omega - k_{Ip}\int_0^t d_\omega d\tau$$
$$- k_{Pp}\hat{k}_{1p}\omega_{0p}^2\left(1-\hat{\beta}_{loss,p}^*\right)^g - k_{Ip}\hat{k}_{1p}\int_0^t\omega_{0p}^2\left(1-\hat{\beta}_{loss,p}^*\right)^g d\tau \tag{8.46}$$

where $\hat{k}_{1p}\omega_{0p}^2 = \hat{Q}_{0p} - \hat{k}_{1p}\left(\omega_{0p} - \omega_p\right)^2$ and $\hat{Q}_{0p} = \hat{k}_{1p}\omega_p^2$. Thus, one may assume that $\hat{k}_{1p}\omega_{0p}^2$ will increase the stability less than $\hat{Q}_{0p}$ term. However, $\hat{k}_{1p}\omega_{0p}^2$ will not contain noise, whereas the $\hat{k}_{1p}\omega_p^2$ will increase the noise level on second potential of ω_p as ω_p is the measured controller output.

The phase-lag due to low pass noise filtering and electric motor response will be compensated by the inclusion of $\hat{k}_{1p}\omega_{0p}^2$ term instead of $\hat{Q}_{0p} = \hat{k}_{1p}\omega_p^2$ in the control law and the *washout filtering* of $\hat{\beta}_{loss,p}^*$.

Thus, the following closed-loop equation is obtained assuming $Q_{mp} = Q_{cp}$:

$$\frac{d}{dt}\omega_p = \frac{1}{J_p}\Big[k_{Pp}\left(\omega_{0p} - \omega_p\right) + k_{Ip}\int_0^t\left(\omega_{0p} - \omega_p\right)d\tau - k_{Pp}d_\omega - k_{Ip}\int_0^t d_\omega d\tau$$
$$- k_{Pp}\hat{k}_{1p}\omega_{0p}^2\left(1-\hat{\beta}_{loss,p}^*\right)^g - k_{Ip}\hat{k}_{1p}\int_0^t\omega_{0p}^2\left(1-\hat{\beta}_{loss,p}^*\right)^g d\tau - Q_{ap} - Q_{fp}\Big]. \tag{8.47}$$

As the term $k_{Pp}\hat{k}_{1p}\omega_{0p}^2\left(1-\hat{\beta}_{loss,p}^*\right) \propto k_{Pp}\frac{d}{dt}\omega_p$, the control is termed the *Direct torque-loss control*.

As can be noticed from (8.47), the benefits of the proposed control law may be stated as follows:

- The proposed controller will increase the stability in a similar way as the inertial control;
- The disturbance estimate is directly included in the control law;
- Control is very robust to parameter inaccuracies;
- The proposed control is non-switching, so problems involving control switching issues do not need to be considered;
- The proposed control is continuous i.e. it will smoothly react to all disturbances with regards to their level;
- The proposed control is applicable and robust in all operating regimes;
- The recovery after the disturbance will depend on the measured, i.e. estimated disturbance.

8.6.4 Simulations

A case study simulation of electrical thruster operating in harsh environmental conditions is performed using MATLAB/SIMULINK and results are presented in Figs. 8.10 to 8.12. Observer, filter and controller parameters are presented in Table 8.6. The simulated thrust loss peak is 95% nominal, which corresponds to almost full propeller emergence.

The following filters/observers are compared in this study:
- *Low pass* – Butterworth second order low pass filter based PI controller;
- *Inertial* – observer-based inertial controller;
- *Direct torque-loss* – observer-based Direct torque-loss controller (*soft anti-spin*).

The noisy measurements in shaft speed ω_p and electrical torque Q_{mp} are simulated by adding the signal perturbations, uniformly distributed, with min/max relative error of ± 1 to 2% and 5% respectively. All variables, as well as the controller gains, are normalized. The nominal speed of the thruster is $\omega_{0p} = 0.3\ \omega_{p,rated}$ and after $t = 30$ seconds it becomes $\omega_{0p} = 0.9\ \omega_{p,rated}$, so the controllers can be compared with different thruster loadings i.e. regimes: low speed vs. high speed regime. The total inertial time constant for the thruster rotating parts is $H = 0.5$ seconds., where J is substituted with 2 H in thruster shaft motion equation.

From the results of the simulations, presented in Figs. 8.11 and 8.12 it can be noticed that with the *Direct torque-loss controller* the shaft speed reference will be reduced every time the thrust loss occurs e.g. propeller goes out of water. This control behavior is similar to anti-spin (Smogeli, 2006) and thus the *direct torque-loss controller* can also be called the *soft anti-spin controller*. As can be seen from Fig. 8.11, the shaft speed fluctuations can be significantly reduced with the *direct torque-loss controller*, however the overall shaft torque fluctuations (i.e. shaft accelerations) will be less with the *inertial controller*. The *direct torque-loss controller* may provide lower shaft torque fluctuations due to chattering induced by the fast reference change, compared to standard *PI controller*. However, the robustness to chattering will be the lowest with the *inertial controller*.

Table 8.6. Observer, filter and controller parameters

	Type of the filter used	**Filter and observer gains**	**Controller gains**
1.	PI controller with Low pass filter	$T_{1fp} = 0.1$, $T_{2fp} = 0.2$	standard PI controller: $k_{Pp} = 10$ p.u., $k_{Ip} = 1$ p.u., $k_{Dp} = 0$ p.u.
2.	Inertial controller with PO – observer	$l_{1Pp} = 20$; $l_{2Pp} = -200$; $H = 0.8$ seconds, $T_{fp} = 0$;	Inertial controller: $k_{Pp} = 3$ p.u., $k_{Ip} = 1$ p.u., $k_{iner,p} = 80$;
3.	Direct torque-loss controller with PO – observer	$l_{1Pp} = 20$; $l_{2Pp} = -200$; $H = 0.8$ seconds, $T_{1fp} = 0.1$, $T_{2fp} = 0.2$	Direct torque-loss controller: $k_{Pp} = 10$ p.u., $k_{Ip} = 1$ p.u., $k_{\beta,p} = 0.2$; $\tau_{\beta,p} = 0.5$;

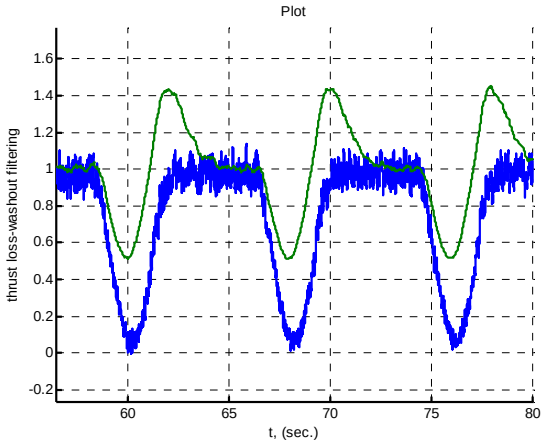

Fig. 8.10. Filtering of torque loss factor $\beta_{loss,p}$ using low pass filter after washout filter, before wash-out filter (------, blue), filtered output (____, green)

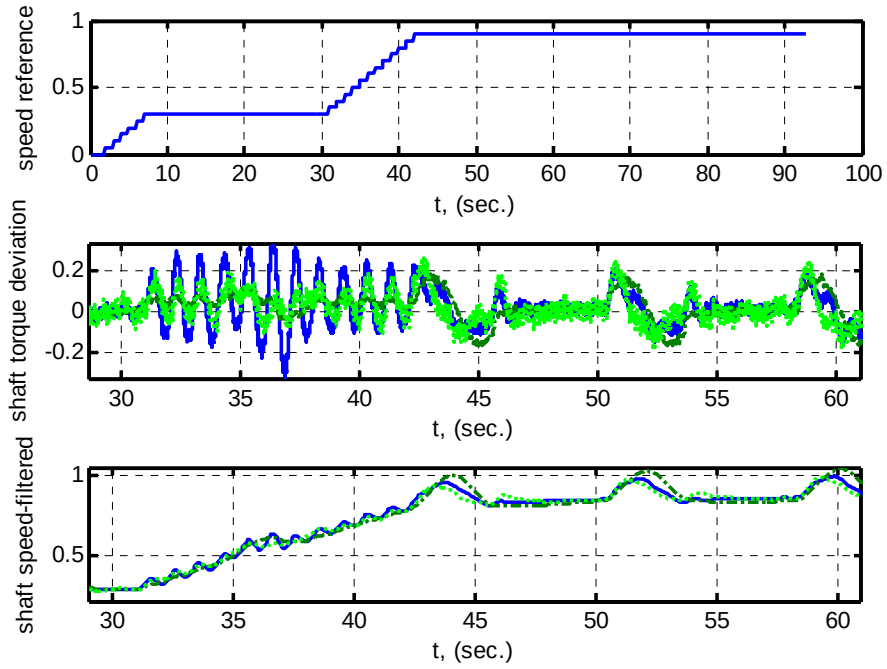

Fig. 8.11. Shaft torque (middle) and shaft speed (lowest) fluctuations with regards to discontinuous speed reference (top) for thruster using filters:
PI controller (——, blue), *inertial controller* (-.-.-.-, dark green),
direct torque-loss controller (------, light green)

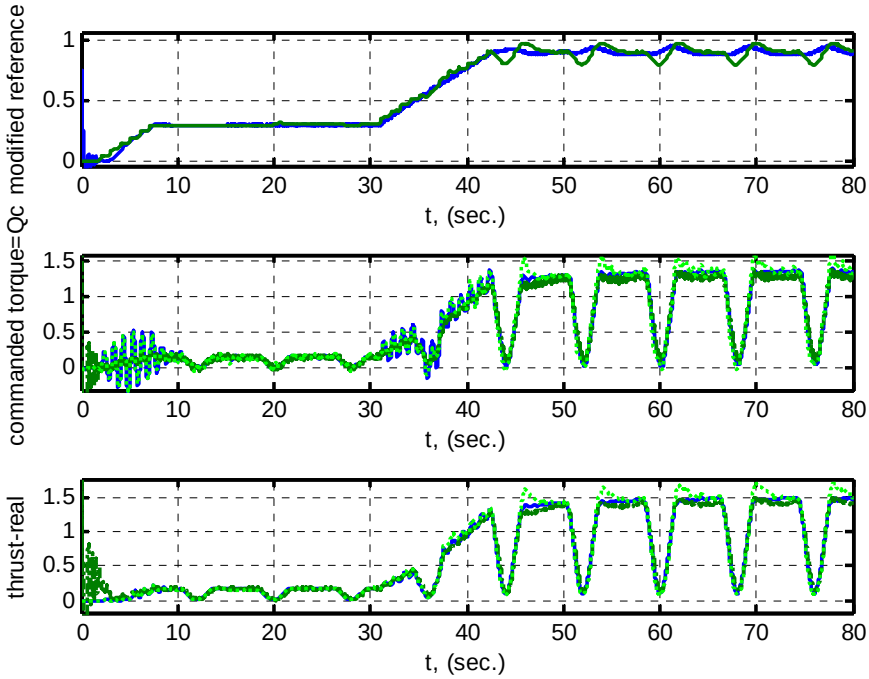

Fig.8.12. Thruster speed reference (top), commanded torque (middle) and real thrust (lowest) using filters: *PI controller* (——, blue), *inertial controller* (-.-.-.-, dark green), *direct torque-loss controller* (------, light green)

8.7 Conclusions

Observer-based speed controllers for thrusters are proposed in this Chapter. The problem of speed control is considered with regards to noise present in the measurement and electrical motor torque for electrical thrusters.

A number of noise-filtering observers (state estimators) are proposed to improve the overall closed-loop control performance of the propulsion when standard proportional-integral (PI) controller is used for the control of marine thrusters. From the simulations performed in SIMULINK/MATLAB it has been concluded that the proportional-integral observer (PIO) may provide the best improvements over the low pass filter when the noise is present.

The *inertial controller* is proposed to improve the controller performance by inclusion of virtual inertia and virtual damping in the control law (Radan *et al.* 2007a). The inertial controller can also be regarded as a nonlinear PID controller with filtered D-term and further improvements in the noise suppression.

The *direct torque-loss controller* has been proposed to improve the control performance of electrical thrusters and engines. *Direct torque-loss controller* is based on the anti-spin control concept (Smogeli *et al.*, 2004a) but provides more robustness to parameter inaccuracies and to variations in the operating regimes. The *torque-loss controller* has been compared to the *inertial* controller. It appears that the *inertial controller* may suppress the shaft torque fluctuations still better than the *direct torque-loss controller*. However, the later will suppress the shaft fluctuations better. The *inertial controller* will have the lowest shaft torque fluctuations of all simulated controllers. This may be beneficial from the vibration aspect, as the *inertial controller* will induce the fluctuations with the lowest frequency compared to other controllers.

The proposed control method is mainly analyzed for the speed control of electrical thrusters due to the importance of having good noise suppression in the controller output signal. Similar analysis and comparison of simulation results are possible for other applications of speed control. It is believed that the *inertial controller* and *direct torque-loss controller* could be applied on rotating machinery in general, without the need to install any additional sensors or actuators, namely: electrical motor drives, prime movers (engines, turbines, etc.), generating-sets, compressors, pumps, and similar.

Chapter 9

Conclusions and recommendations

9.1 Conclusions

This thesis has focused on control of marine electrical power system for increased overall vessel performance.

In Chapter 2, the functionality and operation of existing power and energy management system had been explained. The power system modeling was given in the appendices. The main objectives and constraints of the design were presented together with concepts of redundancy, single point failures, and vessel and PMS fault vulnerability. These are important concepts, constantly repeated in the motivation and validation of proposed PMS solutions. Further, the blackout dynamics and generator allocation control had been modeled and number of constraints and equipment limitations are identified. These constraints are used in Chapter 4 to provide the energy management solutions. Important section in Chapter 2 is about the load limiting control. There, the consequences of present control philosophy have been analyzed with regards to the blackout prevention and overall system performance.

Chapter 3 described the blackout prevention control. Various existing solutions are presented and analyzed with regards to speed of blackout detection and detection reliability. It has been emphasized that spurious trips of thrusters, i.e. the false blackout detection rate should be reduced, as it may potentially increase the wear-out rate of thruster's components. The observer-based fast load reduction has been proposed, and its performance was demonstrated in a case study. It was shown that the proposed controller is faster than any existing controller, i.e. the generator breaker trip (the potential blackout) is detected within 50 milliseconds. Moreover, the proposed controller is robust and reliable while the false blackout detections are minimized.

Chapter 4 was about the minimization of operational costs, including the fuel consumption. The operational costs and constraints have been identified, the number of which are specific for the marine vessel operations. Some of them, such as the blackout risk cost can hardly be quantified. Despite that, the blackout risk cost can be included in the proposed cost function. The long-term and short-term unit commitment optimizations had been proposed. Classical convex optimization numerical techniques as well as relatively modern evolutionary based non-convex optimization methods are used successfully through the case studies. The main result was 6% of fuel saved for the existing OSV and 8% for newbuilds. The overall operational costs, e.g. engine start/stop, engine load variations, etc. have also been reduced.

Chapter 5 presented the propulsion load control. The motivations for the load control were defined, and the network load disturbances were defined for the marine power system. Slowly varying power disturbances were separated from the dynamic disturbances and the latter were further analyzed through the propeller disturbance studies. Quasi-static load limiting controllers were proposed, based on the real-time measurements and the probability of load disturbances, i.e. pre-calculated expected number of disturbances in one hour above

the threshold. It was demonstrated that the controller can decrease the frequency fluctuations on the network. This is an important result for the power redistribution controller and its integration with thrust allocation, presented in the Chapter 6. It is also important for the fuel economy as the fuel consumption is proportional to the level of network load fluctuations.

Chapter 6 proposed a new strategy to completely attenuate the frequency and voltage fluctuations on the network. The proposed *power redistribution control* (PRC) will dynamically affect thrusters and other consumers, thereby significantly improve the network stability to any kind of disturbances, including some faults. It has been demonstrated that the proposed PRC will have a minor effect on the vessel responses, e.g. effects on DP and maneuvering will be insignificant.

In Chapter 7, it had been proposed that the PRC can be integrated with the quasi-static load limiting control, presented in Chapter 5, or thrust allocation. Important mechanical limits for the generating-sets and thrusters were included in the controller design. Chapter 7 also presented the proposed frequency-based precise load limiting control. The thrust allocation algorithm has been implemented with the proposed sensitivity to propeller shaft speed fluctuations when operating with PRC. Thus, it is believed that the PRC is integrated for the optimal vessel performance. Moreover, it has been discussed how the proposed integrated network control concept can be used for the increased robustness to faults and blackout.

Chapter 8 was about speed control of thrusters, and propulsion engines. It dealt with the speed control for an isolated machine, e.g. thruster, propulsion engine or generating-set. The main goal of the Chapter was to find the control that will reduce the damages and wear-out rates of the mechanical components of the machine. An electrical thruster was used to demonstrate control strategies that were applicable to propulsion engines and generating-sets, as well. A number of observers were proposed in order to separate i.e. suppress (attenuate) the noise in the speed measurement. Further, several controllers were proposed that may be combined with proposed noise attenuating observers. The proposed control strategies did not require any additional sensors. The advantages of proposed inertial controller and direct torque-loss controller, combined with the proportional-integral observer were demonstrated through the case studies.

This thesis has demonstrated the importance of high-level power management control to operational cost reductions and blackout prevention, in addition to controller integration between the power system and the propulsion system for the optimum vessel performance.

Based on evaluation of the performance across all operating regimes for the power and propulsion control, the simulation results indicated that the proposed *integrated power network control* was advantageous solution for the maximum blackout prevention, minimum wear-out rate of thrusters and generators, and the minimization of overall operational costs including the fuel and environmental costs.

9.2 Recommendations for future work

The theoretical work and simulations of the proposed power network control strategies have reached a point where preliminary full-scale testing is possible. With the experience gained from this, full-scale industrial implementation should be close at hand.

In Chapter 4, various operational costs have been identified and described. The cost functions are mainly formulated qualitatively. The exact quantitative behavior could be obtained once the present model start to be used and then can be improved based on the full scale real time measurements for the specific vessel. In addition, the blackout cost is very difficult to estimate quantitatively but it could be further analyzed. Such analysis is outside the scope of this thesis.

In Chapter 6, the proposed power redistribution controller redistributes the power load to fast acting consumers i.e. thrusters and achieves very effective reductions in the network load fluctuations. Since the thrusters are already subjected to thrust losses with propellers slipping in water, the effect of the load redistribution to thrust accuracy is low. The effect of load fluctuations reductions will be much lower when the thrusters are operated at the low load. If other consumer(s) injects the load fluctuations to the network, then there will be limited possibilities to reduce these fluctuations. In this case, other consumers not analyzed in this thesis could be used – these are various energy dependant consumers such as electrical heaters, HVAC, some types of compressors (dependent on the purpose), etc.

In Chapter 7, the integration aspects of the PRC control strategy have been demonstrated through the simulations with quasi-static load limiting control and good results are obtained. It remains to further investigate the overall operation of the PRC system with thrust allocation.

The diesel engine transient fuel consumption is based on the transients on engines for agriculture tractors varied from 0.3% up to approximately 13% during front end loading. It remains to obtain a similar model for the marine engines. This may not be easy as it requires extensive change in the load of the engines which may damage the engine. Easier results could be obtained by data logging of measurements on full scale vessels in the operations, subject to harsh weather conditions.

As discussed in Chapter 8, it appears that the *inertial controller* may suppress the shaft torque fluctuations better than the *direct torque-loss controller*, however the latter will suppress the shaft fluctuations better. It is indicated in the case study that the *inertial controller* can induce the lowest frequency fluctuations to the power transmission parts compared to other controllers. This should be further investigated and effects of the various available and proposed control strategies compared in order to find the controller with minimum mechanical wear-our rate of the power transmission parts. The transmission gears should also be included in the studies. The proposed *inertial controller* and the *direct torque-loss controller* are analyzed for the electrical thrusters. However, the frequency converter effects have not been included assuming that the frequency converter will have a very high bandwidth. This may not be true for the very high frequency noise introduced by the cascaded speed controller in the outer loop. Similar analysis and comparison of simulation results are possible for other applications of proposed controllers, namely: generating-set, main propulsion engine and propulsion engine with shaft-generator. These systems are not

equipped with the frequency converter, and thus would be easier to analyze. However, the shaft torque fluctuations induced by the diesel engine periodical cylinder combustion would have to be considered.

Bibliography

ABB AS (2003), Kleven Verft AS, MSB 1&2 690 V, Single Line Diagram and Operation of Viking Energy, *Eidesvik AS, Trials from June 23th to 25th*

Ådnanes, A.K., A.J. Sørensen and T. Hackman (1997), Essential Characteristics Of Electric Propulsion and Thruster Drives in DP Vessels, *Proc. of Dynamic Positioning Conference*, Houston, US

Ådnanes, A.K. (1999), Optimization of Power and Station Keeping Installations by a Total System Design Approach, *Dynamic Positioning Conference*, Houston, US

Ådnanes, A.K. (2003), Maritime Electrical Installations and Diesel Electric Propulsion, *Lecture Notes*, Trondheim: Dept. Marine Technology, NTNU, Norway
http://www.ivt.ntnu.no/imt/electricship/papers/electric_propulsion_adnanes.pdf

Ådnanes, A.K. (2004), Maritime Electrical Installations, *Lecture Slides***,** Department of Marine Technology, NTNU, Trondheim, Norway

Ådnanes, A. K. (2005), Small size Anchor Handling and Supply Vessel, *Tech. Report*, ABB Marine AS

Allen, E., N. LaWhite, Y. Yoon, J. Chapman, and M. Ilic (2001), Interactive Object-Oriented Simulation of Interconnected Power Systems Using SIMULINK, *IEEE Transactions On Education*, Vol. 44, No. 1, Feb. 2001

Anderson, P.M. and A.A. Fuad (2003), Power System Control and Stability, *1st edition: Iowa State University Press, 1977 and 2nd edition: John Wiley and Sons, IEEE Press*, 2003

Aoyagi, S., Y. Hasegawa, T. Yonekura and H. Abe (2001), Energy efficiency improvement of series hybrid vehicle, JSAE *Review journal, Society of Automotive Engineers of Japan, Inc. and Elsevier Science B.V.*, July 2001

Arntsen, T. (2005), Static optimization of load sharing, Statisk optimalisering av lastfordelingen, (in Norwegian), *MSc-thesis*, Department of Marine Technology, NTNU, Spring 2005

Arroyo, J.M. and A.J. Conejo (2004), Modeling of start-up and shut-down power trajectories of thermal units, *Power Systems, IEEE Transactions*, Vol.: 19, Is.: 3, pp: 1562- 1568, ISSN: 0885-8950, Aug. 2004

Atassi, A. N., H. K. Khalil (1999), A Separation Principle for the Stabilization of a Class of Nonlinear Systems, *IEEE Trans. Automatic Control*, pp. 1672-1687

Bakkeheim, J., Ø. N. Smogeli, T. A. Johansen, A. J. Sørensen (2006), Improved Transient Performance by Lyapunov-based Integrator Reset of PI Thruster Control in Extreme Seas, *IEEE Conf. Decision and Control*, San Diego, USA, 2006

Bakkeheim, J., L. Pivano, T. A. Johansen and Ø. N. Smogeli (2007a), Integrator Reset Anti-spin for Marine Thrusters Operating in Four-Quadrants and Extreme Sea Conditions, *IFAC Conference on Control Applications in Marine Systems* (CAMS'07), Bol, Croatia

Bakkeheim, J., Ø. N. Smogeli, T. A. Johansen and A. J. Sørensen (2007b), Lyapunov-based Integrator Resetting with Application to Marine Thruster Control, *IEEE Transactions on Control Systems Technology*

Bansal, R.C. (2006), A Bibliographical Survey Of Evolutionary Computation Applications In Power Systems (1994–2003), *International Journal of Power and Energy Systems*

Bansal R. C. (2005), Optimization Methods for Electric Power Systems: An Overview, *International Journal of Emerging Electric Power Systems*: Vol. 2, Iss. 1, Article 1021

Barsali, S., C. Miulli and A. Possenti (2004), A control strategy to minimize fuel consumption of series hybrid electric vehicles, *IEEE Transactions on Energy Conversion*, Vol. 19, No. 1, pp.187–195

Beale, S. and B. Shafai (1989), Robust control design with a proportional integral observer, *International Journal of Control*, 50, 97-111

Bertsekas, D.P. (1995) Dynamic Programming and Optimal Control, *Belmont, MA:Athena Scientific*

Black, J. W. and M. Ilic (2002), Demand-Based Frequency Control for Distributed Generation, *IEEE PES Summer Meeting*, Vol.1 (2002): 427 – 432

Blanke, M., M. Kinnaert, J. Lunze and M. Staroswiecki (2006), Diagnosis and Fault-tolerant Control, *Springer*

Bose, B. K. (2002), Modern Power Electronics and AC Drives, *Upper Saddle River: Prentice Hall*

Busawon, K. K. and P. Kabore (2001), Disturbance attenuation using proportional integral observers, *International Joumal of Control*, pp. 618-627, 2001

Carlton, J. S. and D. Vlasic (2005), Ship vibration and noise: Some topical aspects, *1st International Ship Noise and Vibration Conference*, London, UK

Claeys, G., N. Retiere, N. Hadjsaid, P. Lemerle, E. Varret, R. Belhomme (2001), Dynamic Modeling Of Turbo- Charged Diesel Engine For Power System Studies, *IEEE/ PICA'2001*, Sydney, Australia

Chen, C.T. (1999), Linear System Theory and Design, *Oxford University Press*, London

Chen, J., J. Patton and H. Y. Zhang (1996), Design of unknown input observers and robust fault detection filters, *International Journal of Control*, pp. 85-105

Clarke, N.J. (2004), Marine electrical power systems, *2nd Intern. Conference on Power Electronics, Machines and Drives*, 2004 (PEMD 2004)

Comes Sanz, J. M. (2004), LQGLTR Speed Control of the Field Oriented Induction Motor with Multirate Kalman Filter, *IEEE International Conference on Industrial Technology (ICIT)*

Conachey, R.M. (2005), Development of Machinery Survey Requirements Based on Reliability-Centered Maintenance, *2005 SNAME Marine Technology Conference & Expo.*

Cranch, N. and D. Phillips (2003), DP Design and Control Systems, DP and Integrated Control Systems Networks, *Dynamic Positioning Conference*, Huston, US

Dabroom, A. M. and H. K. Khalil (1999), Discrete time Implementation of High-gain Observers for Numerical Differentiation, *Int. J. Control*, pp. 1523-1537

Dahler, G., J. Roaldsøy, E. Sandberg (2006), Det Norske Veritas' methodology for propulsion shaft design – A cost-saving and reliable supplement to the IACS simplified code, *Proceedings of SNAME Symposium on Propellers /Shafting 2006*, 2006-09-12/13, Williamsburg VA, US

Davey, K. (2005), Ship Component In-Hull Optimization, *Marine Technology Society Journal*, Vol. 39, no 2, 2005

Design team (2003), Design Report-DRILLSHIP Nereus, University of Michigan, Department of Naval Architecture and Marine Engineering, *International Student Offshore Design Competition*

Deter, D. (1997), Principal Aspects of Thruster Selection, *Dynamic Positioning Conference*, 21 - 22, October, Houston, US

Drakunov, S. and V. Utkin (1995), Sliding Mode Observers. Tutorial, *Proc. of the 34th Conference on Decision and Control*, New Orleans, LA, Dec. 1995

Emadi, A., (2003) Vehicular Electric Power Systems: Land, Sea, Air, and Space Vehicles, *NewYork: Marcel Dekker*

English, P. (2001), The Evolution of Marine and Drilling Drives in Today's Market, ALSTOM Power Conversion Ltd (Rugby, UK), *Dynamic Positioning Conference*, September 18-19

Evans, M. J., and J. S. Rosenthal (2003), Probability and Statistics: The Science of Uncertainty, *W. H. Freeman*, 2003

European commission, EU and Energy Research, (http://ec.europa.eu/)

Faltinsen, O.M. (1990), Sea Loads on Ships and Offshore Structures, *Cambridge University Press*

Faltinsen, O.M., (2005), Hydrodynamics of High Speed Marine Vehicles, *Cambridge University Press*

FEV Engine Technology, Inc. (1995), Emissions and Performance Characteristics of the Navistar T444E DI Diesel Engine Fueled with Blends of Biodiesel and Low Sulfur Diesel Fuel, Phase 2 *Final Report*, 1995

Fletcher, R. (2000), Practical Methods of Optimization, *Wiley*; 2 Sub Edition

Fossen, T. I. and J. P. Strand (2001), Nonlinear Passive Weather Optimal Positioning Control (WOPC) System for Ships and Rigs: Experimental Results, *Automatica* 37(5), 701—715.

Fossen, T.I. (2002), Marine Control Systems: Guidance, Navigation and Control of Ships, Rigs and Underwater Vehicles, *Marine Cybernetics AS*, Trondheim, Norway

Fossen, T. I. and T. I. Johansen (2006), A Survey of Control Allocation Methods for Ships and Underwater Vehicles, *Invited paper at the 14th IEEE Mediterriaen Conference on Control and Automation*, Ancona, Italy, 2006

Frank, P.M., and J. Wunnenberg (1989), Robust fault diagnosis using unknown input observer scheme, In R. J. Patton, P. M. Frank and R. N. Clark (Eds) *Fault Diagnosis in Dynamic Systems; Theory and Application*, Prentice Hall, Englewood CliOEs

Franklin, G. F., J. D. Powell and A. Emami-Naeini (2006), Feedback Control is Dynamic Systems, *Pearson Prrentice Hall*, 2006

Gauthier, J. P., H. Hammouri and S. Othman, (1992), A simple observer for nonlinear systems, Application to bioreactors, *IEEE Transactions on Automatic Control*, 37, 875-880

Gravdahl, J.T. and O. Egeland (1999), Compressor Surge and Rotating Stall: Modeling and Control, *Springer Verlag*
(http://www.itk.ntnu.no/ansatte/Gravdahl_Jan.Tommy/papers/CompressorBook.pdf)

Guzzella, L. and A. Amstutz (1998), Control of diesel engines, *IEEE Control Systems*, 0272-1708, Oct

Guzzella L., A. Sciarretta (2007), Vehicle Propulsion Systems - Introduction to Modeling and Optimization, *Springer Verlag*

Häkkinen, P. (1997), Fire resistant engine room, Maritime Safety '97, Espoo, 19 March 1997

Häkkinen, P. (1998), How to achieve the fire resistant engine room, Fire Europe, Dec. 98, s. 19-22

Häkkinen, P. (2003), Reliability of Machinery Plants and Damage Chains, World Maritime Technology Conference San Francisco USA, 17-20 Lokakuuta, US

Hannett, L. N. and A. Khan (1993), Combustion Turbine Dynamic Model Validation from Tests, *IEEE Transactions on Power Systems*, Vol. 8, No. 1, Feb

Hansen, J. F. (2000), Modeling and Control of Marine Power Systems, *PhD thesis*, Dept. Engineering Cybernetics, NTNU, Trondheim, Norway, 2000

Hansson, P.A., M. Lindegn, M. Nordin, and O. Pettersson (2003), A methodology for measuring the effects of transient loads on the fuel efficiency of agricultural tractors, *Applied Engineering in Agriculture*, 19(3), 251-257

Hassouneh, M.A., H. C. Lee and E.H. Abed (2004), Washout filters in feedback control: benefits, limitations and extensions, Proceedings of the American Control Conference, July

He, B. and M. Jang (2006), Optimization-based energy management of series hybrid vehicles considering transient behavior, *Int. Jounal of Alternative Propulsion*, Vol. 1, No. 1

Hu, Z., Chen, L., Gan, D. and D. Chattopadhyay, (2006), Allocation of Unit Start-Up Costs Using Cooperative Game Theory, *IEEE TRANSACTIONS ON POWER SYSTEMS*, VOL. 21, NO. 2, May

Hunt, I. V.W. (2000), Diesel Engine Generators for Black Start and Supply Emergencies, *Electrical Engineers Association Annual Conference*, Auckland, US

IACS (2004), Requirements Concerning Machinery Installations-Iacs Req. 2004, *International Association Of Classification Societies* - IACS

Ibrir, S. (2001), New Differentiators for Control and Observation Applications, *Proc. ofAmerican Control Coiference*, Arlington, VA, pp. 2522-2527

Jenman, C. (2001), Insufficient Power, *Dynamic Positioning Conference*, Huston, US

Johansen, T. A. (2004), Optimizing nonlinear control allocation, *IEEE Conf. Decision and Control*, Nassau, Bahamas, pp. 3435-3440

Johansen, T. A., T. I. Fossen and P. Tøndel (2004a), Efficient Optimal Constrained Control Allocation via Multi-Parametric Programming, *AIAA Journal of Guidance, Control and Dynamics*, 28, 506-515.

Johansen, T. A., T. I. Fossen and S. P. Berge (2004b), Constrained Nonlinear Control Allocation with Singularity Avoidance using Sequential Quadratic Programming, *IEEE Transactions on Control Systems Technology* 12(1), 211-216.

Journée, J. M. J. (2000), Theoretical Manual of SEAWAY (Release 4.18), *Technical Report* 1216, Delft University of Technology, Netherlands

Journée, J. M. J. and W.W. Massie (2001), Offshore Hydromechanics, March 2001, *Lecture notes*, Delft University of Technology

Kallah, A. (1997a), Electrical Power Plant and Thruster Systems Design Considerations for Dynamically Positioned Vessels, Marine Technology Society, *Dynamic Positioning Conference*

Kallah, A. (1997b), A Comparison of Thruster Propellers and Variable Speed Drives for DP Vessels, Cegelec., *Dynamic Positioning Conference*, 21 - 22 October

Karnavas, Y. L. and D. P. Papadopoulos (1999), Maintenance oriented algorithm for economic operation of an autonomous diesel–electric station, *Electric Power Systems Research*, Vol. 51, pp: 109–122

Khiar, D., J. Lauber, T. Floquet, T.M. Guerra (2005), An observer design for the instantaneous torque estimation of an IC engine, Vehicle Power and Propulsion, *IEEE Conference*, Sept.

Klimstra, J. (2004a), Optimum Load Step Response of Fuel-Injected Reciprocating Gas Engines, *CIMAC Congress*, Kyoto, Japan

Klimstra, J. (2004b), The Cascade Principle: a Power Plant based on Multiple Modular Units, *Modernising Central European Electricity Markets Conference 2004*, Prague

Klimstra, J. (2004c), Power Plant Operation Optimisation through Business Partnership, *POWER-Gen Europe 2004*, Barcelona

Koot, M., J. T. B. A. Kessels, Bram de Jager, W. P. M. H. Heemels, P. P. J. van den Bosch, and Maarten Steinbuch (2005), Energy Management Strategies for Vehicular Electric Power Systems, *IEEE Transactions On Vehicular Technology*, Vol. 54, No. 3, May

Koot, M. (2006), Energy management for vehicular electric power systems, *PhD thesis, Technische Universiteit Eindhoven*, ISBN-10: 90-386-2868-4

Koot, M., J. Kessels, B. de Jager and P. van den Bosch (2006), Fuel reduction potential of energy management for vehicular electric power systems, *Int. J. Alternative Propulsion*, Vol. 1, No. 1, 2006

Koushan, K. (2004), Environmental and Interaction Effects on Propulsion Systems used in Dynamic Positioning, an Overview, *Proc. 9th Int. Symp. Practical Design of Ships and Other Floating Structures* (PRADS'04), Lübeck-Travemünde, Germany

Kovudhikulrungsri, L. and T. Koseki (2006), Precise Speed Estimation From a Low-Resolution Encoder by Dual-Sampling-Rate Observer, *IEEE/ASME Transactions on Mechatronics*, Volume: 11, Issue: 6, pp: 661-670

Koushan, K. (2006), Dynamics of Ventilated Propeller Blade Loading on Thrusters, *World Maritime Technology Conference* (WMTC'06), London, UK

Kudva, P., N. Viswanadham, and A. Ramakrishna (1980), Observers for Linear Systems with Unknown Inputs, *IEEE Transaction on Automatic Control*, AC-25, pp. 113-1 15, 1980

Kundur, P. (1994), Power System Stability and Control, *McGraw-Hill*, New York

Kweon, T. and D. Hyun (1999), High-performance speed control of electric machine using low precision shaft encoder, *IEEE Truns. Power Electronics*, I5(5): 838-849

Lauvdal, T. and A.K. Ådnanes (2000), Power Management System with Fast Acting Load Reduction for DP Vessels, *Dynamic Positioning Conference*, Huston, US

Lazarewicz and M. L., A. Rojas, Grid Frequency Regulation by Recycling Electrical Energy in Flywheels, *IEEE Power Engineering Society General Meeting*, Denver, US

Lee, T.Y., and C.L. Chen (2007), Unit commitment with probabilistic reserve: An IPSO approach, *Energy Conversion and Management*, Volume 48, Issue 2, Pages 486-493

Levander O. (2006), Novel propulsion machinery solutions for ferries, Wärtsilä Corporation - *Ship Power*, Finland

Lewis, F. L., C. T. Abdallah and D. M. Dawson (1993), Control of Robot Manipulators, *Macmillan*, New York

Lin, C.C., H. Peng, J. W. Grizzle, and J. Kang (2003), Power Management Strategy for a Parallel Hybrid Electric Truck, *IEEE Transactions on Control Systems Technology*, vol. 11, pp. 839-849

Lindgren, M. (2004), Engine exhaust gas emissions from non-road mobile machinery, *PhD thesis*, Dept. of Biometry and Engineering, Swedish University of Agricultural Sciences, (http://diss-epsilon.slu.se/archive/00000644/01/Agraria481.pdf)

Lu, Q., S. Yuanzhang, M. Shengwei (2001), Nonlinear Control Systems and Power System Dynamics, *Norwell, MA: Kluwer Academic Publishers*

Mahon, L.L.J. (1992), Diesel Generator Handbook, *Butterworth and Heinemann*

Malik, A.S. and B.J. Cory (1997), Impact of DSM on energy production cost and start-up and shut-downcosts of thermal units, *Fourth International Conference on Advances in Power System Control, Operation and Management* (APSCOM-97), Asian Inst. of Technology., Bangkok

MAN B&W (2005), Project Guides for Marine Plants,Dual-fuel Engine 48/60DF, L+V 48/60 B, L+V 32/40

MAN B&W (2006), Project Guide for Marine Plants Dual-fuel Engine 51/60 DF, Status: 08.2006

MAN Diesel SE (2006), Project Guide for Marine Plants, Diesel Engine 48/60B, 2006 (www.manbw.com)

MAN B&W, Vibration Characteristics of Two-stroke Low Speed Diesel Engines

Mariani, E. and S.S. Murthy (1997), Control of Modern Integrated Power Systems, *Advances in Industrial Control*, Springer-Verlag

Marino, R., and P. Tomei (1995), Nonlinear Control Design, *Prentice Hall*

Massoumnia, M. A., G. C. Verghese and A. S. Willskey (1989), Failure detection and identification. *IEEE Transactions on Automatic Control*, 34, 316± 321

May, J., J. and Foss, H. (2000), Power Management System for the "Deepwater Horizon" a Dynamically Positioned All Weather Semisubmersible, *Dynamic Positioning Conference*,

Huston, US

May, J. J. (2003), Improving Engine Utilization on DP Drilling Vessels, *Dynamic Positioning Conference*, Huston, US

Machowski, J., J. Bialek and J. R. Bumby (1997), Power System Dynamics and Stability, *Wiley*

Matt, C. F., L. S. R. Vieira, G. F. W. Soares and L. P. T. de Faria (2005), Optimization of the Operation of Isolated Industrial Diesel Stations, *6th World Congress on Structural and Multidisciplinary Optimization*, Rio de Janeiro, Brazil

Michalewicz, Z., Dasgupta, Le Riche, D. R.G. and M. Schoenauer (1996), Evolutionary Algorithms for Constrained Engineering Problems, *International Syposium on Methodologies for Intelligent Systems*

Milosevic, M and G. Andersson (2005), Generation Control in Small Isolated Power Systems, *North American Power Symposium* (NAPS), Ames, USA, 2005

Minsaas, K.J., H.J. Thon and W. Kauczynski (1987), Estimation of Required Thruster Capacity for Operation of Offshore Vessels under Severe Weather Conditions, *PRADS*, Trondheim, Norway, pp. 411–427

Morren, J., J. Pierik and Sjoerd W.H. De Haan (2006), Inertial response of variable speed wind turbines, *Electric Power Systems Research*, Vol. 76, Issue 11: 980-987

Murry, R.J. and B.F. Mitchell (1994), Cost savings from a practical predictive-maintenance program, *Proceedings of the Reliability and Maintainability Symposium*, Anaheim, CA, US

Niemann, H. H., J. Stoustrup, B. Shafai, and *S.* Beale (1995), "LTR design of proportional integral observers", *International Journal ofRobust and Nonlinear Control*, pp. 671-693

Nikolaos I. Xiros, Nikolaos P. Kyrtatos (2000), A Neural Predictor Of Propeller Load Demand For Improved Control Of Diesel Ship Propulsion, *Proc. of the 15th IEEE Inter. Symposium on Intelligent Control* (ISIC 2000), Rio, Patras, GREECE

Nilsen, R. (2005), Discussions on modeling of marine power system and marine electric thruster drives, *personal communications*, Department of Electrical Power Engineering, NTNU, 2005

Nguyen T. D., Sørensen A. J. and Quek S. T. (2007a), Design of High Level Hybrid Controller for Dynamic Positioning from Calm to Extreme Sea Conditions, *Automatica*, **43**(5), pp. 768–785

Nguyen T. D., Sørensen A. J. and Quek S. T. (2007b), Multi-Operational Hybrid Controller Structure for Station Keeping and Transit Operations of Marine Vessels, *To appear in IEEE Transaction on Control System Technology*

Olsbu, A., P. A. Loeken and l. E. Grossmann (1988), A Mixed-Integer Programming Model For The Design And Planning Of Power Systems In Oil Production Platforms, *Engineering Costs and Production Economics*, Vol. 14, pages: 281-296, Elsevier Science Publishers B.V., Amsterdam

Olsbu, .A., P. A. Loeken and I. E. Grossmann (1985), Simultaneous synthesis and economic optimization of the power system on an oil/gas production platform, *12th IFIP Conference*, Budapest

Oppenheim, A.V., A. S. Willsky and S. H. Nawab (1997), Signals and Systems, Second edition, *Prentice Hall*, New Jersey, US

Papadimitriou, C.H. and K. Steiglitz (1998), Combinatorial Optimization: Algorithms and Complexity, *Dover Publications*, Unabridged edition, 1998

Perez-Guerrero, R.E. and J.R. Cedenio-Maldonado (2005), Economic Power Dispatch with Non-Smooth Cost Functions Using Differential Evolution, *Proceedings of the 37th Annual North American Power Symposium*, 2005

Pivano, L., T.A. Johansen, Ø.N. Smogeli and T.I. Fossen (2007a), Nonlinear Thrust Controller for Marine Propellers in Four-Quadrant Operations, *American Control Conference* (ACC2007), July 11-13, 2007, New York, USA

Pivano, L.,J. Bakkeheim, T.A. Johansen and Ø.N. Smogeli (2007b), A Four-Quadrant Thrust Controller for Marine Propellers with Loss Estimation and Anti-Spin, *IFAC World Congress*, Seoul, Korea

Price, W.G. and R.E.D. Bishop (1974), Probabilistic Theory of Ship Dynamics, *Chapman and Hall*, London

Rao, S.S. (1996), Engineering Optimization: Theory and Practice, 3rd Edition, *Wiley-Interscience*, 3 Sub edition

Radan, D., T.A. Johansen, A.J. Sørensen, A.K. Ådnanes (2005), Optimization of Load Dependent Start Tables in Marine Power Management Systems with Blackout Prevention, *WSEAS Trans. on Circuits and Systems* , Issue 12, Vol. 4, pp. 1861-1867

Radan, D., A.J. Sørensen, T.A. Johansen and A.K. Ådnanes (2006a), Probability Based Generator Commitment Optimization in Ship Power System Design, *WSEAS Trans. on Systems* , Issue 8, Vol. 5, pp. 1901-1907

Radan, D., Ø.N. Smogeli, A.J. Sørensen and A.K. Ådnanes (2006b), Operating Criteria for Design of Power Management Systems on Ships, *Proc. of the 7th IFAC Conference on Manoeuvring and Control of Marine Craft (MCMC'06)*, Lisbon , Portugal

Radan D., Asgeir J. Sørensen, Tor Arne Johansen (2007a), Inertial Control of Marine Engines And Propellers, *IFAC Conference on Control Applications in Marine Systems (CAMS'07)*, Bol, Croatia

Radan D., Asgeir J. Sørensen, (2007b), A New Concept of Integrated Power Control In Marine Electric Power System, *Conference on Electrical Equipment and Technical Safety on Board of Ships*, SCHIFFBAUTECHNISCHE GESELLSCHAFT e.V., Sept. 19th, Hamburg

Radan D., Asgeir J. Sørensen, Alf Kåre Ådnanes, Tor A. Johansen (2008), Reducing Power Load Fluctuations on Ships Using Power Redistribution CONTROL, *Marine Technology Jounal-SNAME*, (*Accepted*)

Radan, D. (2004a), Power Electronic Convereters for Ship Propulsion Electro Motors, *Tech. Report*, Department of Marine Technology, project: Energy-Efficient All Electric Ship, NTNU, Trondheim, Norway

Radan, D. (2004b), Marine Power Plant Control System- Power / Energy Management System, *Tech. Report*, Department of Marine Technology, project: Energy-Efficient All Electric Ship, NTNU, Trondheim, Norway

Ruth, E. (2005), Modelling and control of controllable pitch thrusters subject to large losses. *Master thesis*, Department of Marine Technology, Norwegian University of Science and Technology, Trondheim, Norway 2005

Ruth, E. and Ø.N. Smogeli (2006), Ventilation of controllable pitch thrusters, *Marine Technology and SNAME news*, vol. 43, pp. 170—179, October 2006

Ruth, E., Ø.N. Smogeli, and A.J. Sørensen (2006), Overview of propulsion control for surface vessels, *7th IFAC Conference on Manoeuvring ans Control of Marine Craft*, Lisbon, Portugal

Ruth, E., A. J. Sørensen, and T. Perez (2007), Thrust allocation with linear constrained quadratic cost function, *Conference on Control Applications in Marine Systems*, Bol, Croatia

Saif, M. (1997), An Observer Based Approach for Fault Diagnosis, *Proc. IASTED lnternational Conf.*, control 97, Cancun, Mexico, pp.239-242, 1997

Savoy, S. (2002), ENSCO 7500 Power Management System Design, Functionality and Testing, *Dynamic Positioning Conference*, Huston, US

Sciarretta, A., M. Back, and L. Guzzella (2004), Optimal Control of Parallel Hybrid Electric Vehicles , *IEEE Transactions On Control Systems Technology*, Vol. 12, No. 3

Sciarretta A. and L. Guzzella (2007), Control of Hybrid Electric Vehicles - A Survey of Optimal Energy-Management Strategies, *IEEE Control Systems Magazine*, Vol. 27, No. 2, pp. 60-70

Shafai, B. and R. L. Carroll, (1985), Design of proportional integral observers for linear time varying multivariable systems. *Proceedings of the IEEE CDC*, Piscataway, NJ

Shafai, B., C.T. Pi, and S. Nork (2002), Simultaneous Disturbance Attenuation and Fault Detection using Proportional Integral Observers, *Proc. Of American Control Conference*, Anchorage, AK, pp. 1643-1649, 2002

Slotine, J.J.E., J.K. Hedrick and E.A. Misawa (1987), On Sliding Observers for Nonlinear Systems, *Journal of Dynamic Systems, Measurement and Control*, Vol. 109, pp 245-252

Smogeli, Ø. N., J. Hansen, A. J. Sørensen and T. A. Johansen (2004a), Anti-spin Control for Marine Propulsion Systems, *Proc. of the 43rd IEEE Conf. on Decision and Control*, Bahamas

Smogeli, Ø. N., A. J. Sørensen and T. I. Fossen (2004b), Design of a hybrid power/torque thruster controller with thrust loss estimation, *Proceedings of the IFAC Conference on Control Applications in Marine Systems* (CAMS'04), Ancona, Italy

Smogeli, Ø.N. (2006), Control of Marine Propellers: from Normal to Extreme Conditions, *PhD thesis*, Dept. Marine Technology, NTNU, Trondheim, Norway, 2006

Sørensen, A.J., A.K. Ådnanes, T.I. Fossen and J.P. Strand (1997), A New Method of Thrusters Control in Positioning of Ships Based on Power Control, *4th IFAC Conf. on Manoeuvring and Control of Marine Craft*, Brijuni, Croatia

Sørensen, A. J., Quek, S. T. and Nguyen, T. D. (2005), Improved Operability and Safety of DP Vessels Using Hybrid Control Concept, *OSV Singapore*

Sørensen, A.J. and A.K. Ådnanes (2005), Reconfigurable Marine Control Systems and Electrical Propulsion Systems for Ships, *ASNE Reconfiguration and Survivability Symposium*, Florida, US

Stephen, S. and L. Vandenberghe (2004), Convex Optimization, *Cambridge University Press*

Theotokatos, G. and N.P. Kyrtatos (2001), Diesel Engine Transient Operation with Turbocharger Compressor Surging, *SAE World Congress*, Detroit, US

Tienhaara, H. (2004), Guidelines to Engine Dynamics and Vibration, *Wärtsilä Corporation*

Tilli, A. and M. Montanari, (2001), A low-noise estimator of angular speed and acceleration from shaft encoder measurements, *Journal Automatika*, 42(2001) 3-4, 169-176

Tronstad, T. and J. Burknes (2004), The fuel cells in ships: safety and reliability, *1st European Hydrogen Energy Conference*

Tupper, E. C. (1996), Introduction to Naval Architecture, *Butterworth-Heinemann*

Utkin, V., J. Gulder, M. Shijun (1999), Sliding Mode Control in Electro-mechanical Systems, *Series in Systems and Control*, CRC; 1 edition (April 22, 1999), ISBN-10: 0748401164

Wang, M.S., J. H. Chen, and S. H. Wang (2004), Filter Design of a Servomotor Encoder, *IEEE Asia-Pacific Conference on Circuits and Systems*

Wärtsilä (2007), Air emissions legislation review for internal combustion engines, *Report, Wärtsilä Finland Oy*, Vaasa, Finland

Watson, D.G.M. (2002), Practical Ship Design, *Elsevier Ocean Engineering Series*, Elsevier, ISBN-13: 978-0080440545, January, 2002

Weinmann, A. (1991), Uncertain Models and Robust Control, *Springer-Verlag*, New York

Westergard, J.P. (2006), Defining the diesel engine constraints and discussions on fast load reduction issues, *personal communications*, Wärtsila, 2006/2007

White D. (2004), Reduction In Carbon Dioxide Emissions: Estimating The Potential Contribution From Wind-Power, *Report, The Renewable Energy Foundation*

Wood, A.J. and B. F. Wollenberg (1996), Power Generation, Operation and Control, Second Ed., *John Wiley and Sons*

Young, Y. and S. Kinnas (2003), Performance prediction of surface-piercing propellers, *Journal of Ship Research*

Appendix A

Modeling of marine power system

In order to design and test the various control solutions presented in this thesis a simulator have to be used. This Chapter describes the basic modeling principles of marine power system simulator based on the well known models used for the design, analysis and control of the on-land power system. The marine power system is modeled as an isolated power system, with small transmission line impedance between the power generators and consumers. The main goal is to design the simulator capable to have fast speed of computation and low parameter dependence (data requirement), while having the required accuracy necessary for the safe testing of ideas e.g. power management and control solutions. Thus, modeling simplifications used to reduce the data requirements and to increase the simulation speed are given.

A.1 Power generation

The power generation plant consists of synchronous generators powered by diesel engines, gas (dual fuel) engines, gas- and/or steam-turbines. The fuel cells are also considered for the marine application as well (Tronstad and Burknes, 2004).

Unlike the on-land centralized power system, a marine power system is an isolated system, and typically all power generators and power consumers are located at the vessel.

The marine power generation system is easily affected by the consumer load due to small difference between the installed power and the consumed power. The reasons for this can be found in minimizing the installation costs, described in Chapter 2, and the operational costs e.g. power/energy management system (PMS/EMS). The PMS/EMS is starting and stopping generators in order to reduce the operational costs of the power plant, as described in Chapter 4 of this thesis. As the number of operating generating sets is minimized, the sensitivity of the power system to the consumer load fluctuations will be maximized. Therefore, the power network (grid) of the marine isolated power system may be regarded as "*weak*" network, unlike the so called "*stiff*" networks or "*one-machine-infinite-bus-system*", traditionally used in the electrical power engineering. The infinite bus system is represented by the so called "classical model", i.e. the voltage source behind the transient reactance (Anderson and Fuad, 2003), and operate with fixed voltage and frequency e.g. heaving infinite inertia.

The infinite bus systems will not be presented in this thesis as a great deal of information can be found in the referenced literature, e.g. Kundur (1994), Anderson and Fuad (2003), Machowski *et al.* (1997), Lu *et al.* (2001) and the references therein. These useful references also describe detailed modeling of generators, steam-, gas-, and hydro-turbines, in addition to providing details about the frequency and voltage control.

The *weak* power grid is described more in detail in e.g. Hansen (2000), Lu *et al.* (2001) and Milosevic and Andersson (2005) and the references therein. The application for the marine

vessel is thoroughly described in Hansen (2000). In this Chapter, simplified models of the network, derived in Lu *et al.* (2001), Hansen (2000) and Anderson and Fuad (2003) will be presented.

A.1.1 Rotor dynamics of synchronous generator

According to the *Newtons's law*, the relations among angle and angular acceleration of a generator's rotor and the torques imposed on the shaft of the generator set are obtained as:

$$J_g \frac{d}{dt}\omega_g = M_{mg} - M_{eg} - M_{dg}\,, \tag{A.1}$$

where ω_g is the rotor speed, M_{mg} is the mechanical torque imposed on the shaft supplied by the prime mover, M_{eg} is the electromagnetic (electrical) torque of the generator, and M_{dg} is the damping torque in direct proportion to the variations in the shaft speed, see e.g. Lu *et al.* (2001) and Anderson and Fuad (2003). The J_g is the moment of inertia of the rotating parts of the generator set i.e. the rotors of the generator and prime mover together. In this thesis, from this point forward, the M will be substituted by Q, so the following motion balance equation for the generator is obtained:

$$J_g \frac{d}{dt}\omega_g = Q_{mg} - Q_{eg} - Q_{dg}\,, \tag{A.2}$$

where Q_{mg} is the mechanical (engine) torque, Q_{eg} is the electromagnetic (electrical) torque of the generator, and Q_{dg} is the damping torque.

The rotor position with respect to a synchronously rotating reference ω_{0g} is defined by the rotor power angle δ_g. Then, the rotor velocity can be expressed as:

$$\omega_g = \omega_{0g} + \Delta\omega_g = \omega_{0g} + \frac{d}{dt}\delta_g\,, \tag{A.3}$$

where ω_{0g} is the rotor synchronous speed i.e. $\omega_{0g} = 2\,\pi\,f_0$ which e.g. for the 60 Hz system is $\omega_{0g} = 2\,\pi\,60$. In the per unit system, $\omega_{0g} = 1$. The rotor angular acceleration is expressed as:

$$\frac{d}{dt}\omega_g = \frac{d^2}{dt^2}\delta_g\,. \tag{A.4}$$

In a per unit system, (A.2) can be written as:

$$J_g^* \frac{d}{dt}\omega_g^* = Q_{mg}^* - Q_{eg}^* - Q_{dg}^*\,, \tag{A.5}$$

In the above equation, the base value of torque Q_{Bg} is:

$$Q_B = \frac{S_B}{2\pi n_g}\,, \tag{A.6}$$

where S_B is the power rating of the generator, expressed in VA (volt amperes), and n_g is the generator speed, expressed in revolution per second.

Usually, the time t and the moment of inertia, denoted by H_g are expressed is seconds while all torques are expressed in per unit. Thus, the following motion equation is usually used:

$$\frac{2H_g}{\omega_{0g}}\frac{d}{dt}\omega_g = Q_{mg} - Q_{eg} - Q_{dg}\,,$$

(A.7)

where the inertial time constant is:

$$H_g = \frac{1}{2}\frac{J_g\omega_{0g}^2}{S}\,. \qquad \text{(A.8)}$$

H_g is denoted by the time period it takes for a rotor rotating from a totally static state to reach its rated speed as a 1.0 per unit torque is applied on the shaft from t = 0 seconds.

The electrical power is related to torque through following well known equation:

$$Q_{eg} = \frac{P_{eg}}{\omega_g}\,. \qquad \text{(A.9)}$$

The per unit values of P_{eg} and Q_{eg} are very close to each other and usually set to be equal $P_{eg} = Q_{eg} \Rightarrow \omega_g = \omega_{0g} = 1$ in (A.9), in the on-land power system studies. The isolated marine grid should have an accurate motion equation, and this approximation will not be performed here.

A.1.2 Generator power and coordinate system transformation

The real value of the instantaneous active generator output power for the 3-phase synchronous generator is:

$$P_{eg} = V_{abc}^T I_{abc} = v_a i_a + v_b i_b + v_c i_c\,, \qquad \text{(A.10)}$$

where

- v_a, v_b, v_c are the instantaneous values of the generator's terminal voltages of the phase *a*, *b* and *c*;
- i_a, i_b, i_c are the instantaneous values of the generator's stator currents of three phases;
- $V_{abc}^T = \left[v_a\ v_b\ v_c\right]^T$, $I_{abc}^T = \left[i_a\ i_b\ i_c\right]^T$ and superscript T represents the transpose.

As the base value of power is $P_B = 3\,VI = 3\left(v_B/\sqrt{2}\right)\left(i_B/\sqrt{2}\right)$, where V and I are the effective values of rated voltages and currents, and v_B, i_B are base the values of the instantaneous peak voltages and currents, the per unit instantaneous generator output power is:

$$P_{eg} = \frac{2}{3} V_{abc}^{T} I_{abc} = \frac{2}{3}\left(v_a i_a + v_b i_b + v_c i_c\right), \tag{A.11}$$

where (A.11) is obtained when (A.10) is divided by the base power P_B to obtain per unit values of P_{eg}.

In order to increase the speed of simulation i.e. reduces the calculation load, the 3-phase voltages and currents are usually transformed to *d*-*q*-0 coordinate system which is rotating with the machine rotor. In this way, the magnetic conductivity of the windings is not the periodic function of time *t*, but a constant for an ideal generator. Thus, every parameter of an ideal generator will be a constant and independent of time *t* and the mathematical model becomes the time invariant system (TI), as explained in e.g. Lu *et al.* (2001). Then, the transformation equations for voltages and currents together with their inverse counterparts are shown:

$$V_{dq0} = C\, V_{abc}, \qquad I_{dq0} = C\, I_{abc}, \tag{A.12}$$

$$V_{abc} = C^{-1}\, V_{dq0}, \quad I_{abc} = C^{-1}\, I_{dq0},$$

where:

$$C = \begin{bmatrix} \cos\gamma & \cos\left(\gamma - 2/3\pi\right) & \cos\left(\gamma + 2/3\pi\right) \\ -\sin\gamma & -\sin\left(\gamma - 2/3\pi\right) & -\sin\left(\gamma + 2/3\pi\right) \\ 1/2 & 1/2 & 1/2 \end{bmatrix},$$

$$C^{-1} = \begin{bmatrix} \cos\gamma & -\sin\gamma & 1 \\ \cos\left(\gamma - 2/3\pi\right) & -\sin\left(\gamma - 2/3\pi\right) & 1 \\ \cos\left(\gamma + 2/3\pi\right) & -\sin\left(\gamma + 2/3\pi\right) & 1 \end{bmatrix},$$

where $\gamma = \int_0^t \omega(t)\, dt$.

According to theory of electromagnetics, when the resistances of the armature winding are ignored, the phase voltages are obtained from the flux linkages as:

$$V_{abc} = \frac{d}{dt}\psi_{abc}, \tag{A.13}$$

which is in *d*-*q*-0 coordinates:

$$C^{-1} V_{dq0} = \frac{d}{dt} C^{-1} \psi_{dq0} = C^{-1} \frac{d}{dt}\psi_{dq0} + \frac{d}{dt}\left(C^{-1}\right)\psi_{dq0}, \tag{A.14}$$

where the flux is transformed using the same transformation as for the voltages and currents, and

$$V_{dq0} = \frac{d}{dt}\psi_{dq0} + C\ \frac{d}{dt}\left(C^{-1}\right)\psi_{dq0}\,. \tag{A.15}$$

Taking $\omega = d\gamma / dt$, the following term in (A.15) can be simplified to:

$$C\ \frac{d}{dt}\left(C^{-1}\right) = \begin{bmatrix} 0 & -\omega & 0 \\ \omega & 0 & 0 \\ 0 & 0 & 0 \end{bmatrix}. \tag{A.16}$$

When (A.16) is substituted in (A.15), the following equations can be obtained:

$$\begin{aligned} v_d &= \frac{d}{dt}\psi_d - \omega_g \psi_q\,, \\ v_q &= \frac{d}{dt}\psi_q + \omega_g \psi_d\,. \end{aligned} \tag{A.17}$$

Ignoring the transformer electric potentials, $d\psi_d / dt$ and $d\psi_q / dt$, and assuming the generator rotates with constant speed, the relations between the armature winding voltages and the flux linkages can be obtains as:

$$\begin{aligned} v_d &= -\psi_q\,, \\ v_q &= \psi_d\,. \end{aligned} \tag{A.18}$$

Similarly, the following equations are obtained when the expressions for the phase flux linkages, armature currents, and excitation current are transformed in *d*-*q*-0 frame:

$$\begin{aligned} \psi_d &= x_{ad} I_f - x_d i_d\,, \\ \psi_q &= -x_q i_q\,, \end{aligned} \tag{A.19}$$

where $x_d = \omega L_d$ and $x_q = = \omega L_q$ are stator windings' self inductive reactance, L_d and L_q are inductances, and x_{ad} is the mutual inductive reactance between the stator winding and the field winding.

After substituting (A.19) for the flux linkages and $E_q = x_{ad} I_f$ in (A.18) the following equations are obtained:

$$\begin{aligned} v_d &= x_q i_q\,, \\ v_q &= E_q - x_d i_d\,. \end{aligned} \tag{A.20}$$

The generator power is obtained from (A.11) using the transformations (A.12):

$$P_{eg} = \frac{2}{3} V_{abc}^{T} I_{abc} = \frac{2}{3} V_{dq0}^{T} \left(C^{-1}\right)^{T} \; C^{-1} \; I_{dq0}, \\ = v_d i_d + v_q i_q \tag{A.21}$$

assuming balanced system conditions $v_0 = i_0 = 0$, which are the main interest in the generator control and stability studies.

Substituting the equations for v_d and v_q in (A.21) the following equation follows:

$$P_{eg} = v_d i_d + v_q i_q \\ = E_q i_q + \left(x_q - x_d\right) i_d i_q, \tag{A.22}$$

which can be rewritten as:

$$P_{eg} = E_q^{'} i_q + \left(x_q - x_d^{'}\right) i_d i_q, . \tag{A.23}$$

The flux linkage equations can be also rewritten as:

$$\psi_d = E_q^{'} - x_d^{'} i_d , \\ \psi_q = -x_q i_q , \tag{A.24}$$

where $E_q^{'}$ is the electric potential behind the transient reactance $x_d^{'}$, and in the *q*-axis.

Substituting above equations in (A.18) it follows:

$$v_d = x_q i_q , \\ v_q = E_q^{'} - x_d^{'} i_d . \tag{A.25}$$

When the generator is connected to the network and loaded with active power, the load current will cause an angular difference δ between the terminal voltage of the generator V_t and the idling (no-load) electric potential E_q or $E_q^{'}$:

$$\begin{bmatrix} v_a \\ v_b \\ v_c \end{bmatrix} = V_t \begin{bmatrix} \sin\left(\gamma - \delta\right) \\ \sin\left(\gamma - \delta - 2/3\pi\right) \\ \sin\left(\gamma - \delta + 2/3\pi\right) \end{bmatrix}, \tag{A.26}$$

where V_t is the amplitude of the generator terminal voltage. After transformation to *d*-*q*-0, the following is obtained:

$$\begin{bmatrix} v_d \\ v_q \end{bmatrix} = 2/3 \begin{bmatrix} \cos\gamma & \cos(\gamma - 2/3\pi) & \cos(\gamma + 2/3\pi) \\ -\sin\gamma & -\sin(\gamma - 2/3\pi) & -\sin(\gamma + 2/3\pi) \end{bmatrix} \begin{bmatrix} v_a \\ v_b \\ v_c \end{bmatrix},$$

$$\begin{bmatrix} v_d \\ v_q \end{bmatrix} = \begin{bmatrix} V_t \sin\delta \\ V_t \cos\delta \end{bmatrix}, \tag{A.27}$$

where only the first two rows of the C transformation matrix are included as the last one is not important in the balanced conditions.

From (A.25) and (A.27) the *d*,*q* components of the winding armature current are determined:

$$i_d = \frac{E_q^{'} - V_t \cos\delta}{x_d^{'}}, \tag{A.28}$$

$$i_q = \frac{V_t \sin\delta}{x_q}.$$

Substituting the (A.28) and (A.27) in (A.23) the following equation for the electrical power is obtained:

$$P_{eg} = E_q^{'} \frac{V_t}{x_q} \sin\delta + \left(\frac{1}{x_q} - \frac{1}{x_d^{'}} \right) \frac{V_t^2}{2} \sin 2\delta \,. \tag{A.29}$$

Taking the magnitudes of the terminal voltage and the armature winding current as $V_t = \sqrt{v_d^2 + v_q^2}$ and $I = \sqrt{i_d^2 + i_q^2}$, the reactive power can be calculated from apparent power and active power as:

$$\begin{aligned} Q_{eg} &= \sqrt{S_{eg}^2 - P_{eg}^2} = \sqrt{V_t^2 I^2 - P_{eg}^2} \\ &= \sqrt{\left(v_d^2 + v_q^2\right)\left(i_d^2 + i_q^2\right) - \left(v_d i_d + v_q i_q\right)^2} \\ &= v_q i_d - v_d i_q, \end{aligned} \tag{A.30}$$

where the apparent power $S_{eg} = V_t I$.

Substituting the (A.28) and (A.27) in (A.30) the following equation for the reactive power is obtained:

$$Q_{eg} = \frac{E_q^{'} V_t}{x_d^{'}} \cos\delta - \left(\frac{1}{x_d^{'}} + \frac{1}{x_q} \right) \frac{V_t^2}{2} + \left(\frac{1}{x_q} - \frac{1}{x_d^{'}} \right) \frac{V_t^2}{2} \cos 2\delta \,. \tag{A.31}$$

A.1.3 Field winding

The voltage equation of the field winding is:

$$V_f = r_f i_f + \frac{d}{dt}\psi_{fd}, \tag{A.32}$$

where V_f is the voltage of the field winding, proportional to the output of the automatic voltage regulator (AVR), I_f is the field current, ψ_{fd} is the flux linkage and r_f is the field winding resistance.

Multiplying (A.32) with x_{ad}/r_f the following equation for the field winding is obtained:

$$E_f = E_q + T_{d0}\frac{dE_q'}{dt}, \tag{A.33}$$

where:

- $E_q = x_{ad} i_f$ is the idling electric potential;
- $T_{d0} = \frac{x_f}{r_f}$ is the time constant of the field winding, in seconds;
- $E_q' = \frac{x_{ad}}{x_f}\psi_{fd}$;
- $E_f = V_f \frac{x_{ad}}{r_f}$ is obtained in a similar manner as in (A.24) and (A.25).

In per unit values, E_f=V_f and the following dynamic equation of field winding can be used:

$$\frac{dE_q'}{dt} = -\frac{1}{T_{d0}}E_q + \frac{1}{T_{d0}}V_f. \tag{A.34}$$

Thus, the generator has been modeled based on the following approximations:

- The voltage losses caused by the armature resistances were ignored in (A.13);
- Flux linkages produced by the currents in the damping windings are neglected in (A.25);
- The damper effects are completely neglected and their effect is transferred to the damping torque in the swing equation (A.2), as will be seen later in the full model;
- The component of electric potential called “transformer electric potentials” $d\psi_d/dt,\ d\psi_q/dt$;
- It has been assumed that the waveform of the terminal voltage is always sinusoidal;
- The active power (A.29) is only valid for the synchronous operation of generators and power system due to assumption that $\omega_g = \omega_{0g} = 1$ in (A.18).

However, despite these assumptions it has been shown that the power equation (A.29) can meet the accuracy requirements of the mathematic models used to analyze the stability problems and dynamic performance of the power system.

A.1.4 Generator in the multimachine system

The load of each bus is modeled as a constant impedance *Z*, where the current vectors for the *k* number of generators on-line can be expressed as:

$$\begin{aligned}
\bar{I}_1 &= \bar{E}_1 \bar{Y}_{11} + \bar{E}_2 \bar{Y}_{12} + \bar{E}_3 \bar{Y}_{13} + \ldots\ldots + \bar{E}_k \bar{Y}_{1k} \\
\bar{I}_2 &= \bar{E}_1 \bar{Y}_{21} + \bar{E}_2 \bar{Y}_{22} + \bar{E}_3 \bar{Y}_{23} + \ldots\ldots + \bar{E}_k \bar{Y}_{2k} \\
&\ldots\ldots \\
\bar{I}_k &= \bar{E}_1 \bar{Y}_{k1} + \bar{E}_2 \bar{Y}_{k2} + \bar{E}_3 \bar{Y}_{k3} + \ldots\ldots + \bar{E}_k \bar{Y}_{kk} ,
\end{aligned} \tag{A.35}$$

where $\bar{Y}_{ij} = 1/\bar{Z}_{ij}$ is the corresponding component of the network admittance matrix, $\bar{I}_i$ is the complex current vector that the generator *i* injects into the power network, $\bar{E}_i$ and $\bar{E}_j$ are the complex vectors of the transient electric potentials $\bar{E}'_{qi}$, $\bar{E}'_{qj}$ or idling electric potentials $\bar{E}_{qi}$, $\bar{E}_{qj}$, and $i, j \in (1, k)$. The $\bar{Y}_{ij} = \bar{Y}_{ji}$ and the admittance matrix is symmetric.

Then the each individual generator will deliver this current to the network:

$$\bar{I}_i = \bar{E}_i \bar{Y}_{ii} + \sum_{\substack{j=1 \\ j \neq i}}^{k} \bar{E}_j \bar{Y}_{ij} , \tag{A.36}$$

where the current delivery will depend on the contribution of other generators, besides loads.

The apparent power of the generator *i*, sending the power to the network in complex form is:

$$\bar{W}_{eg,i} = P_{eg,i} + jQ_{eg,i} = \bar{E}_i \bar{I}_i^* , i, \in (1, k), \tag{A.37}$$

where $\bar{I}_i^*$ is the complex conjugate of $\bar{I}_i$, and *j* is now used as a complex number, $j = \sqrt{-1}$.

After substituting (A.36) into (A.37) the following equation is obtained:

$$\bar{W}_{eg,i} = \bar{E}_i \left(\bar{E}_i^* \bar{Y}_{ii}^* + \sum_{\substack{j=1 \\ j \neq i}}^{k} \bar{E}_j^* \bar{Y}_{ij}^* \right). \tag{A.38}$$

Expressing the complex admittance as:

$$\begin{aligned}
\bar{Y}_{ij} &= Y_{ij} e^{j\phi_{ij}} = G_{ij} + jB_{ij} \\
G_{ij} &= Y_{ij} \cos\phi_{ij} , \text{ and } B_{ij} = Y_{ij} \sin\phi_{ij} ,
\end{aligned} \tag{A.39}$$

where G_{ij} and B_{ij} are conductance and susceptance of the node *ij*, and ϕ_{ij} is the impedance angle. The following equation for the apparent power is obtained:

$$\bar{W}_{eg,i} = E_i^2 Y_{ii} \cos\phi_{ii} + E_i \sum_{\substack{j=1 \\ j \neq i}}^{k} E_j Y_{ij} \cos\left(\delta_{ij} - \phi_{ij}\right) + j \left(- E_i^2 Y_{ii} \sin\phi_{ii} + E_i \sum_{\substack{j=1 \\ j \neq i}}^{k} E_j Y_{ij} \sin\left(\delta_{ij} - \phi_{ij}\right) \right), \tag{A.40}$$

where $\delta_{ij} = \delta_i - \delta_j$ and hence $\delta_{ij} = -\delta_{ji}$. When E is replaced with E'_{qj} then x'_d should be used for the generator reactance. As defined in (A.37), the real part of (A.40) represents the active power $P_{eg,i}$ and the imaginary part is the reactive power $Q_{eg,i}$.

Expressing above equation in rectangular coordinates for G_{ij} and B_{ij} the active and reactive power are obtained:

$$P_{eg,i} = E_i^2 G_{ij} + E_i \sum_{\substack{j=1 \\ j \neq i}}^{k} E_j \left(G_{ij} \cos\delta_{ij} + B_{ij} \sin\delta_{ij} \right), \tag{A.41}$$

$$Q_{eg,i} = - E_i^2 B_{ii} + E_i \sum_{\substack{j=1 \\ j \neq i}}^{k} E_j \left(G_{ij} \sin\delta_{ij} - B_{ij} \cos\delta_{ij} \right),$$

due to $G_{ij} = Y_{ij} \cos\phi_{ij}$ and , as defined in (A.39). The mutual admittance $\overline{Y}_{ij}$ only involves the impedances of the transformers and transmission lines (transmission lines are relatively very small on the marine vessel) and the proportions of resistance R/X in these impedances are very small, so the impedance angles are nearly 90^0. This indicates that the cos $\pi/2 = 0$ in (A.41) and the following simplified equations are typically accepted:

$$P_{eg,i} = E_i^2 G_{ij} + E_i \sum_{\substack{j=1 \\ j \neq i}}^{k} E_j B_{ij} \sin\delta_{ij}\,, \tag{A.42}$$

$$Q_{eg,i} = - E_i^2 B_{ii} + E_i \sum_{\substack{j=1 \\ j \neq i}}^{k} E_j G_{ij} \sin\delta_{ij}\,.$$

A.1.5 Multimachine system model

Combining the equations for the rotor motion in (A.7), the electrical power in (A.40), and filed winding dynamics (A.34), the following system is obtained (Lu *et al.*, 2001):

$$\frac{d}{dt}\delta_{g,i} = \omega_{g,i} - \omega_{0g,i}\,, \tag{A.43}$$

$$\frac{d}{dt}\omega_{g,i} = \frac{\omega_{0g}}{2H_{g,i}} Q_{mg,i} - \frac{\omega_{0g}}{2H_{g,i}} \frac{1}{\omega_{g,i}} P_{eg,i} - \frac{D_{dg,i}}{2H_{g,i}} \left(\omega_{g,i} - \omega_{0g,i} \right),$$

$$P_{eg,i} = E_i'^2 Y_{ii} \cos\phi_{ii} + E_i \sum_{\substack{j=1 \\ j \neq i}}^{k} E'_j Y_{ij} \cos\left(\delta_{ij} - \phi_{ij} \right),$$

$$\frac{dE'_{q,i}}{dt} = -\frac{1}{T_{d0,i}} E_{q,i} + \frac{1}{T_{d0,i}} V_{f,i}\,.$$

where $D_{g,i}$ is the damping constant from the damper and the engine, which has typically small value.

The relation between q-axis transient potential and the q-axis potential is:

$$E_{q,i} = E'_{q,i} + I_{d,i}\left(x_{d,i} - x'_{d,i}\right). \tag{A.44}$$

The currents are obtained from (A.36) in a similar manner as powers in (A.40) and (A.41):

$$\begin{aligned} I_{d,i} &= -E_i B_{ii} + \sum_{\substack{j=1 \\ j\neq i}}^{k} E_j Y_{ij} \sin\left(\delta_{ij} - \phi_{ij}\right), \\ I_{q,i} &= E_i G_{ii} + \sum_{\substack{j=1 \\ j\neq i}}^{k} E_j Y_{ij} \cos\left(\delta_{ij} - \phi_{ij}\right), \end{aligned} \tag{A.45}$$

and then inserting (A.45) into (A.44), and then into (A.34) the final equation is obtained:

$$\frac{dE'_{q,i}}{dt} = -\frac{1 + B_{ii}\left(x_{d,i} - x'_{d,i}\right)}{T_{d0,i}} E'_{q,i} + \frac{x_{d,i} - x'_{d,i}}{T_{d0,i}} \sum_{\substack{j=1 \\ j\neq i}}^{k} E'_{q,i} Y_{ij} \sin\left(\delta_{ij} - \phi_{ij}\right) + \frac{1}{T_{d0,i}} V_{f,i}. \tag{A.46}$$

The model is finally:

$$\begin{aligned} &\frac{d}{dt}\delta_{g,i} = \omega_{g,i} - \omega_{0g,i}, \\ &\frac{2H_{g,i}}{\omega_{0g}} \frac{d}{dt}\omega_{g,i} = Q_{mg,i} - \frac{1}{\omega_{g,i}} P_{eg,i} - D_{dg,i}\left(\omega_{g,i} - \omega_{0g,i}\right), \\ &P_{eg,i} = E'^{2}_{i} Y_{ii} \cos\phi_{ii} + E_i \sum_{\substack{j=1 \\ j\neq i}}^{k} E'_j Y_{ij} \cos\left(\delta_{ij} - \phi_{ij}\right), \\ &\frac{dE'_{q,i}}{dt} = -\frac{1 + B_{ii}\left(x_{d,i} - x'_{d,i}\right)}{T_{d0,i}} E'_{q,i} + \frac{x_{d,i} - x'_{d,i}}{T_{d0,i}} \sum_{\substack{j=1 \\ j\neq i}}^{k} E'_{q,i} Y_{ij} \sin\left(\delta_{ij} - \phi_{ij}\right) + \frac{1}{T_{d0,i}} V_{f,i}. \end{aligned} \tag{A.47}$$

The above model belongs to the affine class of nonlinear systems:

$$\frac{d}{dt}x = f(x) + \sum_{i=1}^{k} g_i(x) u_i, \tag{A.48}$$

where the details are given in (Lu *et al.*, 2001).

A.2 Diesel engine model

Several different prime mover types have been used in the marine application of power generation system:

- Turbocharged medium speed diesel engine;
- Gas turbine;
- Steam turbine.

Gas turbines, steam turbines and hydro turbines have been traditionally used for on-land power generation, and references with extensive modeling and control details can be found in e.g. Anderson and Fuad (2003), Kundur (1994), Hannett and Khan (1993), and references therein.

However, the main prime mover in the marine industry is a diesel-engine (Ådnanes, 2003). As mentioned in Hansen (2000), the diesel engines have been modeled with different complexity. The modeling complexity will depend on the application ranging from air-flow models, cylindrical combustion models, control and/or observer models, diagnosing models e.g. fluctuating torque estimation from speed measurements, etc.

A typical model useful for the power system dynamic studies may only take into account the mechanical dynamics of the process. Thus, it may be defined by steady state data and geometrical characteristics, see e.g. Guzzella and Amstutz (1998). Based on the Guzzella and Amstutz (1998), the following diesel engine model is proposed in this thesis to be used with power system simulations:

$$Q_{mg} = \tilde{Q}_{mg}\left(t - \tau_e\right), \qquad \text{(A.49)}$$
$$\tau_e = 1...1.125 \text{ seconds.}$$

It is assumed that all cylinders have the same crank-angle phase difference. It should be noticed that additional delays will be introduced by the controller hardware.

The engine's mean torque can be determined from:

$$\tilde{Q}_{mg} = H_{LHV} m_f \eta_{ind}, \qquad \text{(A.50)}$$
$$\eta_{ind} = \left(a_1 + a_2 P_{mg} + a_3 P_{mg}^2\right)\left(1 - a_4 \lambda^{a_5}\right),$$

where:
- η_{ind} is the indicated efficiency;
- H_{LHV} is the fuel lower heating value (42 707 kJ/kg for heavy fuel oil);
- ω_e is the engine crankshaft speed, The engine crankshaft speed is linearly proportional to the generator shaft speed. It depends on the gear box transmission ratio. In order to reduce the mechanical losses, marine diesel-generators are usually delivered without a gearbox, so typically $\omega_e = \omega_g$;
- $v = 1$ for two-stroke and $v = 2$ for four-stroke engines;
- N_c is the number of cylinders;
- m_f is the mass of fuel injected into one cylinder in one cycle;
- λ is the air/fuel ratio;
- P_{mg} is the engine load, obtained from the generator active power as $P_{mg} = P_g / \eta_m$ where η_m is the mechanical efficiency;
- a_i parameters to be adjusted for the engine.

Air to fuel ratio can be approximately found from:

$$\lambda = \frac{\dot{m}_f}{\dot{m}_{ca}}. \qquad \text{(A.51)}$$

The mass flow and the mean fuel-pressure relations are:

$$p_f = \frac{H_{LHV}}{V_d} m_f \,, \qquad \text{(A.52)}$$
$$m_f = \frac{v 2\pi}{\omega_e} \dot{m}_f \,,$$

where V_d is the engine's displaced volume, and dm_f/dt is the fuel mass flow to the engine commanded by the generating set speed controller i.e. governor.

The third order model is used to relate the charging air pressure to the fuel pressure:

$$p_{ca} = \frac{1}{\tau_{e1} s + 1} \frac{1}{\tau_{e2} s + 1} \frac{1}{\tau_{e3} s + 1} p_f \,. \qquad \text{(A.53)}$$

The three time-constants can be associated with physical properties of the system, e.g. exhaust system dimension, supercharger lags, etc.

The mass of the charge air can be found from the ideal gas law as:

$$\dot{m}_{ac} = m_{ac} \frac{\omega_e}{v 2\pi} \,, \qquad \text{(A.54)}$$
$$m_{ac} = p_{ac} \frac{V_{IR}}{R \vartheta_{ac}} \,,$$

where V_{IR} is the engine's displaced volume, R is the gas constant, and ϑ_{ac} is the charging air temperature. To avoid need of extending the model dynamics the charging air temperature can be assumed to be constant.

A.3 Control of generating set

The overall control structure for the marine generating set is presented in Fig. A.1. The speed is influenced by the changes in the generator electric torque, which depends on the generator active power. Thus, the prime mover will have to respond to fast changes of active power in order to keep the shaft speed i.e. network frequency close to the reference. This may be a problem when the load is changing fast as the diesel engine response is limited to torque build up speed dependent on the charging air pressure build up speed; see (A.53). Thus, the electrical load must be limited from the PMS in order to reduce the frequency fluctuations on the generators i.e. to match the load to the available engine torque.

The voltage is controlled by the automatic voltage regulator (AVR), presented in Fig. A.2. The AVR is receiving the measurement of the terminal voltage and responds very fast to any changes. The requirement from the class societies is to accomplish the voltage recovery after the transient in less than 0.5 seconds, see e.g. *Det Norske Veritas* (DVN). The required speed of the voltage recovery is 5 seconds, which is 10 times slower than for the voltage. Therefore

affecting the voltage control onboard the marine vessel may violate the class society rule constraints, and hence it may not be recommended. This is unlike the usual control strategies developed for the on-land power systems, where the field voltage control was dominating over the frequency control.

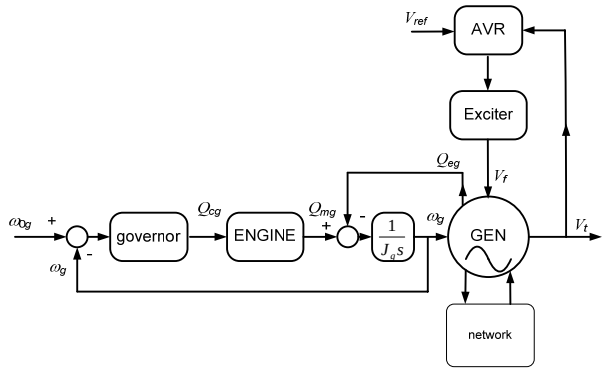

Fig. A.1. Control structure of generating-set

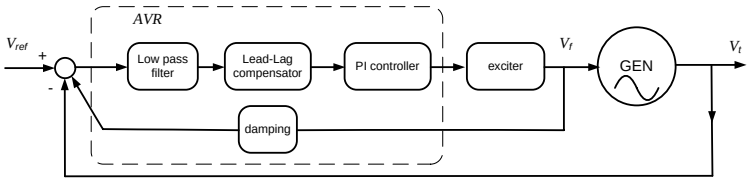

Fig. A.2. Control structure for the voltage control

A.4 Consumer load

The consumers are modeled according to their typical behavior regarding dynamics, power and reactive power i.e. power factor, see e.g. Kundur (1994).

A.4.1 Electric loads

Two static load models are typically used; constant impedance and constant power, see e.g. Allen *et al.* (2001), Hansen (2000) and the references therein.

Constant impedance load

The constant impedance loads are usually used in the power system studies, see e.g. Kundur (1994), Anderson and Fuad (2003). In the constant impedance model, Z is obviously treated as a fixed quantity; therefore, the constant impedance load is represented by the equation:

$$v = -Z\, i\,, \qquad \text{(A.55)}$$
$$Z = RI + XJ\,,$$

$$I = \begin{bmatrix} 1 & 0 \\ 0 & 1 \end{bmatrix},\ J = \begin{bmatrix} 0 & -1 \\ 1 & 0 \end{bmatrix},$$

where v and i are voltage and current vectors, and $v = \begin{pmatrix} V_d & V_q \end{pmatrix}^T$, $i = \begin{pmatrix} I_d & I_q \end{pmatrix}^T$. The admittance is then related as:

$$i = -Y v\,. \tag{A.56}$$

Constant power load

To simulate the load behavior of a constant power load, the admittance of the load becomes a state variable with the following dynamics (Allen *et al.*, 2001):

$$\frac{d}{dt}G = \frac{1}{\tau_z}\left(P_{\text{ref}} - P\right), \tag{A.57}$$
$$\frac{d}{dt}B = \frac{1}{\tau_z}\left(Q_{\text{ref}} - Q\right),$$

where:

- P_{ref} and Q_{ref} are active and reactive power summations from all loads on the bus, i.e. desired power on the bus;
- P and Q are instantaneous power;
- τ_z is the time constant.

A.4.2 Electric thruster model

Models based on representation of induction motor losses, synchronous motor losses and converter losses are proposed in Hansen (2000). Similar models are used in this thesis. These models are based on the simplified representations of the losses in the active power and changes in the power factor due to e.g. frequency converter. The VSI-PWM frequency converter, typically used with induction motor will give the power factor about 0.95 on the supply side of frequency converter. This is due to VSI-PWM will have a diode rectifier. The cycloconverter is based on thyrisors on the rectifier side and inverter side of the drive. Thus, the power factor for cycloconverter, used with synchronous motor will depend on the load, i.e. may decrease linearly for load below 50% rated, see e.g. Ådnanes *et al.* (1997), Hansen (2000) and the references therein.

A.5 Simulations of marine power system

A case study demonstrating the described modeling is presented in Figs. A.3 to A.5.

One side of the two split system of the typical platform supply vessel (PSV) is simulated. The 2 MW aft thruster is in the operation, together with 1 MW static load. Two gen-sets, each 1.75 MW are online, so 3.5 MW is the power generating capacity in the system.

It should be noticed from the simulations that the generators are more prone to frequency fluctuations than the voltage fluctuations, as shown in Fig. A.3. In fact, the frequency drops

for 6% after t = 50 seconds due to fast thruster loading. The voltage drop is almost insignificant. Although in this study VSI-PWM frequency converter is used, similar behavior can be noticed with any kind of frequency drive used in marine applications e.g. CSI, cycloconverter.

Fig. A.5 shows the behavior of the system when one generator is connected in the network. Only one generator, namely gen-1 operates on the network. The gen-2 will connect after being synchronized to the network in about t = 9 seconds. After the connection, the generator will slowly accept the half of the network load, and hence it's load will increase to 0.4 p.u.

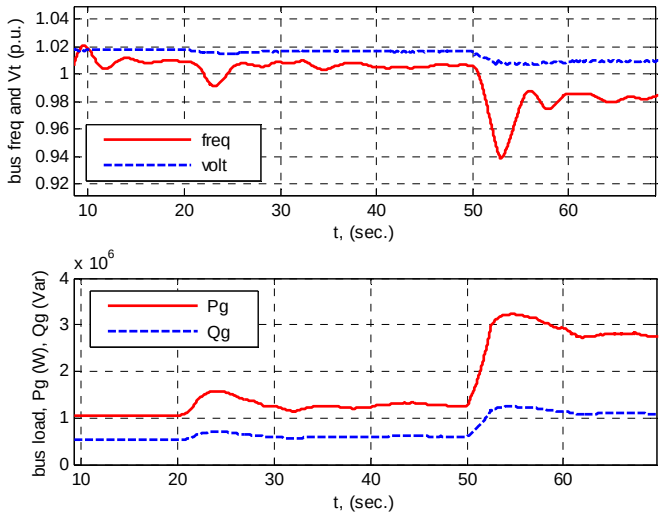

Fig. A.3. Bus frequency and voltage (upper) and bus active and reactive power load (lower)

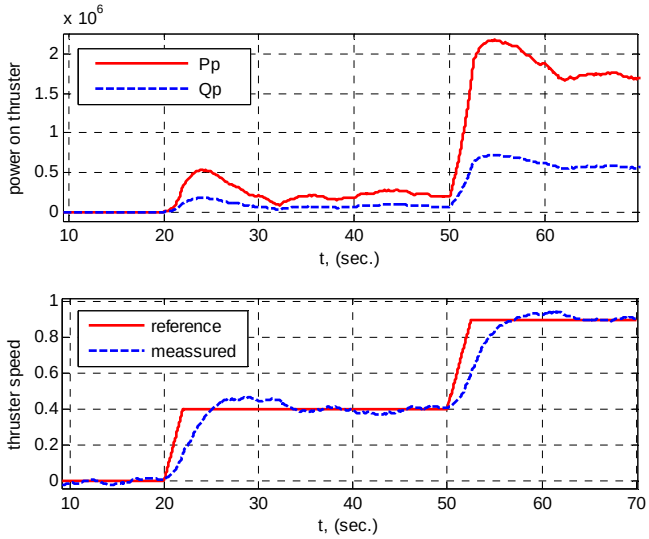

Fig. A.4. Active and reactive power on thruster (upper) thruster speed (lower)

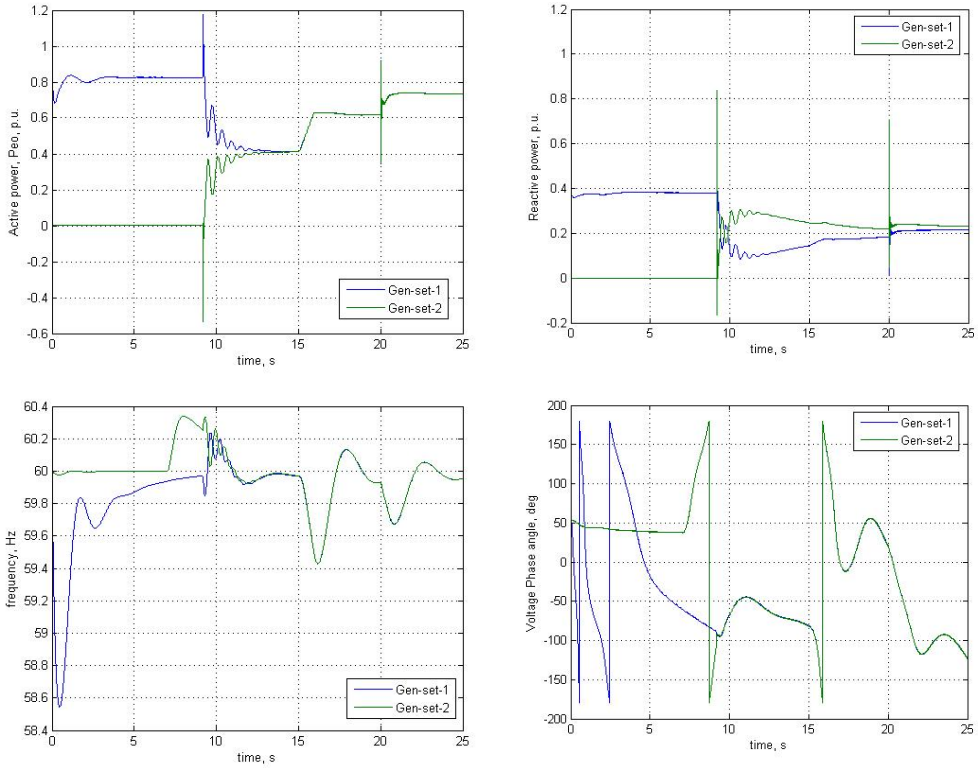

Fig. A.5. Generator 2 is synchronizing with generator 1, and starting to share load equally

Appendix B

Control plant models

B.1 Control plant model of power generating system

The motion equation for the mean acceleration of the power generating system may be expressed as follows (Anderson and Fuad, 2003; Kundur, 1994):

$$\frac{d\delta_g}{dt} = \omega_g - \omega_{0g}\,, \tag{B.1}$$

$$\frac{d\omega_g}{dt} = \frac{\omega_{0g}}{2H_{N_{on}}}\left[Q_{mg} - Q_{dg} - Q_{eg}\right]$$

$$= \frac{\omega_{0g}}{2H_{N_{on}}}\left[Q_{mg} - \frac{D_g}{\omega_{0g}}\left(\omega_g - \omega_{0g}\right) - Q_{eg}\right]$$

where ω_g is the mean rotor angular speed for all generators in the system (in per unit - pu), ω_{0g} is the nominal speed, Q_{mg} is the mechanical torque, Q_{eg} is the electrical torque, and Q_{dg} is the damping torque. The torques is expressed in per unit system (pu). The damping coefficient D_g accounts for the electrical load damping and the mechanical damping in pu. H_{Non} is the system inertial time constant in seconds. The frequency deviation between the mean and the nominal speed gives the derivative of the rotor angle $\delta_g(t)$ in radians.

The equivalent system inertia can be determined from:

$$H_{N_{on}} = \sum_{i=1}^{N_{on}} H_i\,, \qquad H_i = \frac{1}{2}\frac{J_{gi}\omega_{0g}}{S_{r,gi}} \tag{B.2}$$

where J_{gi} is the moment of inertia for the gen-set, and $S_{r,gi}$ is the rated power per generator, usually given in kVA. The equation (B.1) defines the mean acceleration of all the generators in the system, which is defined as the acceleration of a fictitious inertial center. At the instant of load impact the source of energy supplied by the generators is the energy contained in their magnetic fields and is distributed according to the synchronizing power coefficients between the generators and the bus (common node). At the end of a brief transient, the various generators will share the increase in load as a function only of their inertia constants (Anderson and Fuad, 2003).

B.2 Basic control plant model of thruster

The following thruster model is usually used for the control (Sørensen *et al.*, 1997; Smogeli *et al.*, 2004):

$$\frac{d}{dt}\omega_p = \frac{1}{J_p}\left(Q_{mp} - Q_{ap} - Q_{fp}\right), \tag{B.3}$$
$$\frac{d}{dt}Q_{mp} = \frac{1}{T_{mp}}\left(Q_{cp} - Q_{mp}\right),$$

where J_p is the moment of inertia of the shaft, motor, gear, propeller, and added mass of the propeller, Q_{ap} is the load torque, Q_{fp} is the friction torque, T_{mp} is the motor time constant. The commanded torque Q_{cp} is the output from the thruster controller. The thruster control system is shown in Fig. B.1.

In general, Q_{fp} friction is assumed to be more significant on small thrusters typically used on underwater vehicles and in experimental setups than on large thrusters used on surface vessels (Smogeli, 2006). Thus, the friction may for most applications be viewed as a sum of a static friction torque Q_s and a linear component, dependant on shaft speed:

$$Q_{fp}\left(\omega_p\right) = \text{sign}(\omega_p)Q_{s,fp} \; + \; k_f\omega_p \,. \tag{B.4}$$

The motor torque is somewhat delayed after the commanded torque:

$$Q_{mp} = Q_{cp} - T_{mp}\dot{Q}_{mp} = k_{Pp}\left(\omega_{0p} - \omega_p\right) - T_{mp}\dot{Q}_{mp} \,. \tag{B.5}$$

Due to small value of T_{mp}, the thruster dynamics is sometimes disregarded in the analysis, then $T_{mp}\dot{Q}_{mp} = 0$. For the shaft speed control, it should be considered in the *control plant model* as part of the important dynamics.

B.2.1 Control plant model with filtering

In addition to this, a low pass filtering of speed measurement should be included in the model. This is due to the noise in the speed measurement:

$$\frac{d}{dt}\omega_{fp} = \frac{1}{T_{fp}}\left(\omega_p - \omega_{fp}\right). \tag{B.6}$$

where ω_{fp} is filtered speed, and T_{fp} is a time constant of the first-order Butterworth low pass filter. It should be noticed that many different filter designs may be used to filter a speed, e.g. second order Butterworth low pass filter, notch filter, etc. (Oppenheim *et al.*, 1997). The equation (B.6) is used only to include some of the filtering dynamics in to the control plant model.

Thus, a new thruster *control plant model* is defined:

$$\frac{d}{dt}\omega_{fp} = \frac{1}{T_{fp}}\left(\omega_p - \omega_{fp}\right), \tag{B.7}$$

$$\frac{d}{dt}\omega_p = \frac{1}{J_p}\left(Q_{mp} - Q_{ap} - Q_{fp}\right),$$

$$\frac{d}{dt}Q_{mp} = \frac{1}{T_{mp}}\left(Q_{cp}^{f} - Q_{mp}\right).$$

B.2.2 Cascaded control structure of electrical thruster control

The models (B.3) and (B.7) are generic models of the electrical thruster. Fig. B.1 shows the cascaded control structure of DC motor drives, where the same basic structure for any electrical thruster drive is indicated.

This cascaded control structure will be shortly explained on the example of speed control of DC motor. The DC motor dynamics are governed by following equations:

$$\frac{d}{dt}\omega_p = \frac{1}{J_p}\left(k_t i_p - Q_{ap} - Q_{fp}\right), \tag{B.8}$$

$$\frac{d}{dt}i_p = \frac{1}{L}\left(u_p - Ri_p - \lambda_0\omega_p\right),$$

where i_p is armature current, k_t is the torque constant, R is the armature resistance, L is armature inductance, λ_0 is back-EMF (electro-motor force) constant, u_p is terminal voltage, Q_{ap} and Q_{fp} are load torque and friction torque respectively.

One can notice the obvious analogy between DC motor dynamics in (B.8) and generic model in (B.3). In Fig. B.1 it can be noticed that the motor commanded torque Q_{cp} is proportional to demanded current i_{0p} where the real current i_p is obtained at the output which is proportional (α) to real motor torque Q_{mp}:

$$Q_{cp} \;\alpha\; i_{0p}, \qquad \text{and} \qquad Q_{mp} \;\alpha\; i_p. \tag{B.9}$$

For the speed controller in the outer loop, the current control loop is regarded as an ideal current source where the demanded current reference i_{0p} will be tracked immediately (Utkin *et al.*, 1999). However, if necessary, the drive behavior may be modeled as a first order low pass filter (Utkin *et al.*, 1999; Smogeli, 2006). Since marine power and propulsion systems are relatively large inertial systems (e.g. thrusters, engines, generating-sets) compared to other applications (e.g. computer hard-disk drive) this assumption may hold for most of the cases.

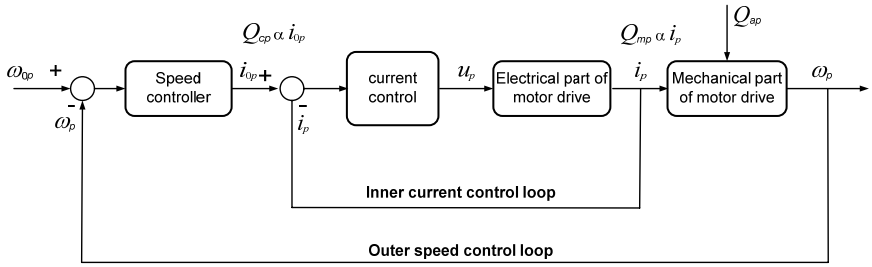

Fig. B.1. Cascaded control structure of DC motor drives, indicating the same basic structure for any electrical thruster drives (Utkin *et al.*, 1999)

R A P P O R T E R
UTGITT VED
INSTITUTT FOR MARIN TEKNIKK
(tidligere: FAKULTET FOR MARIN TEKNIKK)
NORGES TEKNISK-NATURVITENSKAPELIGE UNIVERSITET

UR-79-01 Brigt Hatlestad, MK:	The finite element method used in a fatigue evaluation of fixed offshore platforms. (Dr.Ing. Thesis)
UR-79-02 Erik Pettersen, MK:	Analysis and design of cellular structures. (Dr.Ing. Thesis)
UR-79-03 Sverre Valsgård, MK:	Finite difference and finite element methods applied to nonlinear analysis of plated structures. (Dr.Ing. Thesis)
UR-79-04 Nils T. Nordsve, MK:	Finite element collapse analysis of structural members considering imperfections and stresses due to fabrication. (Dr.Ing. Thesis)
UR-79-05 Ivar J. Fylling, MK:	Analysis of towline forces in ocean towing systems. (Dr.Ing. Thesis)
UR-80-06 Nils Sandsmark, MM:	Analysis of Stationary and Transient Heat Conduction by the Use of the Finite Element Method. (Dr.Ing. Thesis)
UR-80-09 Sverre Haver, MK:	Analysis of uncertainties related to the stochastic modelling of ocean waves. (Dr.Ing. Thesis)
UR-85-46 Alf G. Engseth, MK:	Finite element collapse analysis of tubular steel offshore structures. (Dr.Ing. Thesis)
UR-86-47 Dengody Sheshappa, MP:	A Computer Design Model for Optimizing Fishing Vessel Designs Based on Techno-Economic Analysis. (Dr.Ing. Thesis)
UR-86-48 Vidar Aanesland, MH:	A Theoretical and Numerical Study of Ship Wave Resistance. (Dr.Ing. Thesis)
UR-86-49 Heinz-Joachim Wessel, MK:	Fracture Mechanics Analysis of Crack Growth in Plate Girders. (Dr.Ing. Thesis)
UR-86-50 Jon Taby, MK:	Ultimate and Post-ultimate Strength of Dented Tubular Members. (Dr.Ing. Thesis)

UR-86-51 Walter Lian, MH:	A Numerical Study of Two-Dimensional Separated Flow Past Bluff Bodies at Moderate KC-Numbers. (Dr.Ing. Thesis)
UR-86-52 Bjørn Sortland, MH:	Force Measurements in Oscillating Flow on Ship Sections and Circular Cylinders in a U-Tube Water Tank. (Dr.Ing. Thesis)
UR-86-53 Kurt Strand, MM:	A System Dynamic Approach to One-dimensional Fluid Flow. (Dr.Ing. Thesis)
UR-86-54 Arne Edvin Løken, MH:	Three Dimensional Second Order Hydrodynamic Effects on Ocean Structures in Waves. (Dr.Ing. Thesis)
UR-86-55 Sigurd Falch, MH:	A Numerical Study of Slamming of Two-Dimensional Bodies. (Dr.Ing. Thesis)
UR-87-56 Arne Braathen, MH:	Application of a Vortex Tracking Method to the Prediction of Roll Damping of a Two-Dimension Floating Body. (Dr.Ing. Thesis)
UR-87-57 Bernt Leira, MR:	Gaussian Vector Processes for Reliability Analysis involving Wave-Induced Load Effects. (Dr.Ing. Thesis)
UR-87-58 Magnus Småvik, MM:	Thermal Load and Process Characteristics in a Two-Stroke Diesel Engine with Thermal Barriers (in Norwegian). (Dr.Ing. Thesis)
MTA-88-59 Bernt Arild Bremdal, MP:	An Investigation of Marine Installation Processes - A Knowledge - Based Planning Approach. (Dr.Ing. Thesis)
MTA-88-60 Xu Jun, MK:	Non-linear Dynamic Analysis of Space-framed Offshore Structures. (Dr.Ing. Thesis)
MTA-89-61 Gang Miao, MH:	Hydrodynamic Forces and Dynamic Responses of Circular Cylinders in Wave Zones. (Dr.Ing. Thesis)
MTA-89-62 Martin Greenhow, MH:	Linear and Non-Linear Studies of Waves and Floating Bodies. Part I and Part II. (Dr.Techn. Thesis)
MTA-89-63 Chang Li, MH:	Force Coefficients of Spheres and Cubes in Oscillatory Flow with and without Current. (Dr.Ing. Thesis)
MTA-89-64 Hu Ying, MP:	A Study of Marketing and Design in

	Development of Marine Transport Systems. (Dr.Ing. Thesis)
MTA-89-65 Arild Jæger, MH:	Seakeeping, Dynamic Stability and Performance of a Wedge Shaped Planing Hull. (Dr.Ing. Thesis)
MTA-89-66 Chan Siu Hung, MM:	The dynamic characteristics of tilting-pad bearings.
MTA-89-67 Kim Wikstrøm, MP:	Analysis av projekteringen for ett offshore projekt. (Licenciat-avhandling)
MTA-89-68 Jiao Guoyang, MR:	Reliability Analysis of Crack Growth under Random Loading, considering Model Updating. (Dr.Ing. Thesis)
MTA-89-69 Arnt Olufsen, MK:	Uncertainty and Reliability Analysis of Fixed Offshore Structures. (Dr.Ing. Thesis)
MTA-89-70 Wu Yu-Lin, MR:	System Reliability Analyses of Offshore Structures using improved Truss and Beam Models. (Dr.Ing. Thesis)
MTA-90-71 Jan Roger Hoff, MH:	Three-dimensional Green function of a vessel with forward speed in waves. (Dr.Ing. Thesis)
MTA-90-72 Rong Zhao, MH:	Slow-Drift Motions of a Moored Two-Dimensional Body in Irregular Waves. (Dr.Ing. Thesis)
MTA-90-73 Atle Minsaas, MP:	Economical Risk Analysis. (Dr.Ing. Thesis)
MTA-90-74 Knut-Aril Farnes, MK:	Long-term Statistics of Response in Non-linear Marine Structures. (Dr.Ing. Thesis)
MTA-90-75 Torbjørn Sotberg, MK:	Application of Reliability Methods for Safety Assessment of Submarine Pipelines. (Dr.Ing. Thesis)
MTA-90-76 Zeuthen, Steffen, MP:	SEAMAID. A computational model of the design process in a constraint-based logic programming environment. An example from the offshore domain. (Dr.Ing. Thesis)
MTA-91-77 Haagensen, Sven, MM:	Fuel Dependant Cyclic Variability in a Spark Ignition Engine - An Optical Approach. (Dr.Ing. Thesis)
MTA-91-78 Løland, Geir, MH:	Current forces on and flow through fish farms.

	(Dr.Ing. Thesis)
MTA-91-79 Hoen, Christopher, MK:	System Identification of Structures Excited by Stochastic Load Processes. (Dr.Ing. Thesis)
MTA-91-80 Haugen, Stein, MK:	Probabilistic Evaluation of Frequency of Collision between Ships and Offshore Platforms. (Dr.Ing. Thesis)
MTA-91-81 Sødahl, Nils, MK:	Methods for Design and Analysis of Flexible Risers. (Dr.Ing. Thesis)
MTA-91-82 Ormberg, Harald, MK:	Non-linear Response Analysis of Floating Fish Farm Systems. (Dr.Ing. Thesis)
MTA-91-83 Marley, Mark J., MK:	Time Variant Reliability under Fatigue Degradation. (Dr.Ing. Thesis)
MTA-91-84 Krokstad, Jørgen R., MH:	Second-order Loads in Multidirectional Seas. (Dr.Ing. Thesis)
MTA-91-85 Molteberg, Gunnar A., MM:	The Application of System Identification Techniques to Performance Monitoring of Four Stroke Turbocharged Diesel Engines. (Dr.Ing. Thesis)
MTA-92-86 Mørch, Hans Jørgen Bjelke, MH:	Aspects of Hydrofoil Design: with Emphasis on Hydrofoil Interaction in Calm Water. (Dr.Ing. Thesis)
MTA-92-87 Chan Siu Hung, MM:	Nonlinear Analysis of Rotordynamic Instabilities in High-speed Turbomachinery. (Dr.Ing. Thesis)
MTA-92-88 Bessason, Bjarni, MK:	Assessment of Earthquake Loading and Response of Seismically Isolated Bridges. (Dr.Ing. Thesis)
MTA-92-89 Langli, Geir, MP:	Improving Operational Safety through exploitation of Design Knowledge - an investigation of offshore platform safety. (Dr.Ing. Thesis)
MTA-92-90 Sævik, Svein, MK:	On Stresses and Fatigue in Flexible Pipes. (Dr.Ing. Thesis)
MTA-92-91 Ask, Tor Ø., MM:	Ignition and Flame Growth in Lean Gas-Air Mixtures. An Experimental Study with a Schlieren System. (Dr.Ing. Thesis)

MTA-86-92 Hessen, Gunnar, MK:	Fracture Mechanics Analysis of Stiffened Tubular Members. (Dr.Ing. Thesis)
MTA-93-93 Steinebach, Christian, MM:	Knowledge Based Systems for Diagnosis of Rotating Machinery. (Dr.Ing. Thesis)
MTA-93-94 Dalane, Jan Inge, MK:	System Reliability in Design and Maintenance of Fixed Offshore Structures. (Dr.Ing. Thesis)
MTA-93-95 Steen, Sverre, MH:	Cobblestone Effect on SES. (Dr.Ing. Thesis)
MTA-93-96 Karunakaran, Daniel, MK:	Nonlinear Dynamic Response and Reliability Analysis of Drag-dominated Offshore Platforms. (Dr.Ing. Thesis)
MTA-93-97 Hagen, Arnulf, MP:	The Framework of a Design Process Language. (Dr.Ing. Thesis)
MTA-93-98 Nordrik, Rune, MM:	Investigation of Spark Ignition and Autoignition in Methane and Air Using Computational Fluid Dynamics and Chemical Reaction Kinetics. A Numerical Study of Ignition Processes in Internal Combustion Engines. (Dr.Ing. Thesis)
MTA-94-99 Passano, Elizabeth, MK:	Efficient Analysis of Nonlinear Slender Marine Structures. (Dr.Ing. Thesis)
MTA-94-100 Kvålsvold, Jan, MH:	Hydroelastic Modelling of Wetdeck Slamming on Multihull Vessels. (Dr.Ing. Thesis)
MTA-94-102 Bech, Sidsel M., MK:	Experimental and Numerical Determination of Stiffness and Strength of GRP/PVC Sandwich Structures. (Dr.Ing. Thesis)
MTA-95-103 Paulsen, Hallvard, MM:	A Study of Transient Jet and Spray using a Schlieren Method and Digital Image Processing. (Dr.Ing. Thesis)
MTA-95-104 Hovde, Geir Olav, MK:	Fatigue and Overload Reliability of Offshore Structural Systems, Considering the Effect of Inspection and Repair. (Dr.Ing. Thesis)
MTA-95-105 Wang, Xiaozhi, MK:	Reliability Analysis of Production Ships with Emphasis on Load Combination and Ultimate Strength. (Dr.Ing. Thesis)
MTA-95-106 Ulstein, Tore, MH:	Nonlinear Effects of a Flexible Stern Seal Bag on Cobblestone Oscillations of an SES. (Dr.Ing. Thesis)

MTA-95-107 Solaas, Frøydis, MH:	Analytical and Numerical Studies of Sloshing in Tanks. (Dr.Ing. Thesis)
MTA-95-108 Hellan, øyvind, MK:	Nonlinear Pushover and Cyclic Analyses in Ultimate Limit State Design and Reassessment of Tubular Steel Offshore Structures. (Dr.Ing. Thesis)
MTA-95-109 Hermundstad, Ole A., MK:	Theoretical and Experimental Hydroelastic Analysis of High Speed Vessels. (Dr.Ing. Thesis)
MTA-96-110 Bratland, Anne K., MH:	Wave-Current Interaction Effects on Large-Volume Bodies in Water of Finite Depth. (Dr.Ing. Thesis)
MTA-96-111 Herfjord, Kjell, MH:	A Study of Two-dimensional Separated Flow by a Combination of the Finite Element Method and Navier-Stokes Equations. (Dr.Ing. Thesis)
MTA-96-112 Æsøy, Vilmar, MM:	Hot Surface Assisted Compression Ignition in a Direct Injection Natural Gas Engine. (Dr.Ing. Thesis)
MTA-96-113 Eknes, Monika L., MK:	Escalation Scenarios Initiated by Gas Explosions on Offshore Installations. (Dr.Ing. Thesis)
MTA-96-114 Erikstad, Stein O., MP:	A Decision Support Model for Preliminary Ship Design. (Dr.Ing. Thesis)
MTA-96-115 Pedersen, Egil, MH:	A Nautical Study of Towed Marine Seismic Streamer Cable Configurations. (Dr.Ing. Thesis)
MTA-97-116 Moksnes, Paul O., MM:	Modelling Two-Phase Thermo-Fluid Systems Using Bond Graphs. (Dr.Ing. Thesis)
MTA-97-117 Halse, Karl H., MK:	On Vortex Shedding and Prediction of Vortex-Induced Vibrations of Circular Cylinders. (Dr.Ing. Thesis)
MTA-97-118 Igland, Ragnar T., MK:	Reliability Analysis of Pipelines during Laying, considering Ultimate Strength under Combined Loads. (Dr.Ing. Thesis)
MTA-97-119 Pedersen, Hans-P., MP:	Levendefiskteknologi for fiskefartøy. (Dr.Ing. Thesis)
MTA-98-120 Vikestad, Kyrre, MK:	Multi-Frequency Response of a Cylinder Subjected to Vortex Shedding and Support

	Motions. (Dr.Ing. Thesis)
MTA-98-121 Azadi, Mohammad R. E., MK:	Analysis of Static and Dynamic Pile-Soil-Jacket Behaviour. (Dr.Ing. Thesis)
MTA-98-122 Ulltang, Terje, MP:	A Communication Model for Product Information. (Dr.Ing. Thesis)
MTA-98-123 Torbergsen, Erik, MM:	Impeller/Diffuser Interaction Forces in Centrifugal Pumps. (Dr.Ing. Thesis)
MTA-98-124 Hansen, Edmond, MH:	A Discrete Element Model to Study Marginal Ice Zone Dynamics and the Behaviour of Vessels Moored in Broken Ice. (Dr.Ing. Thesis)
MTA-98-125 Videiro, Paulo M., MK:	Reliability Based Design of Marine Structures. (Dr.Ing. Thesis)
MTA-99-126 Mainçon, Philippe, MK:	Fatigue Reliability of Long Welds Application to Titanium Risers. (Dr.Ing. Thesis)
MTA-99-127 Haugen, Elin M., MH:	Hydroelastic Analysis of Slamming on Stiffened Plates with Application to Catamaran Wetdecks. (Dr.Ing. Thesis)
MTA-99-128 Langhelle, Nina K., MK:	Experimental Validation and Calibration of Nonlinear Finite Element Models for Use in Design of Aluminium Structures Exposed to Fire. (Dr.Ing. Thesis)
MTA-99-129 Berstad, Are J., MK:	Calculation of Fatigue Damage in Ship Structures. (Dr.Ing. Thesis)
MTA-99-130 Andersen, Trond M., MM:	Short Term Maintenance Planning. (Dr.Ing. Thesis)
MTA-99-131 Tveiten, Bård Wathne, MK:	Fatigue Assessment of Welded Aluminium Ship Details. (Dr.Ing. Thesis)
MTA-99-132 Søreide, Fredrik, MP:	Applications of underwater technology in deep water archaeology. Principles and practice. (Dr.Ing. Thesis)
MTA-99-133 Tønnessen, Rune, MH:	A Finite Element Method Applied to Unsteady Viscous Flow Around 2D Blunt Bodies With Sharp Corners. (Dr.Ing. Thesis)
MTA-99-134 Elvekrok, Dag R., MP:	Engineering Integration in Field Development Projects in the Norwegian Oil and Gas Industry. The Supplier Management of Norne. (Dr.Ing.

	Thesis)
MTA-99-135 Fagerholt, Kjetil, MP:	Optimeringsbaserte Metoder for Ruteplanlegging innen skipsfart. (Dr.Ing. Thesis)
MTA-99-136 Bysveen, Marie, MM:	Visualization in Two Directions on a Dynamic Combustion Rig for Studies of Fuel Quality. (Dr.Ing. Thesis)
MTA-2000-137 Storteig, Eskild, MM:	Dynamic characteristics and leakage performance of liquid annular seals in centrifugal pumps. (Dr.Ing. Thesis)
MTA-2000-138 Sagli, Gro, MK:	Model uncertainty and simplified estimates of long term extremes of hull girder loads in ships. (Dr.Ing. Thesis)
MTA-2000-139 Tronstad, Harald, MK:	Nonlinear analysis and design of cable net structures like fishing gear based on the finite element method. (Dr.Ing. Thesis)
MTA-2000-140 Kroneberg, André, MP:	Innovation in shipping by using scenarios. (Dr.Ing. Thesis)
MTA-2000-141 Haslum, Herbjørn Alf, MH:	Simplified methods applied to nonlinear motion of spar platforms. (Dr.Ing. Thesis)
MTA-2001-142 Samdal, Ole Johan, MM:	Modelling of Degradation Mechanisms and Stressor Interaction on Static Mechanical Equipment Residual Lifetime. (Dr.Ing. Thesis)
MTA-2001-143 Baarholm, Rolf Jarle, MH:	Theoretical and experimental studies of wave impact underneath decks of offshore platforms. (Dr.Ing. Thesis)
MTA-2001-144 Wang, Lihua, MK:	Probabilistic Analysis of Nonlinear Wave-induced Loads on Ships. (Dr.Ing. Thesis)
MTA-2001-145 Kristensen, Odd H. Holt, MK:	Ultimate Capacity of Aluminium Plates under Multiple Loads, Considering HAZ Properties. (Dr.Ing. Thesis)
MTA-2001-146 Greco, Marilena, MH:	A Two-Dimensional Study of Green-Water Loading. (Dr.Ing. Thesis)
MTA-2001-147 Heggelund, Svein E., MK:	Calculation of Global Design Loads and Load Effects in Large High Speed Catamarans. (Dr.Ing. Thesis)

MTA-2001-148 Babalola, Olusegun T., MK:	Fatigue Strength of Titanium Risers - Defect Sensitivity. (Dr.Ing. Thesis)
MTA-2001-149 Mohammed, Abuu K., MK:	Nonlinear Shell Finite Elements for Ultimate Strength and Collapse Analysis of Ship Structures. (Dr.Ing. Thesis)
MTA-2002-150 Holmedal, Lars E., MH:	Wave-current interactions in the vicinity of the sea bed. (Dr.Ing. Thesis)
MTA-2002-151 Rognebakke, Olav F., MH:	Sloshing in rectangular tanks and interaction with ship motions. (Dr.Ing. Thesis)
MTA-2002-152 Lader, Pål Furset, MH:	Geometry and Kinematics of Breaking Waves. (Dr.Ing. Thesis)
MTA-2002-153 Yang, Qinzheng, MH:	Wash and wave resistance of ships in finite water depth. (Dr.Ing. Thesis)
MTA-2002-154 Melhus, Øyvin, MM:	Utilization of VOC in Diesel Engines. Ignition and combustion of VOC released by crude oil tankers. (Dr.Ing. Thesis)
MTA-2002-155 Ronæss, Marit, MH:	Wave Induced Motions of Two Ships Advancing on Parallel Course. (Dr.Ing. Thesis)
MTA-2002-156 Økland, Ole D., MK:	Numerical and experimental investigation of whipping in twin hull vessels exposed to severe wet deck slamming. (Dr.Ing. Thesis)
MTA-2002-157 Ge, Chunhua, MK:	Global Hydroelastic Response of Catamarans due to Wet Deck Slamming. (Dr.Ing. Thesis)
MTA-2002-158 Byklum, Eirik, MK:	Nonlinear Shell Finite Elements for Ultimate Strength and Collapse Analysis of Ship Structures. (Dr.Ing. Thesis)
IMT-2003-1 Chen, Haibo, MK:	Probabilistic Evaluation of FPSO-Tanker Collision in Tandem Offloading Operation. (Dr.Ing. Thesis)
IMT-2003-2 Skaugset, Kjetil Bjørn, MK:	On the Suppression of Vortex Induced Vibrations of Circular Cylinders by Radial Water Jets. (Dr.Ing. Thesis)
IMT-2003-3 Chezhian, Muthu	Three-Dimensional Analysis of Slamming. (Dr.Ing. Thesis)
IMT-2003-4 Buhaug, Øyvind	Deposit Formation on Cylinder Liner Surfaces

	in Medium Speed Engines. (Dr.Ing. Thesis)
IMT-2003-5 Tregde, Vidar	Aspects of Ship Design: Optimization of Aft Hull with Inverse Geometry Design. (Dr.Ing. Thesis)
IMT-2003-6 Wist, Hanne Therese	Statistical Properties of Successive Ocean Wave Parameters. (Dr.Ing. Thesis)
IMT-2004-7 Ransau, Samuel	Numerical Methods for Flows with Evolving Interfaces. (Dr.Ing. Thesis)
IMT-2004-8 Soma, Torkel	Blue-Chip or Sub-Standard. A data interrogation approach of identity safety characteristics of shipping organization. (Dr.Ing. Thesis)
IMT-2004-9 Ersdal, Svein	An experimental study of hydrodynamic forces on cylinders and cables in near axial flow. (Dr.Ing. Thesis)
IMT-2005-10 Brodtkorb, Per Andreas	The Probability of Occurrence of Dangerous Wave Situations at Sea. (Dr.Ing. Thesis)
IMT-2005-11 Yttervik, Rune	Ocean current variability in relation to offshore engineering. (Dr.Ing. Thesis)
IMT-2005-12 Fredheim, Arne	Current Forces on Net-Structures. (Dr.Ing. Thesis)
IMT-2005-13 Heggernes, Kjetil	Flow around marine structures. (Dr.Ing. Thesis)
IMT-2005-14 Fouques, Sebastien	Lagrangian Modelling of Ocean Surface Waves and Synthetic Aperture Radar Wave Measurements. (Dr.Ing. Thesis)
IMT-2006-15 Holm, Håvard	Numerical calculation of viscous free surface flow around marine structures. (Dr.Ing. Thesis)
IMT-2006-16 Bjørheim, Lars G.	Failure Assessment of Long Through Thickness Fatigue Cracks in Ship Hulls. (Dr.Ing. Thesis)
IMT-2006-17 Hansson, Lisbeth	Safety Management for Prevention of Occupational Accidents. (Dr.Ing. Thesis)
IMT-2006-18 Zhu, Xinying	Application of the CIP Method to Strongly Nonlinear Wave-Body Interaction Problems. (Dr.Ing. Thesis)
IMT-2006-19 Reite, Karl Johan	Modelling and Control of Trawl Systems.

	(Dr.Ing. Thesis)
IMT-2006-20 Smogeli, Øyvind Notland	Control of Marine Propellers. From Normal to Extreme Conditions. (Dr.Ing. Thesis)
IMT-2007-21 Storhaug, Gaute	Experimental Investigation of Wave Induced Vibrations and Their Effect on the Fatigue Loading of Ships. (Dr.Ing. Thesis)
IMT-2007-22 Sun, Hui	A Boundary Element Method Applied to Strongly Nonlinear Wave-Body Interaction Problems. (PhD Thesis, CeSOS)
IMT-2007-23 Rustad, Anne Marthine	Modelling and Control of Top Tensioned Risers. (PhD Thesis, CeSOS)
IMT-2007-24 Johansen, Vegar	Modelling flexible slender system for real-time simulations and control applications.
IMT-2007-25 Wroldsen, Anders Sunde	Modelling and control of tensegrity structures. (PhD Thesis, CeSOS)
IMT-2007-26 Aronsen, Kristoffer Høye	An experimental investigation of in-line and combined in-line and cross flow vortex induced vibrations. (Dr.avhandling, IMT)
IMT-2007-27 Zhen, Gao	Stochastic response analysis of mooring systems with emphasis on frequency-domain analysis of fatgue due to wide-band processes. (PhD-thesis CeSOS).
IMT-2007-28 Thorstensen, Tom Anders	Lifetime Profit Modelling of Ageing Systems Utilizing Information about Technical Condition. Dr.ing. thesis, IMT.
IMT-2007-29 Ye, Naiquan	Fatigues Assessment of Aluminium Welded Box stiffener Joints in ships. Dr.ing.-Thesis, IMT.
IMT-2007-30 Pákozdi, Csaba	A Smoothed Particle Hydrodynamics Study of Two-dimensional Nonlinear Sloshing in Rectangular Tanks. Dr.ing.thesis, IMT.
IMT-2007-31 Thorhus, Runar	Alliances in Development of Short-sea Transport systems. Dr.ing.thesis, IMT.
IMT-2008-32 Norum, Viggo L.	Analysis of Ignituin and Combustion in Otto Lean-Burn Engines with Prechambers. Dr.ing. thesis, IMT.

IMT-2008-32 Berntsen, Per Ivar B.	Structural Reliability Based Position Mooring. PhD-thesis, IMT.
IMT-2008-33 Refsnes, Jon Erling G.	Nonlinear Model-Based Control of Slender Body AUVs. PhD-thesis, IMT.